Author:
Bacon, Travis J

Title:
Noradrenergic modulation of hippocampal CA1 and CA3 networks

Noradrenergic modulation of hippocampal CA1 and CA3 networks

Travis James Bacon

SWBio Doctoral Training Programme

UNIVERSITY OF BRISTOL

A dissertation submitted to the University of Bristol in accordance with the requirements for award of the degree of Doctor of Philosophy in the Faculty of Life Sciences

September 2019

Word count: 46,229

Abstract

The release of neuromodulators within the hippocampus regulates the encoding of memories. The locus coeruleus (LC) is a brainstem nucleus that projects diffusely throughout the cortex, releasing noradrenaline (NA) and – within the hippocampus – this release acts as a novelty signal, with the LC switching from tonic firing in familiar spaces to burst firing when an animal enters a novel environment.

To explore the relatively understudied modulatory effects of NA on hippocampal synaptic inputs and post-synaptic firing properties we used a combination of whole-cell patch-clamp recordings in mouse *ex vivo* hippocampal slices, optogenetic manipulations and computational modelling.

Bath application of NA attenuated both excitatory and feed-forward inhibitory responses at the Schaffer collateral-CA1 (SC-CA1) synapse, resulting in a reduced spike output in response to synaptic stimulation. However, high-frequency inputs were able to overcome this attenuation and shift the excitatory/inhibitory (E/I) ratio towards excitation – a novel result consistent with a role of NA in prioritising high frequency (perhaps salient) drives.

At mossy fibre-CA3 (MF-CA3) synapses NA decreased feed-forward inhibition but spared excitatory inputs. The effect of NA on naturalistic granule cell firing patterns was further examined using a Tsodyks-Markram model of the MF-CA3 synapse, which suggested that a reduction in the ability of feed-forward inhibitory interneurons to recover from depression underscored the enhanced E/I ratio.

In contrast to the effects of high concentrations of bath-applied NA, optogenetically-evoked NA augmented CA1 spike output through a β-AR mechanism and a potential inhibition of transient voltage-gated K^+ channels. These effects were recapitulated with a sub-micromolar concentration of bath-applied NA, highlighting the importance of concentration and spatiotemporal release patterns of neuromodulators when investigating their effects in *ex vivo* slices. Utilising fast-scan voltammetry and a genetically-encoded fluorescent NA sensor, we show that optically-evoked physiological release of NA is much lower than the bath-applied concentrations used in the literature.

Acknowledgements

This PhD could not have been completed without the help and support of a vast number of people. First and foremost, a strong word of thanks goes to my supervisors, Jack Mellor and Tony Pickering, for their endless support and encouragement. Their optimism, patience and imparted knowledge have helped me grow, both as a scientist and as a person, and I shall miss our meetings and discussions.

Thanks, as well, to all members (past and present) of the Mellor and Pickering labs. In particular, to Matt Udakis, for the competitive MATLAB-ing, and for bringing music to the lab, coffee to the office and margaritas into my life.

Thanks also to Michael Ashby, Jon Witton and Sorayah Meftah for their helpful suggestions, and The Banana Club (Arne, Katy, Clara and Em) for their humour and support. Terry Conway and Leslie Raw, my GCSE Science and A-Level Biology teachers, respectively, deserve a mention for sparking and encouraging my enthusiasm for science many moons ago.

Finally, I wouldn't have made it this far without the support of my friends and family. Breaks to visit old friends from QE and Leeds always make me laugh until my sides ache, and for that I'm forever grateful and long may these friendships last.

Mum, Dad and Connor, thanks for blessing me with such a wonderful upbringing and listening to me ramble on over the phone about my research. Sue, Andy, Ben and James, thanks for welcoming me into your family with such open arms. Finally, a special thank you to my wife Sophie, for your love, encouragement and all the wonderful memories we've made and will continue to make.

Author's declaration

I declare that the work in this dissertation was carried out in accordance with the requirements of the University's Regulations and Code of Practice for Research Degree Programmes and that it has not been submitted for any other academic award. Except where indicated by specific reference in the text, the work is the candidate's own work. Work done in collaboration with, or with the assistance of, others, is indicated as such. Any views expressed in the dissertation are those of the author.

SIGNED: ..... DATE: .....

Table of contents

List of figures

List of tables

List of abbreviations

ACh	Acetylcholine
aCSF	Artificial cerebrospinal fluid
AIS	Axon initial segment
AMPAR	α-amino-3-hydroxy-5-methyl-4-isoxazolepropionic acid receptor
ANOVA	Analysis of variance
ATP	Adenosine triphosphate
CA1-3	Cornu ammonis 1-3
CAMKII	Ca^{2+}/calmodulin dependent kinase II
cAMP	Cyclic adenosine monophosphate
CCh	Carbachol
CCK	Cholecystokinin
ChR2	Channelrhodopsin-2
CNS	Central nervous system
CRF	Corticotropin releasing factor
CSF	Cerebrospinal fluid
D1-5R	Dopamine 1-5 receptor
D-AP5	D-(-)-2-amino-5-phosphonopentanoic acid
DA	Dopamine
DCG-IV	(2S,2'R,3'R)-2-(2',3'-dicarboxycyclopropyl) glycine
DG	Dentate gyrus
EC	Entorhinal cortex
EEG	Electroencephalogram
EGTA	Ethylene glycol-*bis*(2-aminoethylether)-*N*,*N*,*N*',*N*'-tetraacetic acid
EPSC	Excitatory post-synaptic current
EPSP	Excitatory post-synaptic potential
fEPSP	Field excitatory post-synaptic potential

GABA	γ-aminobutyric acid
GIRK	G-protein gated inwardly rectifying potassium
GPCR	G-protein-coupled receptor
GTP	Guanosine-5'-triphosphate
HCN	Hyperpolarisation-activated cyclic nucleotide-gated
HEPES	4-(2-hydroxyethyl)piperazine-1-ethanesulfonic acid
HFS	High frequency stimulation
I_h	*h*-current
IPSC	Inhibitory post-synaptic current
IPSP	Inhibitory post-synaptic potential
KAR	Kainate receptor
LFP	Local field potential
LFS	Low frequency stimulation
LTD	Long-term depression
LTP	Long-term potentiation
M1-5R	Muscarinic 1-5 receptor
mAHP	Medium after hyperpolarisation
MCH	Melanin concentrating hormone
MEC	Medial entorhinal cortex
MF	Mossy fibre
mGluR	Metabotropic glutamate receptor
MWM	Morris water maze
NA	Noradrenaline
NBQX	2,3-Dioxo-6-nitro-1,2,3,4-tetrahydrobenzo[f]quinoxaline-7-sulfonamide disodium salt
NET	Norepinephrine transporter
NMDA	N-methyl-D-aspartic acid

NMDAR	N-methyl-D-aspartic acid receptor
NPY	Neuropeptide Y
NREM	Non-rapid eye movement
PB	Phosphate buffer
PBS	Phosphate buffered saline
PLC	Phospholipase C
PPR	Paired pulse ratio
P_r	Release probability
PSC	Post-synaptic current
PSP	Post-synaptic potential
PTX	Picrotoxin
PV	Parvalbumin
QX-314	*N*-(2,6-dimethylphenylcarbamoylmethyl)triethylammonium chloride
REM	Rapid eye movement
R_{in}	Input resistance
RMP	Resting membrane potential
sAHP	Slow afterhyperpolarisation
SC	Schaffer collateral
SD	Standard deviation
SEM	Standard error of the mean
SK	Small conductance Ca^{2+}-activated K^+
SST	Somatostatin
STDP	Spike-timing dependent plasticity
SWR	Sharp wave-ripple
SWS	Slow wave sleep
TA	Temporoammonic
TBS	Theta burst stimulation

TEA	tetraethylammonium chloride
TTX	Tetrodotoxin
VGCC	Voltage-gated Ca^{2+} channel
V_m	Membrane voltage
VTA	Ventral tegmental area
WT	Wild-type

Chapter 1: Introduction

1.1 The hippocampus and memory

1.1.1 What is memory?

A memory is the neural representation of a fact or experience that can be retrieved – subconsciously or consciously – to play a critical role in learning to interact with the world. Memory is vital in improving an individual organism's response to the same – or similar – situations, and multiple brain regions are implicated in the formation, storage and retrieval of memories (Richter-Levin and Akirav, 2001; Kennedy and Shapiro, 2004; Fastenrath *et al.*, 2014; Jin and Maren, 2015; Bergmann *et al.*, 2016; Eichenbaum, 2017), with interplay between areas enabling the integration of multiple sensory modalities into the neural representations of semantic (factual), episodic (experiences) and procedural (reflexive motor) memories (Squire, 1986; Squire *et al.*, 1993; Milner, Squire and Kandel, 1998). Semantic and episodic memories – forms of declarative or explicit memory – are distinct from procedural memories in that they are the "knowing what" about situations and can be consciously recalled; unlike the subconscious "knowing how" implicit memories that underlie reflexive sensorimotor behaviours (Bird and Burgess, 2008). Moreover, implicit memories are stored in areas of the brain underlying motor control, such as the cerebellum, basal ganglia and the motor cortex (Schacter, Chiu and Ochsner, 1993); whereas explicit memories involve higher brain regions such as the pre-frontal cortex, hippocampus and the amygdala (Voss and Paller, 2008). Of these, the hippocampus plays a crucial role in integrating multiple sensory modalities into a short-term memory for subsequent long-term consolidation in the cortex (McClelland, McNaughton and O'Reilly, 1995; Nadel and Moscovitsh, 1997; Bayley *et al.*, 2005; Bergmann *et al.*, 2016).

1.1.2 The hippocampus: an overview

Located deep within the temporal lobe, the hippocampus is one of the most important and well-studied structures in memory (Andersen *et al.*, 2007). The significance of the hippocampus in memory formation was highlighted in the seminal case of Patient H.M., wherein the subject developed severe anterograde amnesia – an inability to commit new events to his explicit memory – after a bilateral medial temporal lobectomy to control his epilepsy (Scoville and Milner, 1957). Subsequent work on rodents and primates have recapitulated similar memory deficits following hippocampal loss, underscoring their utility as tractable models of memory (see Squire (1992) for review). In addition to these behavioural similarities, the general architecture of the hippocampal anatomy is comparable between animals and humans (Clark and Squire, 2013). This anatomical structure consists of the dentate gyrus (DG), the *cornu ammonis* (CA) subfields CA3,

CA2 and CA1, the subiculum and the entorhinal cortex (Amaral and Witter, 1989). The term "hippocampus" in this thesis will only concern the DG and CA subfields.

All areas of the hippocampus receive projections from neurons within layers II and III of the medial entorhinal cortex (MEC), however there are prominent layer III projections to the CA1 and subiculum, whereas the DG and the CA3 receive strong layer II inputs (Steward and Scoville, 1976). The classical "tri-synaptic pathway" begins with the layer II projections to the dentate gyrus (DG), mossy fibre projections from DG granule cells to the CA3 pyramidal cells form the second relay point, and the CA3 Schaffer collateral (SC) projections to the CA1 comprise the third node. CA1 projections then transmit the information to the subiculum. Pyramidal neurons in the CA3 also send recurrent projections to other CA3 neurons in the ipsilateral and contralateral hippocampi. These projections are known as the "association" and "commissural" pathways, respectively, and are commonly referred to as A/C projections The two aforementioned MEC inputs are known as the direct (layer III to CA1) or "temporoammonic" (TA) pathway and the indirect (layer II to CA1 via the tri-synaptic pathway) "perforant" pathway (PP) to CA1. This circuit is summarised in Figure 1.1.

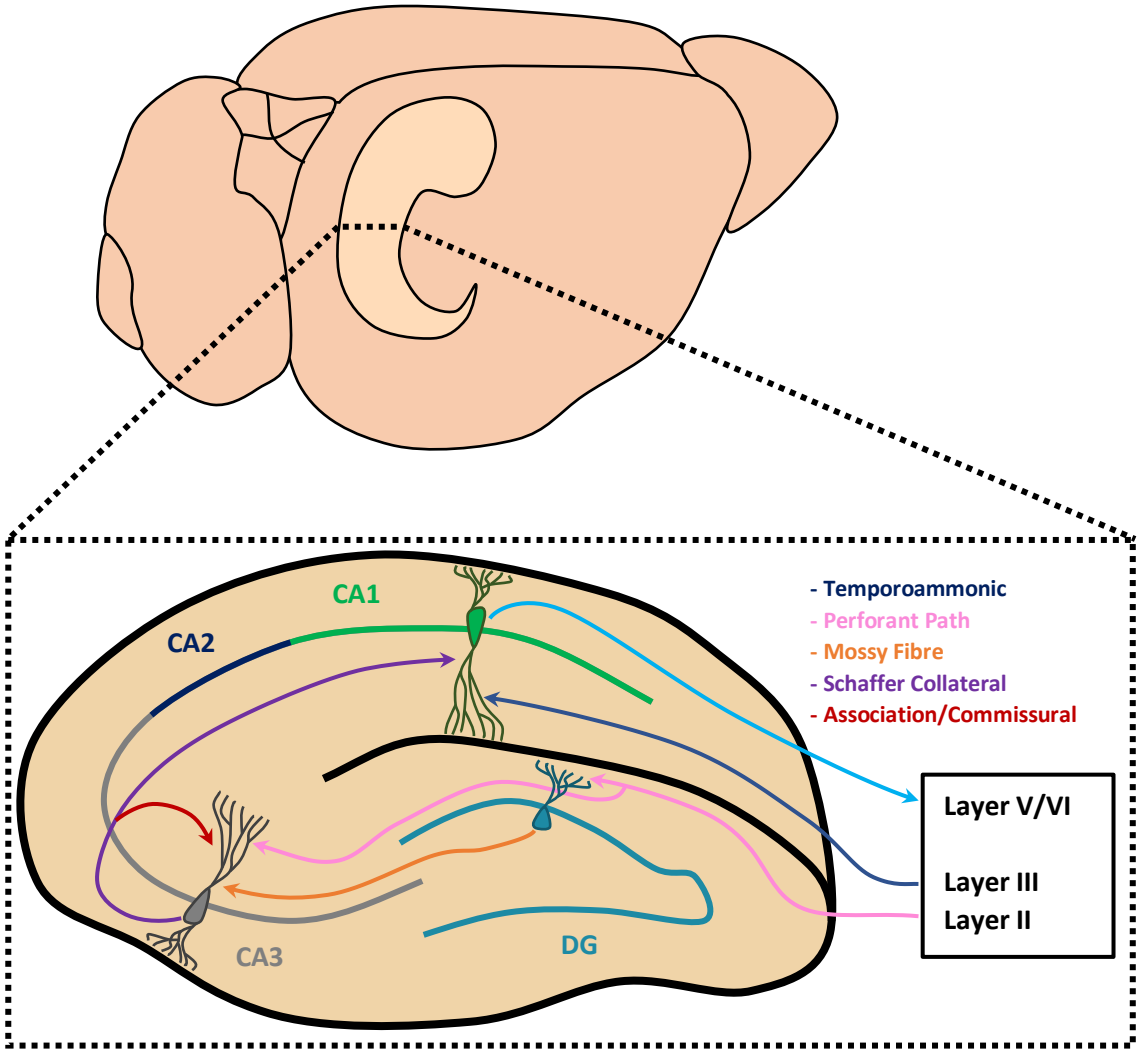

Figure 1.1: *Information flow through the hippocampus. A transverse section of a rodent hippocampus, highlighting the major pathways for information flow.*

Although elegant, this tri-synaptic pathway is somewhat simplistic, ignoring the diverse and complex roles of various interneurons (both feed-forward and feed-back, (Pouille and Scanziani, 2001, 2004; Klausberger *et al.*, 2003, 2004; Klausberger and Somogyi, 2008; Milstein *et al.,* 2015) and the CA2 area of the hippocampus (Shinohara *et al.*, 2012; Kohara *et al.*, 2014; Boehringer *et al.*, 2017). Moreover, despite preservation of the general architecture along the longitudinal axis, the dorsal and ventral hippocampal aspects have shown involvement in distinct types of memory processing: the dorsal aspect plays a strong role in spatial memory (Hughes, 1965; Moser, Moser and Andersen, 1993; Moser *et al.*, 1995; Hock and Bunsey, 1998; Moser and Moser, 1998) whereas the ventral hippocampus is more involved in stress and emotional memory processing (Henke, 1990; Moser and Moser, 1998). These behavioural studies are in line with electrophysiological data suggesting dorsal CA1 contains more place cells (neurons tuned to a particular location in space, discussed in more detail in section 1.1.4.) than the ventral CA1. Moreover, these dorsal CA1 place cells possess more finely tuned place fields than their ventral counterparts (Jung, Wiener and McNaughton, 1994). In addition, recent genome studies have highlighted genetic heterogeneity along the CA1

dorsoventral axis, with dorsal hippocampal gene expression correlating strongly with brain regions related to navigation, and the ventral hippocampus sharing strong gene co-expression with brain areas involved in goal-oriented or emotional behaviour (Dong *et al.*, 2009; Fanselow and Dong, 2010).

Nevertheless, the basic tri-synaptic pathway model preserves hippocampal information flow and permits experimental investigation into the various pathways involved in the processing of this information. A wealth of studies over the last 50 years have interrogated the roles of the three main hippocampal relay nodes in the tri-synaptic pathway – DG, CA3 and CA1 – through carefully placed stimulating electrodes in rodent *ex vivo* slice preparations.

1.1.3 Neuronal intrinsic properties and synaptic transmission

Although the following four sections are not specific to hippocampal neurons, an understanding of basic neuronal properties and interneuronal communication is necessary for the rest of the thesis, and so will be discussed briefly here.

1.1.3.1 Resting membrane potential

Neurons are the key computational units that give rise to processes underscoring consciousness, decision-making, memory and behaviour. The vast neuronal diversity in the brain (Lodato and Arlotta, 2015) is necessary for its plethora of functions, yet despite huge differences in cellular morphology (Ascoli, Donohue and Halavi, 2007), gene expression (Benson *et al.*, 2012; Mo *et al.*, 2015) and intrinsic electrophysiological properties (Tripathy *et al.*, 2015), all neurons are made up of several key compartments. The soma (body) where the nucleus and DNA are stored, axons that send electrical impulses away from the soma to downstream cells, and dendrites that receive inputs from upstream cells (Figure 1.2A). All neurons exist in an extracellular milieu known as cerebrospinal fluid (CSF), the majority of which is produced from the choroid plexus (Swedenborg, 1887). The semi-permeable membrane of neurons allows them to maintain an electrical potential difference – the resting membrane potential (RMP) – of around -65 mV relative to the extracellular CSF. This RMP occurs due to the unequal distribution of ions (chiefly Na^+, K^+ and Cl^-) across the membrane and the selective permeability of the membrane to these ions. Specifically, neuronal intracellular Na^+ concentrations are lower than the surrounding CSF whereas neuronal K^+ concentrations are much higher. Activity of the Na^+/K^+-ATPase pump generates and maintains these concentration gradients, actively extruding Na^+ out of the cell in exchange for K^+ (Skou, 1957, Figure 1.2B). The high expression of leak K^+ channels means that the neuron is far more permeable to K^+, as opposed to Na^+, at rest (Purves *et al.*, 2001).

1.1.3.2 Glutamate transmission triggers action potential firing

Much like the wider brain, communication between neurons within the hippocampus is mediated by excitatory and inhibitory neurotransmitters. This communication acts to perturb the RMP, shifting it to more (depolarised) or less (hyperpolarised) potentials (Figure 1.2C). Excitatory synaptic transmission is mediated by the release of the neurotransmitter glutamate from pyramidal neurons and DG granule cells (Biscoe and Straughan, 1966; Nadler *et al.*, 1976; Petroff, 2002), whilst γ-aminobutyric acid (GABA) release from interneurons conveys inhibitory transmission (Biscoe and Straughan, 1966).

Glutamate and GABA can both activate two distinct receptor types: ionotropic and metabotropic. Ionotropic transmission is the faster of the two, as well as the most common, and for glutamate is mediated by α-amino-3-hydroxy-5-methyl-4-isoxazolepropionic acid receptors (AMPARs), N-methyl-D-aspartic acid receptors (NMDARs) and kainate receptors (KARs). All of these receptors are tetrameric and are permeable to cations upon glutamate binding (Traynelis *et al.*, 2010).

Metabotropic glutamate receptors (mGluR1-8) are all G-protein-coupled receptors (GPCRs) that can be sub-divided into three groups, all comprising seven trans-membrane domains but coupled to different G-protein signalling cascades. Group I (mGluR1 and mGluR5) couple to the G_q signalling pathway, leading to activation of phospholipase C (PLC), whereas both group II (mGluR2 and mGluR3) and group III (mGluR4, mGluR6-8) activate the G_i pathway, resulting in an inhibition of adenylyl cyclase and a decrease in cyclic adenosine monophosphate (cAMP) production. Interestingly, kainate receptors are unique in that they can also activate metabotropic signalling cascades, and are known to pre-synaptically regulate glutamate and GABA release in hippocampal pyramidal neurons and interneurons, respectively, via protein kinase C (PKC) activation (Rodríguez-Moreno and Lerma, 1998; Frerking *et al.*, 2001).

Due to the large electrochemical gradients generated by the Na^+/K^+-ATPase pump, rapid changes in the neuronal membrane potential can occur in response to the opening of ligand-gated ionotropic channels and voltage-sensitive ion channels in the membrane. The rapid influx of positive cations though ionotropic glutamate receptor channels (predominantly AMPARs) rapidly depolarises neurons and when a threshold is reached (~ -45 mV for hippocampal neurons), voltage-gated Na^+ channels open, allowing a swift and transient depolarisation of the neuron. As the neuron approaches ~ +40 mV, these channels shut and voltage-gated K^+ channels open, causing the K^+ ions accumulated in the neuron to flow down their electrochemical gradient into the extracellular space, repolarising the neuron back to its RMP (after a brief overshoot that is corrected by the Na^+/K^+-ATPase). This transient and rapid change in membrane voltage is known as an

action potential, or "spike", and is the basis of neuronal communication. The process is summarised in Figure 1.2D. As the action potential propagates from the soma to the axonal terminals, voltage-gated Ca^{2+} channels (VGCCs) open in the pre-synaptic bouton, causing Ca^{2+} influx, Ca^{2+}-dependent release of neurotransmitter containing vesicles into the synaptic cleft and chemical relay of the electrical signal to the post-synaptic neuron.

1.1.3.3 GABAergic transmission prevents action potential firing

Ionotropic GABA communication is the most common mode of inhibition (Petroff, 2002) and is mediated by ionotropic GABARs ($GABA_ARs$). These exist as anion-permeable, hetero-pentameric channels (Sigel and Steinmann, 2012) and predominantly conduct Cl^- ions. The influx of Cl^- into the cell has the opposite effect to glutamate receptor activation, moving the membrane voltage to more hyperpolarised potentials and reducing a neuron's ability to elicit an action potential. Although it should be noted that during development, the reversal potential for Cl^- (E_{Cl}) is shifted to more negative potentials such that $V_m < E_{Cl}$, rendering Cl^- efflux via $GABA_ARs$ as a depolarising current (Ben-Ari *et al.*, 1989). GABA transmission can also be mediated by slower metabotropic receptors ($GABA_BRs$), GPCRs that are located post-synaptically and pre-synaptically as auto-receptors. Post-synaptically, $GABA_BR$ activation induces a slow IPSP through an increase in G-protein-coupled inwardly-rectifying potassium (GIRK) channels activation (Dutar and Nicoll, 1988; Lüscher *et al.*, 1997). Pre-synaptically, $GABA_BRs$ inhibit VGCCs, reduce cAMP production (through G_i signalling) and directly affect the SNARE (soluble N-ethylmaleimide-sensitive factor attachment protein receptor) complex via $G\beta\gamma$ binding (Sakaba and Neher, 2003; Gassmann and Bettler, 2012). These effects therefore attenuate neurotransmitter release by reducing Ca^{2+} influx and direct inhibition of vesicular fusion machinery.

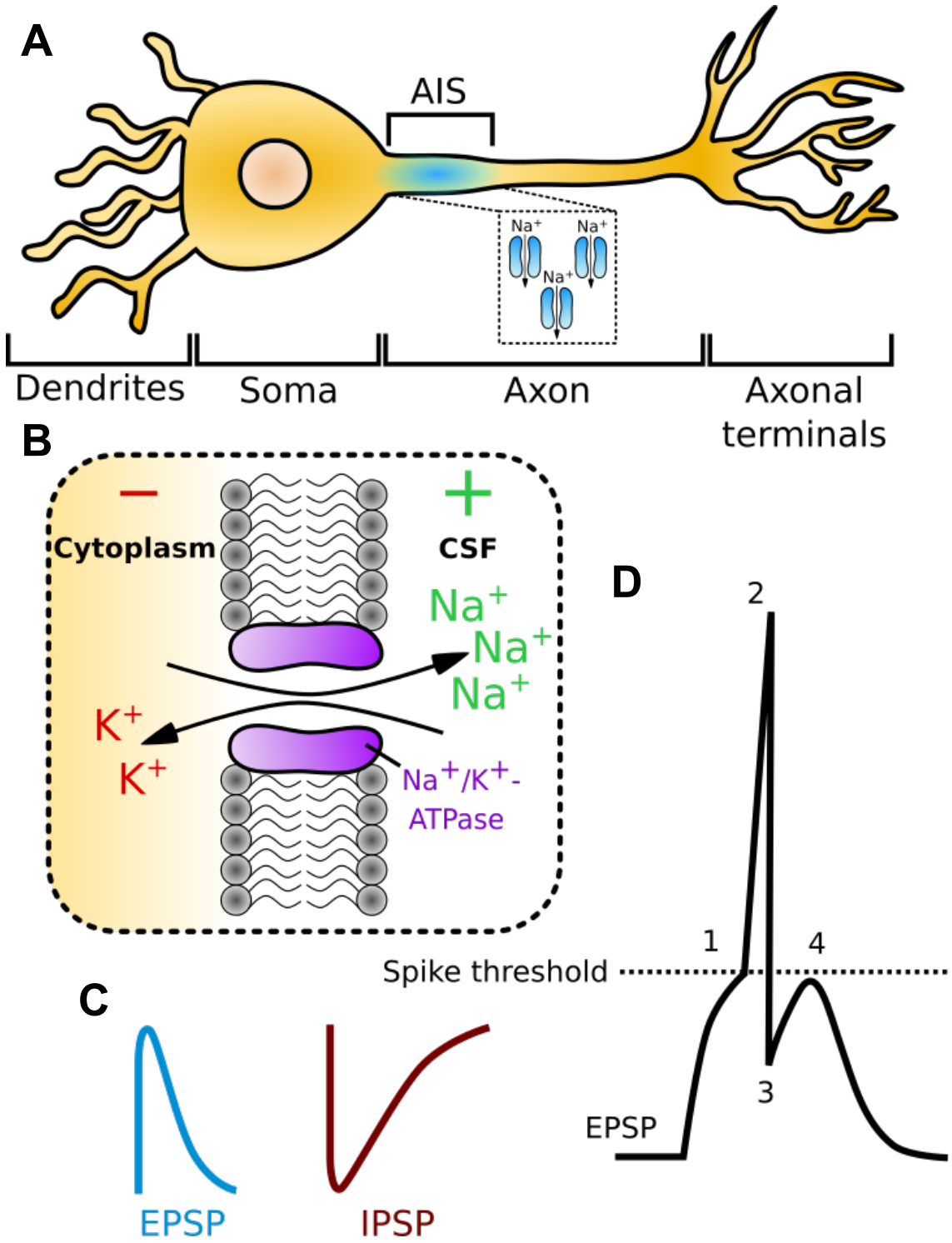

Figure 1.2: *Basic neuronal properties. A) Schematic of a neuron, inset shows the high density of voltage-gated Na^+ channels at the AIS. B) The potential difference across the neuronal membrane is generated by the Na^+/K^+-ATPase exchanging 3 Na^+ ions for 2 K^+ ions, yielding an electrical potential difference of around -65 mV relative to the extracellular CSF. C) Activation of glutamatergic or GABAergic receptors results in excitatory or inhibitory post-synaptic potentials (EPSPs and IPSPs, respectively) in the post-synaptic dendrite. D) Depolarisation of a neuron by an excitatory post-synaptic potential (EPSP) that is sufficient to cross the threshold for action potential generation (1) causes opening of voltage-gated Na^+ channels and rapid depolarisation before these channels close at around +40 mV (2). This closing is concurrent with voltage-gated K^+ channel opening that repolarises the membrane with a slight overshoot that is corrected by the Na^+/K^+-ATPase (3) prior to a slow glutamate removal from the synapse (4).*

1.1.3.4 Additional factors influencing neuronal excitability

Importantly, neurons receive both excitatory and inhibitory inputs simultaneously, and it is their integration at the axon initial segment (AIS, Palay *et al.,* 1968; Clark *et al.,* 2009) that determines whether or not a neuron fires an action potential. Located along the first ~20–60 μm of the axonal shaft (Meeks and Mennerick, 2007; Leterrier, 2018) the concentration of voltage-gated Na^+ (Na_V) channels in the AIS can reach up to ~50 times that seen in proximal dendrites (Meeks and Mennerick, 2007; Kole *et al.*, 2008, Figure 2A). This high density of Na_V channels is thought to underlie action potential initiation, as disruption to the anchoring of Na_V channels increases the spike threshold and reduces action potential fidelity (Lazarov *et al.*, 2018).

In addition to Na_V channels, several K^+ channels also regulate a neuron's so-called intrinsic excitability, dictating its responsiveness to a given synaptic input. For instance, "A-type" voltage-gated K^+ channels (predominantly Kv4.2) in CA1 dendrites display rapid activation and inactivation kinetics, high unitary channel conductance and are activated following EPSP inputs (Maletic-Savatic, Lenn and Trimmer, 1995; Chen and Johnston, 2004). These electrophysiological characteristics, coupled with an expression profile that increases at greater distances from the soma, allow these channels to rapidly shape EPSP amplitudes, prevent single action potentials from eliciting bursting, and suppress back-propagation of action potentials back into the dendrites (Hoffman *et al.*, 1997). In addition, Kv1 K^+ channels (particularly Kv1.1 and Kv1.2) show densest expression at the AIS and soma (Sánchez-Ponce *et al.*, 2012). These are low-voltage activated (LVA), delayed rectifying channels that open in response to small depolarising inputs (Brew, Hallows and Tempel, 2003; Brew *et al.*, 2007;). These properties confer additional dynamics to the electrical properties of the AIS, with slow inactivation effectively suppressing action potential generation by raising the threshold for generation (Dodson, Barker and Forsythe, 2002; Goldberg *et al.*, 2008; Robbins and Tempel, 2012). This is strikingly apparent upon selective blockade of Kv1.1 channels with dendrotoxin-K and in mice genetically engineered to lack the Kv1.1 gene (*kcna1*) (Dodson, Barker and Forsythe, 2002; Brew, Hallows and Tempel, 2003).

Finally, the pre-synaptic targeting and distribution of excitatory and inhibitory inputs relative to each other and to the AIS also play a large part in the integration of these signals (see Spruston (2008) for review). For instance, CA1 pyramidal neurons typically receive cortical inputs via the TA pathway at the distal dendrites, SC inputs from the CA3 more proximally, and SC feed-forward inhibitory interneuron inputs perisomatically (Ishizuka, Weber and Amaral, 1990; Li *et al.*, 1994). Since the AIS dictates action potential firing, this configuration bestows greatest control to the inhibitory inputs. The focus of this thesis will be on the two main feed-forward micro-circuits in the hippocampus: MF-CA3 and SC-CA1 (Figure 1.3).

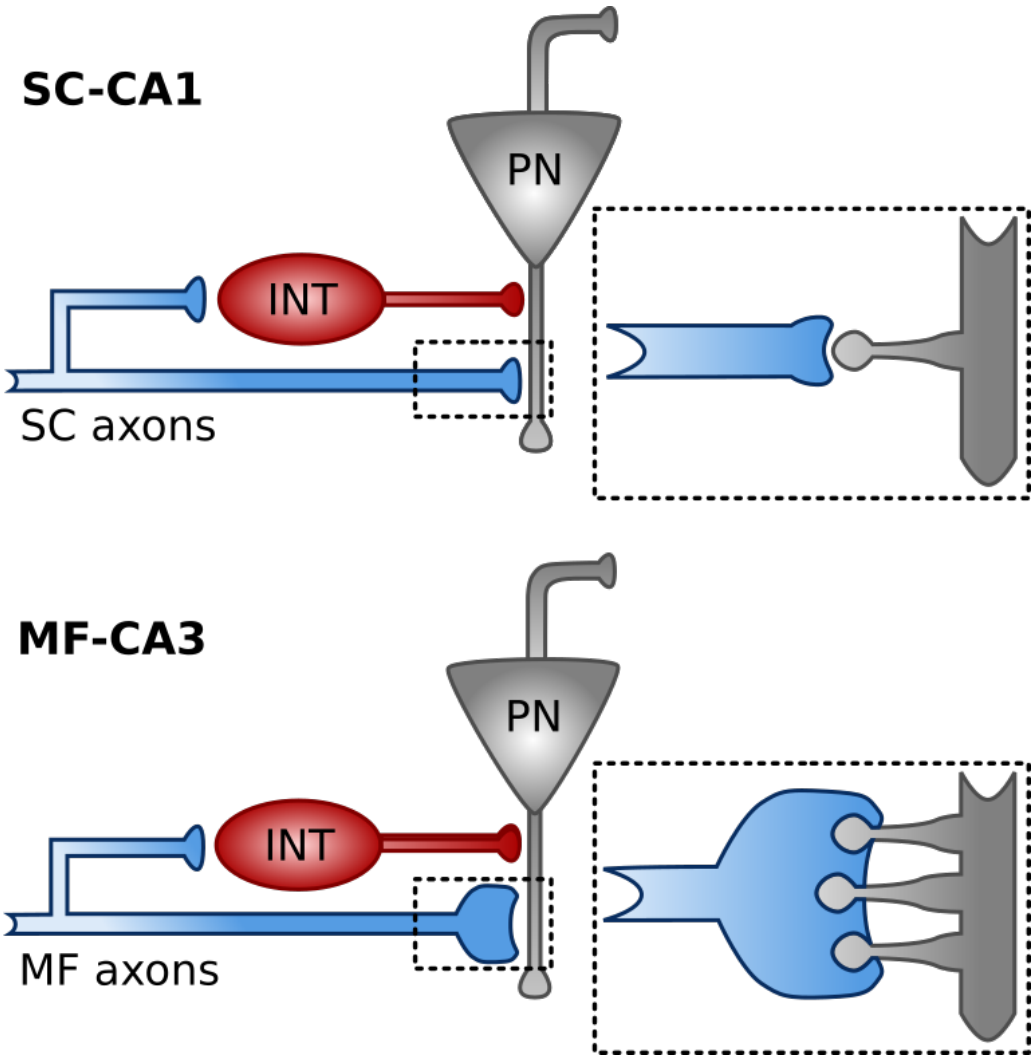

Figure 1.3: *The SC-CA1 and MF-CA3 micro-circuits. Both SC and MF axons directly innervate the dendritic shaft of CA1 and CA3 pyramidal neurons respectively, and also recruit feed-forward inhibition which is targeted perisomatically. Insets denote the structural differences between SC and MF axons: where SC axonal terminals form typical synapses with the CA1 dendrites, the large MF boutons instead envelope the dendritic spines of the CA3 pyramidal neurons. These large boutons contain a far larger number of synaptic vesicles which allow immense facilitation upon repeated stimuli (discussed in greater detail in Sections 1.1.6. and 1.1.7.).*

1.1.3.5 Rate coding

Action potentials are the communication currency of the brain, however since their amplitudes and waveform are largely uniform, neurons code information via the frequency of their action potentials. As will be discussed later in Section 1.2.1.1., various pre- and post-synaptic factors confer particular filtering properties to specific synapses. For instance, DG mossy fibres show frequency-dependent action potential broadening due to the expression of fast-inactivating K^+ channels (Geiger and Jonas, 2000). These synapse-specific filters allow various post-synaptic targets to extract different patterns of information from the same train of action potential inputs (Abbott and Regehr, 2004). Within the hippocampus, rate-coding is particularly important in pyramidal neurons as it permits a simple, yet profoundly useful, indication of an animal's spatial location.

1.1.4 The hippocampus in spatial navigation

The function of the hippocampus stretches beyond its existence as a simple declarative memory storage unit. In the decades following the pioneering foundations laid out by Scoville and Milner, interest and understanding in hippocampal learning and memory grew. The notion that the hippocampus was purely involved in declarative episodic memory abated during the early 1970s when several neuroscientists developed novel methods and technologies to enable recording of neural electrical activity from awake, freely-moving animals. John O'Keefe and John Dostrovsky (O'Keefe and Dostrovsky, 1971) and Jim Ranck (Ranck, 1973) were the leading researchers in this field, and published results showing that individual hippocampal neuron firing activity was exquisitely tuned to the animal's location (O'Keefe, 1976). These neurons became known as "place cells", with each neuron having a unique "place field" where they preferentially fired, with firing frequency diminishing as the animal moved away from this location (Figure 1.4A). Subsequent work on place cells also revealed neurons that respond to non-spatial environmental features including odours (Eichenbaum *et al.*, 1987) and tactile cues (Young, Fox and Eichenbaum, 1994) as well as to the spatial position of the animal, suggesting that the hippocampus integrates both spatial and non-spatial environmental elements in the generation of a cognitive map (Save, Nerad and Poucet, 2000; Leutgeb *et al.*, 2005; Moser, Kropff and Moser, 2008). It is believed this integration is computed within theta cycles and involves place cells spiking in an ordered series representing the succession of locations traversed during exploration. Neurons whose place fields have just been entered fire later in the theta cycle, whereas leaving a place field triggers firing early in the theta cycle (O'Keefe and Recce, 1993). The temporal organisations of such neuronal ensembles are termed theta sequences and can be replayed "off-line" (i.e. during sleep) over a more rapid, compressed timescale, a process thought to underlie memory consolidation (Wilson and McNaughton, 1994; Lee and Wilson, 2002; van de Ven *et al.*, 2016). Intriguingly, spatial location is not topographically mapped (i.e. neighbouring neuronal place fields are no more similar than those of distant neurons, (O'Keefe, 1976; Wilson and McNaughton, 1993), however place field size does increase across the hippocampal dorso-ventral axis (Jung, Wiener and McNaughton, 1994; Kjelstrup *et al.*, 2008).

Importantly, place cells are able to code minor environmental changes through "rate remapping" (where place fields remain stable but the firing rates between environments vary, Leutgeb *et al.*, (2005), Figure 1.4B), or completely novel environments through "global remapping" (where place fields show no correlation between environments, (O'Keefe and Conway, 1978), Figure 1.4C). In addition to place cells, grid cells were later discovered in the medial entorhinal cortex (Hafting *et al.*, 2005). Unlike the highly selective spatial coding of place cells, grid cells exhibit multiple firing fields – spread

across a tessellated, hexagonal pattern – in any given environment. These cells may drive global remapping of place fields; however, their function is still under fierce debate (Rowland *et al.*, 2016). Initial remapping appears to be due to entorhinal inputs to the hippocampus (for review, see Latuske *et al.*, 2017) however recent work implicates neuromodulatory inputs for the stabilisation of globally remapped place fields. For instance, chemo-genetically silencing noradrenergic inputs to the CA3 impairs the encoding of novel environments as place fields (Wagatsuma *et al.*, 2018). The timing of this neuromodulatory input is also important: synthetically driving noradrenergic afferents to release NA into the hippocampus during sleep (when these inputs are typically quiescent) can disrupt memory consolidation and place field encoding (Swift *et al.*, 2018).

The discovery of place cells transformed the way neuroscientists considered hippocampal function: the fact that hippocampal neuronal activity was so strongly modulated by location suggested that its primary function is to encode space, rather than act as a storage component for declarative memory (Squire, 1992). However, the two theories are not necessarily opposed, given that spatial location is a principal component of declarative memory (Tulving, 1972; Leutgeb *et al.*, 2005; Buzsáki and Moser, 2013).

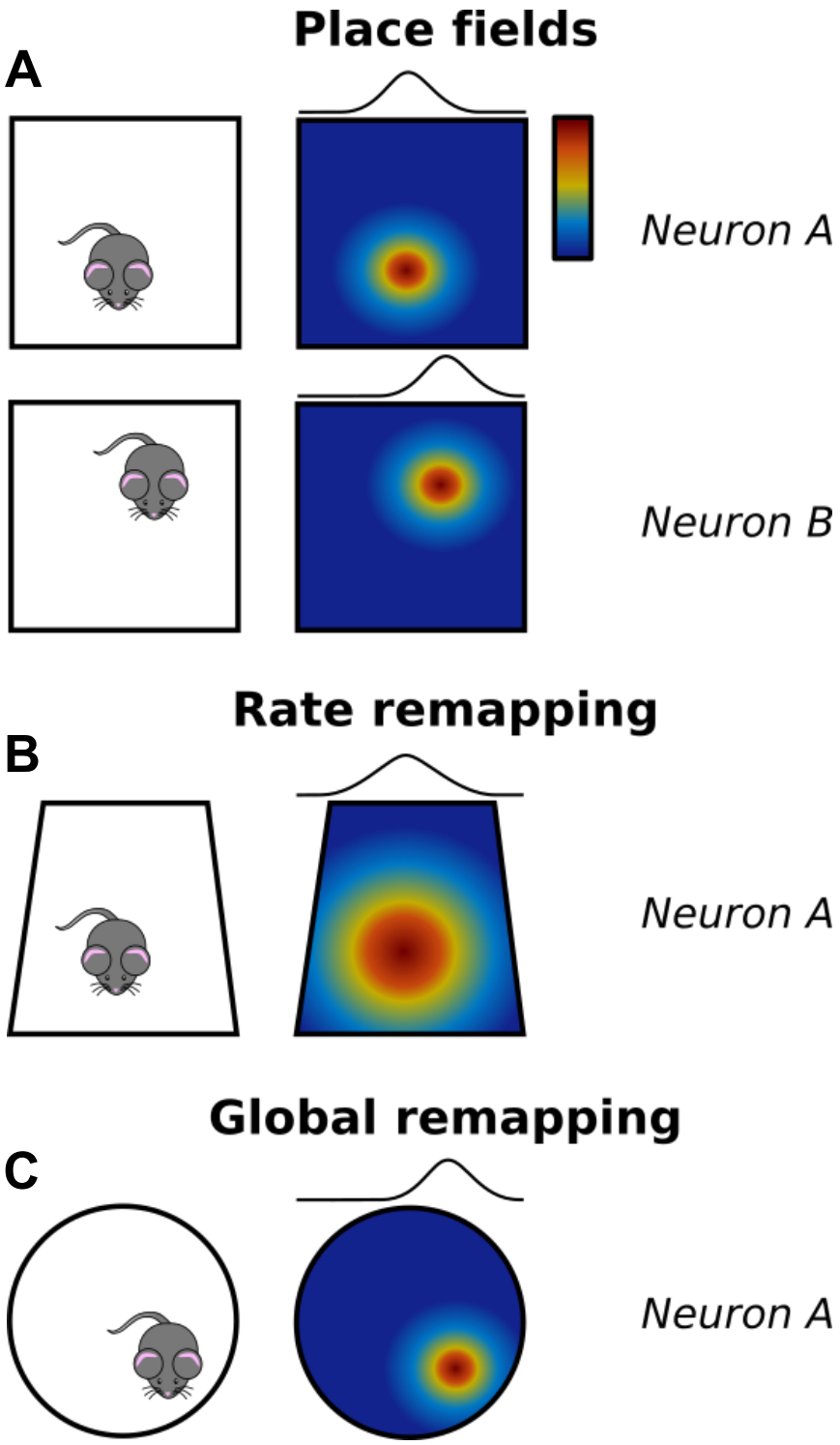

Figure 1.4: *Principles of space encoding by the hippocampus. A) Left: mouse location in arena, right: heat maps illustrating that neurons A and B have unique place fields that are preferentially activated when the mouse is in that location (colour and the Gaussian curve above illustrate the firing frequency in three and two dimensions, respectively). B) Slight changes to the environment induce rate remapping of place fields, where the location is unchanged, but the associated firing frequency is altered. C) If an animal is placed in a completely novel environment, the hippocampal place cells undergo global remapping, where the new place fields bear no resemblance to the previous ones.*

1.1.5 Hippocampal rhythms

The synchronous, rhythmic activity of neuronal populations within the hippocampus can summate, generating several large local field potentials (LFPs), which can be detected using standard electrophysiological apparatus. The dense and organised layering of neurons within the hippocampus facilitates the generation and detection of these LFPs, thus readily lending itself to the study of brain rhythms.

Three main types of brain rhythms occur in the hippocampus: theta (~4-12 Hz), sharp wave-ripple (SW-R) complexes (~110-250 Hz overlaid onto ~0.01-3 Hz sharp waves) and gamma (25-100 Hz), each observed in different behaviours and associated with distinct functional roles (for review, see Colgin, 2016). Crucial to rhythm generation is the presence of interneurons, distinct populations of which are able to inhibit collections of pyramidal neurons via their immense axonal ramifications (Cobb *et al.*, 1995). For instance, it has been estimated that a single chandelier interneuron is able to inhibit over 1,000 pyramidal neurons in the CA1 (Li *et al.*, 1992), and therefore the precise temporal control offered by these arborisations underscores co-ordinated population activity in the hippocampus.

1.1.5.1 Theta

Theta rhythms are involved in exploratory behaviour and the learning of new information, particularly spatial (Winson, 1978; Vertes, 2005). The medial septum (MS) plays a crucial role in hippocampal theta rhythmogenesis (Bland, 1986; Bland and Colom, 1989; Sweeney, Lamour and Bassant, 1992), with lesions producing deficits in the spatial memory of rats (Winson, 1978). In support of this, co-ordinated neuronal firing within the MS at the theta frequency is well-documented and correlates strongly with the theta rhythmicity observed in the hippocampus (Petsche and Stumpf, 1962; Apostol and Creutzfeldt, 1974; Bland, 1986; Stewart and Fox, 1990).

Hippocampal interneurons are rhythmically disinhibited by MS GABAergic afferents (Frotscher and Leranth, 1985; Wainer *et al.*, 1985; Freund and Antal, 1988; Sun *et al.*, 2014). Key to this theta rhythm pacemaker drive is the expression of hyperpolarisation-activated cyclic nucleotide-gated (HCN) and low-voltage activated T-type Ca^{2+} channels in MS interneurons (particularly parvalbumin-expressing (PV+) interneurons, *Talley et al.,* 1999; Varga *et al.,* 2008). HCN channels are strongly activated by hyperpolarisation and slightly open at rest (Robinson and Siegelbaum, 2003), allowing an inward depolarising current (*h*-current) that moves the neuron towards action potential threshold. These slowly become deactivated but the depolarisation towards threshold is facilitated by the T-type Ca^{2+} channels. Subsequent neuronal firing and repolarisation then reactivates HCN channels and the cycle begins again (Robinson and Siegelbaum, 2003; Gangadharan *et al.*, 2016). The effect of this rhythmic MS input on hippocampal

interneurons and, subsequently, pyramidal neurons is observed as the two populations of neurons firing approximately 180° out of phase with each other in *in vivo* electroencephalography (EEG) recordings (Buzsaki and Eidelberg, 1983; Klausberger *et al.*, 2003; Klausberger and Somogyi, 2008).

1.1.5.2 SW-R complexes

Larger in amplitude than theta rhythms, SW-Rs are involved in the replay and consolidation of information during awake and sleep states (Wilson and McNaughton, 1994; Nádasdy *et al.*, 1999; Davidson, Kloosterman and Wilson, 2009). In support of a memory consolidation function, hippocampal SW-Rs occur prior to neocortical spindles during sleep, suggesting a directionality of information flow during consolidation (Siapas and Wilson, 1998). However, Sirota *et al.* (2003) claim a reversal of this relationship, suggesting neocortical input influences this hippocampal replay.

Unlike theta rhythms, SW-Rs are generated internally within the hippocampus, and can be found in acute *ex vivo* hippocampal slices (Kubota *et al.*, 2003). Moreover, low CA3/CA1 ripple coherence suggests SW-Rs are generated locally within each hippocampal subfield (Ylinen *et al.*, 1995), and CA1 SW-Rs can occur even when SC connections from the CA3 are genetically suppressed (although they are smaller in amplitude, Nakashiba *et al.,* (2009). It is thought that a gradual build-up of excitatory activity drives reciprocally connected PV+ interneurons, which start ripple phase-locked spiking that is then relayed back to the CA3 pyramidal neurons. This temporal window allows alternate firing of basket cells and pyramidal cells (Schlingloff *et al.*, 2014).

1.1.6 DG-CA3: Inputs, outputs and functions

1.1.6.1 Inputs

In the rat, some 300,000 CA3 pyramidal neurons receive inputs both directly from the layer II entorhinal cortex via the perforant path (Hjorth-Simonsen and Jeune, 1972; Steward and Scoville, 1976; Boss *et al.*, 1987) and indirectly via mossy fibres originating from granule cells in the dentate gyrus (Blackstad *et al.*, 1970; Claiborne, Amaral and Cowan, 1986; Boss *et al.*, 1987; Amaral and Witter, 1989). The perforant path terminates in the molecular layer of the DG, where some 1,000,000 granule cells reside and from which mossy fibre axons originate (Blackstad *et al.*, 1970; Claiborne, Amaral and Cowan, 1986; Boss *et al.*, 1987; Amaral and Witter, 1989). Emerging from the apical dendrites of CA3 pyramidal cells are thorny excrescences which are enveloped by large MF axonal boutons (3-10 μm in diameter, Acsady *et al.,* 1998). A single CA3 pyramidal neuron receives ~50 MF inputs, resulting in a sparse connectivity estimated at ~0.005% (Claiborne, Amaral and Cowan, 1986; Amaral, Ishizuka and Claiborne, 1990; Rolls, 2013; Evstratova and Toth, 2014). Despite this apparent convergence of MF inputs onto CA3

neurons, it has been estimated that a single CA3 neuron only receives input from one MF granule cell at any given time (Barnes *et al.*, 1990; Lisman, 1999).

In addition to indirect cortical inputs via the DG, CA3 neurons receive recurrent collateral axons projections from neighbouring CA3 neurons (A/C fibres, Schaffer, 1892; Ramón y Cajal, 1899; MacVicar and Dudek, 1979; Traub, Miles and Wong, 1989; Ishizuka, Cowan and Amaral, 1995). This "auto-associative" circuitry is one of the fundamental underpinnings in the CA3's proposed role in memory formation (Lorente de Nó, 1949; Hebb, 1949; Rolls, 2013), with a recall cue provided by direct perforant path inputs (Treves and Rolls, 1992; Rolls, 2013). The recurrent A/C fibres are the most numerous of the inputs to the CA3 (12,000 per cell, compared to 4,000 and 50 for perforant path and mossy fibres, respectively (Amaral, Ishizuka and Claiborne, 1990).

Mossy fibres also contain multiple boutons along their shaft, from which 2-4 tiny filopodial extensions emerge to innervate the dendrites of CA3 inhibitory interneurons (Acsady *et al.*, 1998). The immense web of excitatory interconnectivity would render the CA3 area in a state of runaway hyperexcitability were it not for the mossy fibres' concurrent engagement of GABAergic interneurons (both feed-forward and feed-back) to bring about powerful inhibition (Kandel and Spencer, 1961; Miles, 1990; Acsady *et al.*, 1998; Torborg *et al.*, 2010). Such inhibition may also be supported through potential interneuron recruitment by the CA2 area (Boehringer *et al.*, 2017). Like in CA1, this feed-forward inhibition is much stronger at the pyramidal cell soma than in the dendrites, but unlike in CA1 – where interneurons regulate spike fidelity by dictating a tight temporal window for action potential initiation (Pouille and Scanziani, 2001) – feed-forward inhibition serves to stabilise cell excitability by preventing plateau potentials, action potential bursts and epileptiform activity (Torborg *et al.*, 2010).

1.1.6.2 Outputs

CA3 pyramidal neurons project to two main outputs nodes: neighbouring CA3 pyramidal neurons (via recurrent A/C axons) and the CA1 subfield (via SC axons, Amaral and Witter 1989). The SC axons target CA1 pyramidal neurons and also engage feed-forward inhibition through the recruitment of GABAergic interneurons (Amaral and Witter, 1989; Kwon *et al.*, 2018). Interestingly, one study has shown that SC axonal terminals form areas of concentrated innervation alternating with less densely innervated areas, with an interpeak distance of ~500 μm (Li *et al.*, 1994). Such an observation has not been shown since (and may have been due to incomplete axonal filling), but this focal targeting could play a role in the associative plasticity observed at CA1 synapses (Barrionuevo and Brown, 1983).

CA3 neurons also back-project to the DG region (Li *et al.*, 1994), innervating feed-back inhibition onto the DG. These connections are more apparent in the ventral hippocampus and are thought to prevent seizure-like activity (Scharfman, 2007).

1.1.6.3 Functions: pattern separation, pattern completion and CA1 place field tuning

Three key anatomical features of the DG-CA3 network (lateral inhibition within the DG, sparse MF inputs to CA3 and strong recurrent connectivity within CA3) are thought to imbue the network with the ability to create rapid, single-trial associations between a spatial location and an object or reward (Leutgeb *et al.*, 2007; Rolls, 2013). Episodic memory requires an individual to distinguish different events (i.e. eating a meal in a specific restaurant on a particular day) from one another, and the spatial context of such events is a principal component of this type of memory (Dere *et al.*, 2008; Rolls, 2013; Takeuchi *et al.*, 2016), which may explain its reliance on the hippocampus. The formation of discrete memory representations is accomplished by the DG-CA3 network through a process known as pattern separation, and the recall of this memory occurs through pattern completion (McNaughton and Morris, 1987; Wills *et al.*, 2005; Leutgeb and Leutgeb, 2007; Rolls, 2013). These processes are outlined in Figure 1.5.

Only a subset of DG granule cells are efficiently activated by PP inputs as a result of the powerful lateral inhibition mediated by PV+ interneurons (Espinoza *et al.*, 2018). These interneurons suppress neighbouring granule cells within the DG, ensuring conversion of overlapping cortical synaptic input patterns to non-overlapping ones in the DG and downstream CA3 through a "winner-takes-all" mechanism (Kaski and Kohonen, 1994). There is some discrepancy as to whether DG granule cells exhibit place-related firing: Jung and McNaughton (1993 and Leutgeb *et al.* (2007) showed spatial selectivity and firing rate changes in the place fields of DG neurons when an environment was incrementally altered, suggesting individual environments can indeed be represented by a unique rate pattern in a small number of granule cells. However, Senzai and Buzsaki (2017) recently argued that previous observations regarding place fields in the DG were actually mediated by mossy cells rather than granule cells. Regardless of which DG neurons are spatially-selective, the cortical input to the hippocampus is separated in the DG and is further decorrelated by the aforementioned sparse mossy fibre inputs to CA3.

The ability to recall a memory from partial or corrupted cues is known as pattern completion and relies heavily on recurrently connected auto-associative networks such as that found in the CA3 (Wills *et al.*, 2005; Kesner, 2007; Rolls, 2013). MF inputs to CA3 are relatively weak due to the low release probability (P_r) of the terminals (von Kitzing, Jonas and Sakmann, 1994), therefore the average granule cell firing frequencies measured *in vivo* (0.01–0.1 Hz, Jung and McNaughton 1993) rarely drive CA3 spiking. However, granule cell firing can increase up to ~30 Hz during place cell activity (Henze,

Wittner and Buzsáki, 2002; Gundlfinger *et al.*, 2010), and replaying *in vivo* recorded DG firing patterns into MF-CA3 synapses in *ex vivo* slices reveals immense short-term facilitation of CA3 EPSCs during high-frequency bursts (Henze, Wittner and Buzsáki, 2002; Gundlfinger *et al.*, 2010). It has therefore been postulated that this bi-phasic firing distribution allows the DG input to act as a switch or "detonator synapse" (Henze, Wittner and Buzsáki, 2002; Vyleta, Borges-Merjane and Jonas, 2016), with high frequency bursts causing post-tetanic potentiation, raising the MF terminal release probability and dramatically increasing the reliability of DG-CA3 information transfer (Vyleta, Borges-Merjane and Jonas, 2016). The functional relevance of this becomes clear when one considers that a DG granule cell contacts around 15 CA3 pyramidal cells (Ishizuka, Weber and Amaral, 1990), meaning the post-tetanic potentiation elicited upon "detonation" in a place field would enable the recruitment of an ensemble of these CA3 pyramidal neurons with as little as a single action potential (Vyleta, Borges-Merjane and Jonas, 2016).

The functional connectivity of recurrent CA3-CA3 synapses is stronger than MF-CA3 synapses, and long-term plasticity at the recurrent synapses is thought to bind these neurons together to form ensembles (Zalutsky and Nicoll, 1990; Guzman *et al.*, 2016), and couple this with weaker PP inputs arising from the same populations of cells in the entorhinal cortex also associated with the memory engram (Witter *et al.*, 1989; Treves and Rolls, 1992; Tamamaki and Nojyo, 1993; McMahon and Barrionuevo, 2002). Computational theories of hippocampal function postulate that direct perforant path inputs to the CA3 provides a recall cue, as these inputs are too weak to elicit reliable driving of CA3 neurons required for the initial encoding (Treves and Rolls, 1992). Figure 1.5 illustrates these concepts of pattern separation and pattern completion. Remarkably, the temporal order of pre- and post-synaptic firing is irrelevant in CA3-CA3 long-term plasticity, with symmetrical spike-timing-dependent plasticity (STDP) rules presumably present to allow reliable information storage (Mishra *et al.*, 2016, discussed further in 1.2.1.2.1). Despite such agnostic STDP rules, a crucial component for long-term potentiation of CA3-CA3 synapses is the presence of NMDARs (Zalutsky and Nicoll, 1990; McMahon and Barrionuevo, 2002), with selective CA3 knock-out of NMDARs deteriorating CA1 place fields and impairing pattern completion in the Morris Water Maze (Nakazawa *et al.*, 2002, 2003; McHugh and Tonegawa, 2009).

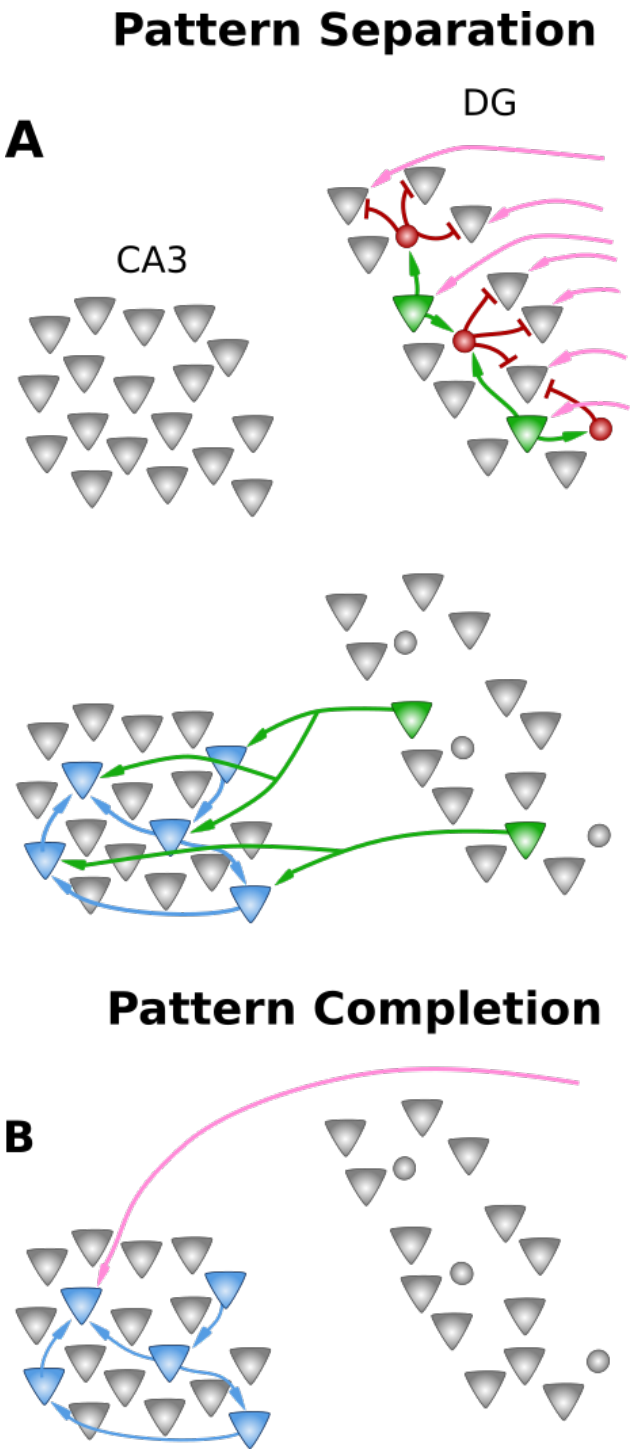

Figure 1.5: *Principles of pattern separation and completion. A) Pattern separation: Top: Incoming cortical firing patterns along the PP (pink) activate DG granule cells (green) which in turn activate local interneurons (red) to bring about lateral inhibition, suppressing neighbouring granule cells until only a subset remains active. Bottom: The MF axons of these granule cells then innervate a sparse subset of CA3 pyramidal neurons (blue), and the associated long-term potentiation that occurs strengthens the connections within these ensembles. B) Pattern completion: a recall cue from the PP, which holds only a subset of the initial cortical information, then activates one of the CA3 pyramidal neurons in the ensembles, but the potentiated synapses allow reactivation of the entire ensemble.*

In addition to its role in memory storage and recall, an additional function of the CA3 recurrent network is the tuning of CA1 place fields (Nakazawa *et al.*, 2004). The direct cortical inputs to CA1 via the TA pathway dominate during exposure to a novel context, carrying general spatial information (due to broadly-tuned place fields in the entorhinal cortex, Quirk *et al.*, 1992). These are rapidly (< 1 hour) overruled by CA3 inputs which bestow more finely tuned place information to the CA1 pyramidal neurons. However genetic ablation of CA3 NMDARs prevent this rapid overriding, with NR1-KO mice taking over a day to sharpen their CA1 place fields (Nakazawa *et al.*, 2003). Given that the CA1 place fields do sharpen eventually, the CA3 is therefore not critical for this refinement, but such a rapid effect supports its role in one-trial learning.

1.1.7 SC-CA1: Inputs, outputs and functions

1.1.7.1 Inputs

The broad anatomy of the hippocampal CA1 area has been well-characterised: pyramidal neurons receive cortical information via two glutamatergic inputs: directly via the TA pathway (TA-CA1, Steward and Scoville., 1976) and indirectly via the tri-synaptic loop, where the final relay is the SC axons of CA3 neurons (SC-CA1, Amaral and Witter, 1989). Like many cortical areas, the CA1 contains distinct populations of excitatory and inhibitory neurons, giving rise to intricate circuit connections and spatiotemporal rules underpinning complex information processing (Silberberg *et al.*, 2005; Klausberger and Somogyi, 2008).

Intriguingly, distal CA1 pyramidal neurons (i.e. those located near the subicular border) receive inputs from CA3 neurons closest to the DG, and proximal CA1 neurons (i.e. those near the CA2) receive projections from CA3 neurons farthest from the DG (shown anatomically by Ishizuka, Weber and Amaral., 1990 and Li *et al.*, 1994, and functionally using glutamate uncaging by Brivanlou *et al.*, 2004). The SC projections are not limited to the originating CA3 neurons' dorsoventral depth (the "lamellae" or transverse plane). Capable of traversing distances of between 100 and 400 μm across the hippocampal longitudinal axis, a single CA3 axon is estimated to innervate between 30,000 and 60,000 CA1 neurons (Li *et al.*, 1994).

A given CA1 pyramidal neuron receives approximately 30,000 synaptic inputs (Megias *et al.*, 2001), and – as seen in the CA3 – the locations and timings of these inputs provide a framework for their integration (Pouille and Scanziani, 2001; Klausberger and Somogyi, 2008). Glutamatergic inputs are concentrated at proximal and distal dendrites in the *stratum radiatum* (Megias *et al.*, 2001; Kajiwara *et al.*, 2008), whereas GABAergic inputs from a variety of interneuron classes innervate distal and proximal dendrites, the axon initial segment and pyramidal cell soma (Megias *et al.*, 2001; Pouille and Scanziani, 2001, 2004; Klausberger *et al.*, 2003, 2004; Klausberger and Somogyi, 2008; Milstein

et al., 2015). The upstream and concomitant positioning of these inhibitory inputs relative to glutamatergic synapses permits precise spike timing and diverse modulation of the glutamatergic signals received in the distal dendrites (Pouille and Scanziani, 2001; Klausberger and Somogyi, 2008; Milstein *et al.,* 2015). Trans-synaptic labelling of CA1 inputs suggests local ipsilateral inhibition is much stronger than long-range inhibition from the contralateral hippocampus (Sun *et al.*, 2014).

In addition to spatial modulation, temporal modulation of CA1 pyramidal neurons can occur due to distinct interneuron types firing at different phases of the hippocampal theta and SW-R oscillations associated with different behavioural states (Klausberger *et al.*, 2003, 2004; Klausberger and Somogyi, 2008; Royer *et al.*, 2012). For instance, bistratified interneurons – which target dendrites receiving SC inputs – fire in time with the CA1 pyramidal neurons during the trough phase of the theta cycle, and this concurrent hyperpolarisation is thought to facilitate the output of CA1 neurons receiving strong excitatory inputs through the de-inactivation of low voltage-activated Ca^{2+} channels (Magee and Johnston, 1995; Magee *et al.*, 1995; Klausberger *et al.*, 2004). This dendritic GABAergic input is important in place field firing as it increases the contrast between neurons in different activation states: facilitating the output of those receiving strong excitatory inputs as an animal enters the place field by de-inactivating voltage-gated ion channels, while the rhythmic hyperpolarisation reduces dendritic excitability and attenuates the spiking probability of pyramidal neurons lacking this coincident excitatory input (Klausberger *et al.*, 2004).

The concept of distinct interneuron classes acting as filters of specific information pathways was also shown by Royer *et al.*, (2012). In this study, optogenetic silencing of dendritically-targeting somatostatin-expressing (SST+) interneurons, but not somatically-targeting PV+ interneurons, dramatically enhanced bursting in CA1 pyramidal neurons. Action potentials arriving in bursts are more reliably relayed to the post-synaptic neuron and are more capable of inducing long-lasting synaptic strengthening (Huerta and Lisman, 1995; Lisman, 1997). Therefore, selective filtering by SST+ interneurons plays a vital role in promoting synaptic plasticity of specific neuronal pathways (Royer *et al.*, 2012).

1.1.7.2 Outputs

The subiculum and the pre-frontal cortex (PFC) are the major output nodes of the CA1 (Cenquizca and Swanson, 2007). The subiculum – in contrast to the strong lateral inhibition present in the DG – appears to be more loosely inhibited and predominantly "bursty" in nature (Taube, 1993; Behr and Heinemann, 1996; Panuccio, Vicini and Avoli, 2012), suggesting that its function is to amplify CA1 outputs on their way to the cortex (O'Mara *et al.,* 2001). Consistent with the hippocampus' role in integrating multiple

sensory modalities, additional outputs from the hippocampus include those to the visual, auditory, somatosensory, gustatory and olfactory areas (Van Groen and Wyss, 1990; Cenquizca and Swanson, 2007). Reciprocal connections with the amygdala are also well-documented (Canteras, Simerly and Swanson, 1992; McDonald, 1998; Pikkarainen *et al.*, 1999; Pitkänen *et al.*, 2000) and underlie the crucial role of the hippocampus in contextual fear memory (Anagnostaras, Gale and Fanselow, 2001; Cenquizca and Swanson, 2007).

1.1.7.3 Functions: comparator and decoder

With a predominant role in spatial and episodic memory, the hippocampus integrates multiple modalities to support spatial (e.g. object recognition and goal-directed navigation), temporal associative (e.g. auditory trace fear), or contextual (e.g. contextual fear) learning (Morris *et al.*, 1982; McEchron *et al.*, 1998; Gewirtz, McNish and Davis, 2000; Clark, Goldberg and Rudy, 2009; Barker and Warburton, 2011; Eichenbaum, 2017). Each of these forms of learning are associated with distinct encoding, retrieval, and consolidation mechanisms both within the hippocampus and wider cortex (Preston and Eichenbaum, 2013). As previously outlined, early theories of the hippocampus' role in memory focused on the CA3 recurrent network and its role in the formation and retrieval of memory ensembles (Wills *et al.*, 2005; Kesner, 2007; Rolls, 2013).

Unlike the highly recurrently connected CA3 network, the neuroanatomy of CA1 does not lend itself to obvious roles in memory formation and recall. However, given that the CA1 pyramidal neurons receive inputs from both grid cells of the entorhinal cortex (via the TA pathway) and place cells located in the CA3 (via the SC pathway), it has been postulated that the major role of the CA1 is to act as a comparator of these two signals to enable novelty detection (Lisman, 1999; Takahashi and Magee, 2009). Anatomical research has suggested these inputs terminate onto distinct CA1 compartments, with distal dendrites in the SLM receiving predominantly TA inputs, whereas more proximal apical dendrites in the *stratum radiatum* are more strongly innervated by CA3 SC axons (Kajiwara *et al.*, 2008). Where inputs from the TA alone have very little post-synaptic effect, signals arriving along the two pathways within 150 ms of each other enables dendritic Ca^{2+}-dependent plateau potentials, a subsequent somatic after-depolarisation and a switching of the CA1 neuron from a single spiking to a burst/complex firing mode (Magee and Carruth, 1999; Takahashi and Magee, 2009, summarised in Figure 1.6). Using voltage-sensitive dyes and pharmacological interventions, Ang, Carlson and Coulter (2005) attributed this "AND" operation at CA1 dendrites to spatial segregation of TA EPSPs by local feed-forward inhibition (also shown by Milstein *et al.* 2015), intrinsic CA1 I_h currents and a co-requirement of NMDAR activation by SC inputs. This non-linear change in CA1 output is therefore the result of comparing the sensory input from the entorhinal cortex to the stored representation in the CA3, with CA1 bursting

indicating a high similarity between the two input streams (Ang, Carlson and Coulter, 2005; Takahashi and Magee, 2009; Milstein *et al.*, 2015). These plateau potentials do not propagate far down the CA1 axons and are attenuated by K^+ channels to prevent distal axon Na^+ channels from inactivation. This "decoding" restores action potentials within complex spikes to full amplitude, enabling accurate voltage-gated Ca^{2+} channel-mediated neurotransmitter release at the terminal boutons and high fidelity post-synaptic signal relay from the CA1 (Apostolides *et al.*, 2016).

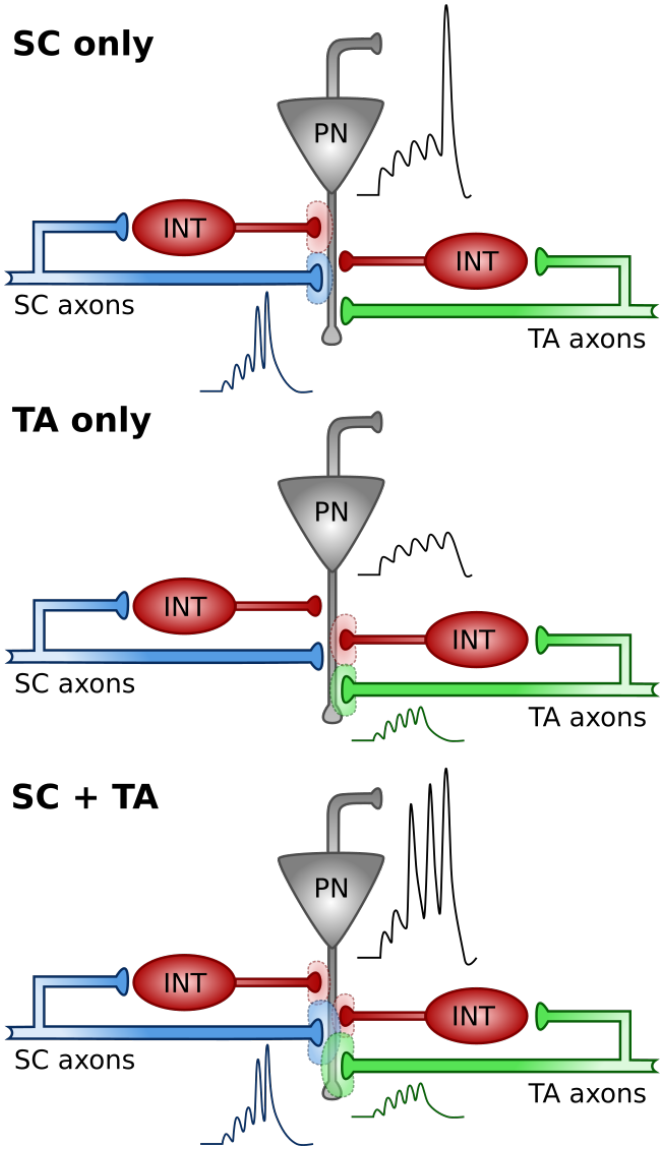

Figure 1.6: *Input comparison in the CA1. Top: SC input alone evokes EPSPs and small dendritic spikes that typically fail to propagate to the soma due to upstream inhibition. Middle: the somatic effects of TA input alone are even weaker due to the increased dendritic distance in combination with upstream inhibition. Bottom: Coincident SC and TA inputs are able to sum supralinearly and can propagate efficiently to the soma to induce action potentials. In addition to coincident excitatory input to the CA1, higher frequency firing of SC and TA axons onto feed-forward neuropeptide Y interneurons cause a depression of these inhibitory inputs to CA1, also allowing SC and TA pathway integration.*

If the roles of the CA3 and DG are primarily to separate out cortical representations into sparse neuronal assemblies and package them together into ensembles for later recall, such representations are now effectively in a format that is not understood by the cortex (Lisman, 1999). CA1 neurons receive information in the form of neuronal firing patterns from the CA3, and so another proposed role of the CA1 is to decode the information derived from these hippocampal CA3 computations back to a representation understood by the cortex (McClelland and Goddard, 1996; Lisman, 1999). An underlying

assumption of the CA1's putative decoder role is that the hippocampus and the cortex use distinct representations (i.e. firing patterns and/or number of cells) for the same information (Lisman, 1999). The changes in representation that are carried out in the DG and CA3 are important in condensing information such that fewer neurons encode any given memory, a concept known as "orthogonalisation", to reduce error rate during recall (McNaughton and Morris, 1987). These hippocampal "memories" are not complete copies but condensed descriptions, a concept based on the fact that the hippocampus is much smaller than the neocortical areas that project to it (McClelland and Goddard, 1996). Anatomical and functional evidence exists to further support the idea of the CA1 as a decoder.

Anatomically, distinct subregions of entorhinal cortex, which presumably carry different types of information, converge on individual granule cells (Johnston and Amaral, 1998), before separation within the hippocampus and re-convergence in the entorhinal cortex (Amaral and Witter, 1989). Functionally, individual CA1 and CA3 neurons in the hippocampus represent space with a Gaussian firing frequency that selectively and uniquely peaks when the animal is in a particular space in a given environment (a "place field" of a place cell), whereas individual DG granule cells can encode several place fields (Leutgeb *et al.*, 2007) and individual entorhinal cortex grid cells instead represent space with multiple, periodic spatial firing fields that form a triangular lattice (Moser, Rowland and Moser, 2015). As spatial information flows from the EC to the DG to the CA3, the representation of space becomes more refined and less "cortex-like". These differences in how individual neurons code space (single spot high resolution in the hippocampus vs. multiple spot lower resolution in the entorhinal cortex) are also shown by the sparsity of activity patterns (~ 2.5% in CA1 and CA3 vs. the less sparse 7% observed in the entorhinal cortex (Barnes *et al.*, 1990; McClelland and Goddard, 1996). McClelland and Goddard, (1996) suggest that the increased sparsity and specificity of the hippocampal representations arises from the pattern separation process in DG and CA3. In support of the CA1 acting as a decoder between the CA3 and cortex, the sparse and selective signals in CA1 become less sparse (i.e. less hippocampal-like) but remain spatially consistent in the subiculum (O'Mara *et al.*, 2009). Such an effect is suggestive of a convergence of a number of CA1 place cells within the subiculum (McClelland and Goddard, 1996). In support of this, the diverged entorhinal efferents (the TA pathway, lateral and medial perforant pathways) projecting to the DG, CA3 and CA1 areas appear to re-converge in CA1, since the entorhinal cortex receives inputs from the CA1 and not CA3 (Amaral and Witter, 1989).

1.1.8 Hippocampal outflow

The integrative pre-processing in the hippocampus (pattern separation in the DG-CA3, novelty or error detection in the CA1 and pattern completion in the CA3 auto-associative

network) forms the first component of the two part "standard model" of memory. Following this initial short-term encoding, the output from the subiculum then allows long-term encoding in the neocortex (Nadel and Moscovitsh, 1997). It has long been appreciated that direct and indirect reciprocal connections between the hippocampus and the medial pre-frontal cortex (mPFC) exist, allowing them to influence one another (Jay, Glowinski and Thierry, 1989; Jay and Witter, 1991; Hoover and Vertes, 2007; Rajasethupathy *et al.*, 2015). This can be measured as correlated electrical activity between the two areas, particularly in the theta rhythm (Siapas and Wilson, 1998; Jones and Wilson, 2005). The nucleus reunions also exhibits reciprocal connections to both structures (Cassel *et al.*, 2013), resulting in a complex, yet continuous, back-and-forth between the two regions during memory encoding, working memory tasks and memory retrieval (Preston and Eichenbaum, 2013; Sigurdsson and Duvarci, 2016).

1.2 Plasticity and modulation of neuronal communication

1.2.1 Synaptic plasticity

Synaptic connectivity – a crucial component in shaping neural dynamics and the resulting computational functions – is relentlessly diverse and extraordinarily complex. Such an existence is underscored by the multiple types of connectivity between specialised groups of neurons (Druckmann *et al.*, 2014; Jiang *et al.*, 2015; Mo *et al.*, 2015; Kwon *et al.*, 2018), and it is well-known that the balance of excitation and inhibition within these neural circuits is exquisitely tuned (Pouille and Scanziani, 2001; Torborg *et al.*, 2010; Bartley and Dobrunz, 2015). This balance can be modulated pre-synaptically through alterations in Ca^{2+} sensing machinery and neurotransmitter release probability (Zucker, 1972; Zucker and Regehr, 2002; Abbott and Regehr, 2004; Jackman *et al.*, 2016) and/or post-synaptically via changes in receptor expression, channel conductance and neuronal intrinsic excitability (Derkach, Barria and Soderling, 1999; Andrasfalvy and Magee, 2004; Liu *et al.*, 2017). These mechanisms can cause short- or long-term alterations and occur in response to changes in selective local inputs, as well as broader rhythmic activity within the network (Markram et al., 1997; Sadowski et al., 2016). The excitatory/inhibitory (E/I) balance is especially vital during early post-natal brain development (Dorrn *et al.*, 2010; Sun *et al.*, 2010), and perturbations can underlie a range of neurological conditions such as epilepsy (Bradford, 1995), Alzheimer's disease (Vico Varela, Etter and Williams, 2019), schizophrenia (Selten, Bokhoven and Kasri, 2018) and autism (Rubenstein and Merzenich, 2003).

Efficient inter-neuronal communication is therefore paramount for healthy brain functioning, however it is the aforementioned plasticity of these neural circuits that gives rise to the immense computational capacity of the brain and higher order functions involved in behavioural modifiability such as learning, memory and cognition (Hebb, 1949; Stevens, 1998; Martin, Grimwood and Morris, 2000; Citri and Malenka, 2008;

Berlucchi and Buchtel, 2009). Neuronal plasticity refers to the flexibility in synaptic strength between neurons in a network, and has its early origins with Ramon y Cajal, who suggested that learning new memories requires new connections to form between neurons (Ramón y Cajal, 1894; Cowan and Kandel, 2001). However, it was the Italian neuropsychiatrist Eugenio Tanzi who proposed that repeated activity along a neuronal path during learning could cause a hypertrophy of associated neurons along that path, thus reducing the interneuronal resistance and making the crossing of electrical impulses easier (Tanzi, 1893). Fellow Italian psychiatrist, Ernesto Lugaro (1898, 1906, 1909), expanded on Tanzi's hypothesis by applying the term "plasticity" to these activity-related synaptic changes, and furthered the idea with his insight into the chemical nature of synaptic transmission. In 1949, Donald Hebb proposed that the repeated firing of cells that were synaptically connected would strengthen the connections between them (Hebb, 1949). This concept in itself was not necessarily novel given the earlier notions by late 19th and early 20th century neuroscientists, but as part of his postulate Hebb described an "irregular arrangement of cells" bound by a lattice-work of strengthened associations across physically modifiable synapses (Cooper, 2005). Thus, the concept of a neuronal assembly – or "ensemble" – with activity-dependent connectivity, was born. A later revision of this hypothesis by Milner (1957) included inhibitory interneurons within the formation of an ensemble. Synaptic plasticity is evident at many synapses throughout the brain (Citri and Malenka, 2008), and the full scope of induction mechanisms and expression is beyond the scope of this thesis. Therefore, this section will predominantly focus on synaptic plasticity research in the hippocampus.

Synaptic plasticity is bi-directional and can arise from pre- and post-synaptic modulation of the mechanisms involved in neurotransmission. Changes to the readily-releasable pool (RRP) of neurotransmitter vesicles (Debanne *et al.*, 1996), voltage-gated Ca^{2+} entry (Castillo, Weisskopf and Nicoll, 1994; Nanou *et al.,* 2016a, 2016b, 2016c), and the Ca^{2+} sensing and exocytotic machinery (Jackman *et al.*, 2016; Turecek and Regehr, 2018) ultimately modulate the release of pre-synaptic neurotransmitter vesicles (Zalutsky and Nicoll, 1990; Schmitz, Mellor and Nicoll, 2001). These effects may be due to repeated activity of the terminal (Jackman *et al.*, 2016) or as a result of retrograde inhibition (i.e. via adenosine receptors, Gundlfinger *et al.*, 2007, or endocannabinoid signalling, Wilson and Nicoll, 2001). In addition, post-synaptic changes in neuronal excitability (Moyer, Thompson and Disterhoft, 1996; Desai, Rutherford and Turrigiano, 1999), receptor expression and AMPAR conductance (Isaac, Nicoll and Malenka, 1995; Katsuki, Izumi and Zorumski, 1997; Benke *et al.*, 1998; Hu *et al.*, 2007), NMDAR activation and the subsequent Ca^{2+}-mediated intracellular signalling cascades (Lisman, Schulman and Cline, 2002) affect how the receiving neuron processes incoming signals. Recruitment of silent synapses may also be involved (Isaac, Nicoll and Malenka, 1995; Reid *et al.*,

2004). The role of glial cells is also important, as a reduction in glia-mediated glutamate re-uptake can result in extra-synaptic spill-over and the activation of NR2B subunit-containing NMDARS that induce long-term depression (LTD) as opposed to long-term potentiation (LTP) (Diamond, 2001; Katagiri, Tanaka and Manabe, 2001; Scimemi, Tian and Diamond, 2009).

As well as the diversity in the locus and mechanisms underscoring synaptic plasticity, there is also a continuum in the time course of such plasticity (Bliss and Lomo, 1973; Zucker and Regehr, 2002; Daoudal and Debanne, 2003; Hiratani and Fukai, 2014a; Monday, Younts and Castillo, 2018). Short-term plasticity typically occurs on the time-scale of tens of milliseconds to several minutes (Zucker and Regehr, 2002), whereas long-term plasticity can persist from hours to days, and even months (Abraham, 2003). The fact that this plasticity exists on a range of time scales adds to the appeal that the adaptable synaptic connections between neurons are a biological correlate of memory. The various types of plasticity – broadly classified here into short-term facilitation, short-term depression, long-term potentiation (LTP) and long-term depression (LTD) – also appear to underlie a plethora of computational functions (Abbott and Regehr, 2004).

1.2.1.1 Short-term plasticity

Short-term plasticity underpins the rapid temporal processing of synaptic inputs (Zucker and Regehr, 2002). In the most basic of terms, if the n^{th} synaptic response/1^{st} synaptic response is >1 then the synapse is characterised as facilitating, whereas if this ratio is <1 then it is depressing (Regehr, 2012). The heterogenous induction and decay rates across cortical systems suggest that the short-term plasticity expressed in each region has been adapted to fit specific temporal requirements throughout the brain (Fisher, Fischer and Carew, 1997). The main function of short-term plasticity is to impose high-, low- or band-pass filtering at a synapse and ensure reliable transmission of relevant information (Lisman, 1997; Goldman, Maldonado and Abbott, 2002; Abbott and Regehr, 2004). For instance, thalamocortical neurons mediate adaptation to repeated stimuli, observed when sensory inputs undergo rapid short-term depression, causing higher order cortical neurons to stop responding (Chung, Li and Nelson, 2002). Within CA1 pyramidal neurons of the hippocampus, there are marked differences in the short-term plasticity properties of dendrites targeted by distinct interneuron populations (Pouille and Scanziani, 2004). These synapses are therefore able to re-route feed-back inhibition across a burst of CA1 action potentials. Specifically, somatically-targeting interneurons are recruited by depressing CA1 synapses early in the stimulus train, whereas dendritically-targeting interneurons are activated by facilitating CA1 synapses later in the train. The recruitment of dendritically-targeted inhibition is more prominent at higher frequencies (Pouille and Scanziani, 2004) and is thought to segregate CA3 inputs

from TA inputs occurring at the distal dendrites (Ang, Carlson and Coulter, 2005), thus allowing the CA1 to function more efficiently as a decoding relay between the CA3 and the cortex (Lisman, 1999).

Short-term plasticity also allows a switch in the E/I balance within neuronal micro-circuits containing feed-forward inhibition. In the CA3, DG granule cells project axons with large mossy fibre boutons onto CA3 pyramidal neurons, which also recruit feed-forward inhibition through small filopodia extending onto interneurons (Acsady *et al.*, 1998). The excitatory MF inputs onto CA3 pyramidal neurons comprise multiple release sites with low release probability (Chicurel and Harris, 1992; Rollenhagen *et al.*, 2007), allowing dramatic facilitation (Mori *et al.*, 2004; Torborg *et al.*, 2010). Conversely, synapses onto interneurons are less facilitating, and can even depress rapidly at high frequencies (Salin *et al.*, 1996; Toth *et al.*, 2000). Therefore, DG granule cell firing at low frequencies prioritises inhibition, whereas higher frequencies are able to efficiently recruit CA3 pyramidal neurons. Taken together, the functional features of these dynamic synapses explain the high-frequency burst firing in CA3 pyramidal neurons when an animal enters a place field (Leutgeb *et al.*, 2007).

Mechanistically, short-term facilitation is reliant on a low initial release probability (P_r) and Ca^{2+} build-up over repetitive stimuli (Regehr, 2012). Transient pre-synaptic activity causes a local, large influx of Ca^{2+} into axonal terminals through VGCCs (Ca_{Local}) which binds rapidly to the low affinity Ca^{2+} sensor synaptotagmin 1 (Syt1). Syt1 then triggers membrane fusion and endocytosis of neurotransmitter-containing vesicles from the readily-releasable pool (RRP). If pre-synaptic activity is sustained, Ca^{2+} equilibrates throughout the pre-synaptic terminal (Ca_{Res}). At a range of facilitating synapses, the enhanced Ca^{2+} influx upon repetitive stimulation binds to the pre-synaptically located Syt7 Ca^{2+} sensor and augments the release probability of the terminal (Sugita *et al.*, 2001; Jackman *et al.*, 2016), potentially through an interaction with Syt1 (Jackman and Regehr, 2017). Crucially, Syt7 possesses slow kinetics but a high affinity for Ca^{2+}, allowing it to produce synaptic facilitation only upon the Ca_{Res} build-up over repetitive stimuli. Where short-term facilitation occurs due to a low initial P_r and a steady recruitment of vesicles, short-term depression occurs due to a high initial P_r and a subsequent depletion of vesicles over repetitive stimuli (Zucker and Regehr, 2002; Regehr, 2012). Figures 1.7 and 1.8 illustrate these two processes.

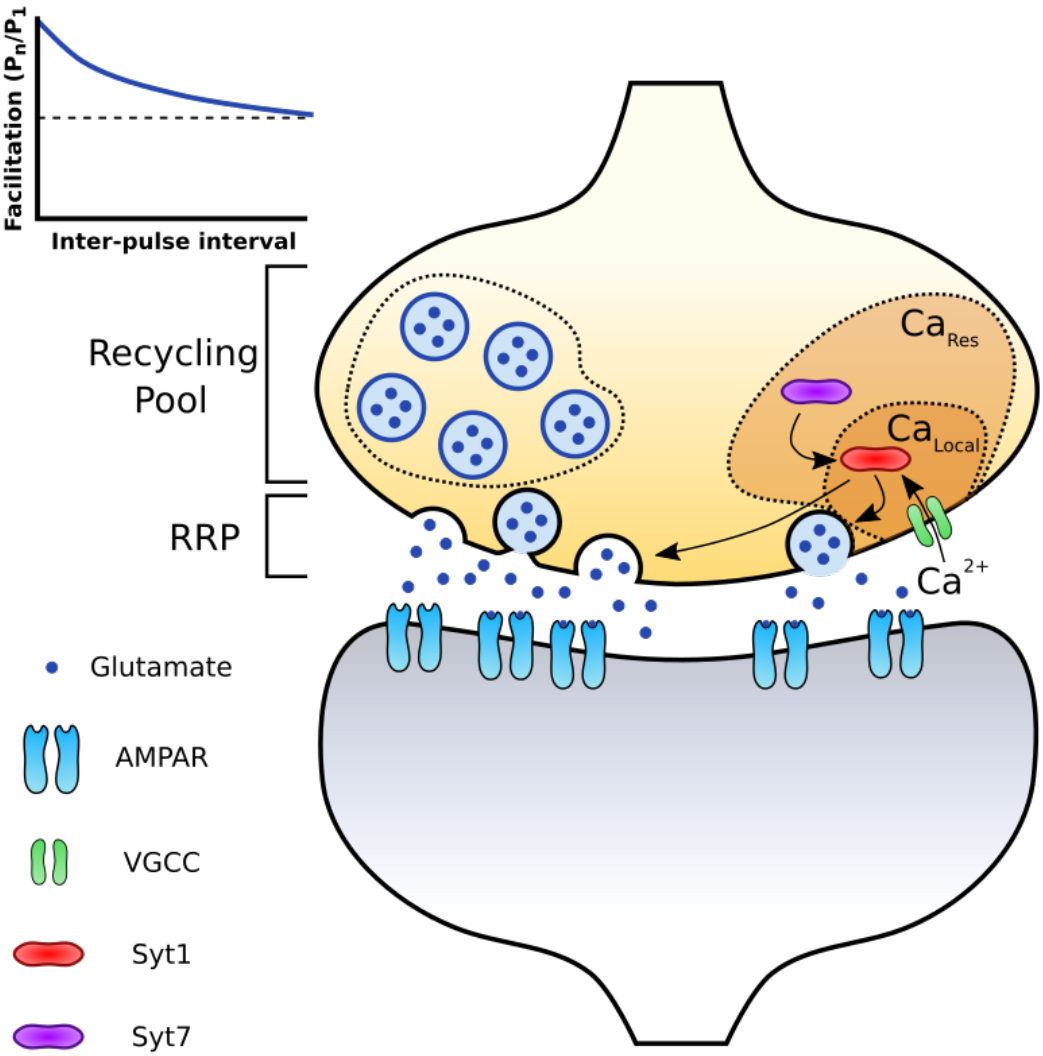

Figure 1.7: *Principles of short-term facilitation. Ca^{2+} influx in response to a single action potential triggers transient Ca^{2+} influx through VGCCs (Ca_{Local}) that binds rapidly to the low affinity Ca^{2+} sensor Syt1 to induce vesicle exocytosis and neurotransmitter release. Repeated action potentials allow an equilibration of Ca^{2+} throughout the pre-synaptic terminal (Ca_{Res}) that binds slowly to the high affinity Ca^{2+} sensor Syt7. Syt7 then raises terminal release probability via a possible interaction with Syt1. Top inset shows that the facilitation ratio (n^{th} peak/1^{st} peak) decreases with increasing inter-pulse intervals.*

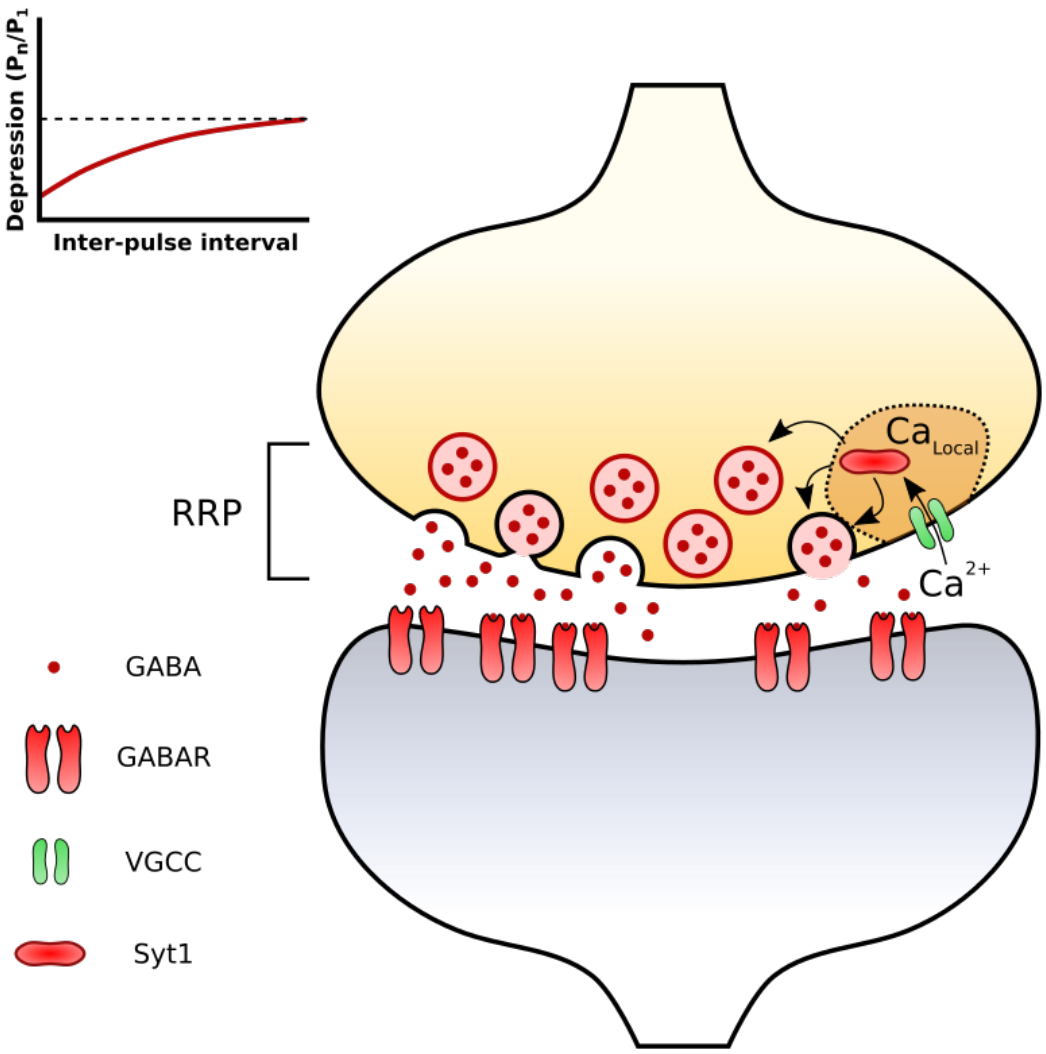

Figure 1.8: *Principles of short-term depression. Axonal terminals of depressing synapses typically possess a high P_r, which – upon repeated Ca^{2+} influx – depletes rapidly. Top inset shows that the depression ratio (n^{th} peak/1^{st} peak) decreases with increasing inter-pulse intervals.*

1.2.1.2 Long-term plasticity

1.2.1.2.1 Long-term potentiation

Long-term potentiation (LTP) is the most extensively studied form of long-term synaptic plasticity and was first evidenced *in vivo* at the perforant path to dentate gyrus synapse in anaesthetised rabbits (Bliss and Lomo, 1973). Following a 100 Hz electrical tetanus to the perforant path, an increase in the DG population response (EPSP amplitude and/or population spike amplitude) was observed. LTP remains the most attractive biological correlate for learning and memory (Nicoll, 2017) and since 1973 it has been evidenced at all major hippocampal synapses *in vitro* (Schwartzkroin and Wester, 1975; Doller and Weight, 1985; Chattarji, Stanton and Sejnowski, 1989; Remondes and Schuman, 2003) and *in vivo* (Buzsaki, 1980; Martinez *et al.*, 2002; Aksoy-Aksel and Manahan-Vaughan, 2013; Gonzalez *et al.*, 2016) and at synapses throughout the brain (Citri and Malenka, 2008).

As *in vivo* recordings became more widespread, it became apparent that – despite the wealth of research examining the mechanisms underlying tetanus-induced LTP – the typical high frequency induction protocol (50-100 stimuli delivered at 100 Hz for 1 second, Bliss and Collingridge, 1993) was not reflective of typical hippocampal neuron firing frequency (Rose and Dunwiddie, 1986). Feder and Ranck (1973) recorded dorsal hippocampal neurons in awake, freely moving rats and observed firing frequencies ranging from 24-96 Hz, with a mean of ~57 Hz. Moreover, neurons typically fired in bursts of three to ten spikes and showed a striking rhythmicity that was phase-locked to a theta rhythm, a hippocampal oscillation associated with exploratory behaviour (Vanderwolf, 1969) and learning (Miller, 1989; Lisman and Idart, 1995). Therefore, more physiologically-relevant induction protocols were subsequently developed. Under natural conditions, when a mouse or rat is exploring, hippocampal pyramidal neurons fire action potentials at a frequency of about 5 Hz, resulting in what is known as "theta rhythm," a sinusoidal oscillation of the hippocampal electroencephalography, which is critical for mnemonic processing (Bland, 1986). This observation led investigators to develop theta burst stimulation (TBS) and primed-burst stimulation (PBS) protocols (Larson and Lynch, 1986; Rose and Dunwiddie, 1986). Hernandez *et al.* (2005) showed TBS protocols to be just as effective as high frequency stimulation (HFS) protocols for inducing LTP at rat SC-CA1 synapses, with early-phase LTP actually greater with TBS. In addition to this, an induction protocol known as spike timing-dependent plasticity (STDP) was developed based on Hebb's postulate. In this protocol, pre-synaptic input and post-synaptic spiking are closely correlated, with shorter time intervals increasing the magnitude of LTP (Magee and Johnston, 1997; Nishiyama *et al.*, 2000).

With the exception of the MF-CA3 synapse, plasticity at all glutamatergic synapses in the hippocampus is dependent upon NMDARs on the post-synaptic membrane

(Collingridge, Kehl and McLennan, 1983; Zalutsky and Nicoll, 1990; Nicoll and Malenka, 1995), although LTP at the SC-CA1 and TA-CA1 synapses also co-requires VGCCs (Remondes and Schuman, 2003; Ahmed and Siegelbaum, 2009; Tigaret *et al.*, 2016). Mg^{2+} ions block NMDARs at the RMP (Konnerth *et al.*, 1990), however sufficient activation of AMPARs during LTP-inducing activity or by back-propagating action potentials causes a local depolarisation that removes this voltage-sensitive block (Mayer, Westbrook and Guthrie, 1984; Nowak *et al.*, 1984). NMDARs therefore become active and allow influx of Ca^{2+} into the post-synaptic compartment that – if sufficient in concentration – binds to calmodulin which in turn activates Ca^{2+}-calmodulin kinase II (CaMKII). The activation of CaMKII then influences AMPAR function by direct phosphorylation of AMPARs and phosphorylation of stargazin. AMPAR phosphorylation at Ser-831 increases channel conductance (Benke *et al.*, 1998; Derkach, Barria and Soderling, 1999) and stargazin phosphorylation facilitates its binding to post-synaptic density-95 (PSD-95) resulting in enhanced trafficking of AMPARs to the post-synaptic membrane (Tomita *et al.*, 2005a; Tomita *et al.*, 2005b).

The expression of LTP at the MF-CA3 is distinct from other hippocampal synapses in that it is NMDAR-independent (Harris and Cotman, 1986; Zalutsky and Nicoll, 1990) and has a pre-synaptic locus that is thought to involve Ca^{2+} influx via VGCCs (Breustedt *et al.*, 2003; Nicoll and Schmitz, 2005).

1.2.1.2.2 Long-term depression

A long-term reduction in synaptic efficacy termed long-term depression (LTD) can be induced with a low frequency synaptic input that is insufficient to induce spiking in the post-synaptic neuron (Dudek and Bear, 1992; Mulkey and Malenka, 1992). Much like LTP, NMDARs and post-synaptic Ca^{2+} influx are required for LTD, however the more modest Ca^{2+} influx through NMDARs and VGCCs causes a reduction in synaptic strength (Cummings *et al.*, 1996). Protein phosphatase 2B (PP2B/calcineurin) mediates this pathway as it has a higher affinity for Ca^{2+} than does CaMKII, allowing preferential activation under lower Ca^{2+} concentrations (Lisman, 1989). Calcineurin activates protein phosphatase 1 (PP1) by dephosphorylating and inactivating CaMKII's regulatory protein, inhibitor-1 (Mulkey *et al.*, 1994; Huang *et al.*, 1999; Allen *et al.*, 2000), allowing PP1 to dephosphorylate CaMKII and reduce its activity (Shields, Ingebritsen and Kelly, 1985). Calcineurin also induces a complex signalling cascade resulting in down-regulation of AMPARs (Beattie *et al.*, 2000). A variation of the Hebbian STDP protocol termed "anti-Hebbian STDP", in which the post-synaptic spike precedes the pre-synaptic EPSP, is also capable of inducing LTD (Markram *et al.*, 1997). Similar to LTD elicited by low frequency stimulation (LFS), lower intracellular Ca^{2+} levels have also been attributed to anti-Hebbian STDP (Nishiyama *et al.*, 2000). Figure 1.9 illustrates the processes underlying canonical LTP and LTD.

Much of the discussion on synaptic plasticity has focused on electrophysiological and behavioural correlates. However, it is possible to structurally quantify long-term changes in synaptic strength by using high-resolution imaging tools. In agreement with electrophysiological findings, LTP and LTD at hippocampal synapses exhibit increased or decreased dendritic spine size, respectively (Matsuzaki *et al.*, 2004; Zhou, Homma and Poo, 2004). In agreement with electrophysiological work, both of these changes also require NMDARs and show synapse selectivity. It has been postulated that maintaining appropriate spine density is important for efficient hippocampal function, with high densities of spines hypothesised to impair changes in synaptic strength (Chechik, Meilijson and Ruppin, 1999). From a computational point of view this makes sense: uncontrolled synaptic strengthening would negate pattern separation processes and increase the likelihood of pattern collision (Houghton, 2016). Not only does runaway LTP impair the encoding of new experiences by limiting network capacity, it also prevents the updating or elimination of old ones. In agreement with this, mice genetically modified to exhibit reduced synaptic pruning show impaired performance in hippocampus-dependent memory tasks and a resistance to LTD induction at the SC-CA1 synapse (Afroz *et al.*, 2016). Pharmacologically preventing synaptic pruning with MK-801 resulted in similar effects.

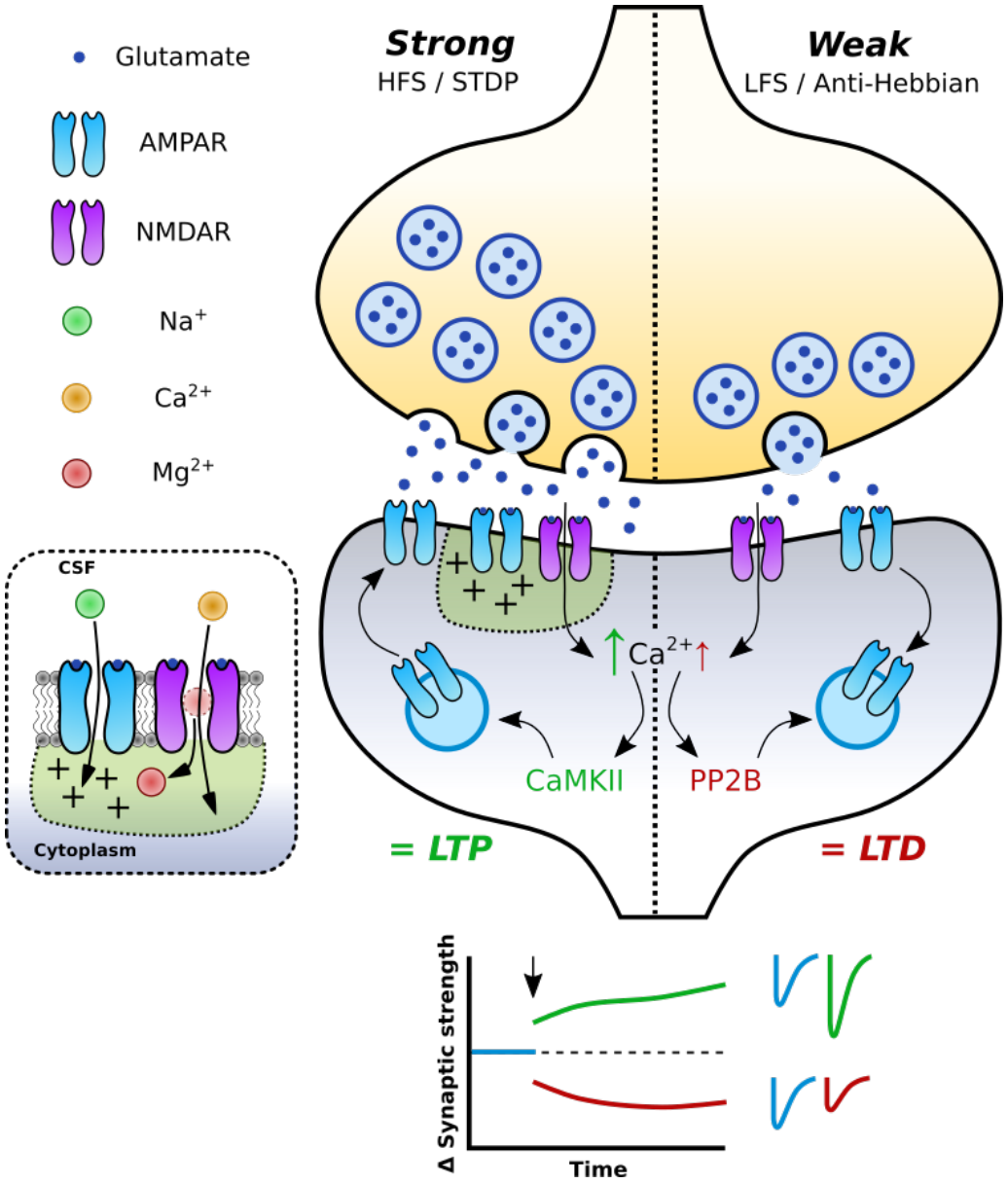

Figure 1.9: *Principles of canonical LTP and LTD. LTP: Strong/Hebbian pre-synaptic activation leading to large quantities of glutamate release activates post-synaptic AMPARs and induces a local depolarisation that removes the voltage-dependent Mg^{2+} block from NMDARs (left inset). This allows high levels of post-synaptic Ca^{2+} influx that activates CaMKII, in turn increasing AMPAR conductance and expression, resulting in LTP. LTD: Weak/anti-Hebbian pre-synaptic activation leading to low levels of glutamate release instead evokes a more modest post-synaptic Ca^{2+} increase that preferentially activates calcineurin (PP2B), leading to AMPAR internalisation and LTD. Bottom inset: typical time course of the change in synaptic strength for LTP (green) and LTD (red), arrow denotes the time of the plasticity induction protocol.*

1.2.1.2.3 Functions of long-term plasticity

There is a certain appeal in long-term synaptic changes existing as a biological correlate of memory. Indeed, animal performance in hippocampus-dependent memory tasks shows a reliance on NMDAR function, correlating well with the NMDAR requirement in LTP and LTD at almost all hippocampal synapses (Morris *et al.*, 1986). Memory and late-phase LTP are also both dependent on protein synthesis (Davis and Squire, 1984). Therefore, it is convenient to suppose that LTP is involved in "remembering" and LTD is crucial for "forgetting" information (Siegelbaum and Kandel, 1991; Tsumoto, 1993). In agreement with this notion, it is possible to apply an LTD-inducing protocol to a previously potentiated pathway to "de-potentiate" this connection (Barrionuevo, Schottler and Lynch, 1980; Bashir and Collingridge, 1994). Using this approach in combination with optogenetics (discussed in Chapter 3), it was shown that selective optical de-potentiation of synapses associated with fear memories in the amygdala could inactivate the fearful behaviour (reduced lever pressing) associated with the memory (Nabavi *et al.*, 2014). Further, optical re-potentiation could re-activate the fearful memory and associated behaviour.

However, rather than the somewhat crude "remember/forget" functions of LTP and LTD, it has been suggested that the two processes act together to encode and refine specific aspects of a memory, with LTD acting to improve network flexibility and storage capacity by filtering out irrelevant aspects of an experience. Evidence for a concerted effort of LTP and LTD in spatial acquisition was shown by Kemp and Manahan-Vaughan, (2004, 2008) and Hagena and Manahan-Vaughan (2011). Here, LTP at all hippocampal synapses was facilitated *in vivo* by a novel empty hole board (PP-DG, SC-CA1, MF-CA3, CA3-CA3), but was impaired by the presence of novel objects. Conversely, LTD was facilitated by novel objects in the hole board, but the facilitation observed at different synapses relied on distinct properties of the novel objects. For instance, SC-CA1 LTD was only facilitated when discrete environment cues were partially concealed by bedding (Kemp and Manahan-Vaughan, 2008), but PP-DG and MF-CA3 LTD was only augmented by large environmental cues (Kemp and Manahan-Vaughan, 2008; Hagena and Manahan-Vaughan, 2011). CA3-CA3 LTD was only enhanced by fully visible, small environmental cues (Hagena and Manahan-Vaughan, 2011). These studies suggest that LTP encodes the general features of an environment, with LTD at specific synapses encoding the more subtle details. Intriguingly, the conditions that facilitate LTP impair LTD and vice versa (Kemp and Manahan-Vaughan, 2004, 2008), hinting at distinct categorisation processing mechanisms mediated by LTP and LTD.

1.2.1.2.4 Complementary roles of short-term and long-term plasticity

It should also be noted that short- and long-term forms of plasticity are not necessarily mutually-exclusive: pre-synaptically expressed long-term plasticity is capable of shifting

synapses between low-, band-, and high-pass filtering modes due to the change in baseline release probability (Monday, Younts and Castillo, 2018). Conversely, computational research has suggested that short-term depression is crucial for maintaining memory capacity through the elimination of "weak" cortical assemblies, allowing the embedding of a stimuli as multiple cell assemblies within the network (Hiratani and Fukai, 2014b). *In vivo*, the sub-threshold LTP protocols in the aforementioned learning-facilitated LTP experiments are typically protocols that induce short-term plasticity, hence short-term plasticity may be converted to LTP under the relevant environmental conditions (Hagena, Hansen and Manahan-Vaughan, 2016). Thus, diverse forms of synaptic plasticity combine in complex ways to modulate local circuit and network computations.

1.2.2 Neuromodulation

Early neuroscience considered a given neuron's output as a function of the simple summation of its transient inhibitory and excitatory inputs, however in the late 1970s and early 1980s it was realised that a third type of input, known as "modulatory", could selectively alter the gain of these binary "on" or "off" synaptic signals (Kupfermann, 1979). The excitatory and inhibitory neurons directly involved in the local circuitry are most strongly involved in the homeostatic regulation of the E/I balance and plasticity, however inputs from modulatory neurons originating in distant brain regions confer further control in shaping the circuit dynamics of areas such as the cortex and hippocampus (Pawlak *et al.*, 2010). The neuromodulators commonly associated with behavioural states include acetylcholine (ACh – uncertainty), noradrenaline (NA – novelty and emotion), dopamine (DA – reward), serotonin (5-HT – reward) (Prince *et al.*, 2016; Avery and Krichmar, 2017; Palacios-Filardo and Mellor, 2019).

Every neural network is subject to neuromodulation (Marder, 2012). Even the simplest neural circuits are complex, and modulation adds extraordinary richness to the dynamics that networks can display. Although we are far from understanding the full extent of modulation that exists in the brain, we do know that these inputs have important consequences for synaptic transmission and plasticity that extend over a range of time-scales (Prince *et al.*, 2016).

1.3 Noradrenergic neuromodulation

1.3.1 The locus coeruleus and noradrenaline

Noradrenaline (NA) is the neuromodulator pertinent to the present work. Released throughout the brain from diffusely projecting locus coeruleus (LC) fibres, this endogenous catecholamine has been widely studied as a neuromodulator in multiple higher brain regions (for reviews, see Marzo, Bai and Otani, 2009; O'Dell *et al.*, 2010, 2015; Tully and Bolshakov, 2010). NA is synthesised from tyrosine through a series of

biochemical reactions that are outlined in Figure 1.10, with the final conversion of DA into NA by dopamine-β-hydroxylase (DβH) occurring within the terminal vesicles. Following its release into the synaptic cleft, NA can act on a variety of noradrenergic receptor subtypes which can be broadly split into three main classes: α1-, α2- and β-ARs (Figure 1.10). All three adrenoceptor subtypes are GPCRs but are coupled to different G-proteins and exhibit distinct affinities for NA, with the rank order of affinity for NA being α2 > α1 > β (O'Rourke *et al.*, 1994; Ramos and Arnsten, 2007; Atzori *et al.*, 2016). α2-ARs and β-ARs couple to G_i and G_s proteins, respectively, thus acting to decrease or increase intracellular cAMP levels through inhibition (α2-ARs) or activation (β-ARs) of adenylyl cyclase (AC). α1-ARs instead couple to G_q proteins, enhancing PLC activity upon activation. These pathways are summarised in Figure 1.10. α2-ARs are rather interesting in that they are also found pre-synaptically on LC terminals, where they act as auto-receptors to self-regulate NA release and potentially gate stress/stimulus-induced LC hyperactivity (Starke and Montel, 1973; Huang *et al.*, 2012).

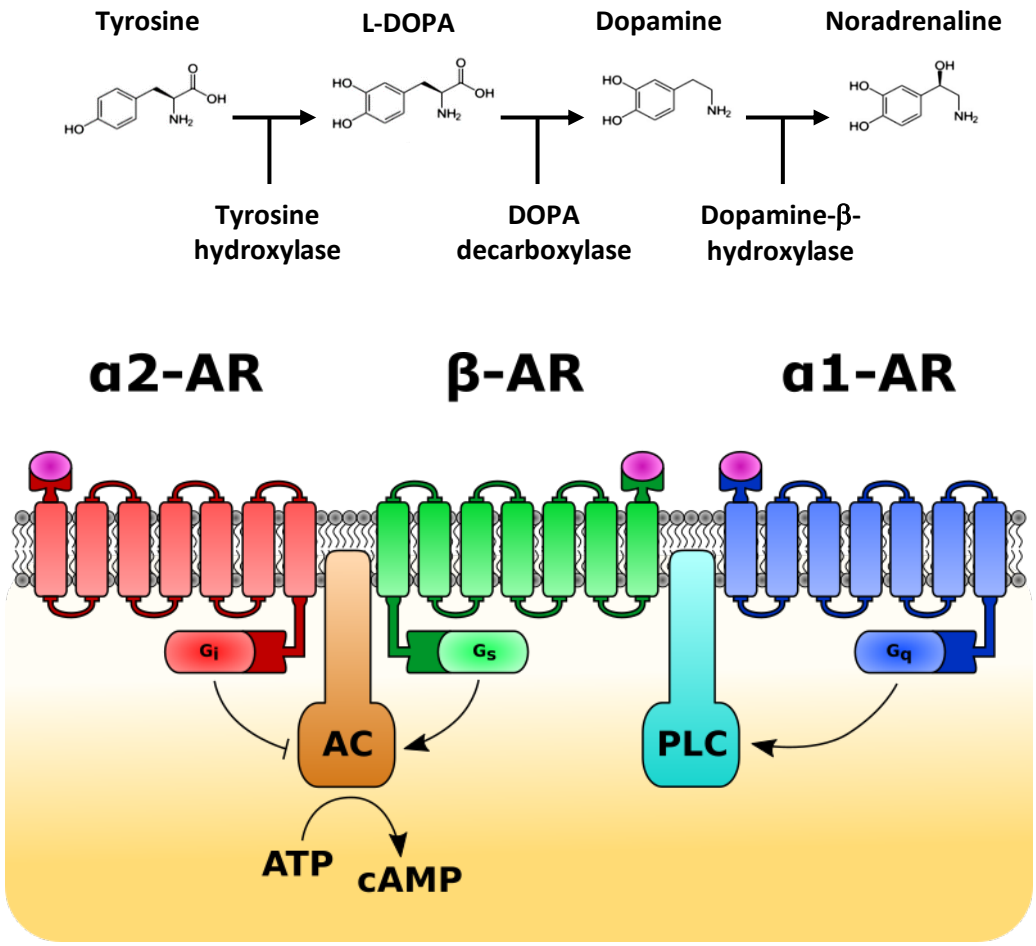

Figure 1.10: *Synthesis of NA and noradrenergic signalling pathways. Top: biochemical synthesis pathway for NA. Bottom: schematic illustrating the signalling cascades following activation of α2-ARs (red), β-ARs (green) and α1-ARs (blue) by NA.*

The LC itself is a small, pontine cluster of neurons (~2,500 in rat, ~10,000 in rhesus macaques and ~50,000 in humans, Maeda and Shimizu, 1972; Sharma *et al.*, 2010; Robertson *et al.*, 2013) located bi-laterally in the brainstem. Despite its size, it sends diffuse projections throughout the brain, innervating distinct cortical areas to co-ordinate their activity and enhance memory, attention and induce waking from sleep (Samuels and Szabadi, 2008; Sara, 2009). These projections are not exclusively ascending, as the LC also sends descending axons via the spinal cord which are involved in analgesia (Millan, 2002; Pertovaara, 2006; Hirschberg *et al.*, 2017). Indeed, the LC's brainstem location and presence across species – including fish (Ekström, Honkanen and Borg, 1992; Ma, 1994) and birds (Bailhache and Balthazart, 1993; Moons *et al.*, 1995) – allow this evolutionarily conserved, archaic structure to partake in a plethora of additional regulatory functions including pain, defensive responses, and vigilance (Samuels and Szabadi, 2008; Sara, 2009; Uematsu, Tan and Johansen, 2015; Aston-Jones and Waterhouse, 2016).

The LC was arguably the first neuromodulatory system to be anatomically outlined in 1941 (Sano, 1941), and characterised functionally 6 years later (Araki, 1947). Unfortunately, these interesting studies were published in Japanese and so the LC existed unbeknownst to many people in western countries until the first comprehensive analysis was carried out by Russell (1955). For many years following this the LC was assumed to exist as a homogenous collection of noradrenergic neurons, however growing evidence now suggests that the LC is comprised of distinct, minimally overlapping sub-domains which preferentially target diverse brain regions. Initial anatomical studies utilising 3D reconstruction (Loughlin, Foote and Bloom, 1986) were recently supported by MAPseq approaches (Kebschull *et al.*, 2016). Moreover, the neurons comprising these LC domains also show distinct electrophysiological properties (Chandler, Gao and Waterhouse, 2014). Indeed, retrograde injections to the spinal cord and pre-frontal cortex of the same viral vector used in the present study (CAV2-PRS-mCherry-ChR2) and a GFP-tagged chemogenetic virus (CAV2-PRS-EGFP-2A-PSAM) further supported the notion of a topographical arrangement of the LC (Li *et al.*, 2016). These were subsequently functionally characterised in analgesia and anxiety behavioural tasks (Hirschberg *et al.*, 2017). In addition to targeted outputs, these distinct modules also appear to receive selective inputs from across the brain, which are then integrated and broadcast globally or selectively (Schwarz *et al.*, 2015).

NA release from the LC during emotional or novel experiences is believed to act as a gating mechanism, flagging the experience as salient (Aston-Jones and Bloom, 1981; Sara, Vankov and Herve, 1994; Vankov, Herve-Minvielle and Sara, 1995). During quiet wakefulness, LC neurons fire at a tonic rate of ~1 Hz, a lower rate during drowsiness and slow-wave sleep (SWS) (Aston-Jones and Bloom, 1981; Aston-Jones *et al.*, 1994) and are

completely silent during rapid eye movement (REM) sleep (Roussel *et al.*, 1967; Takahashi *et al.*, 2010). However, when presented with a novel or emotionally-rousing stimuli, the LC switches to a burst firing, phasic mode (Aston-Jones and Bloom, 1981; Sara, Vankov and Herve, 1994; Vankov, Herve-Minvielle and Sara, 1995). Although the tonic firing mode has been well-correlated with vigilance (Rajkowski, 1994; Aston-Jones and Cohen, 2005b), it is the phasic firing mode that has received the most attention in attempts to link it with learning, memory and cognition (Aston-Jones and Bloom, 1981; Rajkowski, 1994; Vankov, Herve-Minvielle and Sara, 1995; Waterhouse, Moises and Woodward, 1998).

The hippocampus is an important component of memory formation, consolidation and retrieval (Bird and Burgess, 2008), and is also a major output target of the LC, with all subfields receiving noradrenergic innervation (Milner and Veznedaroglu, 1989; Walling *et al.*, 2012; Wagatsuma *et al.*, 2018). Like other neuromodulators, NA release from the LC is believed to mediate its effects via volume transmission (Umbriaco *et al.*, (1995), however see Walling *et al.*, (2012) for evidence of selective synaptic targeting in the CA3 subfield). LC lesions (Compton *et al.*, 1995), blockade of hippocampal adrenoceptors (Ji, Zhang and Li, 2003), and mutant mice lacking NA all show deficits in memory and learning (Murchison *et al.*, 2004, 2011), leading to the idea that NA is a fundamental regulator of memory processing.

1.3.2 Noradrenergic modulation of the SC-CA1 micro-circuit

Several studies have examined the expression of all adrenoceptor subtypes in the CA1. β-ARs are found in pyramidal neurons and interneurons throughout the CA1 (Hillman, Doze and Porter, 2005; Guo and Li, 2007; Cox, Racca and LeBeau, 2008), whereas α2-ARs are predominantly expressed in pyramidal neurons and α1-ARs are more prominent in interneurons (Milner *et al.*, 1998; Hillman *et al.*, 2005; Papay *et al.*, 2006). The initial research into the modulatory role of NA at the SC-CA1 synapse highlighted NA as a complex neuromodulator, with mixed effects on CA1 pyramidal neuron excitability: β-AR-mediated depolarisation and α2-AR-mediated hyperpolarisation (Madison and Nicoll, 1986; Ul Haq *et al.*, 2012). Subsequent work showed that NA attenuates synaptic inhibitory inputs from CA1 interneurons and enhances population spikes in rat *ex vivo* hippocampal slices (Madison and Nicoll, 1988; Doze, Cohen and Madison, 1991; Heginbotham and Dunwiddie, 1991; Dunwiddie *et al.*, 1992; Bergles *et al.*, 1996). Confusingly, such disinhibition only appears to affect evoked responses, as NA also depolarises interneurons via α1-ARs and enhances tonic spontaneous inhibitory drive onto CA1 pyramidal neurons (Madison and Nicoll, 1988; Bergles *et al.*, 1996). Furthermore, β-AR activation alone was also shown to be sufficient to enhance population spike amplitude through enhanced EPSP-spike coupling (Heginbotham and

Dunwiddie, 1991; Dunwiddie *et al.*, 1992), with no change in excitatory input (also shown by Hu *et al.*, (2007), but see Katsuki, Izumi and Zorumski (1997) for a small decrease). These studies usually utilised specific adrenoceptor agonists or adrenaline (which has a higher affinity for adrenoceptors than NA, Minneman, Theroux and Esbenshade, 1994), and no studies following these attempted to further interrogate the effects of NA on synaptic inputs, short-term dynamics, E/I balance, and – crucially – how this modulation shaped synaptically-evoked CA1 pyramidal neuron output at a single cell level. Intriguingly, Mueller, Hoffer and Dunwiddie (1981) did find a bell-shaped curve for the effects of NA on the SC-CA1 population spike, with lower concentrations (5 μM) enhancing and higher (25-50 μM) depressing the spike amplitude via β-AR and α2-ARs, respectively (however field EPSP amplitude was unaffected). These effects were subsequently recapitulated *in vivo* (Mueller *et al.*, 1982).

Focus instead shifted to the more robust effects of NA: inhibition of the CA1 sAHP (slow after-hyperpolarisation, (Madison and Nicoll, 1982, 1986; Haas and Konnerth, 1983; Dunwiddie *et al.*, 1992; Sah and Isaacson, 1995) and facilitation of SC-CA1 LTP (Katsuki, Izumi and Zorumski, 1997; Hu *et al.*, 2007; Maity *et al.*, 2015, 2016; Liu *et al.*, 2017). Both of these effects are mediated by β-ARs. Given that attenuation of the CA1 sAHP amplitude has been correlated with increased spiking and enhanced learning (Moyer, Thompson and Disterhoft, 1996; Oh *et al.*, 2006; Power *et al.*, 2018), noradrenergic sAHP inhibition – and the associated increase in CA1 spike output – likely plays a role in the facilitation of SC-CA1 LTP (Fuenzalida, Fernandez de Sevilla and Buno, 2007).

In addition to the putative role of sAHP inhibition in LTP, a plethora of studies over the last three decades have shed light on numerous other mechanisms involved in noradrenergically-enhanced LTP. Tetanus-induced LTP can be facilitated by DNA methylation, post-translational histone modifications, AMPAR phosphorylation and increased trafficking to the post-synaptic membrane (Katsuki, Izumi and Zorumski, 1997; Gelinas and Nguyen, 2005; Gelinas *et al.*, 2007; Hu *et al.*, 2007; Makino *et al.*, 2011; Qian *et al.*, 2012; Maity *et al.*, 2015, 2016). These are believed to reduce the frequency threshold for LTP. Non-tetanus protocols that are sub-threshold for LTP (5 Hz for 3 minutes) can also be enhanced via β-AR-mediated protein synthesis (Gelinas and Nguyen, 2005). β-AR-mediated NMDAR Ser1166 phosphorylation via PKA enhances current flow and spine Ca^{2+} influx through NMDARs, and likely contributes to SC-CA1 plasticity (Raman, Tong and Jahr, 1996; Murphy *et al.*, 2014). STDP can also be augmented as a result of SAP-97 down-regulation of Kv1.1 channels, enhancing back-propagating action potentials and widening the temporal window for STDP and associative plasticity (Lin *et al.*, 2003; Liu *et al.*, 2017). Curiously, SC-CA1 LTP induced

by TBS does not seem to be affected by NA (Katsuki, Izumi and Zorumski, 1997), for reasons that are unclear.

1.3.3 Noradrenergic modulation of the MF-CA3 micro-circuit

Within the CA3, β-AR expression has been reported in pyramidal neurons and CCK+ interneurons (Jurgens *et al.*, 2005; Guo and Li, 2007; Cox, Racca and LeBeau, 2008). β-AR expression has also been shown in DG granule cells and interneurons (Milner, Shah and Pierce, 2000; Cox, Racca and LeBeau, 2008), whereas α1-ARs seem to only be found in DG interneurons (Papay *et al.*, 2006). α2-ARs have also been evidenced on CA3 pyramidal neurons in expression studies (Milner *et al.*, 1998), and their activation underlies an anti-epileptic function (Jurgens *et al.*, 2005, 2007; Goldenstein *et al.*, 2009). Moreover, this anti-epileptiform activity persists even in the presence of GABAR blockade, suggesting a direct effect on CA3 pyramidal neurons. Studies examining the functional effects of adrenoreceptors on DG and CA3 interneurons are somewhat lacking, however the distinct cellular expression profiles of these receptors hint at interesting modulatory roles of β-ARs in inhibitory transmission. Interestingly, one study did examine the effects of NA on hilar interneurons synapsing onto DG granule cells and found a marked decrease in the sAHP of these interneurons, as well as an increase in spontaneous IPSC input to granule cells (Bijak and Misgeld, 1995).

In agreement with noradrenergic influences in the CA1, β-AR depolarising and α2-AR hyperpolarising effects have been reported in CA3 pyramidal neurons and DG granule cells (Lacaille and Schwartzkroin, 1988; Ul Haq *et al.*, 2012). Functionally, activation of CA3 α2-ARs has potent anti-epileptic properties, dramatically reducing neuronal burst firing (Jurgens *et al.*, 2005, 2007; Goldenstein *et al.*, 2009). β-AR activation inhibits the sAHP in granule cells (Haas and Rose, 1987), enhances the phosphorylation of the DG synapsins I and II (vesicle-associated proteins linked to neurotransmitter release) and increases excitatory synaptic output from the DG (Parfitt, Hoffer and Browing, 1991; Parfitt *et al.*, 1992). In agreement with these findings, β-ARs enhance glutamate release from DG synapses (Lynch and Bliss, 1986). It should be noted that these studies examined increases in total DG synapsin phosphorylation and glutamate release, and so may not be reflective of specific changes in mossy fibre terminals. Moreover, the EPSP amplitudes in the Parfitt, Hoffer and Browing (1991) study were recorded in the *stratum lacunosum-moleculare* (where entorhinal cortex inputs, but not mossy fibres, are typically located), as opposed to the hilar or CA3 pyramidal regions. Indeed, using the same concentration of the β-AR agonist, isoproterenol, Huang and Kandel (1996) did not observe any enhancement in excitatory transmission at the MF-CA3 synapse.

Isolated CA3 recurrent and mossy fibre AMPAR currents are inhibited by NA, by a possible pre-synaptic α1-AR mechanism, in hippocampal cultures (Scanziani, Gähwiler

and Thompson, 1993). In presumed *in vivo* DG interneurons, NA was found to be inhibitory via α1-AR activation (Pang and Rose, 1987) and electrical stimulation of the LC inputs to CA3 also induced suppressing effects mediated by α1-ARs in anaesthetised rats (Curet and de Montigny, 1988). The mechanism of this α1-AR-mediated suppression is unclear and confusing, given that α1-ARs mediate excitatory effects in CA1 interneurons (Madison and Nicoll, 1988; Bergles *et al.*, 1996).

Substantial evidence also suggests NA can enhance LTP at the MF-CA3 synapse (Hopkins and Johnston, 1984, 1988; Gray and Johnston, 1987; Huang, Li and Kandel, 1994; Huang and Kandel, 1996). Much like the LTP-enhancing effects at the SC-CA1 synapse, the increase in magnitude and duration of MF-CA3 LTP is underscored by a β-ARs, with several studies indicating a pre-synaptic enhancement of VGCC activity in granule cells as a possible mechanism (Hopkins and Johnston, 1984, 1988; Gray and Johnston, 1987). In agreement with this, Huang and Kandel (1996) also showed that NA-enhanced LTP at the MF-CA3 can occur even when glutamatergic transmission is blocked during the induction protocol. They further showed that, like NA-enhanced LTP at the SC-CA1 synapse, NA could convert sub-threshold LTP to full LTP at the MF-CA3 synapse. This enhancement affected both the early phase (protein synthesis-independent) and late phase (protein synthesis-dependent) components of MF-CA3 LTP. They were unable to replicate this at CA3-CA3 synapses, supporting similar findings by Weisskopf *et al.* (1994).

1.3.4 Effects of LC activation on synaptic plasticity and memory *in vivo*

Given that novelty induces LC burst firing, it is plausible that the aforementioned learning-facilitated enhancements of LTP and LTD in relation to novel aspects of an environment are mediated by NA (Kemp and Manahan-Vaughan, 2004, 2008; Hagena and Manahan-Vaughan, 2011). Indeed, learning-facilitated LTP related to a novel environment is critically dependent on β-AR activation at all hippocampal subfields, as is the encoding of spatial content with LTD (Kemp and Manahan-Vaughan, 2008; Hagena and Manahan-Vaughan, 2012; Goh and Manahan-Vaughan, 2013; Hagena, Hansen and Manahan-Vaughan, 2016). Moreover, optogenetic inhibition of the LC can impair performance on a hippocampus-dependent contextual fear memory task and disrupt place field formation and stability (Wagatsuma *et al.*, 2018). Intriguingly, the mere presence of NA does not improve hippocampus-dependent memory since optogenetic activation of the LC during sleep spindles (when the LC is typically quiescent) actually impairs spatial memory and disrupts place fields (Swift *et al.*, 2018)

1.3.5 The locus coeruleus, neuropeptides and dopamine

Historically, the LC has been thought to solely release NA, however it was shown by Holets *et al.* (1988) that up to 80% of LC neurons also contain galanin and a smaller

subset of ~20% contain neuropeptide Y (Holets *et al.*, 1988). It is now known that the LC can co-release corticotropin releasing factor (CRF), orexin, endogenous opioids, substance P, melanin concentrating hormone (MCH), neuropeptide Y (NPY) and somatostatin (SST). The release of these neuropeptides onto neighbouring LC neurons can increase (CRF, orexin, substance P) or decrease (endogenous opioids, MCH, SST, NPY) LC activity to mediate arousal and response to stress (see Zitnik (2016) for review).

More recent reports suggest that the LC may additionally release dopamine (DA) (Kempadoo *et al.*, 2016; Takeuchi *et al.*, 2016; Wagatsuma *et al.*, 2018). Takeuchi *et al.*, (2016) found that mice performed better on a foraging task if they were exposed to a novel environment between the training and test trials, and this effect could be recapitulated by optogenetically-activating the LC in a non-novel environment. This effect was blocked by a D1/D5 receptor antagonist, SCH23390. However, this compound is also known to be a potent (IC_{50} < 300 nM) and direct inhibitor of G-protein-coupled inwardly rectifying K^+ (GIRK) channels (Kuzhikandathil, Oxford and Carolina, 2002). GIRK channels themselves are strongly expressed in the hippocampus (Saenz *et al.*, 2008) where they regulate neuronal excitability (Luján, Maylie and Adelman, 2009), and dysfunction of these channels has been linked to poorer spatial learning and memory, which may have been a confound in the Takeuchi *et al.* (2016) study (Wickman *et al.*, 2000; Luján, Maylie and Adelman, 2009; Lüscher and Slesinger, 2010; Cooper *et al.*, 2012; Sánchez-rodríguez *et al.*, 2017).

Although the present research predominantly focuses on noradrenergic modulation, it is worth considering the possibility of a dopaminergic effect. This is not only based on the aforementioned research, but also the fact that NA and DA show affinity for one another's receptors (Cornil and Ball, 2008; Sun *et al.*, 2018; Feng *et al.*, 2019) and these receptors utilise the same intracellular downstream signalling cascades (Girault and Greengard, 2004; Beaulieu and Gainetdinov, 2011; O'Donnell *et al.*, 2012). For instance, DA binds to rat α2-ARs with a 10-20-fold lower affinity than NA (Cornil and Ball, 2008); and DA binds to human β-ARs (in HEK293 cells) with ~100-fold lower affinity (Wieland *et al.*, 1996). Both NA and DA have also been shown to enhance memory function, but in response to distinct brain states (arousal/novelty and reward, respectively (Lisman and Grace, 2005; Duszkiewicz *et al.*, 2019).

1.4 Brief aims

This review of the literature has shown that the effects of NA on hippocampal function are potent but varied and often contradictory. There is also little research examining the effects of NA on synaptic transmission and short-term plasticity at a single-cell level, and many studies use exogenous bath application of adrenoceptor subtype-selective agonists as opposed to the endogenous neuromodulator. This is useful in examining the isolated roles of adrenoceptor subtypes and how these contribute to hippocampal function given selective activation, but this may only provide a part of the overall picture. Given that all adrenoceptors are present in the hippocampus, and NA is capable of activating all of these subtypes, examining the effects of concentration and spatiotemporal release perhaps provides a more useful picture. Furthermore, the majority of research into noradrenergic neuromodulation was obtained using rat hippocampal slices, however the genetic toolbox for mice eclipses that for rats. It is therefore of benefit to re-examine the effects of NA in mice at the two main hippocampal feed-forward micro-circuits: the SC-CA1 and the MF-CA3 synapses. This thesis aims to integrate the observed effects of NA on intrinsic neuronal properties, synaptic inputs and synaptically-evoked spike output. In addition, the work outlined in this thesis utilised recent advances in optogenetic targeting to evoke endogenous NA from within hippocampal slices and compared these effects to those obtained with bath application of the neuromodulator.

Initial characterisation of the noradrenergic modulation of the SC-CA1 feed-forward micro-circuit with bath-applied NA will be discussed in Chapter 2, and subsequently compared with the effects obtained with optogenetically-evoked release in Chapter 3. Chapter 4 will then examine the effects of bath-applied NA at the MF-CA3 synapse in response to regular and irregular synaptic inputs, and these results will be compared with the effects of ACh in modulating MF-CA3 E/I balance using a computational model of the MF-CA3 feed-forward micro-circuit. Finally, exploratory work using modern techniques (fast-scan cyclic voltammetry and genetically encoded fluorescent sensors) to determine the concentration of NA released by hippocampal LC terminals upon optogenetic stimulation will be reviewed in Chapter 4.

Chapter 2: Effects of bath-applied NA on the SC-CA1 micro-circuit

2.1 Introduction

The SC-CA1 synapse is one of the most well-characterised synapses of the hippocampus (Andersen *et al.*, 2007), and a fine example of the exquisite tuning present in many neuronal networks. Glutamatergic SC axons from CA3 pyramidal cells not only provide direct excitatory drive to CA1 pyramidal neurons, but also terminate onto the dendrites of GABAergic interneurons in the *stratum radiatum* which in turn synapse onto CA1 pyramidal neurons (Amaral and Witter, 1989; Witter *et al.*, 1989; Andersen *et al.*, 2007; Sun *et al.*, 2014; Kwon *et al.*, 2018). This recruitment of feed-forward inhibition is essential in maintaining the E/I balance in this micro-circuit and ensuring precise spike timing and integration (Pouille and Scanziani, 2001; Bartley and Dobrunz, 2015). This micro-circuit is summarised in Figure 2.1.

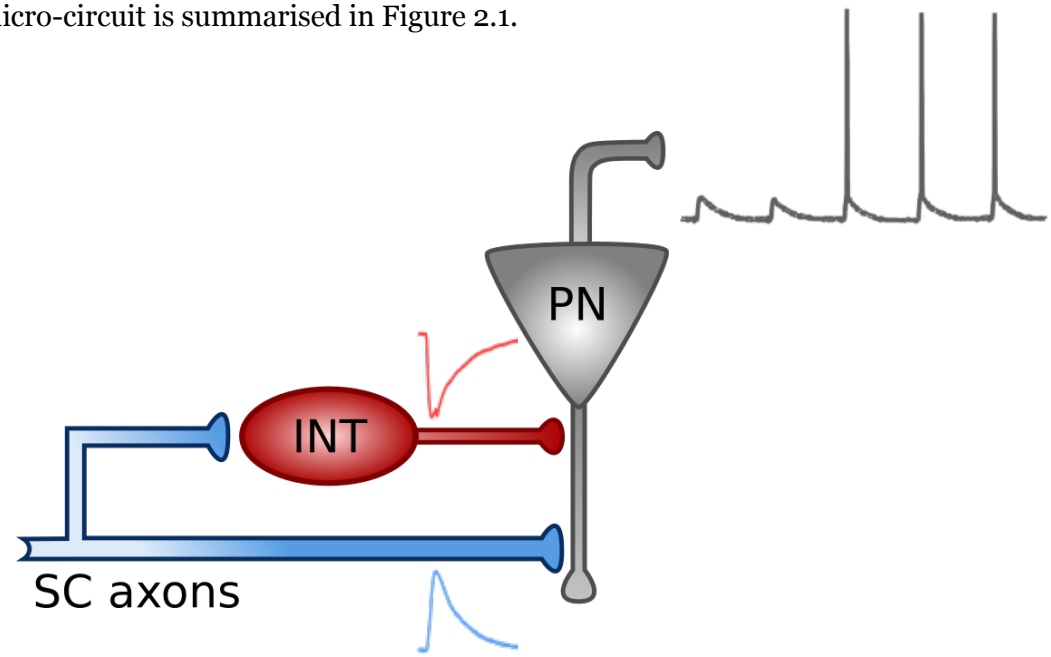

Figure 2.1: *Inputs and outputs of the SC-CA1 feed-forward micro-circuit. Incoming SC axons from CA3 synapse directly onto distal CA1 pyramidal neuron (PN) dendrites, and also onto CA1 inhibitory interneurons (INT) which then synapse onto more proximal dendrites. The combined input determines spike output.*

As outlined in Chapter 1, the effects of NA on CA1 neuronal excitability and synaptic transmission have been examined and the results are varied and contradictory, largely due to differences in adrenoceptor subtype activation. The effects of bath-applied NA on synaptic transmission in the hippocampus were initially studied with a focus on population spiking activity (Madison and Nicoll, 1988; Doze, Cohen and Madison, 1991) or, more recently, as part of broader studies looking at synaptic plasticity (Katsuki, Izumi and Zorumski, 1997; Hu *et al.*, 2007). Examining post-synaptic potentials has its merits (i.e. it is possible to measure "true" voltage changes in a neuron and their integration at

the soma) but does not allow isolation of specific (excitatory or inhibitory) synaptic inputs in an intact micro-circuit. Moreover, a profound feature of the SC-CA1 micro-circuit that has not been examined is the noradrenergic effects on the short-term plasticity of its excitatory and feed-forward inhibitory components. Given the role of NA in attenuating the frequency-dependence of LTP (Katsuki, Izumi and Zorumski, 1997; Hu *et al.*, 2007), we postulated that NA may also confer frequency-dependent effects on SC-CA1 short-term plasticity.

There is also a wealth of research examining the noradrenergic inhibition of the sAHP and the associated increased CA1 spike output in response to somatic current injection (Madison and Nicoll, 1982, 1986; Haas and Konnerth, 1983; Dunwiddie *et al.*, 1992; Sah and Isaacson, 1995), however no studies have examined the effects of NA on synaptically-evoked spike output at a single-cell level, and such effects would likely be linked to changes in synaptic input.

SC-CA1 LTP, on the other hand, is very-well characterised and predominantly modulated by β-ARs (Jędrzejewska-Szmek *et al.*, 2017). First observed in 1975 (Schwartzkroin and Wester, 1975), LTP at the SC-CA1 synapse has since been extensively characterised (Andersen *et al.*, 1977; Lynch *et al.*, 1983; Emptage *et al.*, 2003; Barria and Malinow, 2005). Like many forms of LTP expressed throughout the brain, LTP at SC-CA1 synapses is strongly NMDAR-dependent, regardless of whether it is induced using HFS (Collingridge, Kehl and McLennan, 1983; Harris, Ganong and Cotman, 1984; Morris *et al.*, 1986) or STDP protocols (Magee and Johnston, 1997; Nishiyama *et al.*, 2000). As outlined in Chapter 1, a plethora of studies have examined the role of NA in modulating long-term enhancement of SC-CA1 synaptic strength (Katsuki, Izumi and Zorumski, 1997; Lin *et al.*, 2003; Gelinas and Nguyen, 2005; Gelinas *et al.*, 2007; Hu *et al.*, 2007; Makino *et al.*, 2011; Qian *et al.*, 2012; Maity *et al.*, 2015, 2016; Liu *et al.*, 2017). The majority of these studies have implicated changes in AMPAR phosphorylation and trafficking as major underlying factors underscoring β-AR-enhanced SC-CA1 LTP. However, NA activation has also been shown to enhance NMDAR activity through PKA phosphorylation (Raman, Tong and Jahr, 1996; Murphy *et al.*, 2014), suggesting an additional substrate for noradrenergically-enhanced LTP. Intriguingly, several lines of evidence also point towards an additional, indirect, modulation of NMDARs by NA.

Crucial to this line of thought is the concept that NMDARs in CA1 pyramidal neurons are tonically regulated by SK channels (Ngo-Anh *et al.*, 2005; Faber *et al.*, 2008). SK channels are Ca^{2+}-activated K^+ channels that hyperpolarise the post-synaptic spines where NMDARs are located, thus preventing their activation (Buchanan *et al.*, 2010). However, inhibition of these SK channels by ACh or glutamatergic spill-over (acting at M1 muscarinic or mGluR1 receptors, respectively) results in disinhibition of NMDARs

and a potentiation of STDP at the SC-CA1 synapse (Buchanan *et al.*, 2010; Tigaret *et al.*, 2016, 2018). SK channel sensitivity to intracellular Ca^{2+} can also be reduced by protein kinase CK2 phosphorylation activity (Bildl *et al.*, 2004; Allen *et al.*, 2007), and in dorsal root ganglion neurons, NA reduces the Ca^{2+} sensitivity of a subtype of SK channels, SK2, via increased phosphorylation by CK2 (Maingret *et al.*, 2008). Recent work in the amygdala has also shown that down-regulation of SK channels by β-ARs enhances LTP (Faber *et al.*, 2008). Given the wealth of research implicating SK2 channels in CA1 pyramidal neuron intrinsic excitability and synaptic plasticity (Bond *et al.*, 2004; Ngo-Anh *et al.*, 2005; Hammond *et al.*, 2006; Bloodgood and Sabatini, 2007; Lin *et al.*, 2008, 2010) we postulated that NA may down-regulate the expression and/or Ca^{2+} sensitivity of SK channels in CA1 pyramidal neurons, and this may play a role in NA-mediated LTP. Such a finding would also implicate SK channels as a convergent regulatory mechanism for NA and ACh in enhancing NMDAR function and the associated increase in synaptic strength at the SC-CA1 synapse.

In summary, no research has examined the effects of NA on the short-term dynamics of both the excitatory and inhibitory synaptic components of the SC-CA1 micro-circuit. There is also little research on how modulation of this input affects synaptically-evoked CA1 pyramidal cell output (as opposed to the somatically-induced spiking utilised in most sAHP studies). Finally, several studies imply that NA – like ACh and glutamate – can modulate SK channel function, however the idea of such a common mechanism existing between these neuromodulators for enhancing LTP has yet to be established.

The key questions were:

1) How does NA affect excitatory and inhibitory synaptic transmission and short-term dynamics at the SC-CA1 synapse in mice?

2) How does modulation of this synaptic input affect the synaptically-evoked spike output of CA1 pyramidal cells?

3) Is NA involved in the modulation of SK channels to facilitate STDP at the SC-CA1 synapse?

We used whole-cell voltage-clamp recordings and a caesium-based intracellular solution to isolate evoked mono-synaptic excitatory and feed-forward inhibitory synaptic inputs to CA1 pyramidal neurons. We show that NA attenuates both EPSCs and IPSCs, and the attenuation of excitatory inputs dramatically reduced the spike output of CA1 pyramidal neurons in current-clamp recordings. However, at higher stimulation frequencies the attenuation of the excitatory inputs becomes less pronounced, suggesting noradrenergic modulation may impose a high-pass filter on SC-CA1 synaptic transmission. Together, these findings provide further support for the notion that NA enhances signal-to-noise

at the SC-CA1 synapse. We were unable to demonstrate modulation of NMDAR function or STDP with NA, however some tentative explanations are proposed.

2.2 Materials and methods

2.2.1.1 Ex vivo slice preparation

Isolated transverse hippocampal slices were prepared from male (P21-P70) C57BL/6J mice. Following cervical dislocation, brains were immediately removed and immersed in ice-cold sucrose-based cutting solution containing the following (in mM): 205 sucrose, 10 glucose, 26 $NaHCO_3$, 2.5 KCl, 1.25 NaH_2PO_4, 0.5 $CaCl_2$, and 5 $MgSO_4$. Individual hippocampi were excised from the brain, mounted on agar and 400 µm transverse slices (dorsal only) were cut using a VT1200 vibratome (Leica). Following dissection and slicing, slices were transferred to aCSF containing the following (in mM): 119 NaCl, 10 glucose, 26 $NaHCO_3$, 2.5 KCl, 1 NaH_2PO_4, 1.3 $MgSO_4$, and 2.5 $CaCl_2$, maintained at ~35°C for 30 min, and then stored at room temperature. Slices were left for a minimum of 1 h after dissection before recordings were made. All solutions were saturated with 95% O_2 and 5% CO_2 and all experiments were performed in accordance with Home Office guidelines (UK Animal Scientific Procedures Act (1986)) as directed by the University of Bristol Home Office Licensing Team.

2.2.2 Electrophysiological recordings and analysis

Slices were submerged in a custom-designed recording chamber perfused at 2-4 ml/min with aCSF (as above) at 31-32°C, heated via an inline heating system (TC-324, Warner Instruments). CA1 pyramidal cells were visualised using infrared-differential interference contrast (DIC) optics on an Olympus BX-50WI microscope. Flow rate was maintained by a 101U/R peristaltic pump (Watson Marlow) and aCSF was removed via a Dymax 5 vacuum pump (Charles Austin).

Patch electrodes with a resistance of 2–8 MΩ were pulled from borosilicate filamented glass capillaries (1.5 OD x 0.86 ID x 100 L mm, Harvard Apparatus) using a vertical puller (PC-10, Narishige) or horizontal puller (P-87, Sutter Instruments). Table 1 summarises the intracellular solutions and their associated experiments used in this PhD.

Experiment	***Recording configuration***	***Intracellular composition***	***Estimated liquid junction potential***
Synaptic currents (EPSCs, IPSCs, sEPSCs and sIPSCs)	Voltage-clamp	130 $CsMeSO_3$, 4 NaCl, 10 HEPES, 0.5 EGTA, 10 TEA, 2 Mg-ATP, 0.5 Na-GTP, 1 QX-314, pH 7.4, 280-290 mOsm.	14.8 mV
sAHP currents	Voltage-clamp	117 $KMeSO_3$, 8 NaCl, 10 HEPES, 0.2 EGTA, 4 Mg-ATP, 0.3 Na-GTP, 1 MgCl, pH 7.4, 280-290 mOsm	13.5 mV
Compound EPSP decays	Current-clamp	120 $KMeSO_3$, 8 NaCl, 10 HEPES, 0.2 EGTA, 4 Mg-ATP, 0.3 Na-GTP, 10 KCl, pH 7.4, 280-295 mOsm	12.1 mV
Spike probability Rheobase (Chapter 4)	Current-clamp	125 K-Gluconate, 5 NaCl, 10 HEPES, 0.2 EGTA, 4 Mg-ATP, 0.3 Na-GTP, 1 $MgCl_2$, pH 7.4, 280-290 mOsm	14.8 mV
STDP	Voltage-clamp		

Table 1: *Intracellular recording solutions and their associated experiments.*

Whole-cell patch-clamp recordings from CA1 pyramidal neurons were obtained using an AxoPatch 200B amplifier (Molecular Devices), and the current signals were filtered at 2 or 5 kHz (synaptic currents) or 1 kHz (sAHP currents), and digitised at 10 kHz (synaptic recordings) or 50 kHz (spike probability and rheobase recordings) using a CED Power 1401 data acquisition board and Signal acquisition software (version 5.11, Cambridge Electronic Design).

Series resistance was monitored throughout the experiments and synaptic recordings were rejected from analysis if the series resistance (R_{Ser}) increased by more than 30% or was >35 MΩ (synaptic experiments) or 60 MΩ (sAHP experiments). For all recordings, a stable 10 minute baseline was achieved prior to a 10 minute drug application. Liquid junction potential was not corrected for, but the estimated values were calculated using the JPCalc tool in pClamp (version 10.3, Barry, 1994) and these are outlined for each intracellular solution in Table 1.

Electrophysiological recordings were analysed on-line using Signal software or offline using MATLAB 2017a or Microsoft Excel. For all recordings (except spike probability experiments) consecutive traces were averaged together to produce a mean response every minute. For spike probability experiments, traces were analysed individually, and

the extracted parameters were averaged together to generate minute averaged data. Data are plotted as the mean ± standard error of the mean (SEM). Data was tested for normality before appropriate statistical tests were carried out in GraphPad 7. *, **, *** and **** denote $p < 0.05$, 0.01, 0.001 and 0.0001, respectively. Traces and graphs were generated in GraphPad Prism 7 and MATLAB 2017a.

2.2.3 Synaptic current recordings

For voltage-clamp synaptic experiments, cells were clamped near the $GABA_A$ reversal potential (E_{GABAA}, -60.7 ± 2.9 mV, n = 7) or the glutamate reversal potential (E_{Glut}, +3.4 ± 2.0 mV, n = 5) to isolate EPSCs and IPSCs, respectively. At -65 mV $GABA_AR$ channels are open but no net flux occurs across these channels, isolating EPSCs (Figure 2.2, left). Conversely, at +3 mV there is no net flow across glutamate receptor channels, thus isolating IPSCs (Figure 2.2, right). These reversal potential values were obtained by isolating $GABA_AR$ transmission (using 20 µM NBQX and 50 µM D-AP5) or glutamate transmission (using 50 µM PTX and 1 µM CGP-55845) and stimulating the *stratum radiatum* Schaffer-collateral inputs to CA1 with a monopolar electrode. The stimulation intensity was adjusted to achieve current amplitudes of 50-150 pA (EPSCs) or 200-400 pA (IPSCs).

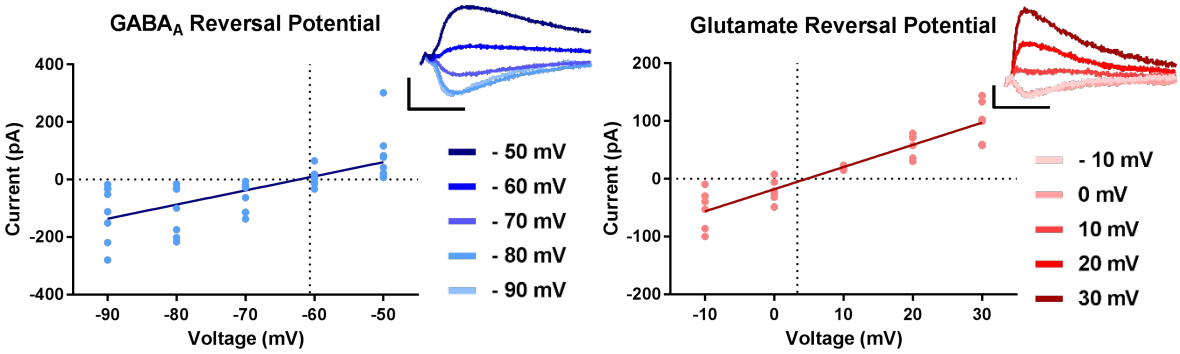

Figure 2.2: *Experimental set-up for recording EPSCs and IPSCs. Reversal potentials for $GABA_A$ (left, n = 7) and glutamate receptors (right, n = 5). Scale bars = 200 pA and 100 ms ($GABA_A$ reversal trace), 50 pA and 100 ms (glutamate reversal trace).*

To examine the effects of NA on synaptic transmission and short-term plasticity at the SC-CA1 synapse, SC synaptic responses were evoked with a train of five 100 µs square voltage pulses delivered by a Digitimer D2SA isolated stimulator every 10 seconds through a monopolar stimulating electrode located in the CA1 *stratum radiatum* layer (Figure 2.3). The stimulation intensity was adjusted to evoke current amplitude of 50-150 pA (EPSCs) or 200-400 pA (IPSCs), and the stimulation frequency cycled between 1, 10 and 50 Hz, and minute averages for each frequency were generated for analysis. In all experiments examining CA1 $GABA_AR$ IPSCs, the AMPAR antagonist NBQX (20 µM) was applied to confirm IPSCs were generated by feed-forward inhibition resulting from SC stimulation and not direct stimulation of the interneurons. Any responses not

inhibited by ≥75% within 10 minutes of NBQX application were discarded from subsequent analysis.

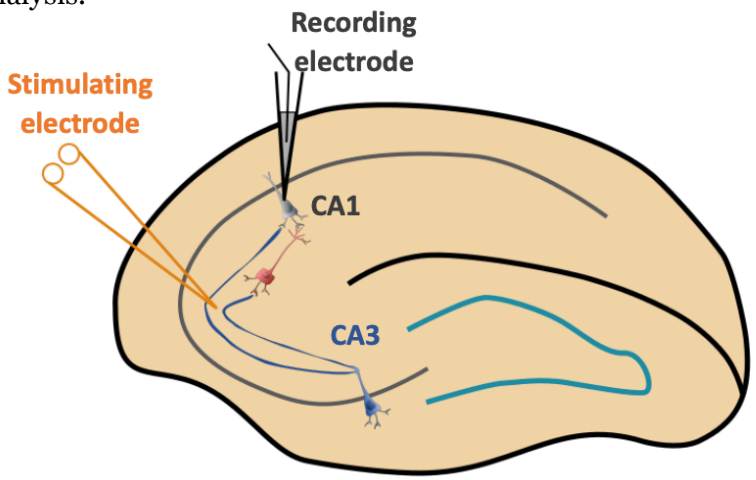

Figure 2.3: *Recording set-up for SC-CA1 EPSCs and feed-forward IPSCs.*

Online analysis used custom cursors to detect the maximum peak amplitude of the first evoked synaptic response, subtracted from the baseline taken 5 ms before the onset of the response. Amplitudes were then normalised to the average peak amplitude for the 10 minutes prior to NA application. Burst facilitation or depression was calculated as the fifth peak divided by the first peak (P5/P1) in CA1 recordings. EPSCs were typically facilitating (P5/P1 > 1, Figure 2.4A), whereas IPSCs were typically depressing (P5/P1 < 1, Figure 2.4B). For 50 Hz recordings, the fifth peak was deconvolved in MATLAB prior to P5/P1 peak analysis, with a curve fit to the decay of the fourth peak and the fifth peak amplitude subtracted from the extracted "baseline" at the fifth peak time point (Figure 2.4C, Wierenga and Wadman, 2003). Paired pulse ratio (PPR, commonly used as a proxy for determining whether the locus of a synaptic change is pre- or post-synaptic) was calculated as P2/P1 (Figure 2.4B).

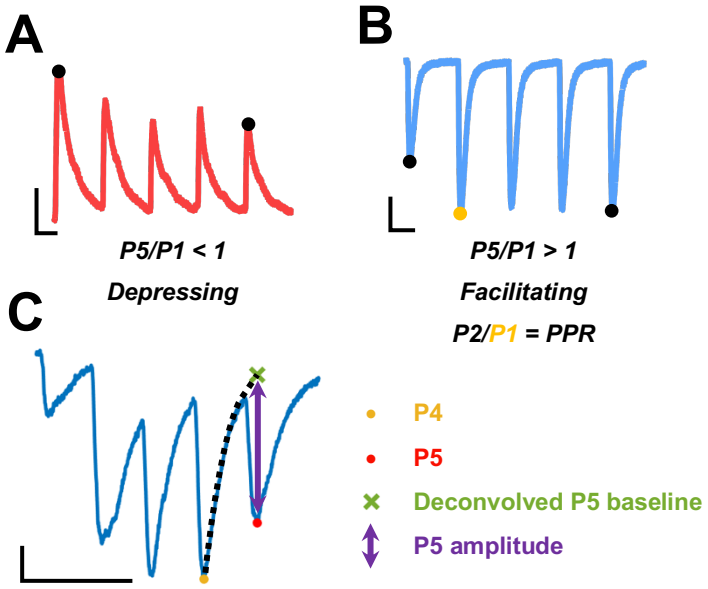

Figure 2.4: *Example traces illustrating the calculation of IPSC and EPSC short-term plasticity ratios. A) Example of depressing IPSCs at 10 Hz. B) Example of facilitating EPSCs at 10 Hz. C) Method for deconvolving the fifth peak prior to calculating the P5/P1 ratio in a 50 Hz stimulation protocol. This was done for both EPSCs and IPSCs using the same method. Scale bars = 100 pA and 50*

2.2.4 Mono-synaptic parvalbumin interneuron IPSCs

To isolate mono-synaptic parvalbumin (PV+) interneuron inputs to CA1, we crossed Ai32-ChR2 mice with PV-Cre mice to drive expression of ChR2 in parvalbumin (PV+) interneurons (Udakis *et al.,* in prep) and delivered two 5 ms 473 nm light pulses (10 Hz, 2.3 mW) to the *stratum radiatum* via the objective lens to optogenetically evoke PV+ IPSCs onto CA1 pyramidal neurons.

2.2.5 sAHP recordings

sAHP currents were elicited by somatically depolarising pyramidal cells by 70 mV from a holding potential of -50 mV for 120 ms every 20 seconds. This induced a slowly decaying (>3 seconds) current. Peak sAHP amplitudes were detected online using a cursor scripted to find the maximum peak of the sAHP current 100 ms after termination of the depolarising pulse. This time point avoided contamination from the medium after-hyperpolarisation (mAHP). This value was then subtracted from a mean baseline value taken 30 ms before the depolarising pulse (Figure 2.5).

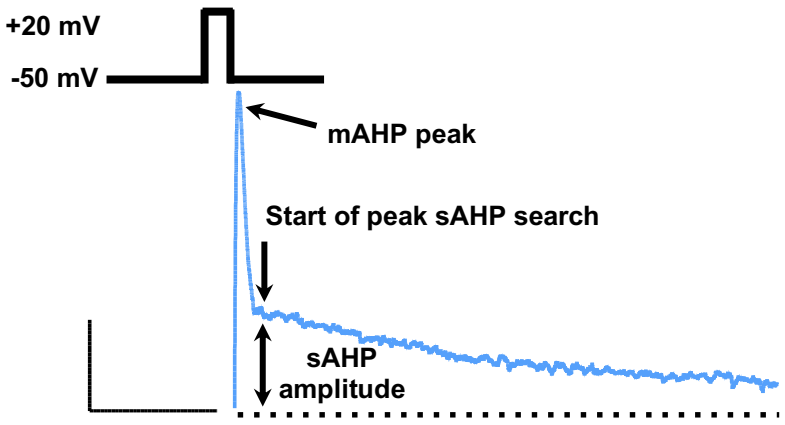

Figure 2.5: *Peak sAHP analysis. The current response to the depolarising pulse (top left inset) was digitally removed. sAHP peak detection avoided the mAHP and the baseline (dotted line) was subtracted to calculate the peak amplitude. Scale bars = 25 pA and 250 ms.*

2.2.6 Spike probability recordings

A bipolar electrode was used to deliver 10 pulses at 10 Hz to SC axons in the *stratum radiatum*, with the stimulation intensity adjusted such that approximately five of the ten EPSPs elicited a spike (i.e. spike probability (S_P) = 0.5). After a stable baseline was established,

To investigate how NA modulates CA1 spike output, 10 square voltage pulses (100 μs) at 10 Hz every 20 seconds were applied through a bi-polar electrode placed in the *stratum radiatum* layer. A bi-polar electrode was required as we were unable to generate reliable spiking using a monopolar electrode. The stimulation intensity was adjusted such that approximately five of the ten EPSPs elicited a spike (i.e. spike probability (S_P) = 0.5), to allow the spike output to either increase or decrease. In reality, this value was usually between 0.4 and 0.6. Membrane potential (V_m) and input resistance (R_{in}) using a small

hyperpolarising current injection were also measured. During recording, a threshold cursor set at 0 mV calculated the number of spikes in each sweep and divided this by 10 to obtain a raw S_P value. Minute averaged raw S_P values were normalised off-line to the 10 minute baseline prior to NA application such that the normalised baseline S_P (whether it be 0.4, 0.5 or 0.6 etc.) became 1. The reason for this is because even though a raw S_P of 0.5 was aimed for, achieving this in practice for every cell is impossible, meaning some recordings had an S_P closer to 0.4 and others closer to 0.6. Normalising the spike probability allowed us to assess the relative change with NA (i.e. 0.4 to 0.8 is a much larger relative increase than 0.6 to 0.8). Following the bath application of NA, the membrane potential (V_m) was reset to its baseline value using a somatic current injection to determine whether the effects of NA were mediated purely through resting V_m changes.

Further analysis was carried out off-line in MATLAB 2017a. Here, a custom-written MATLAB script again detected spikes when the voltage value exceeded a threshold of 0 mV and each EPSP was then sorted into "spiking" and "non-spiking" matrices (Figure 2.6A). Subsequent analysis on the "spiking" matrix calculated the dV/dT of each EPSP and the spike threshold was determined as the voltage at which 30 V/s threshold was exceeded (Figure 2.6B). Additionally, the spike latency (stimulation artefact to spike onset) was also calculated. The high P_R of SC-INT synapses, coupled with the low P_R of SC-CA1 synapses, typically means that the first EPSP in a train is usually insufficient to reach action potential threshold and trigger a spike (Dobrunz *et al.,* 1997; Wierenga and Wadman, 2003; Ali *et al.,* 2004; Sun *et al.,* 2005). This meant that it was possible to quantify synaptic input by using the first EPSP as a proxy, the script also calculated the amplitudes of the first EPSP in each sweep in the "non-spiking" matrix (Figure 2.6C).

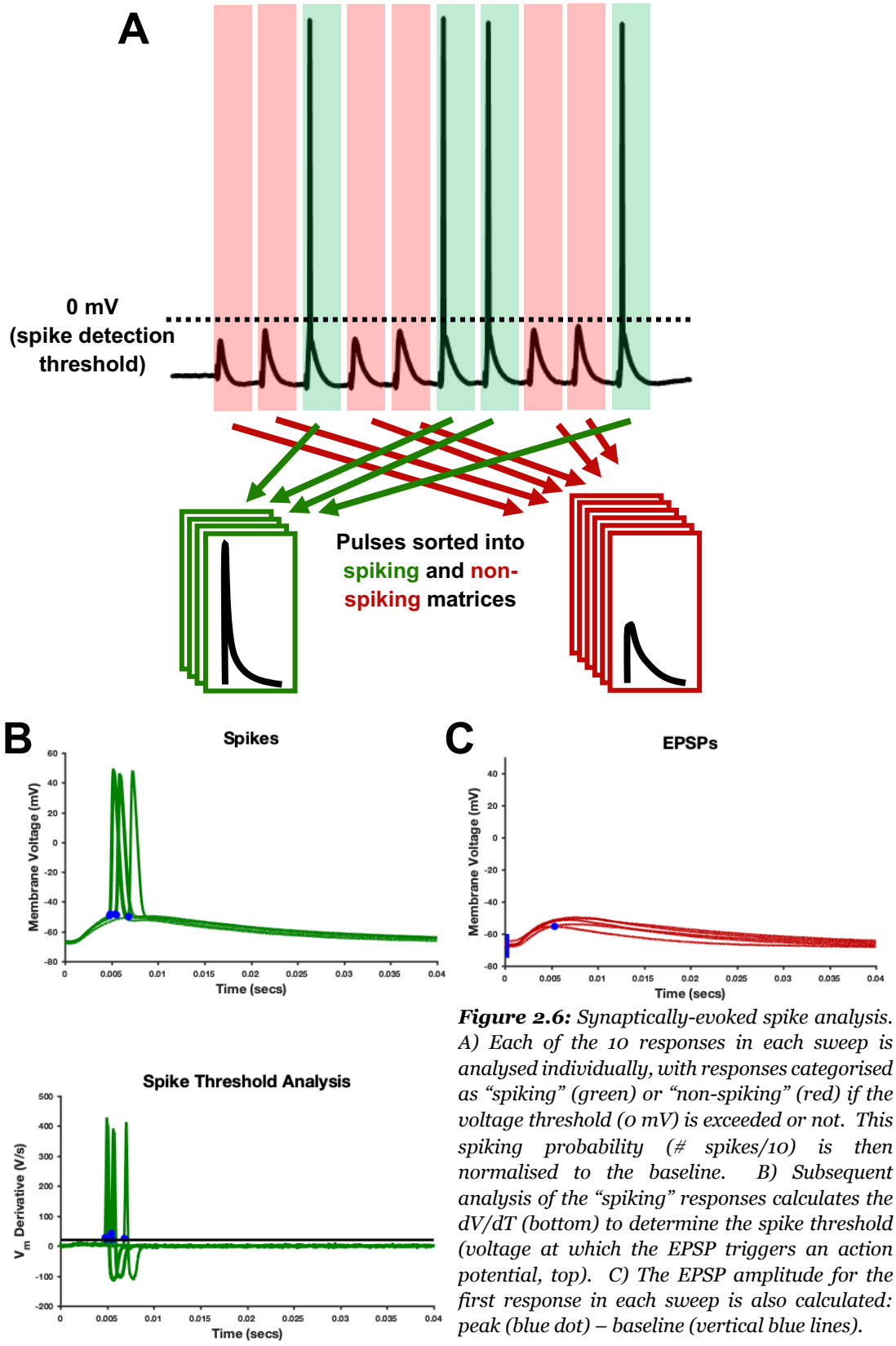

Figure 2.6: *Synaptically-evoked spike analysis. A) Each of the 10 responses in each sweep is analysed individually, with responses categorised as "spiking" (green) or "non-spiking" (red) if the voltage threshold (0 mV) is exceeded or not. This spiking probability (# spikes/10) is then normalised to the baseline. B) Subsequent analysis of the "spiking" responses calculates the dV/dT (bottom) to determine the spike threshold (voltage at which the EPSP triggers an action potential, top). C) The EPSP amplitude for the first response in each sweep is also calculated: peak (blue dot) – baseline (vertical blue lines).*

2.2.7 Compound EPSP decay

SC-CA1 compound EPSPs were elicited using a burst of five 100 μs pulses delivered to the *stratum radiatum* SC axons at 100 Hz using a bi-polar electrode. The stimulation intensity was adjusted such that pulses were sub-threshold for action potential initiation. As we saw very little modulation of the compound EPSPs with NA and apamin, the NMDAR antagonist, D-APV (50 μM), was added at the end of the recording to confirm NMDARs had been activated using this protocol. These experiments were carried out with 50 μM picrotoxin (PTX) and 1 μM CGP-55845 present in the aCSF to block $GABA_A$Rs and $GABA_B$Rs, respectively. Cells with resting membrane potentials > -60 mV were excluded from analysis.

Average traces for baseline and the final 5 minutes of NA/apamin and D-APV application were generated and a single exponential curve was fit from the fifth peak to 50 ms later to quantify the EPSP decay (Figure 2.7). Raw decay constants for baseline and drug conditions as well as NA/apamin and D-APV decay constants normalised to the baseline average trace were analysed.

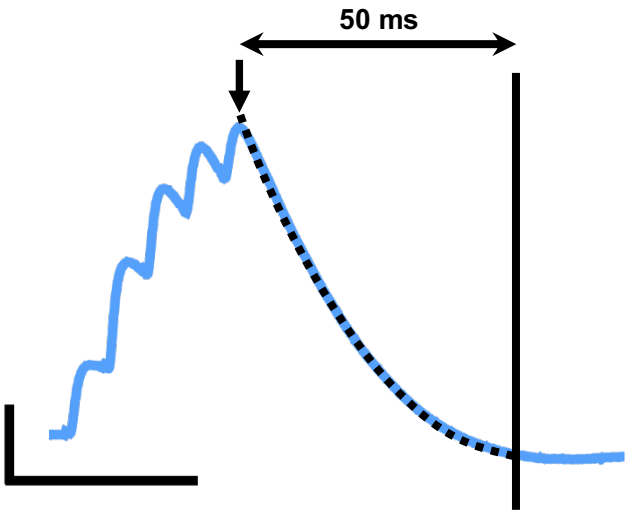

Figure 2.7: *Compound EPSP decay analysis. A single exponential curve was fit from the fifth peak to 500 ms later to calculate the decay rate of the response. Scale bars = 2.5 mV and 50 ms.*

2.2.8 STDP recordings

All STDP recordings were also carried out with 50 μM picrotoxin (PTX) in the aCSF. Bi-polar electrodes were placed in the *stratum radiatum* for both test and control pathways (Figure 2.8A), with responses evoked using a 100 μs pulse. The synaptic responses were measured in voltage-clamp. Stimulation of the test and control pathways was alternated every 7.5 seconds, giving 4 averaged responses per pathway per minute. Upon achieving a stable baseline, the recording configuration was switched to current-clamp to allow the necessary somatic action potentials in the induction protocol. The STDP protocol

consisted of 1 pre-synaptic EPSP paired with a back-propagating action potential 10 ms later (Figure 2.8B). The back-propagating action potential was induced by a 0.5 nA somatic current injection to the patched neuron. 100 of these "1 pre 1 post" pairings were delivered at 5 Hz. Induction protocols were executed within 10 minutes of breaking into the patched neuron to prevent wash-out of LTP machinery. For this reason, the baseline for normalisation was 5 minutes rather than the 10 minutes used in the aforementioned EPSC and IPSC experiments. Recordings were excluded if the control pathway amplitude or R_{Ser} increased or decreased by more than 30% during the course of the experiment.

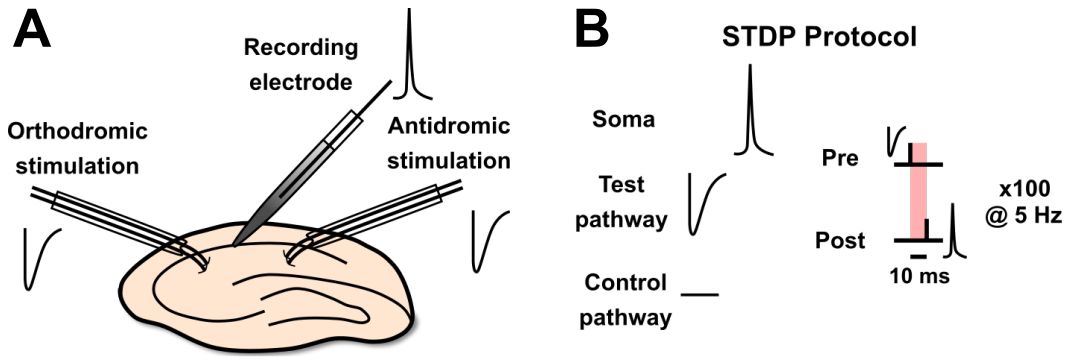

Figure 2.8: *STDP set-up and protocol. A) Bi-polar electrodes were placed in the stratum radiatum to stimulate test and control pathways. B) STDP induction protocol consisted of 100 pairs of pre-synaptic EPSPs followed 10 ms later by a somatically-induced back-propagating action potential.*

Our lab and others have previously shown that the "1 pre 1 post" STDP protocol does not lead to an increase in synaptic strength, as measured by EPSC amplitude (Tigaret *et al.*, 2016, 2018; Liu *et al.*, 2017). However, if a neuromodulator such as NA and ACh is present prior to STDP induction, this protocol does cause an increase in synaptic strength. We therefore perfused our slices with NA-containing aCSF while trying to patch neurons, and then switched to NA-free aCSF upon applying the STDP induction protocol. Our findings suggested that changing two variables simultaneously could be a confound, and so in subsequent experiments we kept NA-containing aCSF perfusing for the entire experiment.

2.2.9 Spontaneous EPSCs and IPSCs

Spontaneous EPSCs and IPSCs (sEPCSs and sIPSCs) were obtained in whole-cell voltage-clamp. Similar to synaptically-evoked EPSCs and IPSCs, they were isolated by holding the CA1 pyramidal neurons at E_{GABA} and E_{Glut} and recording events for one minute, respectively. NA was then bath-applied for 10 minutes and the protocol repeated. Both sEPSCs and sIPSCs were obtained in the same neuron and analysed in WinEDR (version 3.8.5, University of Strathclyde). Events were detected using template analysis (Table 2) and false positives manually removed.

Parameter	sEPSCs	sIPSCs
Amplitude	5 pA	5 pA
Rise time	0.1 ms	0.1 ms
Decay time	3 ms	10 ms

Table 2: *Template values for sEPSC and sIPSC detection.*

2.2.10 Drugs

DL-noradrenaline hydrochloride and picrotoxin (PTX) were purchased from Sigma-Aldrich. Apamin was purchased from Tocris. NBQX di-sodium salt, CGP-55845 and D-APV were purchased from HelloBio. Fresh stock solutions of NA were made up every day in dH_2O and stored on ice. PTX, NBQX di-sodium salt, CGP-55845 and D-APV stock solutions were made up in dH_2O and stored at -20° C.

2.3 Results

2.3.1 Bath-applied NA reduces evoked excitatory and inhibitory neurotransmission at SC-CA1 synapses

Holding CA1 pyramidal cells near the experimentally-determined reversal potentials for $GABA_A$ and glutamate receptors allowed isolation of EPSCs and IPSCs evoked through SC stimulation. Bath application of 20 μM NA induced a depression of mono-synaptic SC-CA1 EPSCs and di-synaptic feed-forward IPSCs: EPSCs were depressed to 69.8 ± 5.3% of baseline amplitude (n = 11, Figure 2.9A and C) and IPSCs to 70.7 ± 8.9% (n = 7, Figure 2.9A and C). These reductions were significantly different to time-matched control EPSCs and IPSCs (90.9 ± 4.6% and 110.4 ± 6.0%, respectively, $p < 0.05$ and $p < 0.01$, n = 8 and 5, unpaired Student's *t*-test, Figure 2.9C). IPSCs were subsequently inhibited by 93.7 ± 1.9% with 10 μM NBQX. To ensure changes in EPSC amplitude were not due to shunting inhibition (Willadt, Nenniger and Vogt, 2013), we also repeated the EPSCs experiments in the presence of picrotoxin (50 μM). Bath-application of NA again caused a significant reduction in EPSC amplitude (68.3 ± 6.6%, $p < 0.05$, n = 3, one-sampled *t*-test, Figure 2.9B).

Intriguingly, the average peak EPSC and IPSC amplitudes after NA application showed similar levels of attenuation that were not significantly different from one another (30.2 ± 5.3% and 29.3 ± 8.9%, respectively, $p > 0.05$, unpaired Student's *t*-test, Figure 2.9D). This suggests that a possible mechanism is a pre-synaptic reduction in glutamate release from SC axons onto both CA1 pyramidal neurons and feed-forward inhibitory interneurons. Moreover, it also indicates that although NA reduces these excitatory and inhibitory inputs to CA1, the overall E/I balance is left intact.

To further examine the possible locus of this modulation, we examined the release probability of mono-synaptic EPSCs. An increase in synaptic release probability is commonly associated with a decrease in paired-pulse ratio (PPR), however we found no change in EPSC PPR in the presence of NA: 1.5 ± 0.1 at baseline vs. 1.5 ± 0.1 in the presence of 20 μM NA (n = 11, $p > 0.05$, paired Student's *t*-test, Figure 2.10A). In contrast to mono-synaptic excitatory inputs, the PPR of inhibitory inputs within a feed-forward micro-circuit is compounded by a range of factors in addition to release probability of the feed-forward interneuron (i.e. the release probability of the afferent glutamatergic fibres, the intrinsic properties of the interneuron etc.), therefore the analysis of di-synaptic inhibitory PPR is of little value and was not performed.

Next, we examined whether NA may be exerting an effect on mono-synaptic inhibitory inputs. To isolate these, we crossed Ai32-ChR2 mice with PV-Cre mice to drive expression of ChR2 in parvalbumin (PV+) interneurons (Udakis *et al.,* in prep), since PV+ interneurons are thought to be one of the major interneuron subtypes mediating

feed-forward inhibition within the SC-CA1 micro-circuit (Pouille and Scanziani, 2001; Sun *et al.*, 2014). We then delivered two 5 ms 473 nm light pulses (10 Hz, 2.3 mW) to the *stratum radiatum* via the objective lens to optogenetically evoke PV+ IPSCs onto CA1 pyramidal neurons. Interestingly, NA had no effect on IPSC amplitude (94.1 ± 9.6% of baseline, n = 4, $p > 0.05$, one-sampled *t*-test, Figure 2.10B) of these responses. We also found no effect on the PPR of these responses (0.5 ± 0.1 at baseline vs. 0.5 ± 0.1 in the presence of NA, n = 4, $p > 0.05$, paired Student's *t*-test, Figure 2.10C), which implies locus of the effects on inhibition observed in Figure 2.9 may be post-synaptic (i.e. the CA1 pyramidal neuron) or result from a change in the release probability of the CA3 SC axons onto the feed-forward interneurons. It should be noted that feed-forward inhibition within the SC-CA1 micro-circuit comprises multiple interneuron subtypes, not just those expressing PV (Klausberger *et al.*, 2003, 2004; Klausberger and Somogyi, 2008). Moreover, due to the distinct spatial localisation of these different inhibitory inputs, the decay kinetics associated with IPSCs originating from different classes of interneurons can vary greatly (Klausberger and Somogyi, 2008). With this in mind, we examined the decay kinetics of electrically-evoked di-synaptic IPSCs in WT mice and optogenetically-evoked in AI32-PV mice. Decay times from PV+ interneurons were faster than those evoked in WT, however this was not significant, likely due to the low number of replicates for the PV+ IPSCs (17.4 ± 2.1 ms and 34.8 ± 5.9 ms, respectively, n = 4 and 7, unpaired Student's *t*-test, Figure 2.10D).

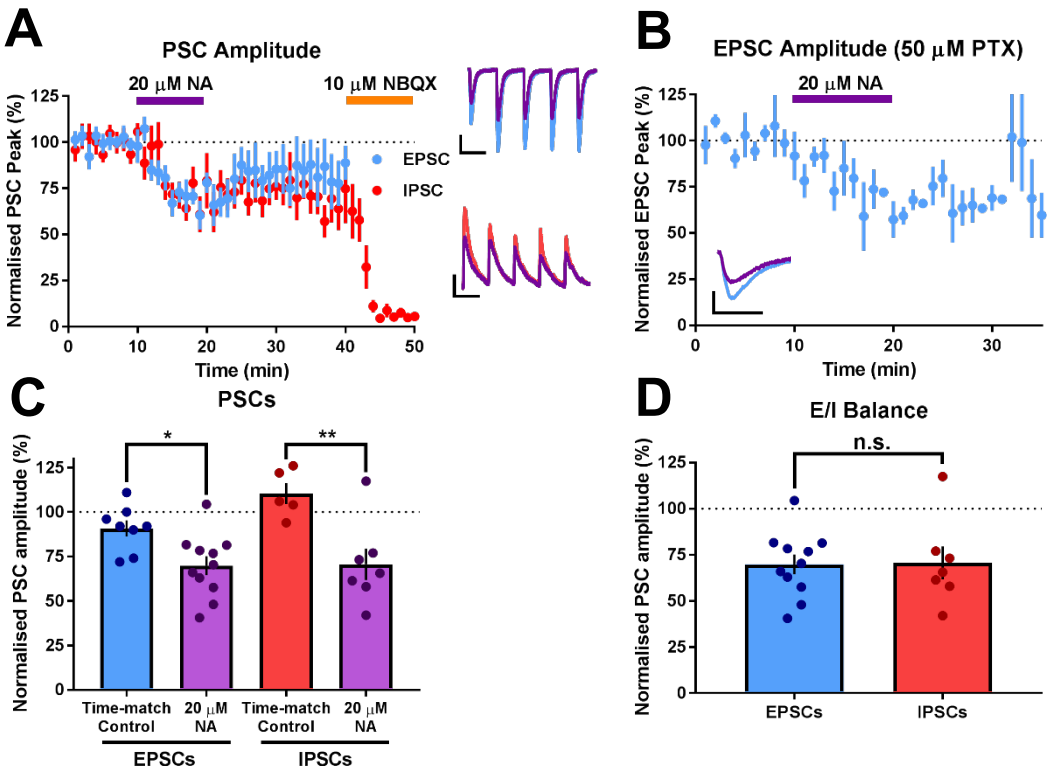

Figure 2.9: *Bath-applied NA attenuates EPSCs and feed-forward IPSCs at the SC-CA1 synapse but preserves E/I balance. A) Bath application of 20 μM NA attenuated SC-CA1 peak EPSC (n = 11) and feed-forward IPSC (n = 7) amplitudes, respectively. IPSCs were subsequently completely blocked with the glutamate receptor antagonist NBQX (20 μM), confirming their di-synaptic feed-forward nature. Insets: average traces of baseline EPSCs (blue) and IPSCs (red) and 5 minutes after NA application (purple). Scale bars = 100 pA and 100 ms (EPSCs), 50 pA and 100 ms (IPSCs). B) A similar attenuation of EPSCs was also observed when slices were bathed in 50 μM PTX throughout the recording. Scale bars = 20 ms and 25 pA. C) Summary data for A, compared to time-matched controls (EPSC control n = 8, IPSC control n = 5). D) Comparing the normalised EPSC and IPSC peak amplitudes suggests the E/I balance at SC-CA1 synapses was unaffected by NA.*

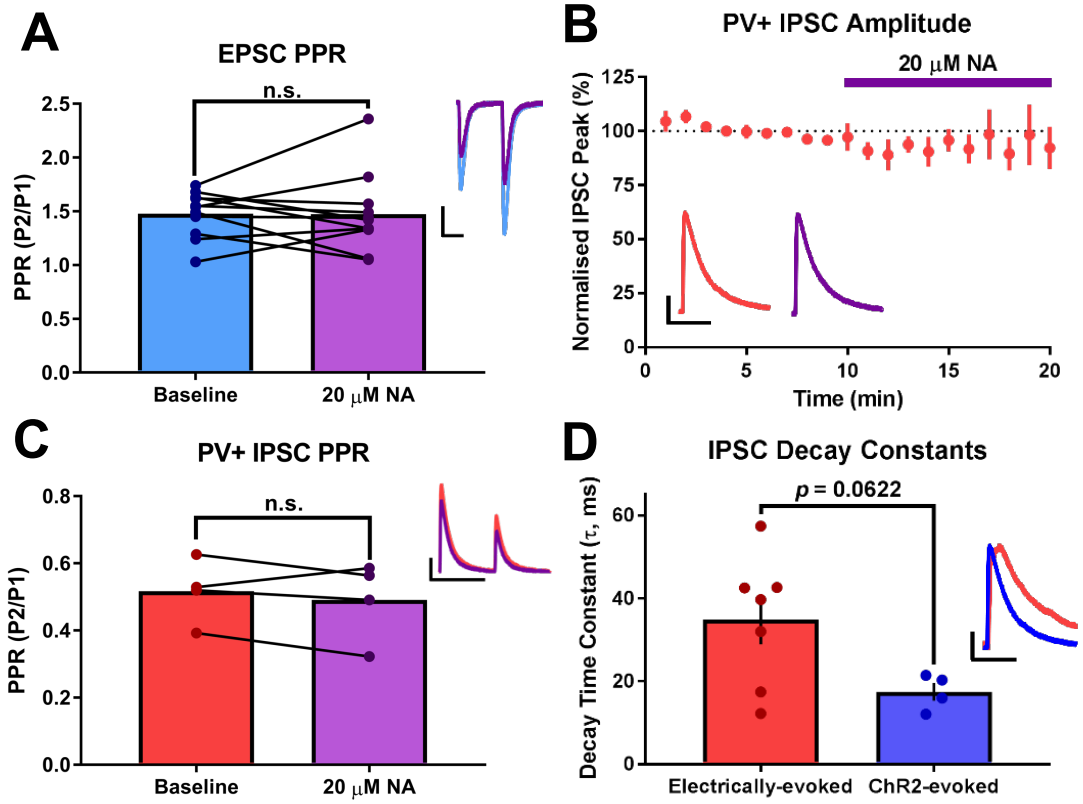

Figure 2.10: *Effects of NA on EPSC PPR and mono-synaptic PV inhibitory inputs. A) EPSC PPR was unaffected by NA (n = 11). Insets are example traces before (blue) and after (purple) NA application. Scale bars = 50 ms and 100 pA. B) IPSCs optogenetically evoked from PV+-ChR2 mice were not affected by NA (n = 4). Insets are example traces before (red) and after (purple) NA application. Scale bars = 50 ms and 100 pA. C) PV+ IPSC PPR was unaffected by NA (n = 4). Scale bars = 200 pA and 100 ms. D) Electrically-evoked feed-forward IPSCs had a longer decay constant than their optogenetically-evoked counterparts, suggesting a mixed population of interneurons mediating the response. Inset shows example traces from electrically-evoked WT (red, n = 7) and optically-evoked (blue, n = 4) responses. Scale bars = 50 ms and 100 pA.*

2.3.2 NA reduces the frequency and amplitude of spontaneous IPSCs more than spontaneous EPSCs

We next examined the effects of NA on spontaneous network activity, again isolating spontaneous EPSCs and IPSCs (sEPSCs and sIPSCs) in voltage-clamp by holding CA1 pyramidal neurons at the $GABA_A$ and glutamate receptor reversal potentials. In line with the higher release probability of interneuron terminals, baseline sIPSCs showed a higher average frequency than sEPSCs (sIPSCs = 4.5 ± 0.8 Hz, sEPSCs = 2.1 ± 0.5 Hz, $p < 0.05$, n = 5, paired Student's *t*-test, Figure 2.11A) and were also of greater amplitude (sIPSCs = 31.3 ± 2.0 pA, sEPSCs = 16.9 ± 1.4 pA, $p < 0.05$, n = 5, paired Student's *t*-test, Figure 2.11B).

Bath application of NA slightly reduced the average frequency of sEPSCs to 1.7 ± 0.3 Hz and the average frequency of sIPSCs to 4.5 ± 0.8 Hz. Neither of these were statistically significant ($p > 0.05$, unpaired Student's *t*-test, Figure 2.11C-D). Examining the cumulative frequencies of the inter-event interval did show a significant reduction with sIPSCs (Kolmogorov-Smirnov test, $p < 0.01$, Figure 2.11E-F) and a reduction with sEPSCs that did have a *p* value of < 0.05 but not the more stringent cut-off of $p < 0.01$.

NA also attenuated the average sEPSC and sIPSC amplitudes (sEPSC = 14.9 ± 1.1 pA, sIPSC = 27.1 ± 2.1 pA, Figure 2.12A-D), however this was only significant with sEPSCs ($p < 0.05$, paired Student's *t*-test). Interestingly, when examining the cumulative frequencies of the sEPSC and sIPSC peak amplitudes, both showed a shift towards smaller amplitude events, however only this was only significant for the sIPSCs (Kolmogorov-Smirnov test, $p < 0.001$, Figure 2.12E-F). These trends suggest lower spontaneous release of both glutamate and GABA onto CA1 pyramidal neurons.

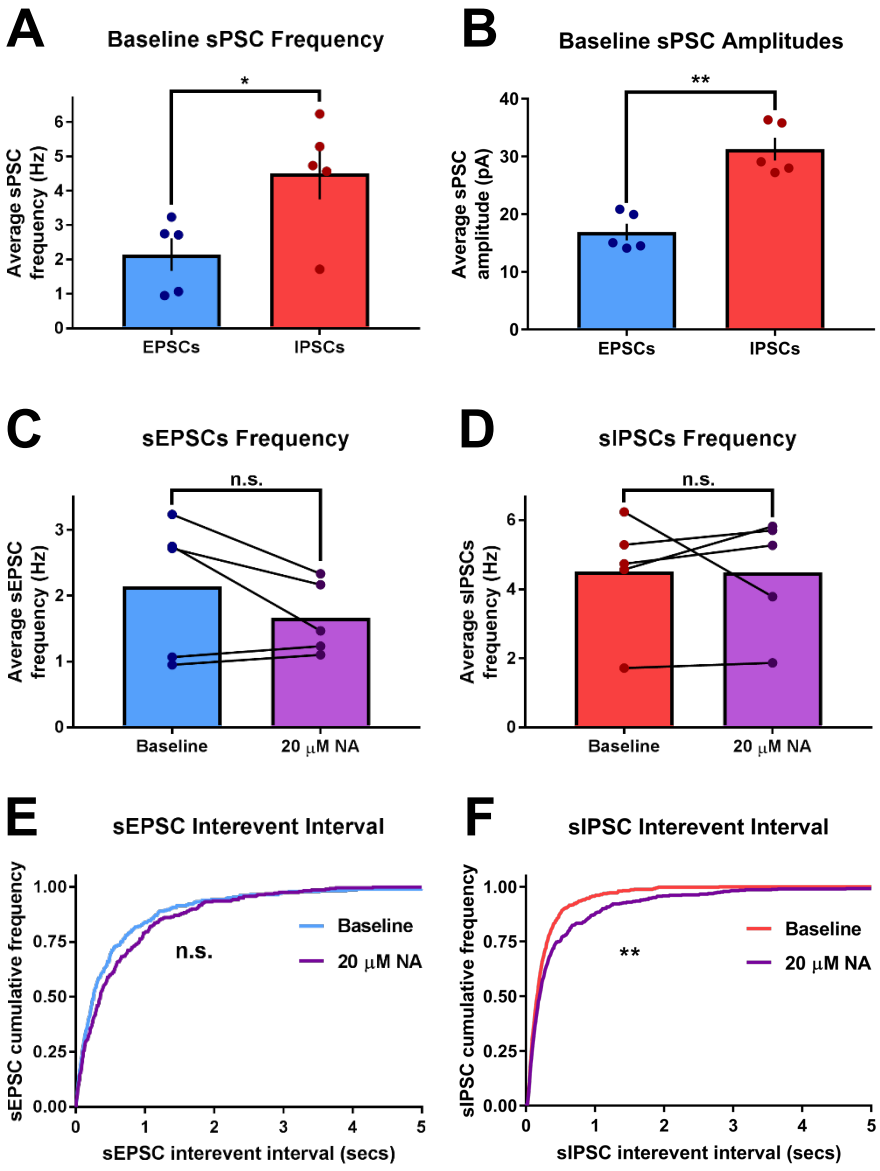

Figure 2.11: *The effects of NA on spontaneous synaptic events. A) Baseline sIPSC frequency was much higher than that of sEPSCs (n = 5). B) Baseline sIPSC amplitude was also greater than sEPSC amplitude (n = 5). C-D) The average number of spontaneous excitatory and inhibitory events was unaffected by NA. E-F) Both sEPSCs and sIPSCs showed longer inter-event intervals in the presence of NA, however this was only significant with sIPSCs.*

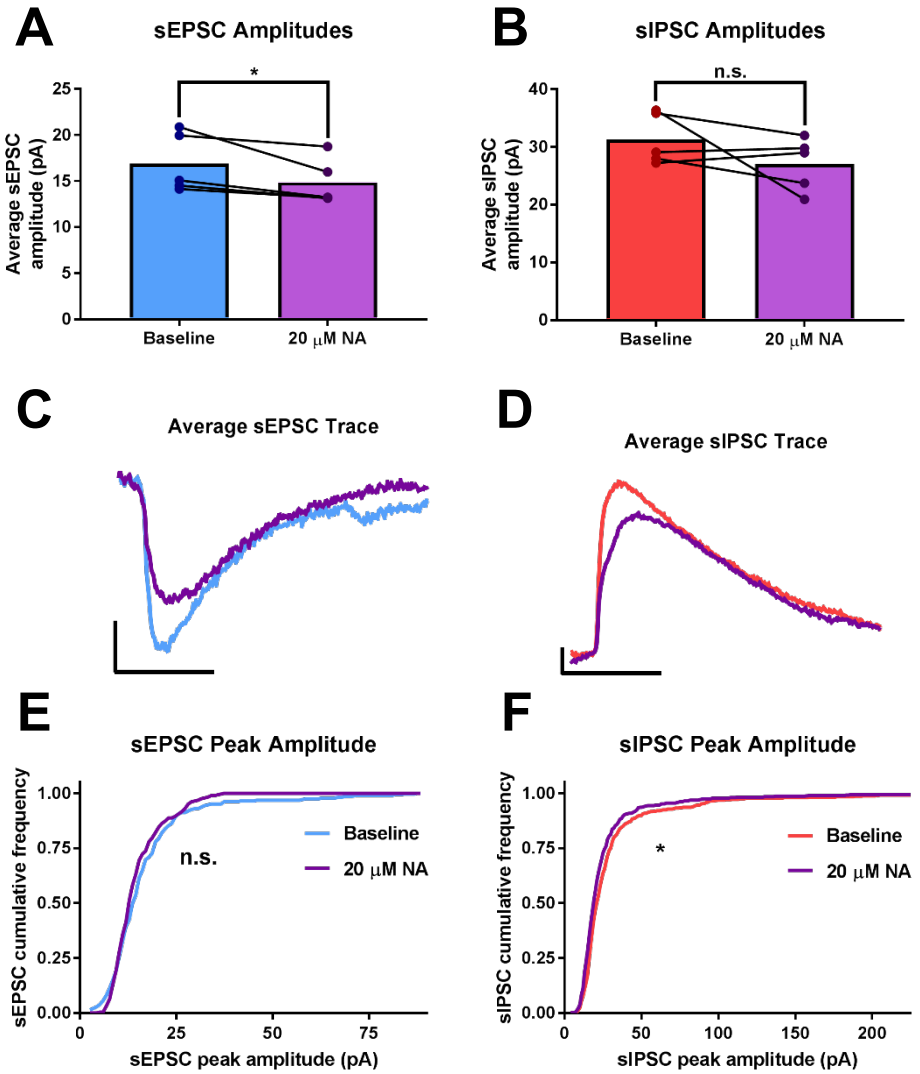

Figure 2.12: *The effects of NA on spontaneous synaptic events (continued). A-B) Average sEPSC and sIPSC amplitudes were slightly reduced by NA, however this was only significant with the former (n = 5). C-D) Average sEPSC and sIPSC traces in the present and absence of NA (n = 5). Scale bars = 5 pA and 10 ms. E-F) Both sEPSCs and sIPSCs showed a shift towards smaller amplitudes in the presence of NA, however this was only significant for sIPSCs.*

2.3.3 NA does not affect the decay kinetics of excitatory or inhibitory responses

The attenuation of EPSCs may have been caused by a change in glutamatergic receptor subtype expression or composition, and so we examined the decay constant of EPSC and feed-forward IPSC responses. However, no significant effect on the EPSC decay time constant was observed: 12.7 ± 1.2 ms at baseline vs. 15.9 ± 2.6 ms in the presence of 20 μM NA ($p > 0.05$, n = 10, paired Student's *t*-test, Figure 2.13A). Similarly, the decay times of IPSCs vary depending on the type of interneuron input, with IPSCs mediated by PV+ interneurons showing much faster decay times than those mediated by SST+ interneurons, due to their more proximal targeting of CA1 pyramidal neuron dendrites (Klausberger and Somogyi, 2008). Therefore, if NA attenuated the inhibitory responses produced by one subtype of interneuron more than another, a change in IPSC decay time may be expected. However, IPSC decay constants were also not significantly affected by NA, (34.8 ± 5.9 ms at baseline vs. 33.5 ± 7.0 ms in the presence of NA, $p > 0.05$, n = 7, paired Student's *t*-test, Figure 2.13B).

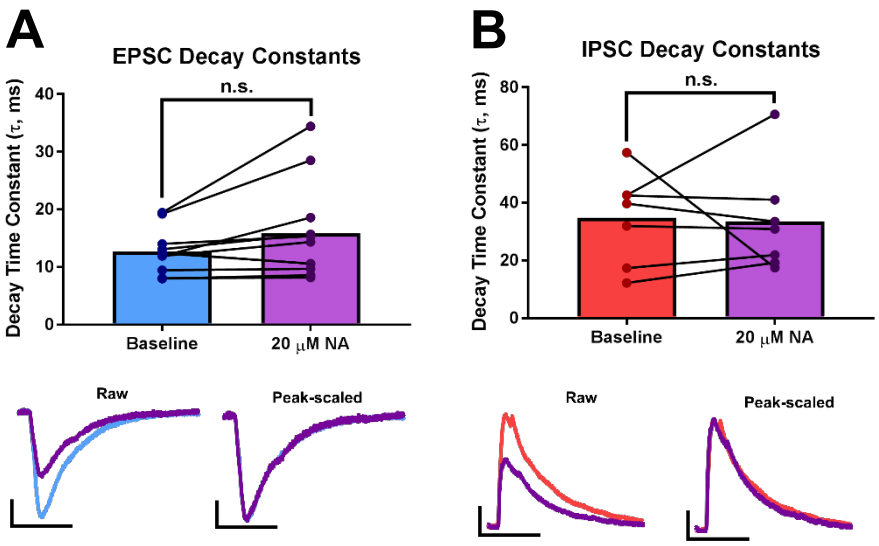

Figure 2.13: *Excitatory (A) and inhibitory (B) decay kinetics are not affected by NA. EPSC n = 10, IPSC n = 7). Insets: single EPSC and IPSC decay constants, scale bars = 25 pA and 20 ms (EPSC), 100 pA and 50 ms (IPSC).*

2.3.4 NA enhances excitatory short-term plasticity at high stimulation frequencies at the SC-CA1 synapse, but leaves inhibitory plasticity unaffected

Due to the low release probability at glutamatergic synapses, SC-CA1 EPSCs typically facilitate when repeatedly stimulated (Dobrunz *et al.,* 1997; Sun *et al.,* 2005). Conversely, inhibitory inputs typically depress, due to the high initial release probability of their afferent SC axons which become depleted over successive stimuli (Wierenga and Wadman, 2003; Sun *et al.,* 2005). We therefore stimulated SC axons with three stimulation frequencies (1, 10 and 50 Hz) to examine the basal short-term plasticity of both excitatory and feed-forward inhibitory synapses, and how these may be affected by NA.

Unsurprisingly, EPSCs did not facilitate at 1 Hz (burst ratio (P5/P1) = 106.0 ± 4.0%, n = 9, $p > 0.05$, one-sampled *t*-test, Figure 2.14A), however significant facilitation was observed at 10 Hz (143.7 ± 10.7%, $p < 0.05$, n = 9, two-way ANOVA with Dunnett's multiple comparison test), which became even more apparent at 50 Hz (174.5 ± 18.0, $p < 0.001$, n = 9, two-way ANOVA with Dunnett's multiple comparison test). Unlike excitatory synapses, IPSCs showed some depression at 1 Hz (85.0 ± 3.9%, n = 7, $p < 0.01$, one-sampled *t*-test, Figure 2.14C), and this attenuation did become slightly more pronounced at 10 Hz (71.2 ± 8.0%, n = 7, $p < 0.05$, two-way ANOVA with Dunnett's multiple comparison test) and at 50 Hz (59.7 ± 16.8%, $p < 0.01$, n = 7, two-way ANOVA with Dunnett's multiple comparison test).

We next examined whether the short-term plasticity was affected by NA. EPSC burst ratios at 1 and 10 Hz in the presence of 20 μM NA (111.6 ± 8.9% and 149.7 ± 12.6%, respectively, n = 9) were not significantly different from that observed at baseline ($p > 0.05$, two-way ANOVA with Sidak's multiple comparison test, Figure 2.14B). However, at 50 Hz the burst ratio was significantly greater than baseline facilitation (261.6 ± 40.0%, n = 9, $p < 0.0001$, two-way ANOVA with Sidak's multiple comparison test). At 1 Hz and 10 Hz, IPSC burst ratios were not significantly different from baseline ratios in the presence of NA (85.4 ± 6.9% and 73.8 ± 9.7%, respectively, $p > 0.05$, n = 7, two-way ANOVA with Sidak's multiple comparison test, Figure 2.14D). At 50 Hz, the depression of the IPSC burst ratio was slightly less than that observed at baseline, but this was not significant (73.6 ± 18.0%, $p > 0.05$, n = 7, two-way ANOVA with Sidak's multiple comparison test).

To further investigate potential changes in the excitatory/inhibitory balance of each response in the burst, the charge transfer (integral) of each pulse burst was analysed and normalised to the first response in each condition. No difference in the normalised charge transfer of EPSCs or IPSCs was observed at 1 Hz and 10 Hz ($p > 0.05$, two-way repeated measures ANOVA with Sidak's multiple comparisons test, n = 9 and 6,

respectively, Figure 2.14E-F). However, at 50 Hz there was significantly greater charge transfer from the third EPSC pulse in the burst onwards in the presence of NA ($p < 0.0001$, $p < 0.001$ and $p < 0.01$ for peaks 3 to 5, compared to the first peak, respectively, two-way repeated measures ANOVA with Sidak's multiple comparisons test, n = 9, Figure 2.14G). No change was observed with the IPSC charge transfer ($p < 0.05$, two-way repeated measures ANOVA with Sidak's multiple comparisons test, n = 6, Figure 2.14E-G)

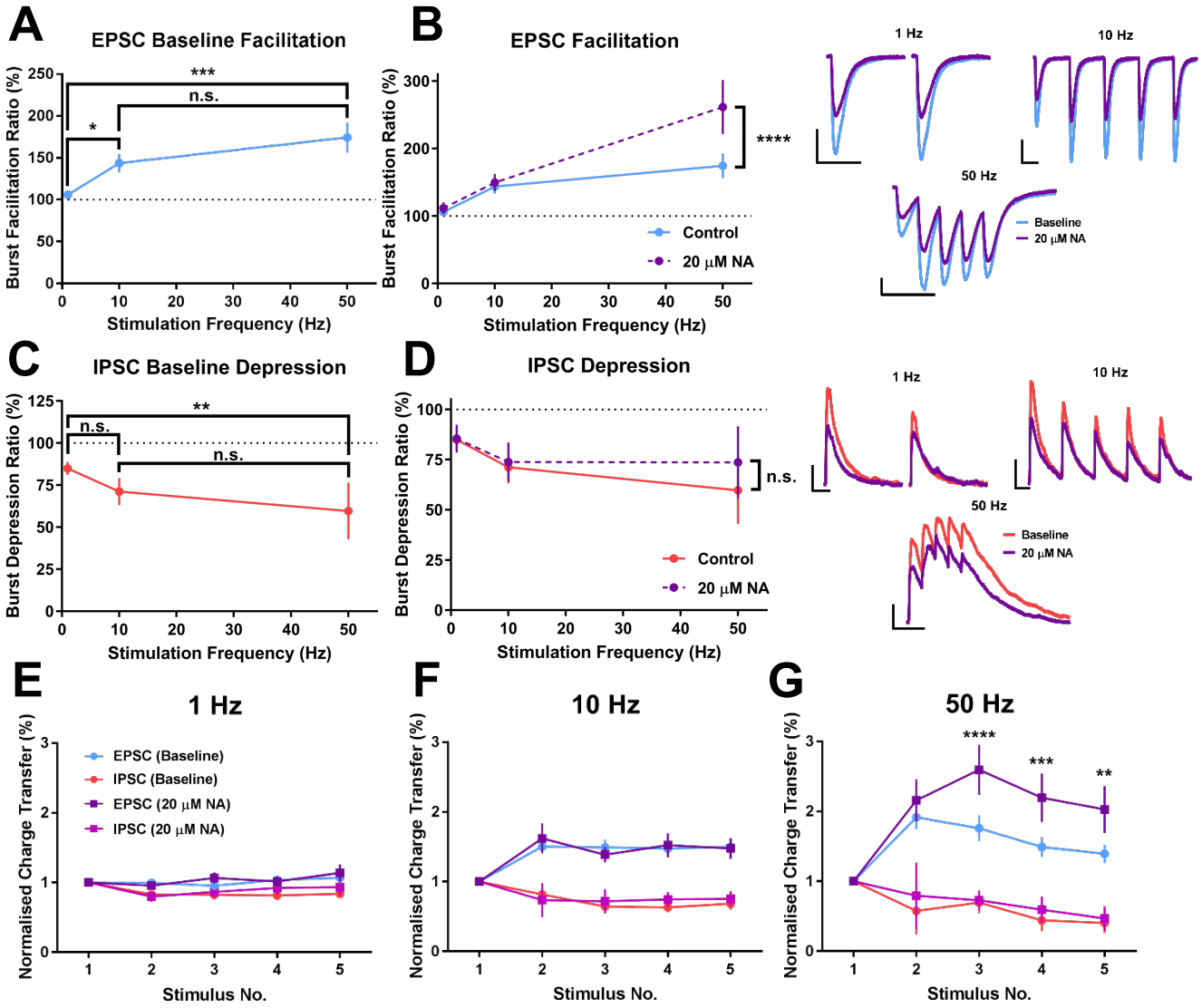

Figure 2.14: *NA selectively modulates the short-term dynamics at the SC-CA1 synapse. A-B) Excitatory SC-CA1 synapses show frequency-dependent facilitation that is enhanced in the presence of NA (n = 9). Insets show example traces for all frequencies, scale bars = 100 pA and 50 ms (n = 7). C-D) Feed-forward inhibitory dynamics at the SC-CA1 synapse are not modulated by NA (n = 6). Insets show example traces for all frequencies, scale bars = 100 pA and 50 ms. E-G) Normalised charge transfer at excitatory or feed-forward inhibitory synapses is not affected by NA at 1 and 10 Hz, however at 50 Hz the balance tips in favour of excitation later in the burst (n = 9).*

2.3.5 NA attenuates spike output via a reduction in SC synaptic input

Given the attenuation of both excitatory EPSCs and feed-forward inhibitory IPSCs, we decided to examine how these changes in synaptic inputs affected the spike output of CA1 pyramidal neurons. Neuronal spike output is reflective of the integrative computations performed by a given neuron and can be influenced by both the synaptic inputs it receives as well as the neuron's own intrinsic excitability. We therefore designed our experiment to allow simultaneous interrogation of intrinsic properties, synaptic input and spike output in the whole-cell patch-clamp configuration. The average baseline resting V_m and input resistance (R_{in}) values were -65.1 ± 2.4 mV and 89.9 ± 10.4 MΩ, respectively. Bath application of 20 μM NA completely abolished the normalised S_P to 0.11 ± 0.10 (Figure 2.15A-C, $p < 0.01$, one-way ANOVA with Dunnett's multiple comparison test, n = 5). Concurrent with this reduction in spike output was a hyperpolarisation of CA1 pyramidal neurons by 2.06 ± 1.31 mV (Figure 2.15D), however we believe this was not the primary cause of the reduction in normalised S_P for two reasons: a) this hyperpolarisation was not statistically significant ($p > 0.05$, one-sampled *t*-test), and b) injecting current to reset the membrane potential back to that seen before NA application (V_m reset) did not recover the S_P (0.18 ± 0.12, $p < 0.01$, one-way ANOVA with Dunnett's multiple comparison test, Figure 2.15A-C). In agreement with our voltage-clamp recordings the amplitude of the first EPSP was significantly reduced (77.2 ± 3.8% of baseline, $p < 0.01$, one-sampled *t*-test, Figure 2.15F) and this did not recover with the V_m reset, suggesting the primary cause of the reduced spike output was a reduction in excitatory SC synaptic input, despite a similar reduction in feed-forward inhibition. NA also slightly reduced input resistance by 1.9 ± 4.2 MΩ, but this was not significant ($p > 0.05$, one-sampled *t*-test, Figure 2.15E).

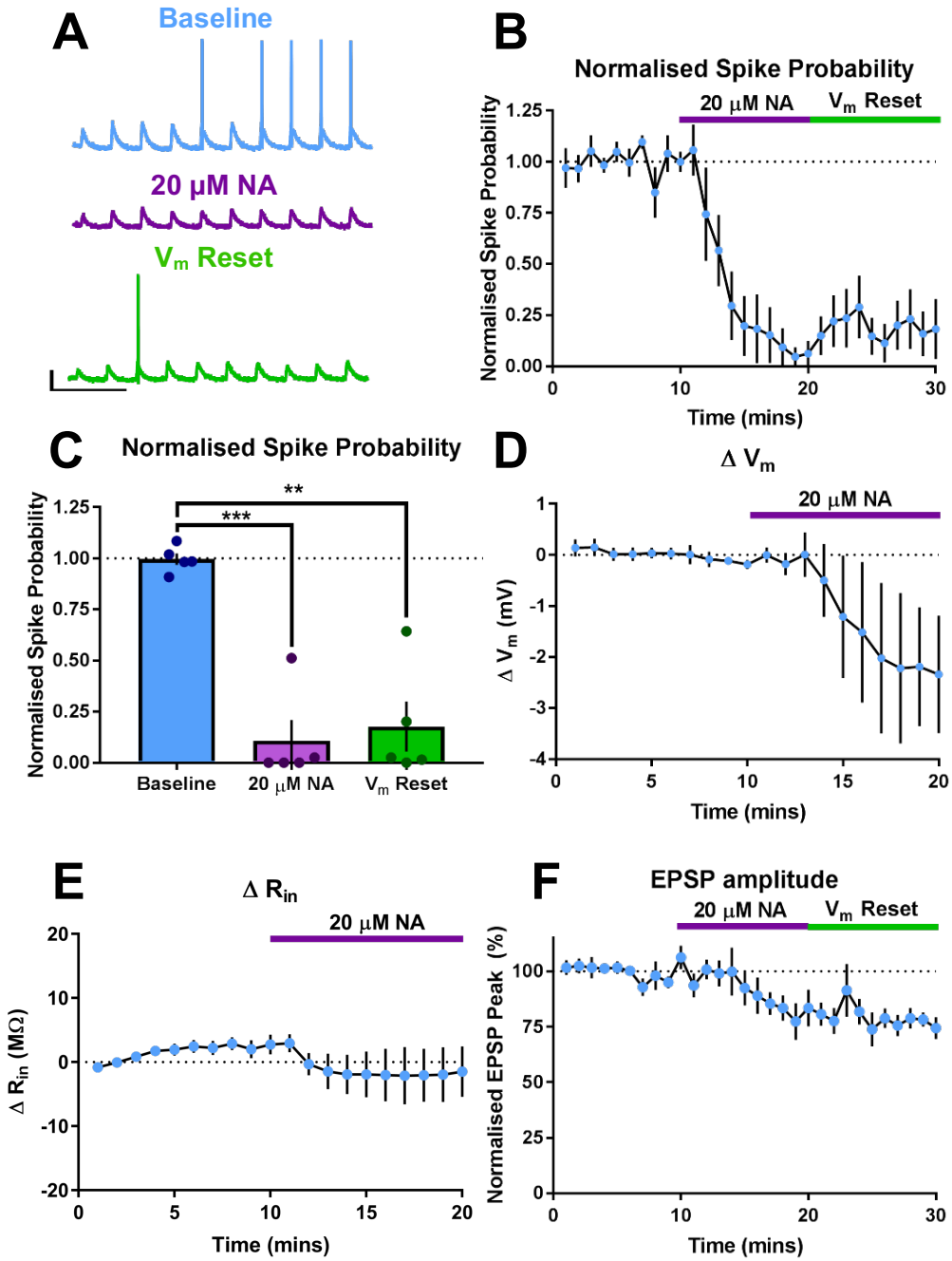

Figure 2.15: *Bath application of 20 µM NA substantially reduced CA1 spike output. A-C) 20 µM NA attenuated CA1 spike output and resetting the V_m to that measured pre-NA application does not recover spiking (n = 5). Scale bars = 25 mV and 250 ms. D-E) 20 µM caused a non-significant hyperpolarisation of CA1 neurons and a decrease in R_{in}. F) Synaptic input was also reduced by 20 µM NA and did not recover with a V_m reset.*

2.3.6 The sAHP is strongly attenuated by NA

We next sought to examine the role of NA in modulating several neuronal mechanisms implicated in LTP. The sAHP, mediated by slowly inactivating Ca^{2+}-activated K^+ channels, is an important regulator of neuronal excitability (Andrade, Foehring and Tzingounis, 2012) and has been implicated in LTP (Bond *et al.*, 2004; Ngo-Anh *et al.*, 2005; Hammond *et al.*, 2006; Bloodgood and Sabatini, 2007; Lin *et al.*, 2008, 2010). The sAHP current occurs in the aftermath of intense pyramidal cell firing (either due to

temporally fast synaptic input or a strong depolarising current injected to the soma) and acts to reduce or prevent further firing for several seconds. Inhibition of this current by NA is well-documented (Madison and Nicoll, 1982, 1986; Haas and Konnerth, 1983; Dunwiddie *et al.*, 1992; Sah and Isaacson, 1995) and bath application of 20 μM NA in our set-up also yielded a similar attenuation of the peak sAHP amplitude to 10.2 ± 8.0 % of baseline. A time-matched control showed that the sAHP did run down over time (84.8 ± 2.2% of baseline after 20 minutes, Figure 2.16A-C), however the reduction seen with NA was still significantly larger (p < 0.0001, unpaired Student's t-test, n = 6 and 4, respectively).

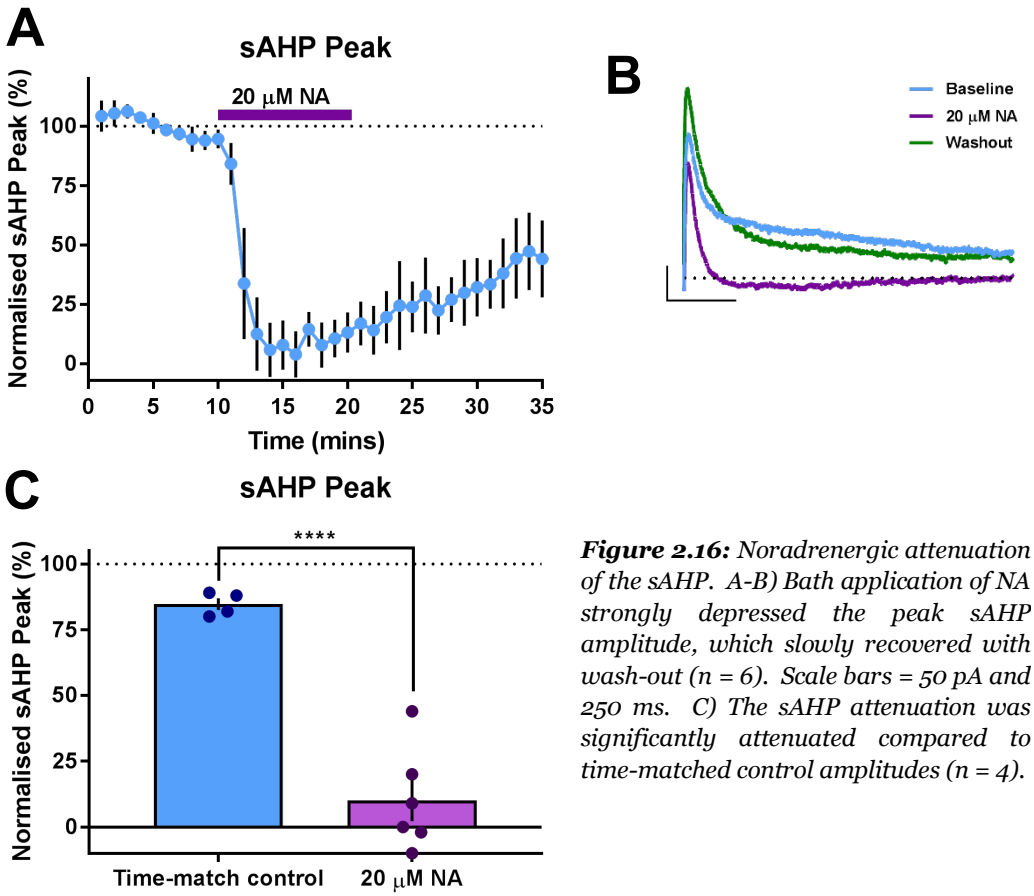

Figure 2.16: *Noradrenergic attenuation of the sAHP. A-B) Bath application of NA strongly depressed the peak sAHP amplitude, which slowly recovered with wash-out (n = 6). Scale bars = 50 pA and 250 ms. C) The sAHP attenuation was significantly attenuated compared to time-matched control amplitudes (n = 4).*

2.3.7 NA does not affect NMDAR function

We next examined whether NA could modulate SK regulation of NMDARs in a manner similar to ACh (Buchanan *et al.*, 2010). If NA positively modulates NMDAR function, the decay constant of compound EPSPs would be expected to increase. Baseline resting V_m for these experiments was -66.1 ± 0.7 mV (n = 21). Surprisingly, bath application of NA actually reduced the compound EPSP decay constant from 44.2 ± 4.5 ms to 38.4 ± 5.1 ms, however this change was not significant (p > 0.05, repeated measures Friedman ANOVA with Dunn's multiple comparison test, n = 11, Figure 2.17A and C). Normalising the decay to the baseline average also showed no change (86.7 ± 7.2% of baseline, p > 0.05, one-sampled t-test, Figure 2.17B and D). To confirm this protocol could detect changes in NMDAR function, we subsequently co-applied an NMDAR antagonist, D-AP5

(50 μM) to the NA-containing aCSF perfusate. This significantly reduced the raw compound EPSP decay constant to 25.5 ± 3.7 ms (p < 0.001, repeated measures Friedman ANOVA with Dunn's multiple comparison test, Figure 2.17A and C) and the normalised EPSP decay constant (60.4 ± 8.0% of baseline, p < 0.001, one-sampled t-test, Figure 2.17B and D).

To test whether NMDAR function could be enhanced by direct SK channel inhibition (as in Buchanan *et al.,* 2010), we repeated the experiments and instead applied 100 nM apamin. Apamin did increase the compound EPSP decay from 36.1 ± 2.8 ms to 42.9 ± 7.9 ms, however this effect was not significant (repeated measures Friedman ANOVA with Dunn's multiple comparison test, n = 10, Figure 2.17E and G). The normalised EPSP decay also showed no significant effect (118.5 ± 16.5% of baseline, p > 0.05, one-sampled t-test, Figure 2.17F and H). Subsequent co-application of 50 μM D-AP5 again significantly attenuated the raw compound EPSP decay constant to 26.4 ± 2.5 ms (p < 0.05, repeated measures Friedman ANOVA with Dunn's multiple comparison test, Figure 2.17E and G). The normalised decay constant was also significantly reduced (74.1 ± 4.7% of baseline, p < 0.001, one-sampled t-test, Figure 2.17F and H).

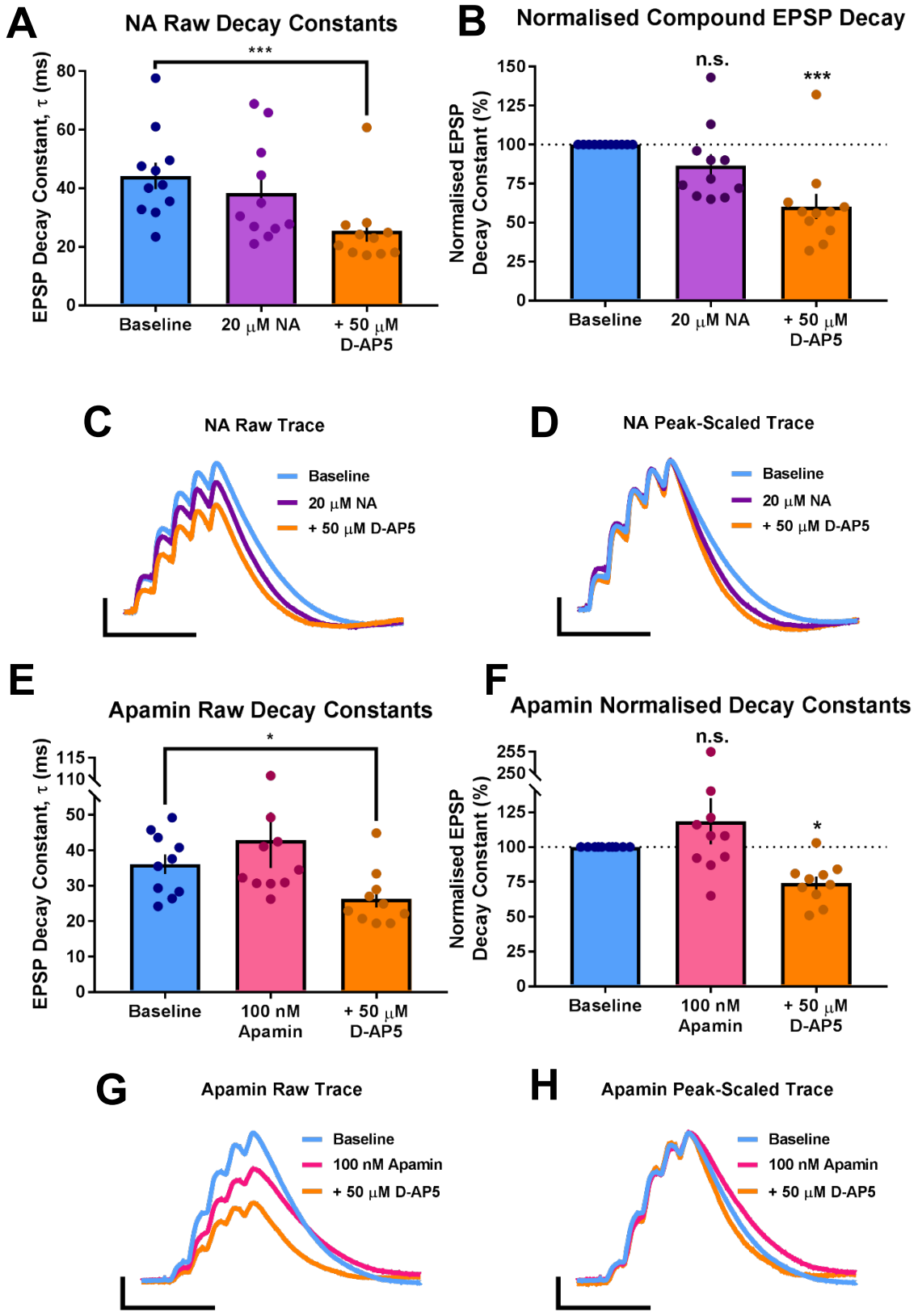

Figure 2.17: *NA and apamin do not modulate SK channels and NMDAR function. A-B) Compound EPSP raw and normalised decay constants showed a small, non-significant attenuation in the presence of NA, but were significantly reduced by the NMDAR antagonist, D-AP5 (n = 11). C-D) Raw and peak-scaled example traces, scale bars = 2.5 mV and 50 ms. E-F) Compound EPSP raw and normalised decay constants showed a small, non-significant increase in the presence of apamin, and again were significantly reduced by D-AP5 (n = 10). G-H) Raw and peak-scaled example traces, scale bars = 2.5 mV and 50 ms.*

2.3.8 NA does not affect STDP

Despite a lack of SK channel modulation, recent work has implicated a novel mechanism for enhanced STDP in the presence of NA: β-AR-mediated down-regulation of Kv1.1 channels, enhancing the capacity for back-propagating action potentials and thus widening the temporal window for STDP (Liu *et al.*, 2017). Although elegant, this STDP work did not ascertain whether such plasticity was homo- or hetero-synaptic, and thus we repeated the experiment and included a control pathway to investigate this.

In agreement with previous research (Tigaret *et al.*, 2016, 2018; Liu *et al.*, 2017), pairing 1 pre-synaptic EPSP with a back-propagating action potential 10 ms later ("1 Pre 1 Post" protocol) resulted in no change in synaptic strength (EPSC amplitude) in either the test or control pathways (test = 109.3 ± 11.3%, control = 112.5 ± 4.6%, n = 8, $p > 0.05$, unpaired Student's *t*-test, Figure 2.18A). Glutamatergic plasticity is strongly affected by intracellular dialysis, and often cannot be induced more than 10 minutes after breaking into the neuron due to the washout of LTP-related machinery. Therefore, we opted to bathe the hippocampal slices in 20 μM NA whilst patching to ensure adrenoceptors had been sufficiently activated prior to STDP induction. Slices were not exposed to NA for more than 30 minutes. Upon cessation of NA and inducing our 1 pre 1 post protocol we observed an increase in both the test and control pathways (213.6 ± 27.5% and 273.0 ± 55.0%, respectively, n = 5, Figure 2.18B). This increase was not significantly different between the two pathways ($p > 0.05$, unpaired Student's *t*-test).

To determine whether the increased EPSC amplitude in the test and control pathways was an effect of NA washout or true hetero-synaptic plasticity we repeated the experiment but did not include the 1 pre 1 post protocol, instead just allowing the neuron to remain at its resting membrane potential following the switch to NA-free aCSF. We again observed an increase in EPSC amplitude in both the test and control pathways, suggesting the aforementioned increase may have been due to NA washout (265.0 ± 52.2% and 267.9 ± 53.6%, respectively, n = 7, Figure 2.18C). There was no significant difference between the test and control pathways ($p > 0.05$, unpaired Student's *t*-test).

We next decided to repeat the STDP experiment with NA present throughout (i.e. to avoid simultaneously changing two variables), and in this case the 1 pre 1 post STDP protocol had no effect on EPSC amplitude on either the test or control pathway (152.0 ± 23.3% and 109.6 ± 10.0%, respectively, n = 12, Figure 2.18D). Once again, no significant difference between the two pathways was found ($p > 0.05$, unpaired Student's *t*-test). The results of all four experiments are summarised in Figure 2.18E.

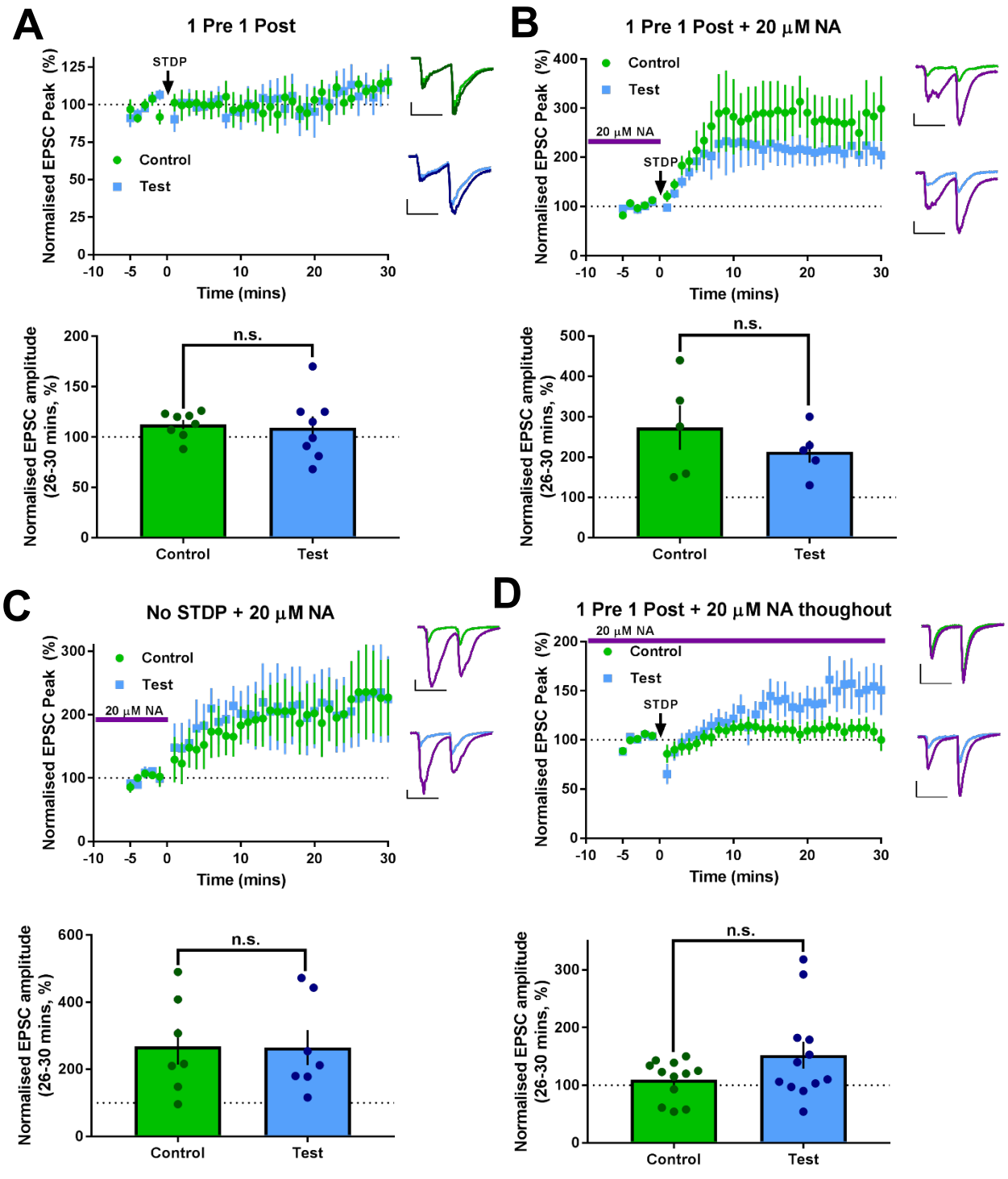

Figure 2.18: *NA does not modulate STDP at the SC-CA1 synapse. A) In agreement with previous research, the "1 pre 1 post" STDP protocol yielded no change in synaptic strength (n = 8). B) Pre-treatment with NA enhanced EPSC amplitudes in both test and control pathways (n = 5). C) No STDP protocol following NA pre-treatment also augmented EPSC amplitudes in both pathways, suggesting the previous effect may be due to NA washout (n = 7). D) Perfusing NA-containing aCSF throughout the experiment induced robust pathway-specific LTP in only a handful of cells (n = 12). All insets: average baseline traces pre-STDP and 26-30 minutes post-STDP protocol, scale bars = 100 pA and 50 ms. E) Summary data for all four conditions.*

2.4 Discussion

Using bath-applied NA, this work has investigated the noradrenergic modulation of the SC-CA1 feed-forward micro-circuit. We have explored the effects of bath-applied NA on SC EPSCs, feed-forward IPSCs, spontaneous network activity, short-term plasticity, CA1 intrinsic properties, spike output, the sAHP, NMDAR function and STDP.

2.4.1 Synaptic transmission

The effects of bath-applied NA on basal SC-CA1 synaptic transmission have typically been examined as part of broader studies looking at synaptic plasticity (Katsuki, Izumi and Zorumski, 1997; Hu *et al.*, 2007), and often in the current-clamp configuration without isolation of specific synaptic inputs (Madison and Nicoll, 1988; Doze, Cohen and Madison, 1991). Therefore, in the present study we also used voltage-clamp recordings to examine the effects of NA on the SC-CA1 synaptic components of the feed-forward micro-circuit. We show that NA attenuates both SC EPSCs and feed-forward IPSCs to a similar degree, allowing preservation of the EI balance. We were interested in keeping the networks as physiological as possible (i.e. maintaining both excitatory and inhibitory inputs to CA1), however a drawback of recording EPSCs in the absence of GABAergic antagonists carried the possibility of shunting inhibition (Willadt, Nenniger and Vogt, 2013). The reduced input resistance as a result of the inhibitory input causes current leak and attenuation of the EPSC, however shunting inhibition in voltage-clamp arising from SC stimulation is thought to be fairly weak (<10%, Wierenga and Wadman, 2003). In addition to this, the degree of EPSC attenuation in the presence of PTX was almost identical to that observed when the neuron was simply held at the $GABA_AR$ receptor reversal potential, confirming that the reduction in EPSC amplitude likely did not contain an inhibitory component.

The effects of NA on SC EPSCs have not been studied at any great length, and the results are contradictory: several studies have reported no change in the peak amplitude of evoked SC excitatory inputs in the presence of NA (Lancaster *et al.*, 2001; Hu *et al.*, 2007) whereas others have shown some attenuation (Katsuki, Izumi and Zorumski, 1997). Our results fall more in line with those reported in Katsuki, Izumi and Zorumski (1997). One key difference between the present and previous studies is that the present work was carried out in acute hippocampal slices from juvenile mice, whereas previous work typically used slices obtained from adult rats. Most adrenoceptor expression analyses have also been examined using adult rats (Jurgens *et al.*, 2005; Guo and Li, 2007; Cox, Racca and LeBeau, 2008), and although expression is likely to be similar between mice and rats, we cannot rule out different expression patterns between species and ages (Erdtsieck-Ernste, Feenstra and Boer, 1991).

The reduction in evoked IPSC amplitudes supports previous findings in the hippocampus (SC-CA1: Doze, Cohen and Madison, 1991, PP-DG: Brown *et al.*, 2005), as well as other brain regions such as the cerebellum (Carey and Regehr, 2009) and lateral amygdala (Tully *et al.*, 2007). Interestingly, where GABAergic feed-forward inputs in the lateral amygdala were directly attenuated by α2-AR-mediated hyperpolarisation of the arbitrating interneurons, attenuation of feed-forward inhibitory inputs in the CA1 may to be due to a reduction in glutamate release from SC terminals, since both excitatory and inhibitory synaptic inputs were reduced to comparable levels. However, we found no change in the PPR (a proxy for pre-synaptic release probability) of EPSCs. This finding was initially puzzling; however, NA also attenuates excitatory inputs to the central amygdala via α2-ARs, with no associated change in the PPR (Delaney, Crane and Sah, 2007). This inhibition results from a decrease in the number of active release sites with no change in release probability. A similar reduction in pre-synaptic neurotransmitter release is present in LC neurons themselves; and is also mediated by α2-autoreceptors through a G_i-coupled signalling cascade (Starke and Montel, 1973). There are several lines of evidence that would implicate the involvement of a pre-synaptic α2-AR mechanism in CA3 SC axons: α2-ARs are expressed on CA3 pyramidal neuron axons (Milner *et al.*, 1998) and epileptiform activity in CA3 can be attenuated by α2-AR activation (Jurgens *et al.*, 2005, 2007; Goldenstein *et al.*, 2009). Moreover, this anti-epileptiform activity persists even in the presence of complete GABAR blockade, suggesting a direct effect on CA3 pyramidal neurons. Whether functional α2-ARs are present on the SC axons of CA3 pyramidal neurons in acute slices remains to be determined, although autaptic excitatory currents in hippocampal cultures show attenuation via a pre-synaptically-mediated α2-AR reduction in glutamate (Boehm, 1999).

Further support for a reduction in SC glutamate release, rather than a direct effect on interneurons, is evident in the absence of modulation of mono-synaptic IPSCs elicited through optogenetic targeting of PV+ interneurons. This data supports the results in Doze, Cohen and Madison (1991), where electrically-evoked mono-synaptic IPSCs were unaffected by NA. The PPR of these inputs was also unaffected, implying either a post-synaptic effect or a reduction in interneuron recruitment by SC axons. Despite supporting previous findings, the conclusions we can draw from the present experiments are somewhat limited for three main reasons: 1) feed-forward inhibitory inputs are comprised of multiple populations and not solely PV+ interneurons (Klausberger and Somogyi, 2008; Sun, *et al.*, 2014); 2) PV+ interneurons are also part of feed-back inhibitory circuits to CA1 pyramidal neurons (Hu, Gan and Jonas, 2014); 3) the difference in decay kinetics between the electrically-evoked and the optogenetically-evoked IPSCs is approaching significance (likely due to lack of replicates), meaning we

can only claim NA does not directly affect PV+ inhibitory inputs. Repeating these experiments to increase the replicates will be of benefit, and utilising additional Cre-inducible ChR2 interneuron mouse lines such as the SST-IRES-Cre (Jackson Laboratory stock no: 013044) and CCK-IRES-Cre (Jackson Laboratory stock no: 012706) will provide a much clearer picture of the effects of NA on different interneuron populations.

2.4.2 Spontaneous network activity

Quantifying the frequency and amplitude of spontaneous (both action potential-dependent and independent) can give an idea of the basal network activity. The frequency of events per minute and the average amplitude of these events are a useful starting point. We found that the number of events was decreased for both sEPSCs and sIPSCs, but neither of these changes was significant. A clearer picture arises when the cumulative frequency is examined instead: the inter-event interval for both sEPSCs and sIPSCs is shifted to longer intervals, indicating a lower frequency. Although this is statistically significant ($p < 0.05$) in both cases, Kolmogorov-Smirnov tests are more prone to false positive errors (as the inter-cell variance is removed), however they can reveal more information regarding the distribution of event amplitude and frequency and are therefore a better measure when examining spontaneous events. Applying a more stringent statistical significance value ($p < 0.01$) means that only the change observed for sIPSCs was significant. Previous work has shown that adrenaline (not NA) actually increases the frequency of sIPSCs in the rat CA1 area (Doze, Cohen and Madison, 1991; Bergles *et al.*, 1996; Hillman *et al.*, 2005, 2009; Jurgens *et al.*, 2007). Doze, Cohen and Madison (1991) and (Bergles *et al.*, 1996) also showed that adrenaline enhances sIPSC frequency through direct depolarisation of CA1 interneurons via α1-ARs. Crucially, adrenaline is a more potent activator of α1-adrenoceptors than NA (Minneman, Theroux and Esbenshade, 1994), so these distinct results may be due to differences in 1) the relative activation of α1-ARs (due to the compound used), and/or 2) differences in α1-AR expression between mice and rats. Further, later studies (Hillman *et al.*, 2005, 2009; Jurgens *et al.*, 2007) used specific α1-AR agonists to support this idea. The use of specific agonists is useful in showing the effects of adrenoceptor subtypes but fails to capture the wider role of NA within the hippocampus. Interestingly, RT-PCR assays and patch-clamp experiments (Hillman *et al.*, 2005; Jurgens *et al.*, 2007) showed that all of the responsive interneurons were SST-expressing and predominantly based in the *stratum oriens*, with only a small population in the *stratum radiatum*. With this in mind, differences in slice orientation may also mean fewer *stratum oriens* interneurons were available for modulation in our slices.

Similar to our observations with evoked synaptic currents, we also observed a reduction in the average sEPSC and sIPSC amplitudes, however this was only statistically

significant for the former. Examining the cumulative frequency of the peak amplitudes provides a more interesting picture: in the presence of NA there was a higher frequency of smaller amplitude sEPSCs and sIPSCs. This was only significant in the latter and also at odds with results published by Bergles *et al.* (1996). Due to a number of recordings being discarded due to noise, the results of these experiments may be underpowered and therefore, more replicates of this experiment are needed. However, we can tentatively propose that NA reduces spontaneous network activity in the CA1 area of the hippocampus, but predominantly affects tonic inhibitory drive to a greater degree than it does tonic excitatory drive. Such an effect would be consistent with theories regarding the role of NA in increasing signal-to-noise (Moore and Bloom, 1979; Woodward *et al.*, 1979).

Future research could isolate the currents more directly with glutamate and GABA receptor antagonists and examine the effects of NA on mini (TTX-insensitive) and spontaneous events. Doze, Cohen and Madison (1991) showed that mini IPSCs in rat hippocampal slices are not affected by NA, but this data is lacking in mice, as is the data on mini EPSCs.

2.4.3 Short-term plasticity

CA1 pyramidal neurons typically receive inputs in bursts (Ranck, 1973; O'Keefe, 1976; Masukawa, Benardo and Prince, 1982; Suzuki and Smith, 1985; Epsztein *et al.*, 2010; Kowalski *et al.*, 2016), therefore examining single synaptic responses provides only a limited insight into the neuromodulation of the SC-CA1 micro-circuit. We therefore examined the effects of NA on the short-term excitatory and inhibitory dynamics of the synapse using three stimulation frequencies: 1, 10 and 50 Hz (Wierenga and Wadman, 2003; Sun *et al.,* 2005).

Initial characterisation showed frequency-dependent facilitation and depression of the mono-synaptic excitatory and feed-forward inhibitory inputs, respectively, in line with previous work (Dobrunz *et al.,* 1997; Ali and Thomson, 1998; Wierenga and Wadman, 2003; Sun *et al.,* 2005). SC-CA1 synapses typically facilitate due to their low initial release probability and the accumulation of intracellular Ca^{2+} with repeated stimulation (Dobrunz *et al.,* 1997; Su *et al.,* 2005), whereas the high initial release probability of the inhibitory interneuron usually leads to a rapid vesicle depletion, depression of synaptic responses over repeated stimuli and, ultimately, diminished interneuron recruitment (Fogelson and Zucker, 1985; Dobrunz *et al.,* 1997; Thomson, 1997; Wierenga and Wadman, 2003; Sun *et al.,* 2005).

Intriguingly, bath application of NA did still reduce the amplitude of all synaptic responses across bursts, but at high (50 Hz) stimulation the relative attenuation was lower for EPSCs later in the stimulus train. This was initially apparent for the peak of

the synaptic EPSCs when examining the burst ratio of the fifth and first peak (P5/P1) but was also true from the third pulse onwards when the normalised charge transfer was calculated. Taken together with the trends observed on sEPSCs and sIPSCs, these data suggest that NA may act to dampen down low-frequency synaptic activity throughout the SC-CA1 micro-circuit and background inhibitory tone within the CA1, but bursts of high-frequency excitatory inputs (i.e. those associated with a place field or sensory input) can overcome the noradrenergic attenuation and relay their signal relatively unimpeded. A similar shift in E/I balance has been shown with DA at feed-forward TA inputs to CA1 (Ito and Schuman, 2007). This study also found no effect on mono-synaptic IPSCs onto CA1 pyramidal neurons, with the E/I shift occurring due to the facilitation dynamics of the excitatory inputs at high frequencies. It would be of interest to examine the effects of interneuron recruitment at high frequencies, for example by recording from fluorescently labelled PV+ interneurons in the current-clamp configuration. It would be expected that in the presence of NA all frequencies of stimulation would lead to an attenuation in interneuron action potential firing, and therefore a reduction in feed-forward IPSCs.

The concept of NA acting as a high-pass filter to enhance signal-to-noise was initially proposed in 1979 by several research groups, (Moore and Bloom, 1979; Woodward *et al.*, 1979). Given the role of feed-forward inhibition in spike generation (Pouille and Scanziani, 2001), the selective reduction of IPSCs later in the stimulus train may allow more efficient action potential initiation at high frequencies. Functionally, this selective attenuation of SC feed-forward IPSCs over EPSCs would allow a wider temporal window for SC-CA1 STDP (Pouille and Scanziani, 2001). A key role of the CA1 is to act as a comparator for incoming signals regarding the present situation (i.e. sensory information relayed from the cortex by TA inputs) and our internal representation of the world (i.e. memory engrams encoded in CA3 ensembles conveyed by SC inputs) (Amaral and Witter, 1989; Witter *et al.*, 1989; Lee *et al.*, 2004). It has been shown that intact feed-forward inhibition at low frequencies only permits linear summation of coincident SC and TA inputs, but at high frequencies the high-pass filtering dynamics allow supralinear summation, dendritic spiking and CA1 burst firing (Lisman, 1999; Ang, Carlson and Coulter, 2005; Takahashi and Magee, 2009; Milstein *et al.*, 2015). Given that low (≤10 Hz), but not high (50 Hz), frequency facilitation is unaffected by NA, this selective enhancement of high-frequency glutamatergic input may therefore sharpen the CA1's function as a comparator and novelty detector.

Repeating the synaptic experiments, but this time alternating between stimulating the TA, SC and both pathways concurrently, may reveal novel gating mechanisms mediated by NA. For instance, if "excitatory" adrenoceptors (β-ARs and α1-ARs) are more abundantly expressed on TA axons and/or the CA1 dendrites that these axons contact,

TA inputs alone may be sufficient to elicit spiking in CA1 pyramidal neurons. The interneurons that modulate TA inputs may also be selectively inhibited by α2-ARs, allowing greater propagation of TA signals. On the other hand, NA may attenuate TA inputs to a much greater degree than that observed at SC inputs. Interestingly, several studies show a selective, pre-synaptic attenuation of TA excitatory and feed-forward inhibitory inputs but a sparing of SC inputs to CA1 by dopamine (Otmakhova and Lisman, 1998; Ito and Schuman, 2007; Rosen, Cheung and Siegelbaum, 2015). As in the present study, high frequency inputs can overcome this attenuation, thus imposing a high-pass filter on incoming cortical information.

Another possible mediator of such noradrenergically-mediated pathway-selectivity could be hyperpolarisation-activated cyclic nucleotide-gated (HCN) channels, cation-selective channels which regulate neuronal excitability and the response to synaptic input in many neurons, including hippocampal CA1 pyramidal neurons (Magee, 1998). HCN channels are open at the resting membrane potential and reduce input resistance, minimising local post-synaptic depolarisation (Shah, 2014). In the CA1, HCN channels – in conjunction with feed-forward inhibition – dampen down TA inputs, prevent plateau potentials, restrict SC and TA pathway integration and limit long-term potentiation at TA-CA1 synapses (Ang, Carlson and Coulter, 2005; Nolan *et al.*, 2005). Genetic deletion of HCN1 channels can enhance TA-CA1 LTP and improve performance in the Morris Water Maze, particularly the speed at which animals learn the location of the hidden platform (Nolan *et al.*, 2005). Interestingly, noradrenergic input can modulate HCN function, with β-AR activation in layer V neurons of the medial pre-frontal cortex enhancing HCN currents (Grzelka *et al.*, 2017), and α2-AR activation reducing them (Barth *et al.*, 2008). Given that HCN channels show increasingly greater expression at more distal locations of CA1 pyramidal neurons dendrites (Magee, 1998), the modulation of these channels (through altered cAMP levels mediated by α2-ARs or β-ARs) would increase or decrease dendritic depolarisation to more distal inputs. Such a mechanism may allow a bias towards TA or SC input and the type of information they carry (sensory information regarding the present situation and stored internal representations, respectively). Given that NA release signifies a state change and the need to learn a new rule set regarding a novel task or space, it may be that NA facilitates dendritic plateau potentials in CA1 via HCN channels located in the distal dendrites. This would then allow long-term potentiation in the TA-CA1 pathway and an improved ability to update the internal representation of the task/space (CA1-CA3) with the current cortical inputs (TA-CA1).

One study has examined the effects of NA on medial and lateral TA inputs (Ito and Schuman, 2012). Here it was found that NA selectively depresses lateral TA inputs over

medial TA inputs, and – similar to the results in the present study – high frequency bursts were able to overcome this attenuation. Taken with the present data, these results highlight an intriguing mechanism for NA to enhance signal-to-noise in the CA1 as well as a biasing effect towards cortical pathways carrying different streams of information. In the case of Ito and Schuman (2012), this was towards the spatial information conveyed by the medial TA, whereas the non-spatial information (i.e. relating to objects or environmental cues) carried by the lateral TA was suppressed (Fyhn *et al.*, 2004; Knierim, Lee and Hargreaves, 2006).

2.4.4 Synaptic output of the CA1

Remarkably, we found that 20 μM NA completely abolished S_P. This did not seem to be directly due to the concurrent hyperpolarisation, but instead appeared to be caused by a reduction in SC excitatory input. Given the evidence from the voltage-clamp experiments that NA appears to act – or enhance – the SC input's function as a high-pass filter, it would be interesting to examine the effects of NA on the spike output of different stimulation frequencies, however there was some difficulty in maintaining spiking stability with 10 Hz in the present study, so we avoided stimulating at higher frequencies to avoid potential plasticity changes. If such experiments were carried out in future, they could provide further support for the shift in E/I balance towards excitation by examining the relative somatic EPSPs and IPSPs. Not all of the S_P experiments in the present study showed an inhibitory component, but if the experiments were repeated in future it would be of benefit to perfuse slices showing an inhibitory component with NBQX at the end of the experiments to determine whether they were feed-forward and obtain a true measure of E/I balance in the presence and absence of NA.

Although the change was not significant, there was also a reduction in CA1 pyramidal neuron R_{in} in the presence of NA. A neuron's R_{in} reflects both cell size and the density of ion channels open at rest. Ohm's Law predicts that for a given inward current, higher values of R_{in} can elicit larger membrane depolarisations. Lower R_{in} values are therefore associated with reduced neuronal excitability, and the R_{in} reduction in the present study may be involved in the attenuated EPSP amplitudes observed in current-clamp, however further work is needed to clarify this.

2.4.5 NMDAR function

NMDARs play several important roles CA1 pyramidal neurons, particularly in LTP and dendritic integration (Collingridge, Kehl and McLennan, 1983; Harris, Ganong and Cotman, 1984; Morris *et al.*, 1986; Takahashi and Magee, 2009), and are targets for noradrenergic modulation (Collingridge, Kehl and McLennan, 1983; Raman, Tong and Jahr, 1996). Compound EPSPs include an NMDAR component that can be enhanced using the SK channel blocker apamin or the M1 AChR agonist, 77-LH-28-1 (Buchanan *et*

al., 2010). We postulated that NA may also modulate NMDARs via SK channels, however neither NA nor apamin enhanced NMDAR function as measured by the compound EPSP decay constant. Reassuringly, D-AP5 did reduce the compound EPSP decay, suggesting NMDARs were involved in the response but were not modulated by NA or apamin. The lack of NMDAR modulation by NA was surprising, but not as surprising as the result that apamin also did not enhance NMDAR function. There are several possible explanations for this. Most of the slices used in this study were from the dorsal aspect of the hippocampus, however there is a differential regulation of NMDARs by SK channels in dorsal and ventral slices (Babiec *et al.*, 2017). Specifically, higher levels of SK3 channels are present in ventral hippocampal slices, resulting in very little NMDAR-mediated EPSP amplification due to this high level of tonic SK channel inhibition. Conversely, dorsal aspects show much greater EPSP amplification due to a relatively lower level of SK channel inhibition, which may explain the lack of modulation in the present study. Moreover, age and species differences are also likely implicated: SK channel modulation of NMDARs was shown in young (P13-15) rats (Buchanan *et al.*, 2010), whereas the present work was carried out in juvenile mice. It is intriguing that in the Buchanan *et al.* (2010) work, NMDAR antagonism brought the compound EPSP decay constant back to baseline levels, whereas in the present study we observed the decay constant become significantly quicker than the baseline measurement. This suggests that, unlike the present work, there was no NMDAR component at baseline in the Buchanan *et al.* (2010) study. We therefore postulate a second explanation for our lack of effect: that NMDAR function was "maxed out" in the more juvenile mice and unable to be further enhanced by SK channel inhibition.

It is also interesting to note that in the Babiec *et al.* (2017) study, the enhanced NMDAR amplification in ventral slices was not apparent unless current was injected to hold neurons at -50 mV or more depolarised membrane potentials before evoking a single (not compound) EPSP. In our experiments, neurons were left to sit at their own resting membrane potential, and we implemented a cut-off value of -60 mV in order to obtain healthy cells and adequate compound EPSPs that did not elicit spikes. Future work could implement the protocol used in Babiec *et al.* (2017) to examine NMDAR modulation by NA.

2.4.6 STDP

Recent research has suggested NA potentiates STDP at the SC-CA1 synapse through increases in back-propagating action potential efficiency (Liu *et al.,* 2017). Although intriguing, the STDP results from this study did not include a control pathway, and so we sought to determine whether NA-STDP at the SC-CA1 synapse was homo- or hetero-synaptic. In agreement with previous research (Tigaret *et al.*, 2016, 2018; Liu *et al.*, 2017), we found that a "1 pre 1 post" STDP protocol was sub-threshold for LTP induction.

However, when we applied NA prior to the STDP protocol, we observed an increase in EPSC amplitude in both pathways. To examine this further, we did not induce the STDP protocol after stopping NA perfusion, but still found a similar increase. Given that the attenuating effect of NA on SC excitatory input does show some degree of wash-out (Figure 2.9A), it therefore appears likely that some of the enhancing effects observed in Liu *et al.* (2017) may be due to washout of NA.

We therefore altered our experiment to include NA perfusion throughout the experiment, however here we found no effect on STDP. The ostensible increase in EPSP amplitude is actually due to two neurons that did show profound LTP. There was no obvious explanation for the strong effect observed in these neurons: series resistance was stable in both cases, both neurons were from mice of similar ages, and one cell was dorsal and the other ventral, so dorso-ventral aspect does not seem to be a factor. It is well-known that STDP is much easier to induce in organotypic slices and younger (<P14) animals (Debanne, Gähwiler and Thompson, 1998; Meredith, Floyer-Lea and Paulsen, 2003; Buchanan and Mellor, 2007) and this is thought to be due to a relative lack of $GABA_AR$-mediated inhibition compared to older acute slices (Meredith, Floyer-Lea and Paulsen, 2003). However, despite routine $GABA_AR$ inhibition, induction of STDP in older animals (>P15) appears to vary between research groups, with some showing success (Nishiyama *et al.*, 2000; Campanac and Debanne, 2008) and other no effect (Wittenberg and Wang, 2006; Remy and Spruston, 2007). Indeed, the present work, like Liu *et al.* (2017) employed $GABA_AR$ inhibition and so this is unlikely to play a role in the lack of STDP observed.

Intriguingly, the answer may lie in the slice preparation solution. Edelmann and Lessmann (2011) found that SC-CA1 STDP could not be induced in slices prepared in sucrose cutting solution, even using stronger induction paradigms, whereas slices prepared using standard aCSF did not show this deficit. Moreover, STDP could be restored in sucrose-prepared slices if they were pre-incubated with DA, but no effect was seen with the β-AR agonist, isoproterenol. The authors were unable to pin-point an exact mechanism for this, since isoproterenol restored several intrinsic action potential properties (i.e. rise time) but not STDP, however they did find that endogenous ambient DA levels were ~40% lower in sucrose-prepared slices. The importance of ambient DA levels for STDP was also shown by blockade of plasticity in aCSF-prepared slices with the D1R receptor antagonist, SCH-23390. However, Zhang, Lau and Bi (2009) found STDP persistence with D1R blockade, and argue that DA extends the temporal window for STDP induction and can convert LTD into LTP with ani-Hebbian induction protocols.

In agreement with differences in cutting solution influencing STDP, the sucrose concentration in Liu *et al.* (2017) study was somewhat lower than in present work (168

mM compared to 205 mM) and contained NaCl (25 mM whereas ours contained none). In future it would be of benefit to repeat these experiments to compare NA effects on STDP on slices obtained using the cutting solutions in Liu and Edelman.

2.5 Additional limitations and future directions

2.5.1 Dorso-ventral distinction in slices

A limitation of the work is the lack of stratification of dorsal and ventral slices. Most of the recent work on the catecholaminergic modulation of CA1 has either focused primarily on dorsal slices (Takeuchi *et al.*, 2016; Liu *et al.*, 2017), or has appeared agnostic to the aspect of the hippocampal slice. In the present study, most of our slices were dorsal to investigate the modulation of mono-synaptic EPSCs and feed-forward IPSCs at the mossy fibre (MF) to CA3 synapse (see Chapter 3), which we found difficult to obtain in ventral slices. Given the – somewhat – segregated roles of the dorsal and ventral poles in spatial and emotional types of memory, respectively (Moser, Moser and Andersen, 1993; Moser *et al.*, 1995; Moser and Moser, 1998), and new reports regarding variations in synaptic transmission and plasticity between the hippocampal poles (Babiec *et al.*, 2017), it would be of benefit to repeat the experiments presented here in ventral hippocampal slices.

2.5.2 Further support for the pre-synaptic α2-AR theory

The notion that the reduction in excitatory and feed-forward inhibitory inputs are mediated by pre-synaptic α2-ARs on SC axons requires further support. The first experiment would be to measure AMPAR-NMDAR ratios: if AMPAR- and NMDAR-mediated currents are both reduced to similar levels, this would again imply a pre-synaptic locus of modulation (Leão and Von Gersdorff, 2002). A second set of experiments exploring the pharmacology of the EPSC and IPSC reduction, using either α2-AR agonists (i.e. clonidine or UK14304) or α2-AR antagonists (i.e. yohimbine or atipamezole) in conjunction with NA, are also necessary.

2.5.3 Irregular spike train stimulation

Examining synaptic responses in response to regular – but rigid – patterns of stimulation can give a useful indication of the general effects of neuromodulators. However, a typical property of neuronal *in vivo* firing patterns are their irregularity or stochasticity, with spike patterns similar to Poisson-like time sequences (Rich, Liaw and Lee, 2014). Examining the effects of NA on the plasticity of irregular spike train stimulation will likely reveal further insights into how NA modulates the dynamics of excitatory and inhibitory synapses in the CA1.

2.5.4 Improvements to the measure of E/I balance

To maintain stable driving forces for excitatory and inhibitory inputs, the data for evoked EPSC and IPSC responses in voltage-clamp were not carried out in the same cells. Repeating these experiments and obtaining data on both types of synaptic current from the same neuron would allow paired correlational analysis and a more powerful measure of E/I balance within neurons.

2.6 General conclusion

The present work has provided new insights into the noradrenergic modulation of the SC-CA1 feed-forward micro-circuit. Specifically, NA gates short-term plasticity through a selective dampening down of background inhibitory activity and boosting of high-frequency glutamatergic neurotransmission, ultimately tipping the E/I balance towards excitation for burst-like inputs. At low frequency synaptic inputs, this reduction in SC excitatory input attenuates spiking, providing further support the notion that NA enhances signal-to-noise and acts as high-pass filter. These effects appear to be mediated pre-synaptically, possibly via α2-ARs. NA does not appear to modulate NMDAR function or STDP, however this could be explained by the use of a sucrose cutting solution and recording from dorsal hippocampal slices. Further work is therefore required to clarify the adrenoceptors underlying the effects on synaptic input and spike output, as well as the role of NA in SK channel and STDP modulation.

Chapter 3: Effects of endogenous NA on the SC-CA1 micro-circuit

3.1 Introduction

For many decades, research into the molecular and synaptic mechanisms underscoring neuromodulation has been carried out primarily using *in vitro* or *ex vivo* preparations. Such research typically involves excision of the neural circuitry of interest (i.e. acute or organotypic slice preparations) or completely removing a particular brain region and culturing the neurons contained therein, with little endogenous local and long-range circuitry left (Lossi *et al.*, 2009; Humpel, 2015; Lossi and Merighi, 2018; Ting *et al.*, 2018). Although such research is somewhat reductionist compared to *in vivo* preparations, this platform permits dynamic functional studies of the living brain across an extensive range of brain regions and animal species and has therefore facilitated a detailed interrogation of neuromodulation (Prince *et al.*, 2016; Palacios-Filardo and Mellor, 2019). For much of this time, the study of neuromodulation in *ex vivo* slice preparations has primarily involved bath-application of exogenous neuromodulators during electrophysiological assays, an approach that cannot recapitulate the precise spatiotemporal release patterns observed *in vivo* (Rosen, Cheung and Siegelbaum, 2015). Such an approach tallied with the traditional idea that neuromodulators simply acted as a "flag" for a particular situation (i.e. DA signals reward, NA indicates novelty etc., Wise and Rompre, 1989; Vankov, Herve-Minvielle and Sara, 1995), however with rapid advances in genetic toolboxes, particularly opto- and chemogenetics, our ability to manipulate and understand neurotransmitter release has developed exponentially (for reviews, see Deisseroth, 2011; Fenno, Yizhar and Deisseroth, 2011; Sternson and Roth, 2014; Repina *et al.*, 2017; Campbell and Marchant, 2018).

Channelrhodopsin-2 (ChR2) is a light-sensitive cation channel (opsin) found endogenously in algae (Nagel *et al.*, 2003), first expressed in mammalian HEK cells and then cultured hippocampal neurons over a decade ago (Nagel *et al.*, 2003; Boyden *et al.*, 2005). Activation of the protein using blue light rapidly depolarises the expressing neurons, causing action potential firing and neurotransmitter release. Using cell population-specific promoters it is now possible to express the opsin in a vast array of neuronal subtypes – excitatory, inhibitory and modulatory – and tease apart their relative contributions to local circuit dynamics, network function and – ultimately – behaviour (Britt, McDevitt and Bonci, 2012; first shown by Adamantidis *et al.*, 2007). An array of opsin variants – and inhibitory counterparts – have now been developed, each with different channel conductances, on/off kinetics and activation wavelengths (see Mattis *et al.*, 2011 for detailed experimental comparisons).

Despite this growing array of optogenetic tools, most of the research has primarily focused on the effects of switching local excitatory and inhibitory circuitry on or off, and how these changes impact local circuits and wider network functions. Stimulating or inhibiting these local glutamatergic and GABAergic inputs are easy to detect and measure, as the synaptic currents are fast and clear (Ntamati and Lüscher, 2016). Moreover, the local neurons expressing ChR2 are typically present in their entirety within the slice, and this presence of the soma and AIS permit successful activation of the neurons despite the relatively low conductance of the ChR2 pore (Boyden *et al.*, 2005). Conversely, long-range projections are more challenging to activate, since high ChR2 expression is needed to counteract its low pore conductance and the lack of soma and AIS. Moreover, these axonal terminals are distant from the somatic site of ChR2 protein synthesis, and so longer incubation times (>3 weeks) are therefore necessary to allow sufficient trafficking of ChR2 to the neuromodulator-containing terminals.

Only a paucity of studies have used optogenetics to examine the long-range neuromodulatory inputs that work on much slower time scales (often *in vivo*, Tsai *et al.*, 2009; Carter *et al.*, 2010; Witten *et al.*, 2011). Carter *et al.* (2010) were the first group to use optogenetics to selectively activate the LC *in vivo*, and showed reliable sleep-to-wake transitions with LC opto-activation, and a frequency-dependent relationship between LC opto-stimulation-frequency and time spent awake.

Even fewer studies have examined the neuromodulatory inputs within *ex vivo* slice preparations. Those that have reveal intriguing details that challenge our long-standing beliefs regarding brain neuromodulatory systems. Results from Takeuchi *et al.* (2015), where the researchers used optogenetics in *ex vivo* slice experiments and *in vivo* behavioural tasks, suggest that the memory enhancing effects of LC burst firing are actually mediated by DA rather than NA. This is an intriguing prospect and, at first glance, appears to be backed up by Kempadoo *et al.* (2016), where optogenetically-evoked monoamine release from LC and ventral tegmental area (VTA) hippocampal terminals in acute slices was examined. Here, HPLC analysis of hippocampal slices and aCSF following opto-burst stimulation of LC terminals did indeed show co-release of NA and DA, however the NA concentration was over 10-fold higher than that of DA. The idea of NA and DA co-release by the LC was actually proposed in 2012 (Smith and Greene, 2012). Here, application of amphetamine caused an increase in endogenous DA release from LC terminals and an increase in D1R-mediated glutamate neurotransmission. This could be prevented by genetic knock-down of TH expression in the LC or blockade of the NA transporter protein (NET). However, NA is rapidly converted from DA in pre-synaptic vesicles containing DβH, therefore the LC terminals must contain DA prior to this conversion otherwise no NA could be synthesised. The use of amphetamine, which is taken up into noradrenergic terminals by NET, prevents

both the transport of DA into DβH-containing vesicles and the breakdown of DA into DOPAC by monoamine oxidase enzymes. DA therefore accumulates in the LC terminals and is reverse-transported down its concentration gradient out into the extracellular space via NET. Therefore, the notion that LC hippocampal terminals release DA under healthy, physiological conditions has still not been properly investigated. Wagatsuma *et al.*, (2018) also found dopaminergic effects with LC opto-stimulation, and offer a tentative proposal that tonic wake firing (1–3 Hz) allows the release of NA alone, but burst firing causes NA and DA co-release because the DβH enzyme is unable to sufficiently convert DA to NA.

Conversely, Liu *et al.* (2017) optically activated hippocampal LC inputs using burst (100 Hz) stimulation and the effects of this (down-regulation of CA1 voltage-gated K^+ channels and the associated increase in neuronal excitability) were blocked by a β-AR antagonist. Therefore, it is still somewhat unclear where DA fits into LC modulation of the hippocampus.

Only one study (Rosen, Cheung and Siegelbaum, 2015) has directly compared the effects of a bath-applied neuromodulator (DA) and its optogenetically-evoked endogenous counterpart in *ex vivo* slices. They found that bath-applied DA depresses perforant path (PP) inputs to CA1 and spares SC inputs, however the inverse is true following 1 Hz tonic opto-stimulation of VTA dopaminergic inputs to the hippocampus. More intriguingly, a phasic-like opto-stimulation protocol had a contrasting effect, instead enhancing SC EPSPs while sparing PP EPSPs. It is therefore apparent that the effects elicited by simply bath-applying a neuromodulator do not necessarily resemble those observed when it is released physiologically in intact organisms, highlighting the need for further examination of neuromodulatory systems with the precise spatiotemporal resolution offered by optogenetics.

In light of the findings by Rosen, Cheung and Siegelbaum, (2015), we postulated that a similar phenomenon may occur with NA. Our key research questions were therefore:

1) Can the effects of bath-applied NA be recapitulated by optogenetically evoked endogenous NA?

2) If so, what are the adrenoceptors and mechanisms underlying these effects?

To allow optogenetic targeting of hippocampal LC terminals, we chose to use the CAV2-PRS-mCherry-ChR2 viral vector, a canine adenovirus (CAV) that drives mCherry-tagged ChR2 expression in catecholaminergic neurons due to the presence of the PRS promoter (Hwang *et al.*, 2001; Li *et al.*, 2016), that has been previously characterised in rats (Li *et al.*, 2016; Hayat *et al.*, 2019). An advantage of using a CAV delivery system is that it is 3-4-fold more effective at transducing catecholaminergic neurons than adenovirus

delivery systems (Li *et al.*, 2016), and an additional advantage of using this delivery system over an AAV equivalent is the increased efficacy for retrograde transport (Bru, Salinas and Kremer, 2010). Given that the LC is such a small injection target (comprising only ~2,500 neurons in adult rats (Robertson *et al.*, 2013), this "back-up" retrograde transport mechanism therefore increases the chances of successful LC transduction (Howorth, Teschemacher and Pickering, 2009). For instance, it is possible to miss the LC cell bodies during injection but, due to the LC's extensive axonal arborisations, the CAV can bind to axonal coxsackievirus and adenovirus receptors (CARs) to undergo endocytosis and retrograde trafficking to the cell body where ChR2 synthesis can occur (Bru, Salinas and Kremer, 2010).

We show that optogenetic activation of LC inputs to the hippocampus can enhance synaptically-evoked spike output via β-AR activation. This β-AR activation enhances EPSP-spike coupling via a possible inhibition of transient voltage-gated K^+ channels. These effects could be recapitulated using a low (600 nM) concentration of NA. SC excitatory and feed-forward inhibitory inputs to the CA1 are not affected by optically-evoked or bath-applied (600 nM) NA, suggesting LC inputs may preferentially target CA1 cell bodies and/or nearby perisomatic locations. These findings are distinct from the effects outlined in Chapter 2, and provide a mechanism by which low levels of endogenous NA (as might be released by activation of the LC in response to salient stimuli or a switch from a sleeping to an awake state) can enhance information transfer in the hippocampus, but higher levels (such as those associated with high levels of LC discharge under stress or anxiety) may block transmission through hippocampal micro-circuits.

The slice preparation and IHC portions of this research were carried out by final year undergraduate students (Florence Caslake Holding and Josie Ryan) supervised by Travis Bacon.

3.2 Methods

3.2.1 Viral vector injections

For optoactivation of LC hippocampal terminals, we unilaterally injected the CAV2-PRS-ChR2-mCherry into the right LC of male C57BL/6J mice. Mice had acclimatised to the animal unit for at least a week prior to viral vector injections and were injected between P24 and P35. For all injections, mice were anesthetised for recovery surgery with an intraperitoneal (IP) injection of a ketamine (70 mg/kg, Vetalar) and medetomidine hydrochloride (0.5 mg/kg, Domitor) cocktail and maintained on a heat pad throughout the surgery.

A burr hole (Ø 1.0 mm) was made over the right hemisphere LC at stereotaxic coordinates from lambda, anterior-posterior (AP): 4.12 mm (corrected using variation from the

average bregma-lambda distance of 4.2 mm, Franklin and Paxinos Mouse Atlas, 3rd edition) and mediolateral (ML): 1 mm. A glass micropipette pulled on a vertical puller (Harvard) containing the viral vector was advanced with a 20° rostral angulation to a depth of 3.9 mm from the brain surface. Three vector injections (250 µL each, at a speed of 125 µL/min) of the CAV2-PRS-ChR2-mCherry viral vector (see Li *et al.* (2016) for more details) were made at depths of 3.5, 3.7 and 3.9 mm.

Following injection, mice received an IP injection of atipamezole hydrochloride reversal agent (1 mg/kg, Anti-sedan) and a subcutaneous injection of buprenorphine hydrochloride (0.1 mg/kg) and were monitored until use in *ex vivo* electrophysiology experiments >3 weeks later.

3.2.2 *Ex vivo* slice preparation

Transverse hippocampal slices were prepared as in Chapter 2 from injected mice (>3 weeks post-injection) or age-matched controls. Isolated transverse hippocampal slices were prepared from male (P50-P70) C57BL/6J mice. Following cervical dislocation, brains were immediately removed and immersed in ice-cold sucrose-based cutting solution containing the following (in mM): 205 sucrose, 10 glucose, 26 $NaHCO_3$, 2.5 KCl, 1.25 NaH_2PO_4, 0.5 $CaCl_2$, and 5 $MgSO_4$. Individual hippocampi were excised from the brain, mounted on agar and 400 µm transverse slices (dorsal only) were cut using a VT1200 vibratome (Leica). 400 µm coronal LC slices from injected mice were also obtained concurrently with hippocampal slices by mounting a dissected brainstem and cerebellum alongside the hippocampi. Following dissection and slicing, slices were transferred to aCSF containing the following (in mM): 119 NaCl, 10 glucose, 26 $NaHCO_3$, 2.5 KCl, 1 NaH_2PO_4, 1.3 $MgSO_4$, and 2.5 $CaCl_2$, maintained at ~35°C for 30 min, and then stored at room temperature. Slices were left for a minimum of 1 h after dissection before recordings were made. All solutions were saturated with 95% O_2 and 5% CO_2 and all experiments were performed in accordance with Home Office guidelines (UK Animal Scientific Procedures Act (1986)) as directed by the University of Bristol Home Office Licensing Team.

3.2.3 Electrophysiological recordings and analysis

Slices were submerged in a custom-designed recording chamber perfused at 2-4 ml/min with aCSF (as above) at 31-32°C, heated via an inline heating system (TC-324, Warner Instruments). CA1 pyramidal cells were visualised using infrared-differential interference contrast (DIC) optics on an Olympus BX-50WI microscope. Flow rate was maintained by a 101U/R peristaltic pump (Watson Marlow) and aCSF was removed via a Dymax 5 vacuum pump (Charles Austin).

Patch electrodes with a resistance of 2–8 MΩ were pulled from borosilicate filamented glass capillaries (1.5 OD x 0.86 ID x 100 L mm, Harvard Apparatus) using a vertical puller (PC-10, Narishige) or horizontal puller (P-87, Sutter Instruments).

3.2.4 Synaptic current recordings

To examine the effects of endogenous NA on synaptic transmission at the SC-CA1 synapse, CA1 neurons were clamped near the $GABA_A$ reversal potential (E_{GABAA}, -60.66 ± 2.86 mV, n = 7) or the glutamate reversal potential (and E_{Glut}, +3.36 ± 2.00 mV, n = 5) to isolate EPSCs and IPSCs, respectively. SC synaptic responses were evoked with a train of five 100 μs square voltage pulses delivered by a Digitimer D2SA isolated stimulator every 20 seconds through a monopolar stimulating electrode located in the CA1 *stratum radiatum* layer. The stimulation intensity was adjusted to evoke current amplitude of 50-150 pA (EPSCs) or 200-400 pA (IPSCs) at a stimulation frequency of 10 Hz, and minute averages for each frequency were generated for analysis. In all experiments examining CA1 $GABA_AR$ IPSCs, the AMPAR antagonist NBQX (20 μM) was applied to confirm IPSCs were generated by feed-forward inhibition resulting from SC stimulation and not direct stimulation of the interneurons. Any responses not inhibited by ≥75% within 10 minutes of NBQX application were discarded from subsequent analysis.

3.2.5 sAHP recordings

As in Chapter 2, sAHP currents were elicited by somatically depolarising pyramidal cells by 70 mV from a holding potential of -50 mV for 120 ms every 20 seconds.

3.2.6 Spike probability recordings

To investigate how endogenous NA modulates CA1 spike output, 10 square voltage pulses (100 μs) at 10 Hz every 20 seconds were applied through a bi-polar electrode placed in the *stratum radiatum* layer. The stimulation intensity was adjusted such that approximately five of the ten EPSPs elicited a spike (i.e. spike probability (S_P) = 0.5), to allow the spike output to either increase or decrease. Membrane potential (V_m) and input resistance (R_{in}) using a small hyperpolarising current injection were also measured. Analysis of spike probability, synaptic input and intrinsic neuronal properties. Unlike in Chapter 2, no V_m reset was required as LC terminal opto-stimulation had no effect on the neuronal membrane potential.

3.2.7 Rheobase experiments

The rheobase injection experiments unique to this chapter were carried out using the intracellular K-gluconate solution described in Chapter 3. CA1 pyramidal neurons were held at -70 mV, and 1 second depolarising current injections were delivered to the soma, with the current injected adjusted such that 1 action potential was elicited. Traces in which only one action potential occurred were tagged and exported to MATLAB, where

a custom-written script calculated the average latency to spike and jitter (SD of the mean latency) for each cell at baseline and in the various conditions used.

3.2.8 Opto-stimulation protocols

Optogenetic stimulation of ChR2-containing LC fibres was accomplished using a 473 nm LED (2.3 mW, Thor Labs) delivered through the 60x objective focused on the patched neuron. All LED pulses were 5 ms in duration.

Several opto-stimulation recordings were used in the experiments presented in this chapter and those in Chapter 5, adapted from various recent studies. Takeuchi *et al.* (2016): 60 pulses at 18 Hz every 20 seconds were used for the initial sAHP recordings. Takeuchi *et al.*, (2016): phasic 25 Hz stimulation consisted of 10 pulses at 25 Hz every 20 seconds, and this was used for spike probability experiments and the genetically encoded fluorescent NA sensor (NA1m) experiments in Chapter 5. Rosen, Cheung and Siegelbaum (2015): 1 Hz tonic stimulation for 10 minutes was used for all other optogenetic work in the present chapter and NA1m experiments in Chapter 5. For the 18 Hz and 25 Hz protocols, the LED pulses ended immediately before the onset of the depolarising current to induce the sAHP or SC stimulation for spike probability experiments, respectively.

3.2.9 Immunohistochemistry

For perfusion fixation, mice were given a terminal IP dose of sodium pentobarbital (100 mg/kg, Euthatal) and, after breathing had ceased and no response to foot pinch was found, the abdomen was opened and the heart exposed. The left ventricle was then injected with 20 ml of 0.01 M phosphate-buffered saline (PBS) and then 4% paraformaldehyde (PFA). The mouse was then decapitated, the scalp cut along the midline and the cerebellum and brain stem were removed and stored in 4% PFA for >24 hours before transferring to 30% sucrose in phosphate buffer (PB) at least 24 hours before slice preparation. The brainstem (for LC slices) or cortex (for hippocampal slices) was then mounted on a freezing cryotome (Leica) using Cryomatrix embedding resin (ThermoFisher Scientific) and 60 μm slices cut manually then stored in 0.1 M PB + 0.02% NaN_3. For hippocampal slices, whole brain coronal slices were generated for IHC, unlike the transverse slices made from dissected hippocampi for electrophysiological experiments. However, some hippocampal slices used for *ex vivo* electrophysiological recordings were also transferred to 4% PFA for >24 hours before IHC post-hoc analysis.

Free-floating slices were washed in 0.1 M PB for 10 minutes (3x) before transfer to 50% alcohol in dH_2O for 30 minutes and washing again in 0.1 M PB for 10 minutes (3x). Slices were then incubated overnight in 0.1 M PB + 0.3% Triton X-100 containing 5% donkey or goat serum (Sigma-Aldrich) and the relevant primary antibodies: rabbit anti-mCherry (1:4000, BioVision) and/or sheep anti-DβH (1:1000, Merck Millipore). The following

day, slices were washed in 0.1 M PB for 10 minutes (x3) and then incubated for >3 hours in 0.1 M PB + 0.3% Triton X-100 containing 2% donkey or goat serum and the relevant secondary antibodies: goat anti-rabbit Alexa-fluor 594 (1:1000, InVitrogen) and/or donkey anti-sheep IgG Alexa-fluor 488 (1:400, Jackson ImmunoResearch). Slices were then transferred to a final solution (0.1 M PB + 1:10,000 DAPI, InVitrogen) to stain for cell nuclei before mounting on glass slides and covering with rectangular glass slips using Fluorsave (Merck Millipore). Slides were stored in a fridge and imaged using a fluorescent microscope (Leica) and LASX imaging software (Leica).

3.2.10 Viral vectors and drugs

CAV2-PRS-ChR2-mCherry was purchased from PVM (Vectorology Platform of Monpellier). DL-propranolol hydrochloride was purchased from Tocris, and stock solutions were made up fresh in dH_2O every day.

3.3 Results

3.3.1 ChR2 expression and functional characterisation in LC neurons

The schematic in Figure 3.1A illustrates the injection of mice with the CAV2-PRS-ChR2-mCherry and Figure 3.1B highlights the strong mCherry expression in the LC. Although well-characterised in rats, we used double immunohistochemistry (IHC) to demonstrate the viral vector also expressed strongly in mice. Figure 3.1B shows dual staining for mCherry and DβH. The CAV2-PRS-ChR2-mCherry was highly specific, with 94.5 ± 2.3% of fluorescent mCherry cell bodies also exhibiting DβH fluorescence (Figure 3.1C). In the hippocampus, strong post-IHC mCherry staining of LC terminals was also observed (Figure 3.1D).

For opto-activation and functional characterisation of the ChR2 protein in LC neurons, we delivered 473 nm pulses through a 60x objective. In whole-cell current-clamp recordings from mCherry-expressing LC neurons, these light pulses (5 x 5 ms) could elicit action potentials reliably up to 25 Hz stimulation frequency before fidelity began to deteriorate (Figure 3.1E-F), in agreement with Carter *et al.* (2010). In voltage-clamp, LC neurons showed typical ChR2 current kinetics: a fast peak followed by a slow steady-state current (Figure 3.1G). These currents reversed at 7.09 mV (Figure 3.1H-I), typical of a mixed cation conductance channel such as ChR2 (Lin, 2011).

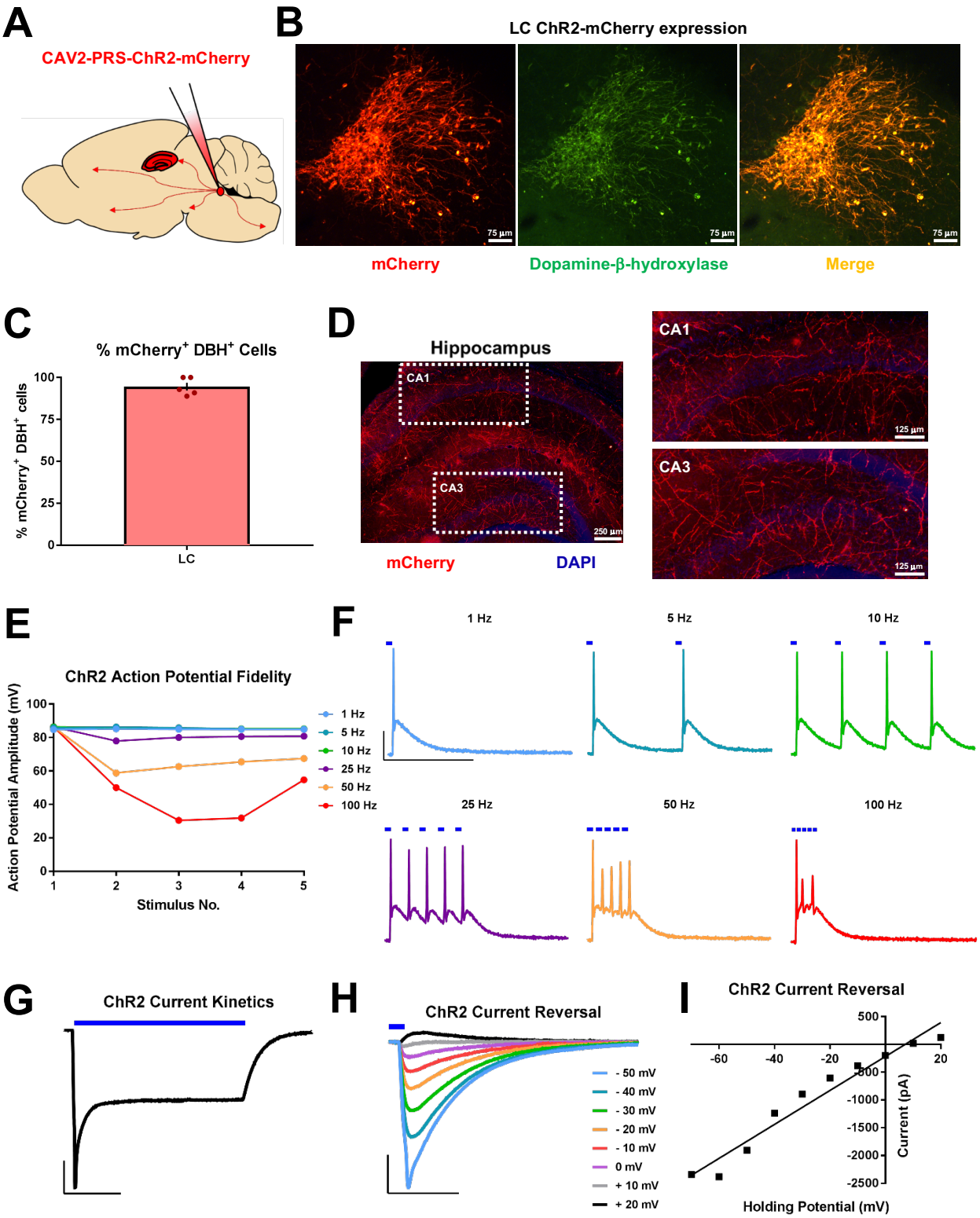

Figure 3.1: *Characterisation of the CAV2-PRS-mCherry-ChR2 viral vector in mice. A) Schematic for viral vector injections. B) mCherry fluorescence co-localised with DβH fluorescence, confirming successful noradrenergic neuronal targeting of the viral vector. C) % of mCherry+ neurons also showing DβH fluorescence (n = 5). D) mCherry fluorescence was also clearly visible in hippocampal terminals, confirming the long-range expression of the ChR2 protein. E-F). In the current-clamp configuration, mCherry-expressing LC neurons could successfully fire action potentials in response to light stimulation up to 25 Hz, before fidelity began to deteriorate. Scale bars = 25 mV and 200 ms. G-I) In voltage-clamp, mCherry-expressing neurons showed typical ChR2 current kinetics (G) that reversed at 7.1 mV (H-I). Scale bars = 500 pA and 50 ms (G), 500 pA and 20 ms (H).*

3.3.2 LC innervation is ubiquitous across the hippocampal dorso-ventral axis but higher in the DG-CA3 subfields

We also examined the LC innervation across the hippocampal dorso-ventral axis, and across the DG-CA3 and CA1 subfields. Coronal hippocampal slices from brains exhibiting LC mCherry expression were imaged and ROIs (DG-CA3 and CA1) were then manually drawn. Fluorescently-labelled fibres can be represented mathematically as structures consisting of curved lines possessing local intensity variations, and these can be detected using a Hessian matrix which describes the curvature of these intensity differences (Sato *et al.*, 1998; Sathyanesan, Ogura and Lin, 2012). Therefore, applying a Hessian matrix specifically extracts line-like structures (Hladuvka and Grôller, 2002) and so a Hessian filter was applied in ImageJ to isolate LC fibres (Meijering, 2003) and the average ROI intensity was quantified. This process is shown in Figure 3.2.

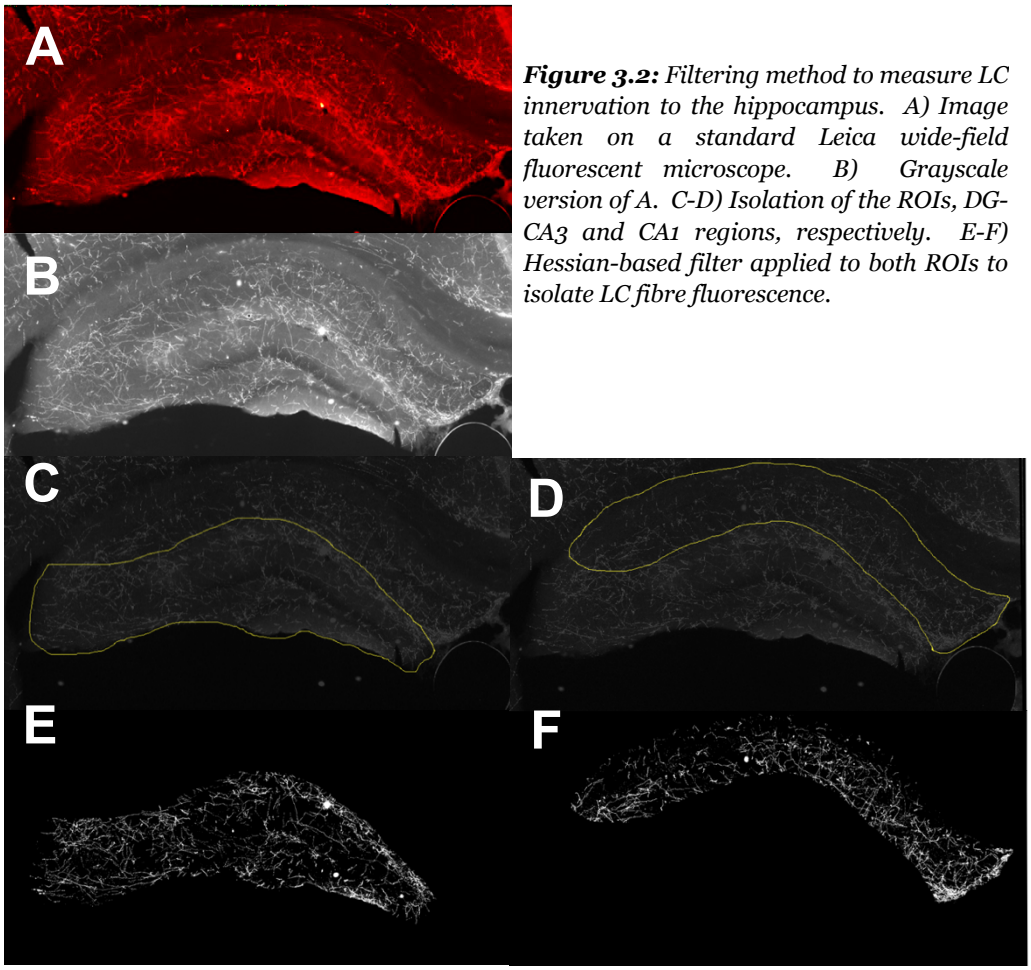

Figure 3.2: *Filtering method to measure LC innervation to the hippocampus. A) Image taken on a standard Leica wide-field fluorescent microscope. B) Grayscale version of A. C-D) Isolation of the ROIs, DG-CA3 and CA1 regions, respectively. E-F) Hessian-based filter applied to both ROIs to isolate LC fibre fluorescence.*

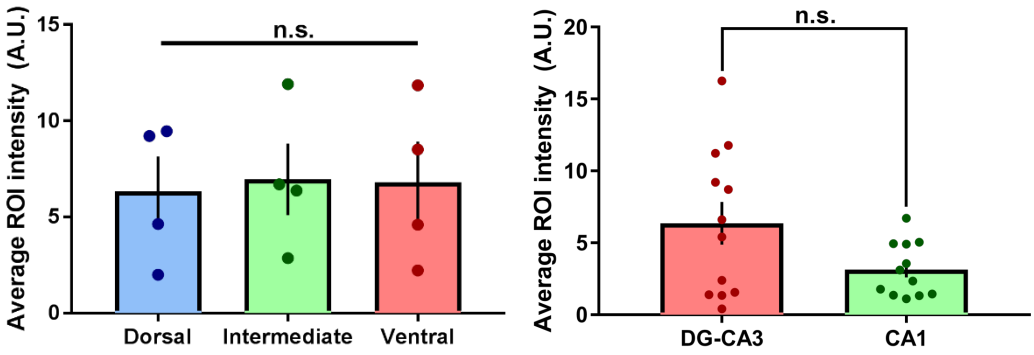

Figure 3.3: *Innervation of the hippocampus by the LC. A) LC innervation was equal across the dorso-ventral hippocampal axis (n = 4). B) The DG-CA3 region was more densely innervated by the LC than the CA1 region (n = 12).*

Intriguingly, little difference in LC innervation was found across the hippocampal dorso-ventral axis (dorsal = 6.3 ± 1.8 A.U., intermediate = 7.0 ± 1.9 A.U., ventral = 6.8 ± 2.1 A.U., n = 4, $p > 0.05$, one-way ANOVA with Dunnett's multiple comparison test). Given this ubiquitous innervation, the hippocampal sub-field data were grouped, and although DG-CA3 innervation by the LC was slightly higher –), in line with previous findings (Milner and Bacon, 1989; Oleskevich, Descarries and Lacaille, 1989; Wagatsuma *et al.*, 2018), statistical analysis of the hippocampal subfields revealed a no significant difference (DG-CA3 = 6.4 ± 1.5 A.U., CA1 = 3.1 ± 0.5 A.U., n = 12, $p > 0.05$, unpaired Student's *t*-test).

3.3.3 Endogenous NA does not attenuate the sAHP

One of the primary research questions was whether endogenous NA released by optoactivation could recapitulate the effects seen with bath-applied NA. Despite more fluorescence in the DG-CA3 subfield, the majority of our bath-applied NA experiments focused on the SC-CA1 synapse due to the initial research questions at the onset of the PhD (i.e. NA effects on short-term SC-CA1 plasticity, spike output and SK channel modulation of NMDARs). Moreover, several groups have reported neuromodulatory effects with opto-stimulation of LC fibres terminating in the CA1 subfield (Takeuchi *et al.*, 2016; Liu *et al.*, 2017). Opto-stimulation of the much more sparsely projecting dopaminergic fibres originating from the VTA has also yielded neuromodulatory effects in the CA1 (Rosen, Cheung and Siegelbaum, 2015).

To investigate the neuromodulatory effects of LC fibres terminating in the CA1, we chose an assay that is known to be highly sensitive to NA: the sAHP current. Although we had demonstrated sAHP inhibition with 20 μM NA (Chapter 2), it has been reported to be sensitive to concentrations as low as 300 nM NA (Madison and Nicoll, 1986). This is closer to the micromolar or sub-micromolar concentrations of NA believed to be released physiologically by noradrenergic terminals (Courtney and Ford, 2014; Muller *et al.*, 2014; Feng *et al.*, 2019).

3-5 weeks after injection of CAV2-PRS-ChR2-mCherry to the right LC, acute transverse hippocampal slices were obtained and we used a phasic opto-stimulation protocol adapted from Takeuchi *et al.* (2016) to excite the LC hippocampal terminals and elicit endogenous NA release from within the hippocampal slice (60 pulses, 5 ms at 18 Hz every 20 seconds). This protocol did cause a modest reduction in the peak sAHP current of CA1 pyramidal neurons (80.3 ± 11.8% of baseline, n = 12, Figure 3.4A-C), however a similar reduction was also seen with non-injected wild-type mice after the same opto-stimulation protocol (76.3 ± 7.8% of baseline, n = 9). Figure 3.4A-C) indicating a possible light and/or heat-induced rundown of the sAHP. These reductions were not significantly different from one another ($p > 0.05$, unpaired Student's *t*-test). Given the possibility that pre-synaptically expressed ChR2 can enhance the release probability of the CA1 expressing terminals (possibly by increasing Ca^{2+} influx, Zhang and Oertner, 2007), we hypothesised that baseline sAHP amplitudes in ChR2-injected animals were smaller due to more tonic release of NA, which may also desensitise the adrenoceptors on the pyramidal neurons (Gainetdinov *et al.*, 2004). We did find that WT mice did have larger baseline amplitudes than ChR2-injected mice, but this was not significant (WT = 66.3 ± 13.3 pA, ChR2-injected = 39.6 ± 9.2 pA, n = 9 and 12, respectively, $p > 0.05$, Mann-Whitney test, Figure 3.4D).

Given our data in Figure 3.3 and additional reports that the CA3 may more densely innervated by the LC than the CA1 (Milner and Bacon, 1989; Oleskevich, Descarries and Lacaille, 1989; Wagatsuma *et al.*, 2018), we repeated the assay in CA3 pyramidal neurons. Opto-activation of LC terminals again attenuated the sAHP, yet this was not significantly different from the non-specific rundown seen in CA1 neurons (81.6 ± 16.6% of baseline, n = 8, $p > 0.05$, Mann-Whitney test, Figure 3.4E-F).

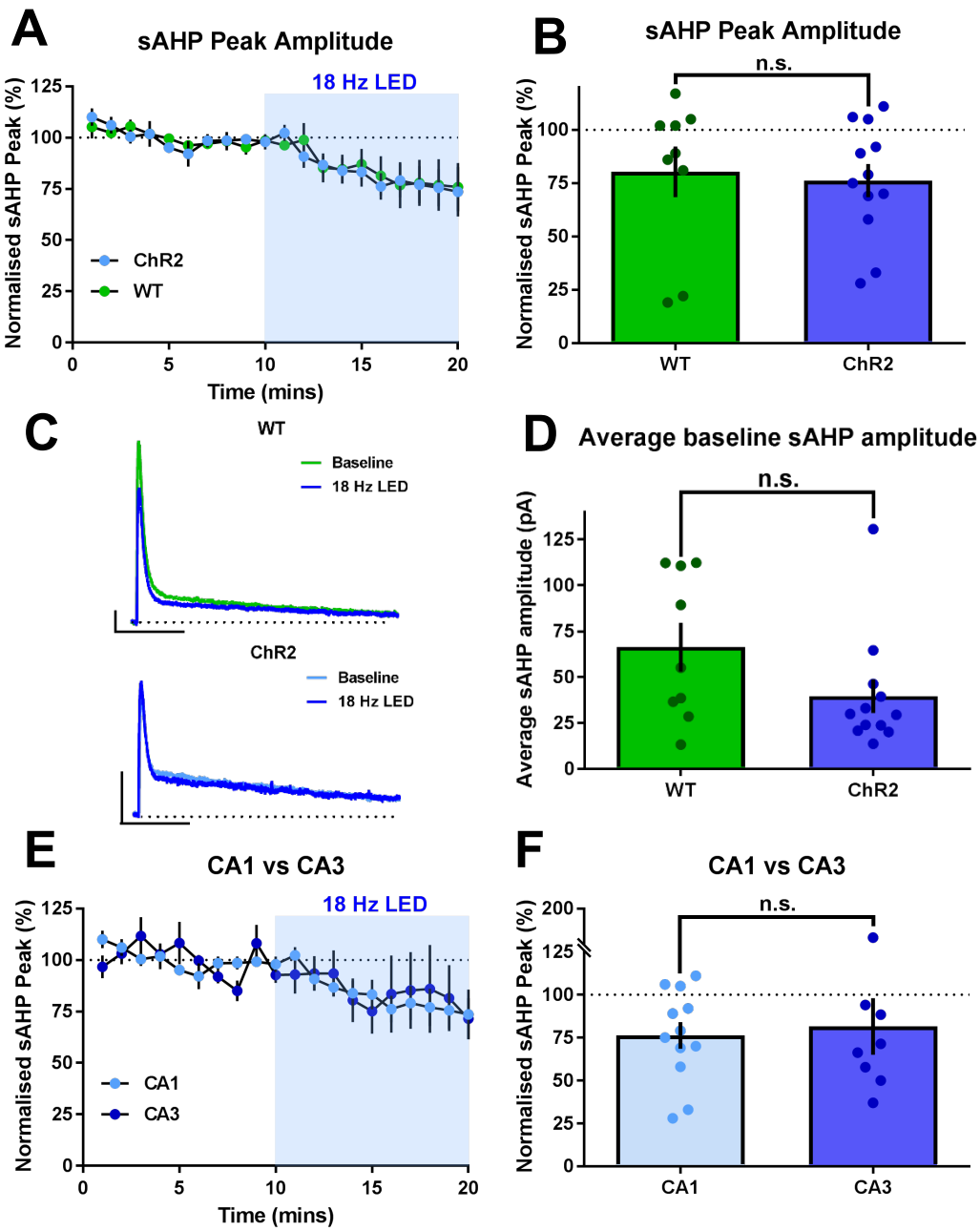

Figure 3.4: *The sAHP is not modulated by 18 Hz phasic-like opto-stimulation in either CA1 or CA3 neurons of ChR2-injected mice. A) Time course plot showing the sAHP peak amplitude of ChR2-injected and WT mice in response to an 18 Hz phasic-like opto-stimulation protocol (ChR2 n = 12, WT n =9). B) Averaged data for A showed no significant difference between the two groups. C) Example traces for WT (top) and ChR2-injected (bottom) mice, scale bars = 25 pA and 500 ms. D) Average baseline sAHP amplitudes were not significantly different in injected and WT mice. E) Time course plot for the normalised sAHP amplitude in response to the same opto-stimulation protocol in CA1 and CA3 neurons (n = 12 and 8, respectively). F) Averaged data for E shows no difference in the sAHP peak between the two hippocampal subfields.*

3.3.4 Endogenous NA enhances spike output via β-ARs

One possible explanation for the lack of effect on the sAHP is that the spatial release pattern of opto-evoked NA was not sufficient to inhibit the channels underlying the sAHP current (Villalobos, 2004; Andrade, Foehring and Tzingounis, 2012). In our bath-applied NA experiments (Chapter 2) synaptically-evoked spike output was another parameter that was strongly attenuated by 20 μM NA, with normalised spike probability (S_P) dramatically reduced from 1.00 ± 0.03 to 0.11 ± 0.10 (as the data is normalised, a

normalised S_P of 1 equates to a raw S_P of ~0.5). To avoid potential heating effects, we also adopted a lower frequency stimulation protocol from Rosen, Cheung and Siegelbaum (2015): continuous 5 ms light pulses at 1 Hz (Figure 3.5A).

Surprisingly, this protocol instead caused a robust enhancement of the evoked spike output to a normalised S_P of 1.4 ± 0.1 in ChR2-injected animals (Figure 3.5B-D and F, n = 12). This difference was significantly different from non-injected WT mice, whose normalised S_P remained unchanged under the same opto-stimulation protocol (Figure 3.5B-E, 0.9 ± 0.2, n = 8, $p < 0.05$, unpaired Student's *t*-test). Intriguingly, no changes in membrane potential (Figure 3.6A-B, WT = -0.01 ± 1.00 mV, ChR2 = -0.19 ± 0.69 mV, $p > 0.05$), R_{in} (Figure 3.6C-D, WT = -4.5 ± 3.4 MΩ, ChR2 = 2.0 ± 5.4 MΩ, $p > 0.05$) or synaptic input (Figure 3.6E-F, WT EPSP = 93.6 ± 2.3%, ChR2 EPSP = 88.1 ± 7.0%, $p > 0.05$) were observed between the two groups (unpaired Student's *t*-tests). The baseline resting V_m values for WT and ChR2-injected mice were -67.0 ± 1.7 mV and -66.1 ± 1.2 mV, respectively. The baseline R_{in} values for WT and ChR2-injected mice were 96.61 ± 5.0 MΩ and 79.89 ± 5.8 MΩ, respectively. Interestingly, spike threshold was significantly reduced in the ChR2-injected animals but not WT controls (ChR2 = -1.9 ± 0.5, WT = -0.4 ± 0.5 mV, $p < 0.05$, Mann-Whitney test, Figure 3.6G-H).

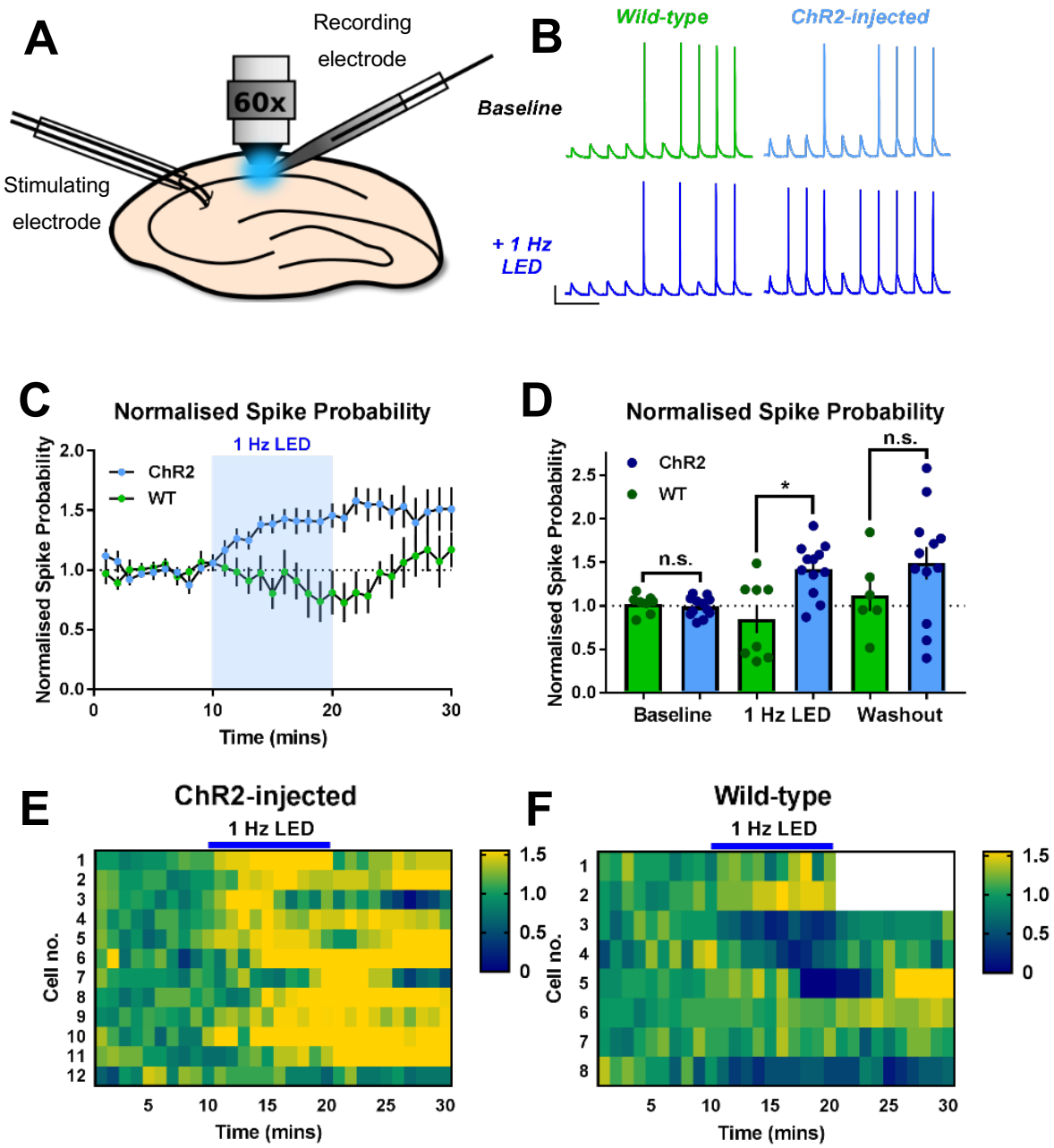

Figure 3.5: *Optogenetically-evoked NA enhances synaptically-evoked spike output in CA1 pyramidal neurons. A) Schematic showing ex vivo slice set-up and optogenetic stimulation. B-C) 1 Hz tonic stimulation (10 minutes) enhanced CA1 spike output in response to SC stimulation in ChR2 (n = 12), but not WT mice (n = 8). Scale bars = 25 mV and 250 ms. D) Averaged data from the final 5 minutes of baseline, 1 Hz LED stimulation and washout for ChR2-injected and WT control mice. E-F) Heat maps showing the normalised S_P for ChR2-injected and WT mice.*

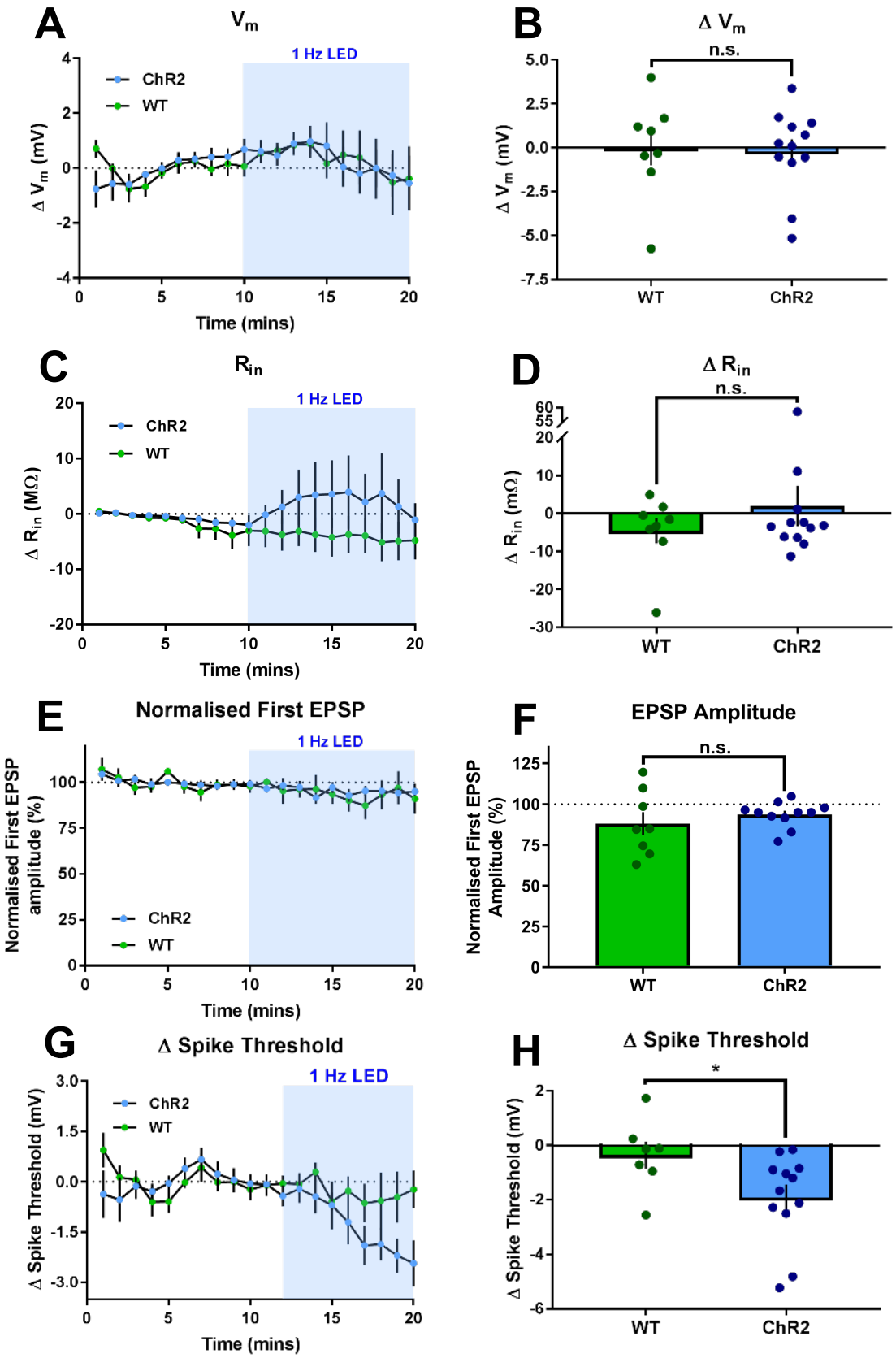

Figure 3.6: *Optogenetically-evoked NA reduces spike threshold but not V_m, R_{in} or synaptic input. A-B) Time-course and averaged data for V_m. C-D) Time-course and average data for R_{in}. E-F) Time-course and averaged data for the first EPSP amplitude. G-H). Time-course and averaged data for spike threshold, the only parameter significantly affected by opto-stimulation in the ChR2-injected mice.*

β-ARs often underlie the excitatory effects of NA, and so we repeated the experiment in the presence of a β-AR-selective antagonist, propranolol (500 nM), for 5 minutes prior to LED stimulation. This concentration had no effect on spike output on its own, and completely occluded the increase in normalised S_P (Figure 3.7A-C, propranolol S_P = 1.0 ± 0.1, propranolol + LED = 1.0 ± 0.2, $p > 0.05$, n = 6, one-Way ANOVA with Dunnett's multiple comparison test).

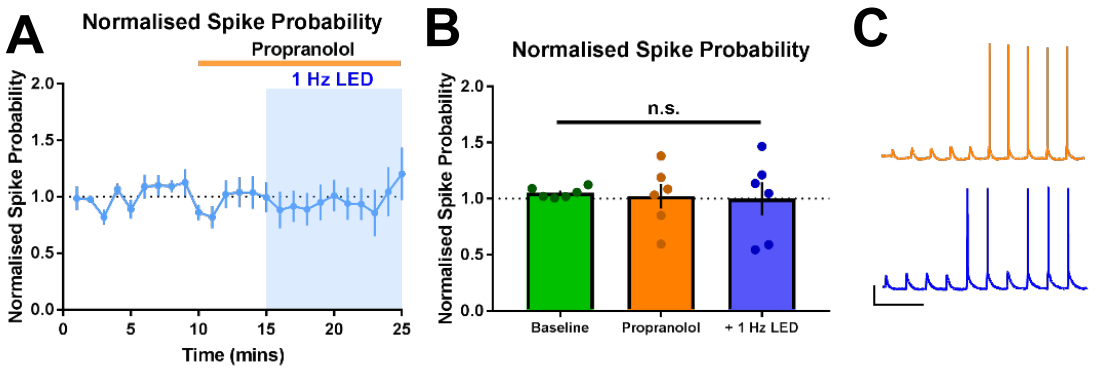

Figure 3.7: *β-AR antagonism prevents the optogenetically-evoked enhancement of synaptically-evoked spike output by NA. A) Time-course showing the lack of effect of propranolol and its prevention of spike output modulation by optically-evoked NA in ChR2-injected mice (n = 6). B) Averaged data for A. C). Example traces for spike output in the presence of propranolol (top) and then with 1 Hz opto-stimulation protocol (bottom). Scale bars = 25 mV and 250 ms.*

3.3.5 Phasic LED stimulation is less efficient at enhancing CA1 spike output

Recent work has suggested different opto-stimulation protocols can elicit distinct neuromodulatory effects (Rosen, Cheung and Siegelbaum, 2015), so we repeated the spike probability protocol with a burst of 10 light pulses (5 ms, 25 Hz) every 20 seconds to see if such effects occurred in our preparation. Baseline resting V_m and R_{in} values were -68.8 ± 2.0 mV and 79.8 ± 3.9 MΩ, respectively. Interestingly, this protocol did significantly enhance normalised S_P from baseline, but to a lower level than that observed using the 1 Hz tonic stimulation (S_P = 1.3 ± 0.1, $p < 0.05$, n = 10, one-way ANOVA with Dunnett's multiple comparison test, Figure 3.8A-D). Similar to the 1 Hz light protocol, we observed no effect on membrane potential (0.1 ± 0.5 mV, $p > 0.05$, one-sampled *t*-test, Figure 3.8E), R_{in} (small decrease of 0.5 ± 2.1 MΩ, $p > 0.05$, one-sampled *t*-test, Figure 3.8F) or the amplitude of the first EPSP (101.8 ± 3.7% of baseline, $p > 0.05$, one-sampled *t*-test, Figure 3.8G). Intriguingly, no effect on spike threshold was observed (increase of 0.3 ± 0.4 mV from baseline, $p > 0.05$, one-sampled *t*-test, Figure 3.8H).

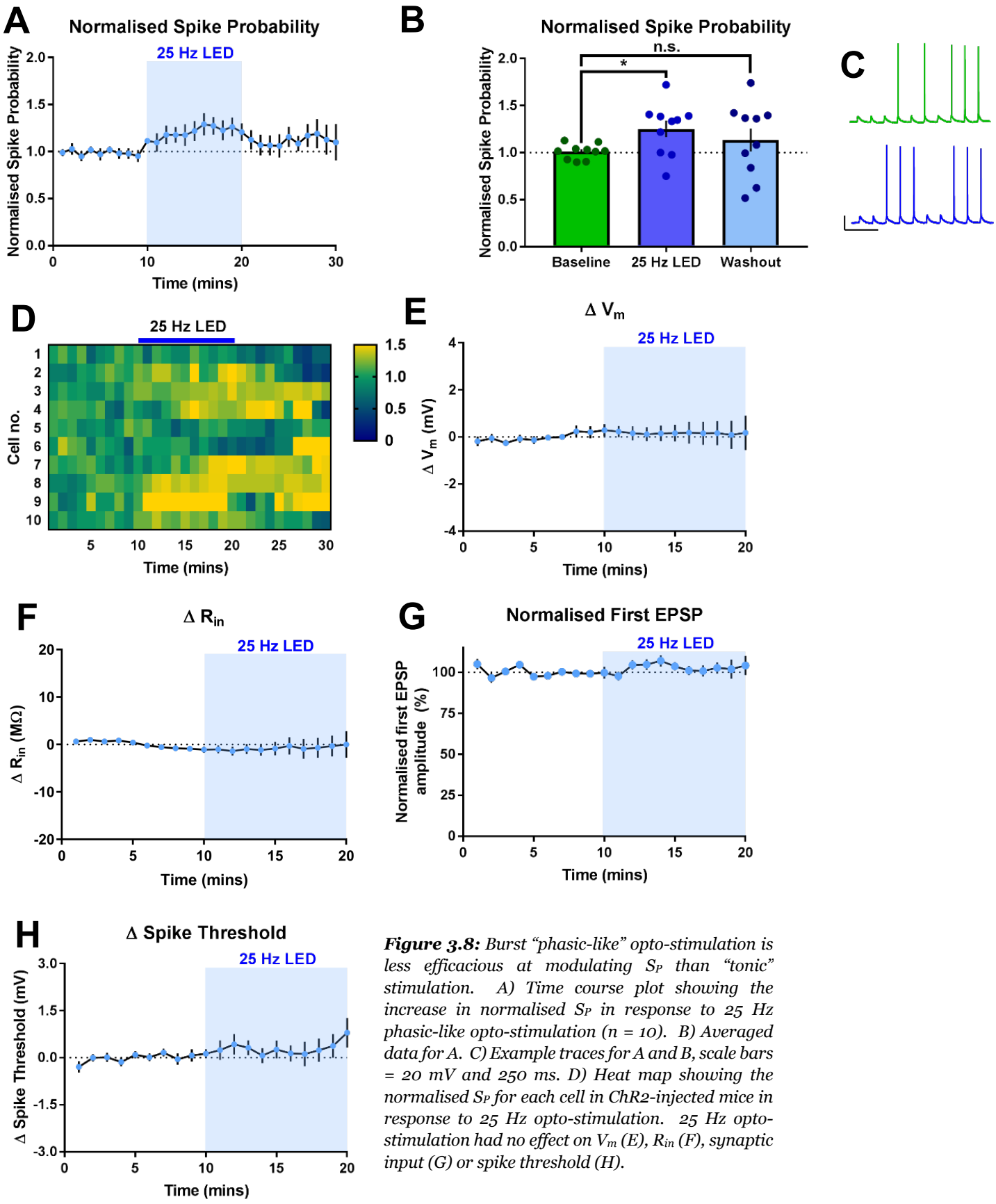

Figure 3.8: *Burst "phasic-like" opto-stimulation is less efficacious at modulating S_P than "tonic" stimulation. A) Time course plot showing the increase in normalised S_P in response to 25 Hz phasic-like opto-stimulation (n = 10). B) Averaged data for A. C) Example traces for A and B, scale bars = 20 mV and 250 ms. D) Heat map showing the normalised S_P for each cell in ChR2-injected mice in response to 25 Hz opto-stimulation. 25 Hz opto-stimulation had no effect on V_m (E), R_{in} (F), synaptic input (G) or spike threshold (H).*

3.3.6 600 nM NA recapitulates the enhanced spike output observed with endogenous NA

A functional dichotomy between bath-applied and endogenous neuromodulators is not unprecedented (Rosen, Cheung and Siegelbaum, 2015), and recent reports suggest that NA release from LC terminals is likely in the low micromolar or even sub-micromolar range (Courtney and Ford, 2014; Muller *et al.*, 2014; Feng *et al.*, 2019). The distinct effects we observed on normalised spike output suggest that optogenetic activation of LC terminals may release a concentration of NA that mediates the β-AR excitatory effects reported here and in previous studies (Liu *et al.*, 2017). In an effort to determine this NA concentration, we repeated the spike probability assay with 200 nM, 600 nM and 2 μM NA.

Unlike the striking effects observed with 20 μM and optogenetically-evoked NA, 200 nM and 2 μM had no appreciable effects on normalised S_P, synaptic input or intrinsic properties (Figures 3.9 and 3.10). 200 nM depolarised neurons by 0.8 ± 0.7 mV (n = 16, $p > 0.05$, one-sampled *t*-test, Figure 3.9E) and reduced R_{in} by 5.9 ± 2.8 MΩ ($p > 0.05$, one-sampled *t*-test, Figure 3.9F). Baseline resting V_m and R_{in} values were -63.0 ± 1.4 mV and 93.6 ± 5.3 MΩ, respectively. Normalised S_P increased slightly upon 200 nM NA application, but this reversed with V_m reset (200 nM NA = 1.1 ± 0.2, V_m reset = 0.9 ± 0.2, n = 8, $p > 0.05$, one-way ANOVA with Dunnett's multiple comparison test, Figure 3.9A-D). Synaptic input (94.7 ± 6.6% of baseline, $p > 0.05$, one-sampled *t*-test, Figure 3.9G) and spike threshold were also unaffected (decrease of 0.7 ± 0.5 mV, $p > 0.05$, one-sampled *t*-test, Figure 3.9H)

With 2 μM NA we observed a small, but non-significant, hyperpolarisation (0.6 ± 0.6 mV, n = 8, $p > 0.05$, one-sampled *t*-test, Figure 3.10E) and a significant reduction in R_{in} by 7.6 ± 2.3 MΩ ($p < 0.05$, one-sampled *t*-test, Figure 3.10F). Baseline resting V_m and R_{in} values were -62.4 ± 1.8 mV and 96.61 ± 5.0 MΩ, respectively. Normalised S_P did not change (2 μM = 1.0 ± 0.2, V_m reset = 1.0 ± 0.2, n = 8, $p > 0.05$, one-way ANOVA with Dunnett's multiple comparison test, Figure 3.10A-D). Synaptic input (98.6 ± 3.5% of baseline, $p > 0.05$, one-sampled *t*-test, Figure 3.10G) and spike threshold were also unaffected (decrease of 0.7 ± 0.5 mV, $p > 0.05$, one-sampled *t*-test, Figure 3.10H).

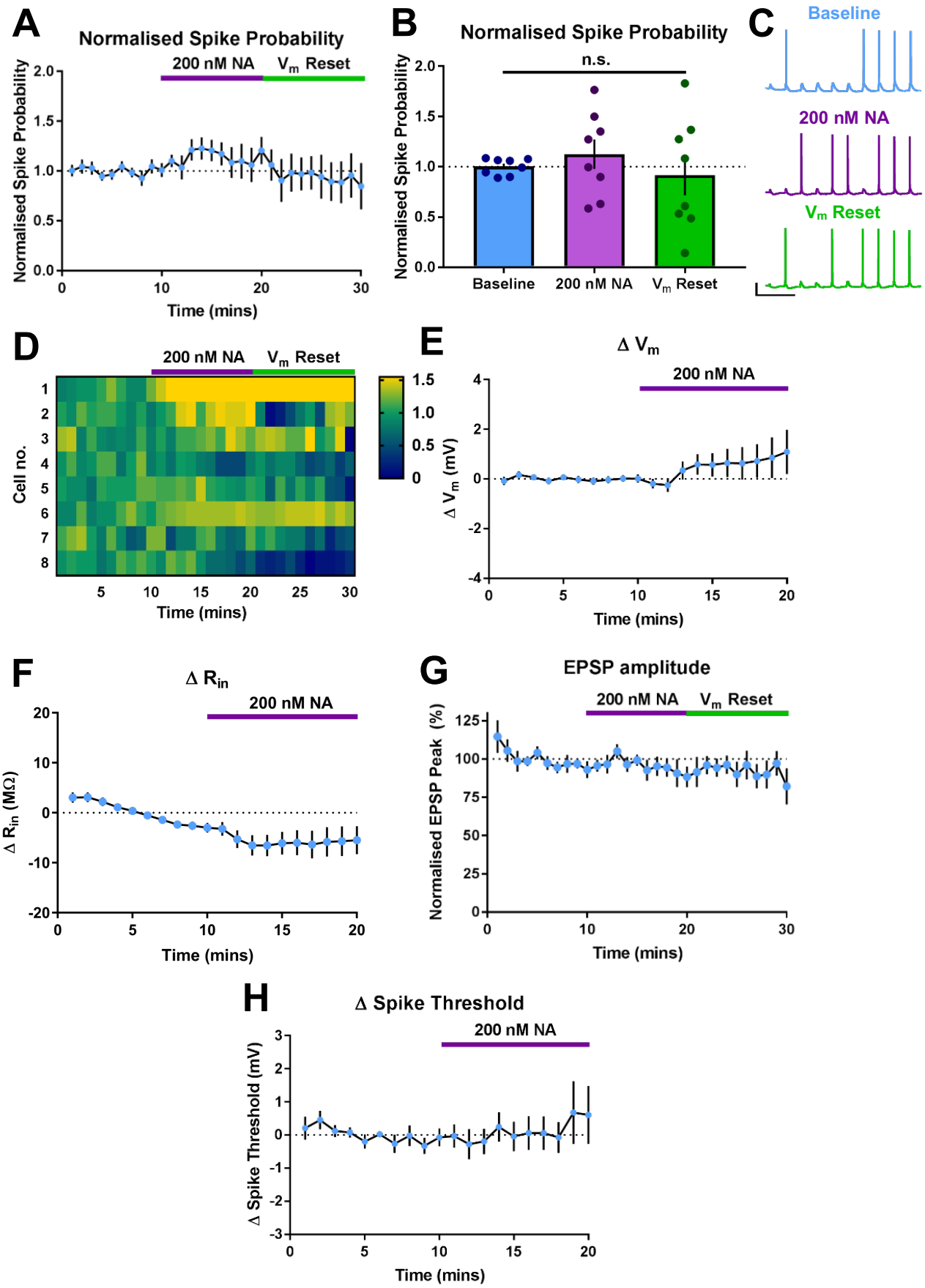

Figure 3.9: *Bath application of 200 nM NA does not modulate spike probability. A) Time course plot showing the normalised S_P in response to 200 nM NA (n = 8). B) Averaged data for A. C) Example traces for A and B, scale bars = 20 mV and 250 ms. D) Heat map showing the normalised S_P for each cell in response to 200 nM NA. 200 nM NA had no effect on V_m (E), R_{in} (F), synaptic input (G) or spike threshold (H).*

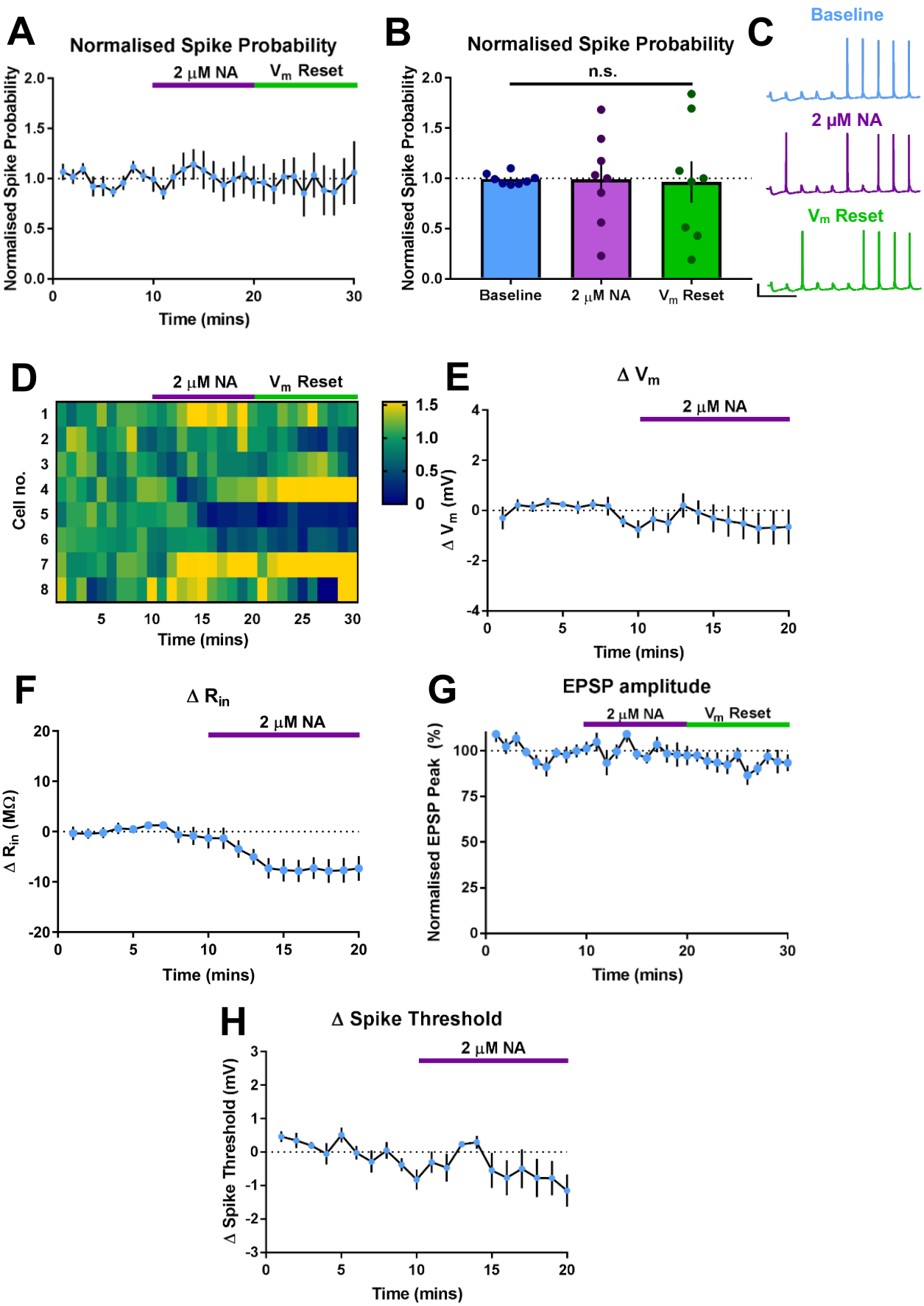

Figure 3.10: *Bath application of 2 μM NA does not modulate spike probability. A) Time course plot showing the normalised S_P in response to 2 μM NA (n = 8). B) Averaged data for A. C) Example traces for A and B, scale bars = 20 mV and 250 ms. D) Heat map showing the normalised S_P for each cell in response to 2 μM NA. 2 μM NA had no effect on V_m (E), synaptic input (G) or spike threshold (H) but did significantly reduce R_{in} (F).*

600 nM NA, however, produced a robust increase in the spike output of CA1 pyramidal neurons, resulting in a normalised S_P of 1.4 ± 0.1 (Figure 3.11A-D, n = 7, $p < 0.05$, one-way ANOVA with Dunnett's multiple comparison test). This increase was sometimes accompanied by a small, non-significant tendency to depolarise (mean = 2.9 ± 1.6 mV, $p > 0.05$, one-sampled *t*-test, Figure 3.11E), however even after resetting the V_m the increase in spike probability persisted, suggesting it was not a simple post-synaptic effect of depolarisation enhancing spiking (1.2 ± 0.2, $p > 0.05$, one-way ANOVA with Dunnett's multiple comparison test, Figure 3.11A-D). R_{in} (decrease of 0.8 ± 3.9 MΩ, $p > 0.05$, one-sampled *t*-test, Figure 3.11F), synaptic input (95.1 ± 13.7% of baseline, n = 7, $p > 0.05$, one-sampled *t*-test, Figure 3.11G), and spike threshold were also not affected (slight increase of 1.7 ± 1.1 mV, $p > 0.05$, one-sampled *t*-test, Figure 3.11H). Baseline resting V_m and R_{in} values were -64.4 ± 2.4 mV and 108.7 ± 10.1 MΩ, respectively.

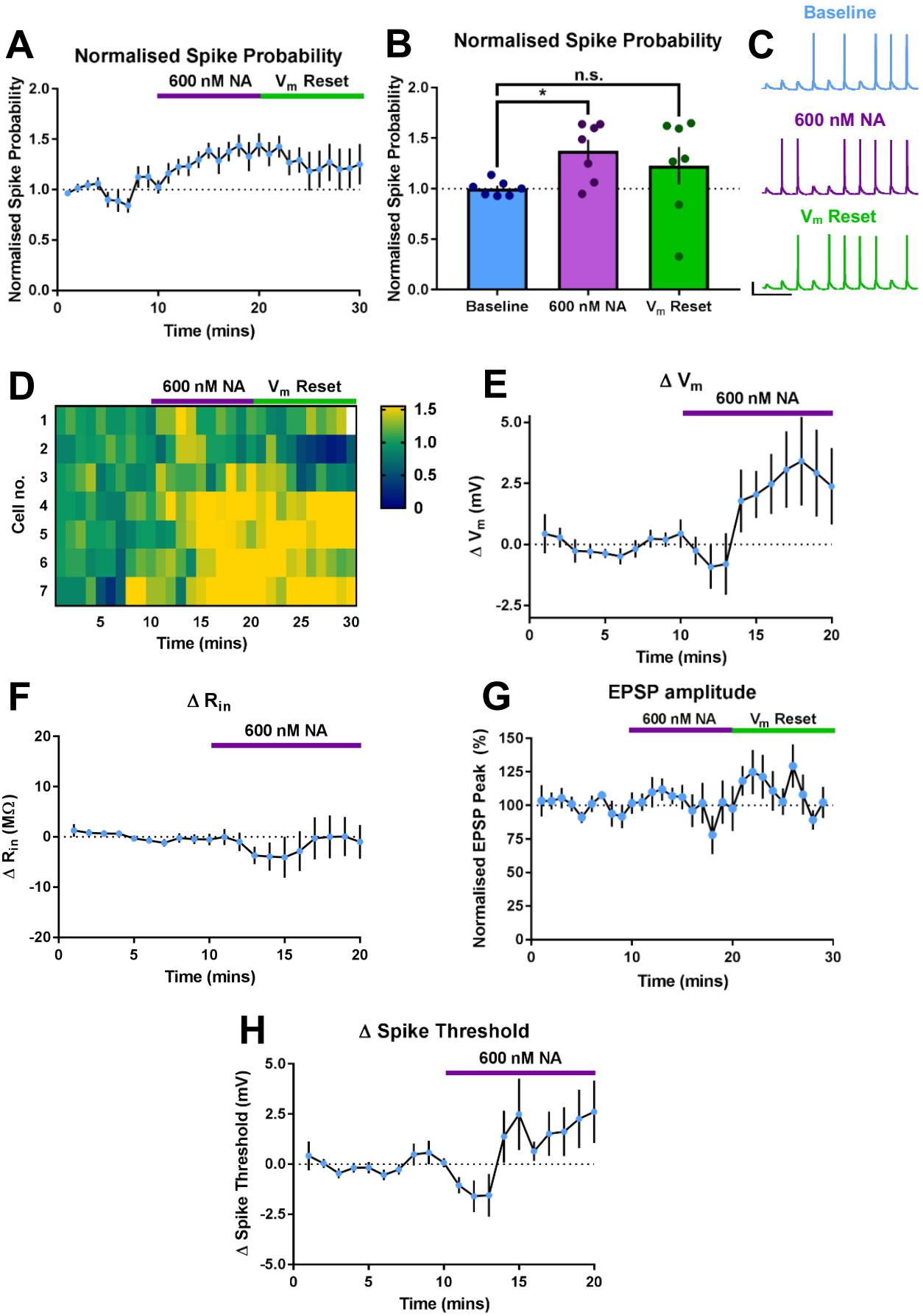

Figure 3.11: *Bath application of 600 nM NA enhances spike probability. A) Time course plot showing the increase in normalised S_P in response to 600 nM NA (n = 7). B) Averaged data for A. C) Example traces for A and B, scale bars = 20 mV and 250 ms. D) Heat map showing the normalised S_P for each cell in response to 600 nM NA. 600 nM NA had no significant effect on V_m (E), R_{in} (F), synaptic input (G) or spike threshold (H).*

Given that we observed a reduction in spike threshold with our 1 Hz opto-stimulation protocol but not with bath application of 600 nM NA (which did produce a similar increase in spike probability), we analysed the baseline spike thresholds in all conditions to determine whether the ChR2-injected animals had a lower spike threshold prior to the release of NA. However, we found no significant differences between the groups (p > 0.05, one-way ANOVA with Tukey's multiple comparison test, Figure 3.13) which, combined with the marginal p value (0.0463) for the reduced spike threshold with the 1 Hz opto-stimulation protocol, suggested we may be underpowered for the analysis of this parameter.

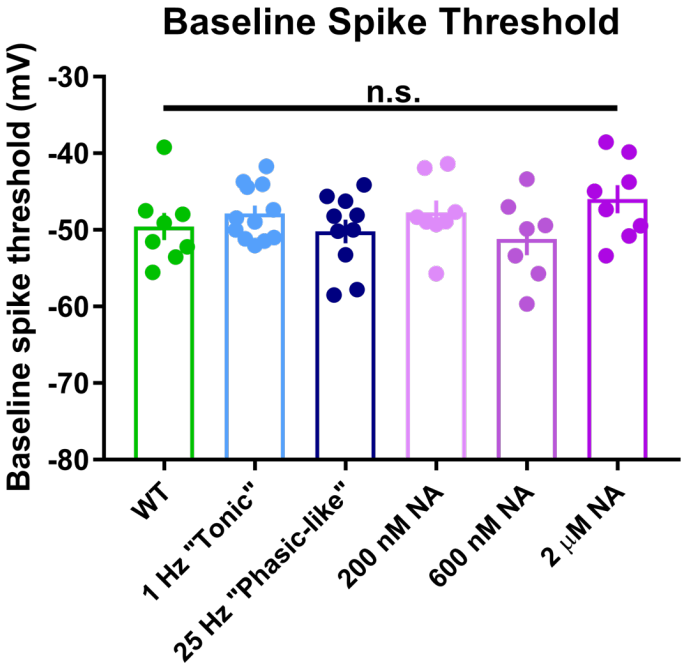

Using our wild-type mice as our "no NA" control, we performed an ANOVA on all the normalised spike probabilities in each condition, which revealed the increases seen with 1 Hz opto-stimulation of the ChR2-injected mice and the bath application of 600 nM NA, and the decrease observed with 20 μM NA as the only significant effects (Figure 3.13A, one-way ANOVA with Dunnett's multiple comparison test). Moreover, plotting the changes in response to the various concentrations of bath-applied NA on a log scale revealed a bell-shaped curve and allowed us to estimate the concentrations of optogenetically-evoked NA with our opto-stimulation protocols. The tonic 1 Hz protocol appeared to be somewhere close to 600 nM NA (Figure 3.12B), whereas the phasic-like burst (25 Hz) protocol evoked a NA concentration that may lie on either one of the shoulders of the curve either side of 600 nM NA (i.e. ~ 300 nM or 1 μM NA, Figure 3.13B).

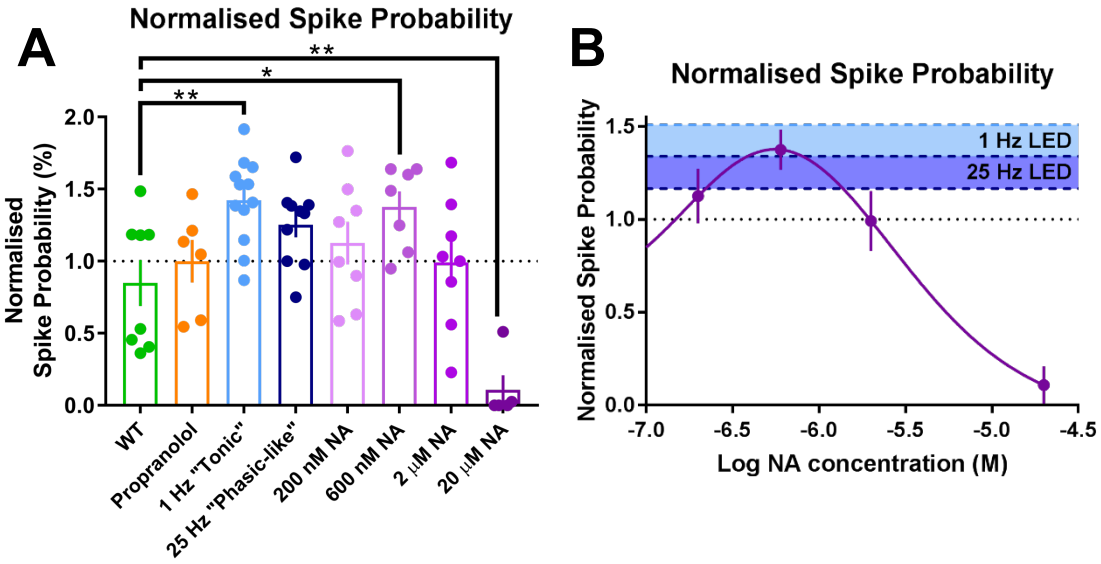

***Figure 3.12**: The increase in spike output with 1 Hz tonic opto-stimulation is recapitulated by bath-application of 600 nM NA. A) Summary of the normalised S_P modulation in all tested conditions. B) Fitting a bell-shaped curve to the bath-applied NA data allowed us to estimate the concentrations of endogenous NA evoked by 1 Hz and 25 Hz opto-stimulation.*

Condition	Parameter				
	V_m	R_{in}	EPSP amplitude	Spike output	Spike threshold
20 μM NA	Hyperpolarisation	↓	↓ *	↓ *	N/A
2 μM NA	No change	↓ *	No change	No change	Small ↓
600 nM NA	Small Depolarisation	No change	No change	↑ *	Small ↑
200 nM NA	No change	↓	No change	No change	No change
WT (1 Hz LED)	No change	No change	No change	No change	No change
ChR2-injected (1 Hz LED)	No change	No change	No change	↑*	↓*
ChR2-injected (25 Hz LED)	No change	No change	No change	↑*	No change

Table 3: *Summary of the effects of bath-applied and endogenous NA on CA1 pyramidal neurons. * denotes a p value < 0.05.*

3.3.7 Endogenous NA and 600 nM NA have no effect on excitatory and inhibitory inputs to the CA1

We sought to determine the common mechanism underlying the enhanced spike output with opto-stimulation and 600 nM NA. Neither endogenous nor 600 nM bath-applied NA appeared to affect SC synaptic input in the current-clamp configuration. Using this first EPSP is a useful proxy for synaptic input to the CA1, but does not give an indication of if and/or how feed-forward inhibitory inputs recruited from SC fibres are affected by NA. We therefore decided to examine this local micro-circuit in more detail using whole-cell voltage-clamp, injecting current to hold the CA1 pyramidal neuron at the experimentally determined reversal potentials for glutamate and GABA receptors. Unlike bath application of 20 μM NA, which significantly attenuated both mono-synaptic EPSCs and feed-forward inhibitory IPSCs (Figure 3.14A), 600 nM NA had no effect on either of these inputs (EPSCs = 88.0 ± 8.3% and IPSCs = 116.5 ± 12.8% of baseline, n = 8 and 6, respectively, $p > 0.05$, one-way ANOVA with Dunnett's multiple comparison test, Figure 3.14C). 1 Hz opto-stimulation of ChR2-injected animals also yielded no changes (EPSCs = 84.2 ± 5.0% and IPSCs = 85.7 ± 7.8% of baseline, n = 6 and 5, respectively, $p > 0.05$, Figure 3.14E). Results of a one-way ANOVA of these data compared to a time-match control is shown in Figure 3.14G-H. The paired-pulse ratio

(PPR) was also not affected in any of these conditions ($p > 0.05$, paired Student's *t*-tests, Figure 3.14B, D and F).

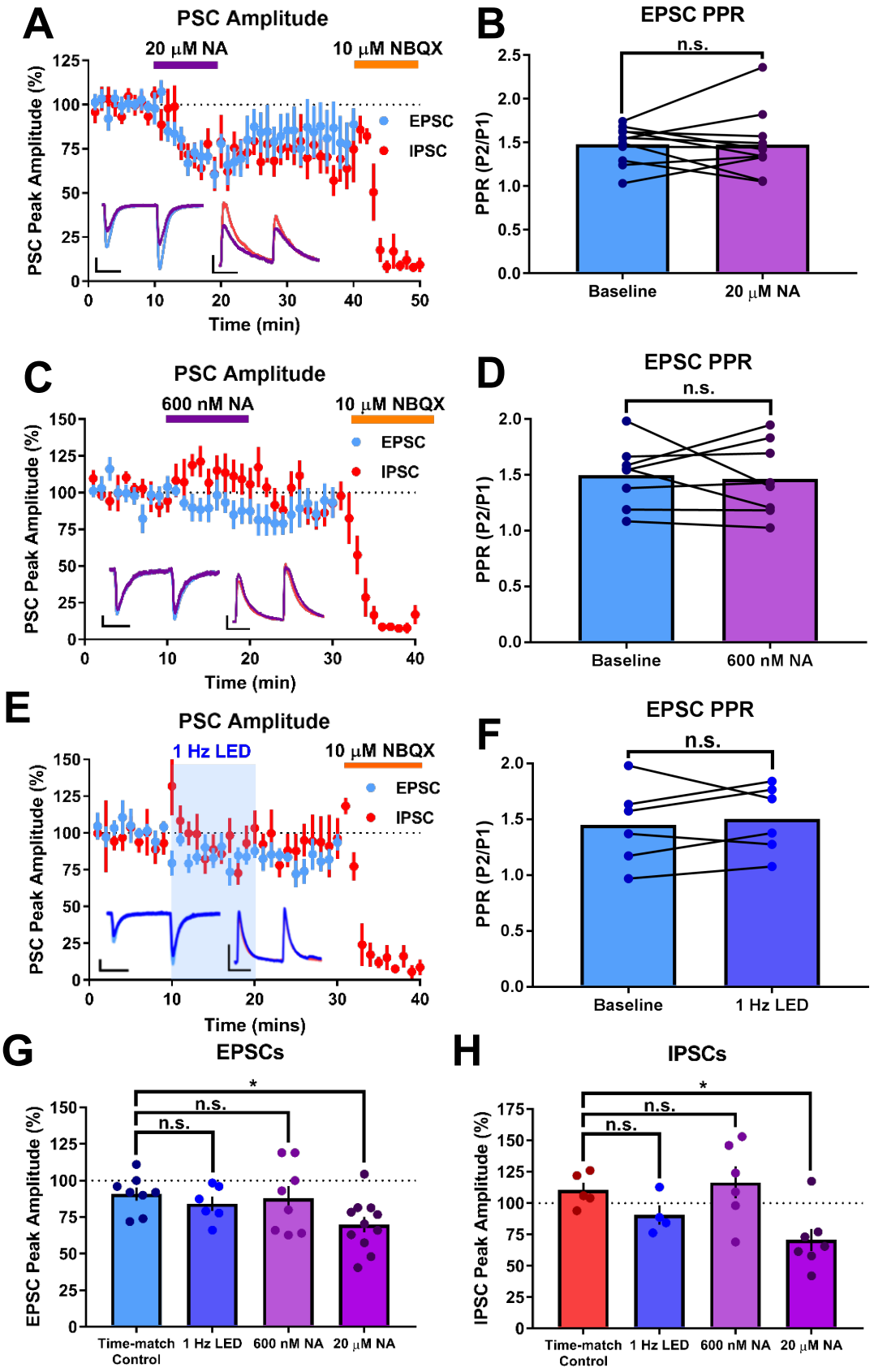

Figure 3.13: *Unlike 20 μM NA, 600 nM NA and optically-evoked NA do not attenuate SC excitatory and feed-forward inhibitory inputs. A, C and E) Time-course traces for 20 μM (A), 600 nM (C) and optogenetically-evoked NA (E) show a reduction in both SC excitatory inputs and feed-forward inhibitory inputs with 20 μM, but not the latter two conditions. Scale bars = 100 pA and 50 ms (both traces in A and IPSCs in C and E), 25 pA and 50 ms (EPSCs, C and E). B, D and F) PPR was not affected by 20 μM (B), 600 nM (D) or optogenetically-evoked NA (F). G-H) Grouped data for each condition.*

3.3.8 600 nM NA, but not endogenous NA, is able to attenuate the sAHP

Due to its role in modulating spike output in response to trains of synaptic input, modulation of the sAHP is one possible mechanism for the enhanced spike output with endogenous and 600 nM bath-applied NA. We first examined whether the sAHP was sensitive to concentrations of NA as low as this, which has been suggested previously (Madison and Nicoll, 1986). Bath application of 600 nM NA indeed caused a reduction in the peak sAHP amplitude that was almost identical to what we previously observed using 20 μM NA (20.6 ± 9.2% of baseline, n = 5, $p < 0.001$, one-way ANOVA with Dunnett's multiple comparison test, Figure 3.15A-E).

Despite a lack of effect on the sAHP with the higher frequency LED stimulation protocol, we decided to repeat the assay with the 1 Hz protocol, since the spike output experiments suggested lower frequency stimulation was more efficient in evoking endogenous noradrenergic modulation. However, although the sAHP was reduced using the 1 Hz opto-stimulation protocol in ChR2-injected mice, this was not as striking as the effects seen with either 20 μM or 600 nM bath-applied NA and was also not significantly different from WT control mice (ChR2 = 84.5 ± 9.6% of baseline, WT = 83.1 ± 5.6% of baseline, n = 9 and 6, respectively, $p > 0.05$, unpaired Student's *t*-test, Figure 3.15F-I).

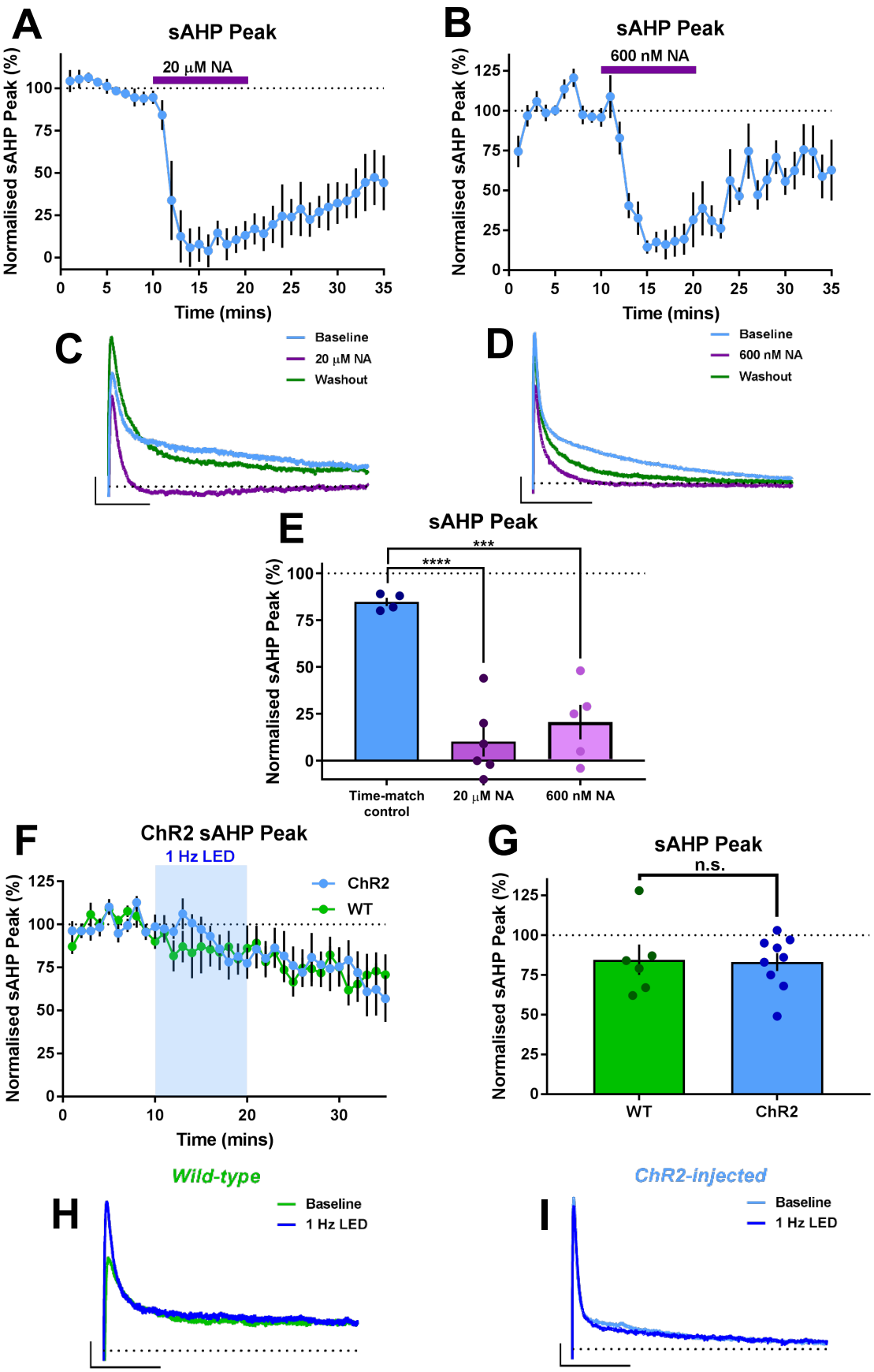

Figure 3.14: *The sAHP is inhibited by 20 μM and 600 nM NA, but not optically-evoked NA. A-D) Time course and example traces of sAHP inhibition with 20 μM (n = 6) and 600 nM NA (n = 5). Scale bars = 50 pA and 250 ms (C), 50 pA and 500 ms (D). E) Averaged data for 20 μM and 600 nM NA versus time-match control (n = 4). F-I) Time course (F), averaged data (G) and example traces for the sAHP in WT (H, n = 6) and ChR2-injected (I, n = 9) mice show no difference between the two groups. Scale bars = 10 pA and 500 ms (WT), 25 pA and 500 ms (ChR2-injected)*

3.3.9 β-AR activation by 600 nM and endogenous NA reduces both spike latency and jitter in response to rheobase injections

Given the lack of effect of endogenous NA on the sAHP, we examined further parameters from the spike probability experiments that were modulated by both endogenous NA and 600 nM NA. We found that spike latency was reduced by both 600 nM NA (baseline = 6.6 ± 0.8 ms, 600 nM NA = 5.6 ± 0.7 ms, n = 7, $p = 0.0527$, paired Student's *t*-test, Figure 3.16C) and opto-stimulation in ChR2-injected mice (baseline = 5.7 ± 0.4 ms, LED = 5.2 ± 0.4 ms, n = 12, $p < 0.05$, paired Student's *t*-test, Figure 3.16A), but not in WT controls (baseline = 6.1 ± 0.4 ms, LED = 5.8 ± 0.3 ms, n = 8, $p > 0.05$, Wilcoxon Matched-Pairs Signed Rank Test, Figure 3.16B).

Spike latency can vary depending on where the SC axons are stimulated, so we decided to re-assess spike latency using the rheobase (the minimum somatic current injection required to evoke a single action potential). Under baseline conditions, K^+ channels (predominantly the Kv1 family) expressed in the somatodendritic region are activated near the action potential threshold and act to suppress action potential firing, resulting in a longer action potential latency and high jitter (SD of the mean action potential latency) (Smart *et al.*, 1998; Liu *et al.*, 2017). Rheobase injections therefore allow a more direct interrogation of the neuromodulation of these K^+ channels and, recently, β-AR activation (via bath-application of NA and optoactivation of ChR2-expressing LC terminals) has been shown to down-regulate the expression of Kv1.1 channels via SAP-97 trafficking, reducing the mean latency and jitter of action potentials evoked using rheobase injections (Liu *et al.*, 2017). This permits more efficient action potential back-propagation, tighter spike-coupling to synaptic inputs and enhanced STDP. We therefore postulated that this mechanism may underlie the enhanced spike output observed with endogenous and 600 nM bath-applied NA.

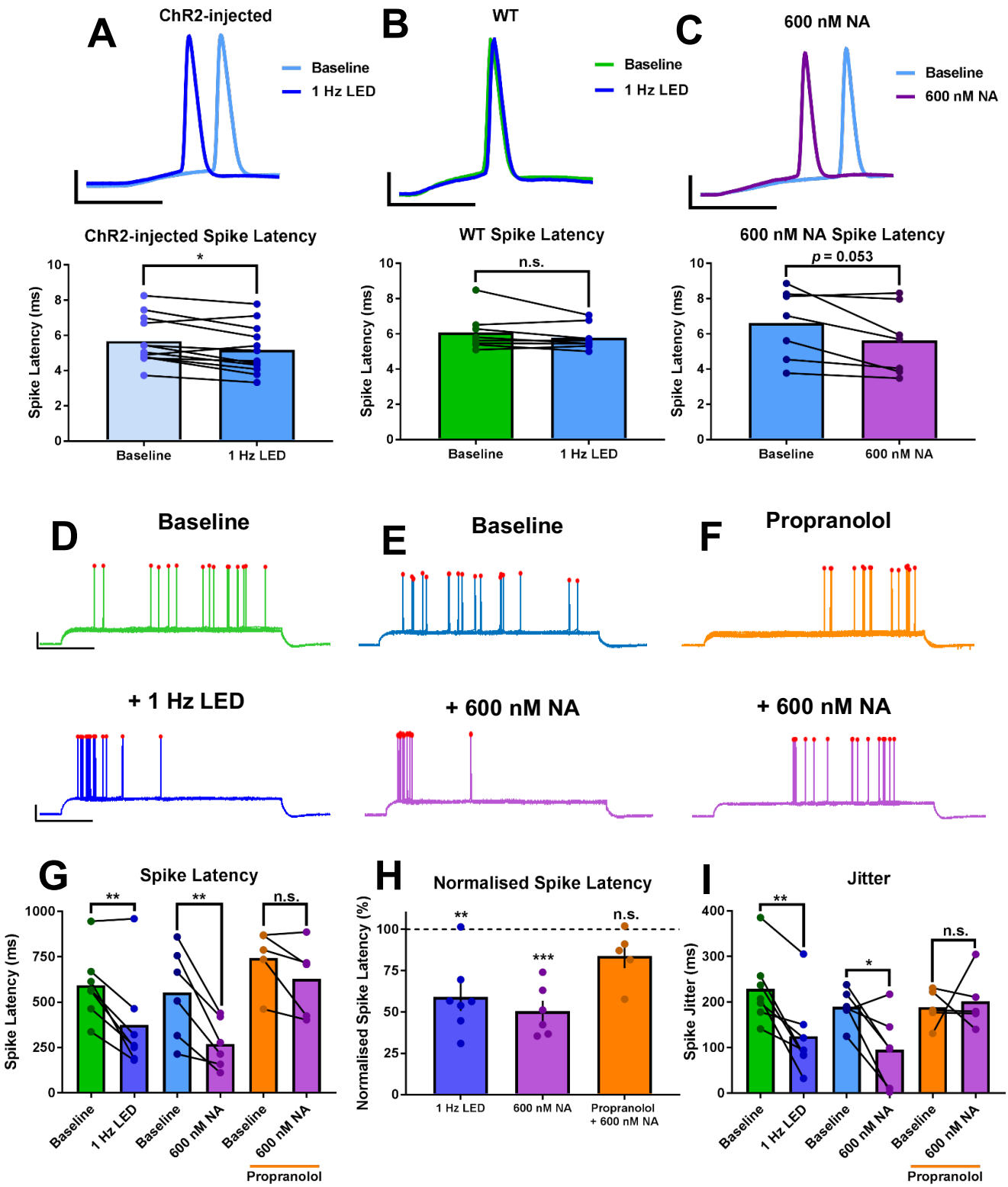

Figure 3.15: *Optically-evoked and 600 nM bath-applied NA reduce spike latency and jitter in response to rheobase injections. A-C) Averaged data and example traces showing that spike latency was reduced with 600 nM NA (C, n = 7) and opto-stimulation in ChR2-injected (A, n = 12), but not WT (B, n = 8), mice. Scale bars = 25 mV and 5 ms. D) Example trace showing a reduction in spike latency and jitter caused by 1 Hz opto-stimulation in ChR2 animals (n = 7). Scale bars = 25 mV and 250 ms. E-F) This effect was recapitulated with 600 nM NA (E, n = 6) and could be blocked with propranolol (F, n = 5). G-I) Averaged data showing the effects of optogenetically-evoked NA and 600 nM NA on spike latency (G), normalised spike latency (H) and jitter (I), as well as the blockade of these effects with propranolol.*

Under baseline conditions, CA1 pyramidal neurons exhibited a mean action potential latency of 594.0 ± 71.4 ms, with a jitter of 229.2 ± 29.7 ms (Figure 3.16D and G, n = 7). However, 1 Hz opto-stimulation of slices from ChR2-injected mice caused a significant reduction in the raw (375.6 ± 103.8 ms, $p < 0.01$, paired Student's *t*-test, Figure 3.16D and G) and normalised spike latency (59.1 ± 8.4%, $p < 0.01$, one-sampled *t*-test, Figure 3.16H), as well as the accompanying jitter (124.7 ± 33.1 ms, $p < 0.01$, paired Student's *t*-test, Figure 3.16I). This effect was recapitulated with 600 nM NA, with raw spike latency significantly reduced from 553.3 ± 103.5 ms to 270.6 ± 55.4 ms ($p < 0.01$, n = 6, paired Student's *t*-test, Figure 3.16E and G), normalised spike latency reduced to 50.5 ± 6.3% ($p < 0.001$, one-sampled *t*-test, Figure 3.16H) and jitter reduced from 189.9 ± 15.67 ms to 95.4 ± 33.3 ms ($p < 0.05$, paired Student's *t*-test, Figure 3.16I). These effects were blocked with propranolol (Figure 3.16F): raw spike latency was not significantly affected (propranolol = 744.4 ± 75.0 ms, + 600 nM NA = 627.7 ± 93.1 ms, $p > 0.05$, n = 5, paired Student's *t*-test, Figure 3.16G), normalised spike latency was showed a non-significant reduction to 83.9 ± 7.6% ($p > 0.05$, one-sampled *t*-test, Figure 3.16H) and jitter showed a non-significant increase (propranolol = 188.8 ± 17.9 ms, + 600 nM NA = 202.0 ± 28.0 ms, $p > 0.05$, paired Student's *t*-test, Figure 3.16I).

3.4 Discussion

Using a viral vector-mediated targeting strategy to enable optogenetic release of endogenous NA from LC terminals in acute hippocampal slices, this work has investigated the noradrenergic modulation of the CA1 subfield. We have explored tonic and phasic-like patterns of optical stimulation to release NA, examined the effects of these on synaptically-evoked firing of CA1 pyramidal neurons and attempted to identify the adrenoceptor subtype and mechanisms underpinning this modulation.

3.4.1 Sub-micromolar concentrations of NA enhance CA1 spike output via a β-AR mechanism

In the present work, we have revealed a functional dichotomy between optogenetically-evoked endogenous NA and bath application of NA (20 μM). Specifically, 20 μM NA completely abolishes synaptically-evoked spiking in CA1 pyramidal neurons, whereas optogenetically-released NA enhances such spike output. Like many of the facilitating effects of NA, this effect appears to be mediated via β-ARs (Dunwiddie *et al.*, 1992; Raman, Tong and Jahr, 1996; Lin *et al.*, 2003; O'Dell *et al.*, 2010; Murchison *et al.*, 2011; Ul Haq *et al.*, 2012; Liu *et al.*, 2017). Interestingly, this effect was recapitulated with a much lower concentration of NA (600 nM) which, although surprisingly low when compared to the typical concentrations of NA used throughout the literature (Madison and Nicoll, 1986; Heginbotham and Dunwiddie, 1991; Hu *et al.*, 2007; Ul Haq *et al.*, 2012), actually falls in line with recent estimates of NA release from LC terminals using

genetically-encoded sensors (Feng *et al.*, 2019). Moreover, our concentration-response curve for NA and normalised S_P agrees with the Yerkes-Dodson inverted-U profile of NA and LC activity reported previously (Devilbiss and Waterhouse, 2000, 2004, 2011; Salgado, Köhr and Treviño, 2012) and outlined in integrative theories of LC function (Berridge and Waterhouse, 2003; Aston-Jones and Cohen, 2005a, 2005b; Sara and Bouret, 2012; Waterhouse and Navarra, 2019). These theories argue that many of the effects modulated by LC activation (i.e. learning and memory, arousal, vigilance) are enhanced by an optimal concentration of NA mediated by an appropriate LC output (the peak of the inverted U-curve). However, chronic and/or high levels of LC firing can lead to distractibility, reduced responses to sensory input and poor task performance. Interestingly, in the visual cortex, bath-application of high (8.75 μM) concentrations of NA cause LTD with both Hebbian and anti-Hebbian STDP protocols via α1-AR activation, whereas low (330 nM) concentrations activate β-ARs and promote potentiation with Hebbian STDP protocols. The mechanisms of these effects were not characterised but agree with our results that a low concentration of NA engages synaptic facilitating mechanisms via β-ARs (Salgado, Köhr and Treviño, 2012).

Although we have not determined the specific mechanisms underpinning this enhanced spike output, we postulate the involvement of a voltage-gated K^+ channel, of the transient rectifier class. Liu *et al.* (2017) recently showed that Kv1.1 is down-regulated by SAP-97 in response to β-AR activation, and this resulted in a profound reduction in the latency and jitter of spikes elicited using rheobase injections. In agreement with these results, we found that both optogenetically-evoked NA and 600 nM NA strongly modulate the latency and associated jitter of spikes elicited with rheobase injections, and these effects are blocked with the β-AR antagonist, propranolol. This, alongside the reduced spike latency observed with synaptic stimulation, suggests an enhanced EPSP-spike coupling in the presence of NA that would improve the precision of consecutive spikes. STDP is crucially dependent on the fidelity of back-propagating action potentials, with wider temporal windows between pre-synaptic input and post-synaptic spiking resulting in less potentiation (Magee and Johnston, 1997; Nishiyama *et al.*, 2000). Therefore, the effect of such noradrenergic modulation would likely be to facilitate STDP at the SC-CA1 synapse, which falls in line with the proposed role of NA in acting as a gating neuromodulator for salient information (Sara, Vankov and Herve, 1994; Sara, 2009; Aston-Jones and Waterhouse, 2016; Liu *et al.*, 2017). Indeed, β-AR activation is known to widen the STDP window at SC-CA1 synapses (Lin *et al.*, 2003).

3.4.2 The effects of NA on spike output are spatiotemporally- and concentration-dependent

Recent work by Rosen, Cheung and Siegelbaum (2015) also highlighted a similar functional discrepancy between bath-applied and endogenous DA evoked using optoactivation protocols similar to those in the present study. We show that this is also the case with NA and further find that such distinct effects are not only concentration-dependent, but also depend on the spatio-temporal release of neuromodulators. Complete inhibition of the sAHP with high concentrations (≥10 μM) of NA have been reported previously (Madison and Nicoll, 1982, 1986; Haas and Konnerth, 1983; Dunwiddie *et al.*, 1992; Sah and Isaacson, 1995), and we also show this using bath application of 600 nM NA in the present study. However, the lack of sAHP modulation with optogenetically-evoked NA release suggests that NA is not released near the K^+ channels giving rise to the sAHP. The precise location of CA1 LC inputs are unknown (Andrade, Foehring and Tzingounis, 2012), but the LC is thought to modulate the network via bulk "volume transmission" (Milner and Veznedaroglu, 1989; Walling *et al.*, 2012). This is in contrast to the CA3 area, where there is some evidence to suggest CA3 pyramidal neurons are synaptically targeted by the LC for more precise regulation (Walling *et al.*, 2012). However, the dichotomy between 600 nM NA and optogenetically-evoked NA on the sAHP would suggest there is at least some degree of CA1 compartmental targeting by LC hippocampal terminals. In acute and cultured hippocampal CA1 neurons, Kv1.1, Kv1.2 and Kv1.6 channels are expressed in the somatodendritic compartment (Grosse *et al.*, 2000), where they regulate spike generation at the axon initial segment (Guan *et al.*, 2006; Liu *et al.*, 2017). Such expression overlaps with that observed for β-ARs (Guo and Li, 2007), and would allow rapid modulation of action potential initiation. Since the molecular identity (and therefore subcellular location) of the K^+ channels underlying the sAHP have yet to be determined (Villalobos, 2004; Andrade, Foehring and Tzingounis (2012), although see King *et al.* (2015) and Turner *et al.* (2016) for the putative candidate KCa3.1) it is plausible that these channels are located in the more distal dendrites and therefore only modulated by saturating concentrations of NA acting on β-ARs. In support of this, the sAHP in CA1 pyramidal neurons can be activated by subthreshold EPSPs, suggesting a dendritic location distant from the soma (Lancaster *et al.*, 2001). Furthermore, using computational modelling, whole-cell patch-clamp recordings and high-speed Ca^{2+} imaging, Power *et al.* (2011) estimated that sAHP-mediating channels are located around 100 μm from the soma in rat basolateral amygdala neurons. This supports previous data in the CA1 also suggesting the sAHP channels are not located at the soma, but dendritically somewhere <200 μm from the cell body (Sah and Bekkers, 1996). Indeed, a more distal – and therefore less readily modifiable – location would not be unlikely

given that the sAHP acts not only to regulate neuronal excitability by counteracting repetitive incoming synaptic barrages in the dendrites (Andrade, Foehring and Tzingounis, 2012), but also shapes the temporal summation of incoming EPSPs (Lancaster *et al.*, 2001).

It is also surprising that, unlike endogenous ChR2 evoked using the tonic 1 Hz opto-stimulation protocol, bath application of 600 nM NA failed to modulate the spike threshold. However, we may be underpowered for the analysis of this parameter for several reasons: 1) there was an increase in spike probability but no change in spike threshold with the phasic-like opto-stimulation protocol; 2) we found no significant differences between baseline spike threshold for any of the conditions, and 3) the *p* value for the spike threshold change with the 1 Hz opto-stimulation protocol was marginal (0.0463).

An interesting disparity between the findings of Rosen, Cheung and Siegelbaum (2015) and the present work are the effects of different light stimulation protocols. Where the tonic and phasic-like light protocols in their study resulted in completely contrasting effects (attenuation and enhancement of SC inputs to CA1, respectively), we find that both cause an increase in synaptically-evoked spike output. It should be noted that our phasic 25 Hz LED protocol was less efficacious in enhancing spike output, only significant when compared to its own baseline and not in an unpaired statistics test against WT control slices (that had received the tonic opto-stimulation protocol). There are a number of possible explanations for this. Firstly, the level of ChR2 expression in the LC terminals within the hippocampus and/or the proximity of the patched CA1 pyramidal neurons to these terminals will vary. Sources of such variability include the accuracy of injection and the time between injection and the electrophysiology experiments. To ensure LC transduction of the viral vector, LC and hippocampal slices were obtained concurrently, and prior to commencing experiments mCherry fluorescence was confirmed in LC slices. If no expression could be confirmed on the electrophysiology rig microscope (e.g. due to poor LC slice quality) then hippocampal slices were stored in 4% PFA after recordings were conducted and mCherry fluorescence was confirmed post-hoc using anti-mCherry antibody staining. The degree of expression was observed to be variable, but we did not try to correlate hippocampal mCherry expression with the magnitude of neuromodulation, which would be advisable for future work. Although very few recordings had to be discarded due to lack of LC transduction, in future it may be of benefit to utilise genetically-manipulated mouse lines (i.e. DβH-Cre or TH-Cre crossed with Cre-ChR2) to further improve ChR2 LC expression. These could also be used in conjunction with opsin variants with improved conductance, such as the ChR2(T159C) variant (Berndt *et al.*, 2011), to examine whether this augments the effects observed in the present work.

Secondly, these experiments were carried out in *ex vivo* slice preparations and therefore slight differences in the flow rate of the aCSF perfusate may affect how quickly the neuromodulator released using opto-stimulation is washed away. Although we have evidenced a degree of neuronal targeting by the LC in the CA1, "bulk transmission" is the prevailing theory for how neuromodulation by the LC occurs (Milner and Veznedaroglu, 1989; Walling *et al.*, 2012). Therefore, 1 Hz tonic stimulation of fibres may allow the concentration to build to a functional level, whereas the less frequent bursts of 25 Hz stimulation may cause the release of a lower concentration that is not sustained in *ex vivo* slice experiments (due to perfusion or NA re-uptake by transporter proteins, for instance, Pacholczyk, Blakely and Amara (1991)). In agreement with this, higher frequency opto-stimulation (>10 Hz) of ChR2-expressing LC terminal *in vivo* causes a depletion in cortical NA levels (Carter *et al.*, 2010). If re-uptake by noradrenaline re-uptake transporters (NETs) were indeed the cause of the discrepancy between our tonic and phasic-like protocols, then the inclusion of a NET inhibitor such as nisoxetine would likely result in a similar increase in normalised S_P. Conversely, the concentration of NA released with the phasic-like protocol may actually be higher than 600 nM and engaging inhibitory mechanisms to counteract the β-AR effects. If this were the case then NET inhibition may result in an attenuation of the effects observed with the tonic opto-stimulation protocol.

Thirdly, an interesting explanation put forward by Jing *et al.* (2018) in their cholinergic sensor study suggests that higher stimulation frequencies may recruit more pre-synaptic auto-inhibition on neuromodulator-releasing neurons, leading to attenuated release and less efficient modulation. Such auto-inhibition does exist on LC terminals (Starke and Montel, 1973) and was proposed to underscore the effects seen by Carter *et al.* (2010) in the pre-frontal cortex. However, this notion is hard to reconcile with the fact that burst firing of the LC promotes enhanced memory and learning (Takeuchi *et al.*, 2016), and that a brief 100 Hz electrical stimulation to the LC can enhance *in vivo* CA1 noradrenaline by two-fold (Lemon *et al.*, 2009), measured by microdialysis 10 minutes post-stimulation. A simpler explanation could be that the increased NA released by 25 Hz stimulation causes a rapid desensitisation of the β-ARs (Florin-Lechner *et al.*, 1996; Gainetdinov *et al.*, 2004). GPCR desensitisation can take the form of a reduction in β-AR expression and/or affinity for NA due to phosphorylation by PKA or βARK (β-adrenoceptor kinase) (Lohse *et al.*, 1990, 1996; Hausdorff, Caron and Lefkowitz, 2019), however changes in expression are not normally seen within 15 minutes of agonist exposure (but see Liggett *et al.*, 1993). Reduced β-AR affinity for isoproterenol can occur within 15 minutes, but since most studies on β-AR desensitisation utilise high concentrations of this specific β-AR agonist (which has a much higher affinity for β-ARs

than NA) it is unknown how rapidly desensitisation would occur with endogenous NA (Insel *et al.*, 1983; McGraw *et al.*, 1998).

Finally, it may be that the axons are unable to reliably follow higher frequency light stimulation (25 Hz was the upper limit when stimulating the cell body), thus causing less NA to be released from their terminals. Using an opsin variant with faster off-kinetics such as ChIEF (Lin *et al.*, 2009) may therefore be more useful in examining the effects of phasic-like opto-stimulation protocols.

In any case, as a result of one or several of these factors, the concentration of NA released using 25 Hz phasic-like opto-stimulation likely lies on one of the shoulders of the bell-shaped curve outlined in Figure 3.12B, suggesting it is too high or too low to exert a reliable increase on spike output.

3.4.3 Excitatory and feed-forward inhibitory components of the SC-CA1 micro-circuit are not attenuated by 600 nM exogenous or endogenous NA

Unlike the distinct effects of 600 nM NA and endogenous NA on the sAHP, we found that neither of these affected the excitatory and feed-forward inhibitory synaptic inputs at the SC-CA1 synapse. This was initially apparent in the current-clamp spike probability experiments, but further clarified in voltage-clamp.

The absence of any effects on synaptic input in both conditions adds further support to the notion that 600 nM NA is indeed mimicking a physiologically-relevant concentration but throws into question the modulation achieved with the much higher concentrations used earlier (Chapter 2) and in previous research. The order of NA's affinity for adrenoceptors is α2>α1>β-ARs (O'Rourke *et al.*, 1994; Ramos and Arnsten, 2007; Atzori *et al.*, 2016), therefore – assuming our proposal in Chapter 2 that SC-CA1 inputs are attenuated by SC pre-synaptic α2-ARs is correct – we would expect to see an effect of 600 nM NA on SC-CA1 synaptic inputs. We did observe a minor reduction in SC-CA1 EPSC amplitude with 600 nM NA, but no effect on feed-forward IPSCs. CA1 interneurons are known to express α1-ARs (Doze, Cohen and Madison, 1991; Bergles *et al.*, 1996; Hillman *et al.*, 2005, 2009; Papay *et al.*, 2006; Hillman, Doze and Porter, 2007), which also underlie excitatory effects of NA via G_q-coupled GPCRs, therefore a conceivable explanation could be that 600 nM NA is exerting a reduction in SC axon glutamate release (observed as a small decrease in the evoked EPSC amplitude) but a concurrent α1-mediated depolarisation of interneurons may still allow sufficient recruitment of interneurons and little change in the feed-forward IPSC amplitude. The lack of effect with endogenous NA could be due to a lower degree of CA3 axonal and/or dendritic targeting of CA1 neurons by the LC, adding further support to the idea that a degree of compartmentalised targeting by the LC exists in the CA1.

Alternatively, an uneven distribution of NA re-uptake machinery may exist in the slice such that low levels of NA in close proximity to the synapse are rapidly removed (thus exerting little effect on synaptic transmission), but a lower level of re-uptake transport proteins around the soma permits the increase in spike output.

3.4.4 Reconciling the effects of tonic and phasic LED protocols with behaviour

Much of the early literature surrounding noradrenergic modulation was concerned with the phasic burst firing that is initiated in the LC nucleus upon novel or emotional stimuli (Aston-Jones and Bloom, 1981; Rajkowski, 1994; Vankov, Herve-Minvielle and Sara, 1995; Waterhouse, Moises and Woodward, 1998). A well-accepted hypothesis is that this switch allows one's attention to be concentrated on the task at hand, sharpening sensory perception, minimising error, improving learning and facilitating the encoding of the experience (Aston-Jones and Bloom, 1981; Waterhouse *et al.*, 1988; Aston-Jones *et al.*, 1994; Rajkowski, Kubiak and Aston-Jones, 1994; Hurley, Devilbiss and Waterhouse, 2004); however, see Clayton *et al.* (2004) for evidence of similar phasic LC activation prior to both correct and incorrect trials). Within the hippocampus, this phasic firing is thought to underpin global remapping of place maps (Wagatsuma *et al.*, 2018; Grella *et al.*, 2019). Intriguingly, LC silence during sleep is vital for the consolidation of these place maps, with opto-stimulation of the LC during sleep impairing place field formation and hippocampus-dependent memory task performance (Swift *et al.*, 2018).

Conversely, tonic LC firing was initially considered to be a "background" quiescent state of LC function during which attention to the task in hand decreases and false-alarm errors increases (Aston-Jones *et al.*, 1996). Therefore, it initially appeared that the tonic firing was a correlate of distractibility, whereas phasic firing signified task engagement (Aston-Jones and Cohen, 2005a, 2005b). However, the tonic mode of LC firing is now thought to play a crucial role in adaptive behavioural adjustments that optimise performance across tasks, effectively maintaining a "scanning" attentiveness (Usher *et al.*, 1999; Kane *et al.*, 2017; Sales *et al.*, 2019). Where phasic LC firing sharpens gain in the relevant neural pathways to optimise performance on a single task, tonic LC activity causes a widespread, persistent increase in gain to render an individual more sensitive to task-irrelevant stimuli if the present task is no longer rewarding (Aston-Jones and Cohen, 2005a, 2005b). Experimentally, the switch between phasic (exploitative) to tonic (explorative) behaviour was shown by Aston-Jones, Rajkowski and Kubiak (1997) when – following reversal of reward contingencies – LC phasic firing diminished and tonic firing increased. This is also observed in humans, where pupil diameter dilates strongly (a proxy for LC phasic firing) in early and easy reward trials, but baseline pupil diameter (positively correlated with LC tonic activity) increases with more difficult tasks, all the way up to the point when the trial series is aborted (Richer and Beatty, 1987; Rajkowski, Kubiak and Aston-Jones, 1993; Gilzenrat *et al.*, 2010). In addition, 1 Hz tonic (but not

10 Hz phasic) opto-activation of the LC also increases locomotor activity in mice (Carter *et al.*, 2010), which functionally may be involved in the foraging task disengagement and enhanced exploration attributed to tonic LC firing by Kane *et al.* (2017).

For the present study, we chose the 1 Hz and 25 Hz opto-stimulation protocols based on the results published by Rosen, Cheung and Siegelbaum (2015) and Takeuchi *et al.* (2016), however *in vivo* LC tonic firing is not fixed at 1 Hz but fluctuates (Aston-Jones and Bloom, 1981) with a subtle relationship with goal-directed task flexibility (Aston-Jones and Cohen, 2005a, 2005b). Indeed, 1 Hz is above that seen in rodents and monkeys during sleep and drowsiness and can produce a substantial increase in LC NA release of ~50%. (Devilbiss, Page and Waterhouse, 2006). However tonic firing can increase up to ~6 Hz during quiet waking and in response to a novel (but less arousing) stimuli (Foote, Aston-Jones and Bloom, 1980). Neurochemically, it has been shown that NA levels in the medial pre-frontal cortex and thalamus increase in a frequency-dependent manner in response to tonic stimulation of the LC (Florin-Lechner *et al.*, 1996; Devilbiss, Page and Waterhouse, 2006; but see Carter *et al.* (2010) for decreases at higher frequency stimulation). These findings indicate that relatively small oscillations in tonic LC discharge rates (i.e. from 3 to 5 Hz) result in notable increases in NA release (~40%), therefore increasing the tonic stimulation frequency in our spike probability experiments may reveal a greater degree of neuromodulation. Moreover, the potential confounding effects regarding phasic-like opto-stimulation outlined earlier may have occluded stronger or more rapid neuromodulation with the phasic-like opto-stimulation frequency akin to LC firing during a salient stimulus.

There is some evidence, however, that suggests higher tonic opto-stimulation may further enhance the effects we observed, and such evidence actually supports the greater modulatory effect we observed with the lower 1 Hz stimulation. Using principal component analysis, Devilbiss, Page and Waterhouse (2006) found that the information encoded by VPM thalamic neurons (as well as the synchronous discharge of synaptically-connected neurons) was highest with 1 Hz LC stimulation, and this functional connectivity actually decreased at 5 Hz. In addition to this, phasic LC firing in response to sensory stimuli depends on tonic LC firing rate, with higher tonic levels associated with weaker phasic responses and poorer task performance (Usher *et al.*, 1999). Task performance and tonic firing frequency were so closely linked that an increase of just 1 Hz (from 2 Hz to 3 Hz) was enough to impair task performance, therefore examining the effects of such minor changes in modulating hippocampal circuitry is of great interest. The aforementioned Yerkes-Dodson inverted U-curve for NA concentration has also been demonstrated in performance levels of working memory (Arnsten and Dudley, 2005; Sara, 2009) and vigilance (Rajkowski, Kubiak and Aston-Jones, 1994). Moreover, chronic high-frequency phasic firing can induce behavioural arrest (Carter et al., 2010)

and elevated tonic firing and is thought to mediate stress-related effects rather than sharpen cognitive function (Valentinol and Foote, 1987).

If tonic LC firing is indeed involved in switching to an exploratory behavioural mode over an exploitative one (Aston-Jones and Cohen, 2005a, 2005b; Sales *et al.*, 2019), an animal will need to be able to remember its spatial location and be able to recognise it while surveying an area. Therefore, a functional role for the enhanced EPSP-spike coupling in response to 1 Hz tonic LC terminal stimulation may be to facilitate STDP at the SC-CA1 synapse through increased neuronal excitability and back-propagating action potentials (Liu *et al.*, 2017). This may even stretch to enhanced TA-CA1 STDP. Indeed, glutamatergic activation of the LC can promote β-AR-dependent potentiation of the perforant path inputs to the dentate gyrus *in vivo* (Walling and Harley, 2004), but the TA inputs to CA1 remain to be properly explored. Moreover, Grella *et al.* (2019) acknowledge that whilst phasic LC activity facilitates global remapping of hippocampal place fields, tonic LC activity may support rate remapping, however this also remains to be investigated.

3.5 Additional limitations and future directions

3.5.1 Further support for the Kv1.1 theory

The idea that the enhancement of synaptically-evoked CA1 spike output is mediated by a reduction in voltage-gated K^+ channels (specifically Kv1.1) requires additional support. Indeed, we have effectively replicated the rheobase results in Liu *et al.* (2017), where they show that the reduction in spike latency and jitter can also be achieved using dendrotoxin-K to block Kv1.1 channels. The species and age of mice are similar in both studies, and so there is little reason to suspect an alternative mechanism, but confirming such results using the same pharmacological and genetic (SAP-97 KO or KvΔ4) manipulations would lend further credence to our hypothesis.

3.5.2 Additional antagonist studies

We have attributed the modulatory effects of NA to β-ARs by showing clear inhibition of endogenously evoked NA using the β-AR antagonist propranolol. We have little reason to suspect dopaminergic involvement (NA acting at DARs and/or DA acting at adrenoceptors) for several reasons: 1) mCherry fluorescence in the LC co-localised strongly with DβH, thus the LC neurons excited by ChR2 are unlikely to contain DA; 2) endogenous release from LC terminals with tonic 1 Hz opto-stimulation is likely insufficient to cause NA vesicle depletion and the recruitment of immature vesicles potentially containing unconverted DA (Wagatsuma *et al.*, 2018); 3) if such DA release did occur then the amount of DA released would therefore be negligible and, since the affinity of DA for β-ARs is 100-fold lower than NA, DA is unlikely to be mediating the effects we have observed (Wieland *et al.*, 1996); 4) low (1 μM) concentrations of bath-

applied DA show an increase in the latency of depolarisation-evoked spiking and an increase in the sAHP that are in direct contrast to our results (Benardo and Prince, 1982; Stanzione *et al.*, 1984; Pockett, 1985); 5) very high (100 μM) concentrations of bath-applied NA in the presence of propranolol and prazosin (α1-AR antagonist) fail to recapitulate the D1R-mediated glutamate increase in CA1, suggesting NA is not an endogenous ligand for D1Rs in the CA1 (Smith and Greene, 2012). Nevertheless, it would be of use to repeat the experiments using a D1/D5 receptor antagonist (i.e. SCH-23390) to categorically rule out the possibility that NA could be acting at DA receptors.

An exciting additional approach would be to utilise the novel opto-β_2AR opsin, a chimeric β-AR adrenoceptor that can be expressed in neurons using the CaMKII promoter and is activated by blue light (Siuda *et al.*, 2015). Expression and activation of this opto-β_2AR opsin in the basolateral amygdala depolarises neurons and increases their firing rate. A drawback of the tool is that the cAMP production is ~16-fold lower than cAMP production by endogenous β-ARs. Since the effects of β-AR on K^+ channels rely on cAMP-mediated PKA (Liu *et al.*, 2017), such a tool may not be reliable in inducing changes in spike probability, despite its possible utility in determining the receptor responsible.

3.5.3 Modulation of TA inputs

Similar to Chapter 2, we have only examined the noradrenergic modulation of SC inputs to CA1. Evoking CA1 spiking though temporoammonic (TA) synaptic inputs is much more difficult than with SC stimulation (Takahashi and Magee, 2009), but given the present evidence that endogenous NA preferentially modulates CA1 function post-synaptically (as opposed to the putative pre-synaptic modulation observed with 20 μM NA in Chapter 2), it would be interesting to investigate if (and how) endogenous NA gates TA inputs. The present data suggest endogenous noradrenergic modulation is focused near the soma, therefore since TA inputs are distal and subject to feed-forward modulation (Lisman, 1999; Ang, Carlson and Coulter, 2005; Takahashi and Magee, 2009; Milstein *et al.*, 2015) there may be little effect on TA inputs alone. However, since the Liu *et al.* (2017) and the present data imply a reduction in voltage-gated K^+ channel expression, back-propagating action potentials resulting from SC inputs may be enhanced, broadening the temporal window for SC and TA integration. Indeed, temporally precise SC and TA inputs enable rapid formation of hippocampal place fields (Bittner *et al.*, 2015), therefore the functional correlate of the facilitated integration by NA could be an enhanced induction of new place field formation and better performance on memory tasks relying on recognising a familiar environment (Remondes and Schuman, 2004; Kinnavane *et al.*, 2016).

3.5.4 Tonic versus phasic LED protocols and regular versus irregular synaptic inputs

In addition to increasing the stimulation frequency for the tonic LED protocol, some adjustments could be made to the phasic-like protocol. In the present work, we arbitrarily assigned our cyclic "LC bursting" to a time-point just prior to SC synaptic events in order to "prime" these inputs. There are two inherent problems with this: the first is that this co-ordinated "LC burst-SC synaptic input" order may not occur *in vivo*. Running the phasic protocol concurrently with the synaptic input may result in more reliable increases in spike output. The second problem is that these SC synaptic inputs are a rigid, regular frequency, where *in vivo* such inputs are highly irregular Poisson-like spike patterns (Rich, Liaw and Lee, 2014). Examining the effects of both tonic and phasic LED protocols on the plasticity of irregular spike train stimulation will likely reveal further insights into how endogenous NA modulates the dynamics of excitatory and inhibitory synapses in the CA1.

3.5.5 Improvements to the measurements of fluorescent LC fibres

The broad findings of our IHC analysis of LC inputs to the hippocampus are in contrast with much of the historical literature, which suggests a greater innervation of the DG-CA3 area over the CA1 (Gage, Thompson and Valdes, 1978; Milner and Bacon, 1989; Oleskevich, Descarries and Lacaille, 1989). Our findings align more closely with recent findings that instead show a non-significant trend towards increased DG-CA3 innervation by the LC (Kempadoo *et al.*, 2016; Wagatsuma *et al.*, 2018), perhaps due to more rigorous and accurate image analysis that were somewhat lacking in earlier studies. Interestingly, previous research has suggested that the ventral pole of the hippocampus is more densely innervated by the LC than the dorsal pole (Gage, Thompson and Valdes, 1978; Loy *et al.*, 1980; Oleskevich, Descarries and Lacaille, 1989) and so we were somewhat surprised to find no difference across the dorso-ventral axis. This uniformity of LC inputs across the dorso-ventral axis may not arise from the same LC module (i.e. distinct LC modules may each target sections along the hippocampal dorso-ventral axis) (Loughlin, Foote and Bloom, 1986; Chandler, Gao and Waterhouse, 2014; Kebschull *et al.*, 2016; Li *et al.*, 2016; Hirschberg *et al.*, 2017), and so potential modular targeting of the hippocampal poles may not be apparent in anterograde tracing studies, but the relative activation of distinct LC modules *in vivo* may underlie selective modulation of the hippocampal poles. Injecting a virus like that used in the present study directly into the LC will fluorescently label terminals in all output nodes throughout the CNS (including dorsal and ventral hippocampal poles); in contrast, retrograde targeting of the LC by injecting the dorsal and ventral hippocampus with different PRS- or DβH-controlled fluorophores would ascertain whether such LC modules exist.

Another reason for the absence of any dorso-ventral selectivity could simply be that we were underpowered, since several animals had to be excluded due to lack of LC

fluorescence (an indicator that the injection had missed its target). However, the use of a Hessian filter and the modern quantitative analysis tools offered by ImageJ are less prone to error than the manual counting methods used in earlier studies. One advantage of the Hessian filter is that it works well with low magnification images, allowing large areas to be analysed without the need for digital stitching of images taken with higher magnification (but admittedly higher resolution) microscopes (Sathyanesan, Ogura and Lin, 2012). Future research could expand on the present work by investigating the fluorescent levels across the hippocampal sublayers, which would inform future optogenetic experiments (for instance, whether it is better to stimulate the pyramidal cell layer or the *stratum radiatum*, depending on where the LC inputs are strongest).

Nevertheless, the digital filtering methods used in the present study do have caveats: autofluorescence caused by bubbles and tissue folding during the mounting of slices are largely reduced but not completely eliminated. The high DG granule cell numbers and immense reciprocal connectivity within the CA3 subfield (Ishizuka, Weber and Amaral, 1990) can result in excitotoxicity and cell death (Choi, 1988), potentially leaving this region most susceptible to autofluorescence and false positive signals in quantitative analysis. Moreover, the manual drawing of the DG-CA3 and CA1 ROIs is open to bias, which may have affected measurements. In future, the ROIs could be drawn on the bright-field image and then applied to the fluorescent counterpart, reducing the potential for such bias.

3.6 General conclusion

Due to their very nature, bath application and optogenetically-evoked release of endogenous NA are unlikely to have identical effects. The present work has provided further support for the notion of this functional dichotomy, and the distinct effects appear to be mediated by differences in spatiotemporal properties as well as concentration. However, we do show that some of the effects of endogenous NA can be recapitulated using a concentration of bath-applied NA that is physiologically relevant.

Specifically, sub-micromolar concentrations of NA enhance the spike output of CA1 pyramidal neurons in response to SC synaptic stimulation. This facilitation is mediated by a β-AR mechanism that potentially down-regulates voltage-gated K^+ channels. We have also shown that tonic opto-stimulation of LC fibres is more efficacious in modulating CA1 spike output, and this may be relevant behaviourally in the exploration of environments. Our results also hint at some level of potential compartmental targeting of the CA1 by LC inputs, as well as a uniformity of these inputs across the dorso-ventral axis.

Chapter 4: Effects of bath-applied NA on the MF-CA3 micro-circuit

4.1 Introduction

The MF-CA3 micro-circuit is thought to play a crucial role in memory formation and retrieval (Treves and Rolls, 1994; Kobayashi and Poo, 2004), with local circuit dynamics and neuromodulators comprising important functions in these processes (Prince *et al.*, 2016, 2017). Our lab has recently shown that ACh strongly attenuates the feed-forward inhibition in the MF-CA3 micro-circuit, dramatically altering the E/I balance and allowing excitation to dominate over inhibition upon repeated stimuli. This disinhibition enables efficient action potential back-propagation and underscores CA3-CA3 STDP upon MF input (Prince *et al.*, 2017).

Given the consistent effects of NA in CA1 and the strong innervation of the MF-CA3 area by the LC (Walling *et al.*, 2012), we undertook experiments to examine whether similar effects occurred in response to NA.

Our key questions were:

1) Does bath-applied NA affect mossy fibre excitatory or feed-forward inhibitory input to CA3 pyramidal neurons?

2) How do these changes impact the short-term dynamics of the synapse in response to physiological patterns of stimuli?

We initially obtained electrically evoked EPSCs and IPSCs in response to both regular stimulation and naturalistic (irregular) spike train protocols. The purpose of the regular stimulation was to determine whether there were any effects on the basal synaptic transmission of excitatory or inhibitory MF responses, and to monitor series resistance. The naturalistic spike train protocol was derived from *in vivo* granule cell recordings, and the synaptic responses were analysed using a realistic short-term plasticity synapse model (Tsodyks and Markram, 1997). The model incorporates several Bayesian pre- and post-synaptic parameters that – after fitting to the *ex vivo* recordings – can show a shift in distribution of the *maximum a posteriori* (MAP). We then incorporated these posterior distribution changes into the model of MF-CA3 synaptic transmission (Appendix I: Prince *et al.*, 2017), where DG granule cell spiking is described by two parameters: a between burst interval (between BI, which describes a background firing rate of DG granule cells) and a within burst interval (within BI, which describes the time between spikes in a burst of granule cell firing). By varying the between and within Bis for excitatory and inhibitory synaptic input we were able to simulate EPSCs and IPSCs across a broad range of frequencies in the presence and absence of NA. We found that,

unlike the striking effects of ACh on the MF-CA3 E/I balance, the effects of NA appear much more modest.

4.2 Materials and methods

4.2.1 Ex vivo slice preparation

Ex vivo hippocampal slices were generated as described in Chapter 2; however, the slices were 500 μm as opposed to 400 μm to improve mossy fibre preservation and the probability of achieving evoked responses.

Isolated transverse hippocampal slices were prepared from male (P28-P70) C57BL/6J mice. Following cervical dislocation, brains were immediately removed and immersed in ice-cold sucrose-based cutting solution containing the following (in mM): 205 sucrose, 10 glucose, 26 $NaHCO_3$, 2.5 KCl, 1.25 NaH_2PO_4, 0.5 $CaCl_2$, and 5 $MgSO_4$. Individual hippocampi were excised from the brain, mounted on agar and 500 μm transverse slices (dorsal only) were cut using a VT1200 vibratome (Leica). Following dissection and slicing, slices were transferred to aCSF containing the following (in mM): 119 NaCl, 10 glucose, 26 $NaHCO_3$, 2.5 KCl, 1 NaH_2PO_4, 1.3 $MgSO_4$, and 2.5 $CaCl_2$, maintained at ~35°C for 30 min, and then stored at room temperature. Slices were left for a minimum of 1 h after dissection before recordings were made. All solutions were saturated with 95% O_2 and 5% CO_2 and all experiments were performed in accordance with Home Office guidelines (UK Animal Scientific Procedures Act (1986)) as directed by the University of Bristol Home Office Licensing Team.

4.2.2 Electrophysiological recordings and analysis

Slices were submerged in a custom-designed recording chamber perfused at 2-4 ml/min with aCSF (as above) at 31-32°C, heated via an inline heating system (TC-324, Warner Instruments). CA1 pyramidal cells were visualised using infrared-differential interference contrast (DIC) optics on an Olympus BX-50WI microscope. Flow rate was maintained by a 101U/R peristaltic pump (Watson Marlow) and aCSF was removed via a Dymax 5 vacuum pump (Charles Austin).

Patch electrodes with a resistance of 2–8 MΩ were pulled from borosilicate filamented glass capillaries (1.5 OD x 0.86 ID x 100 L mm, Harvard Apparatus) using a vertical puller (PC-10, Narishige) or horizontal puller (P-87, Sutter Instruments).

MF-CA3 synaptic responses were evoked via a monopolar stimulating electrode in the DG granule cell layer (Figure 4.1). Due to the low threshold for mossy fibre plasticity, MF-CA3 responses were elicited using minimal stimulation every 20 seconds using 4 pulses at 20 Hz. This protocol also allowed comparison with Dr. Luke Prince's CA3 recordings and their modulation by cholinergic receptors. The Tsodyks-Markram model is designed to model a single synapse, and so the use of minimal stimulation was necessary to activate as few synapses as possible and improve subsequent fitting of the data. The mGluR2/3 agonist DCG-IV (1 μM), which selectively blocks glutamate release from mossy fibre terminals, was applied to determine the EPSCs and di-synaptic feed-forward IPSCs were due to mossy fibre stimulation. Any responses not inhibited by ≥75% within 10 minutes of DCG-IV application were discarded from subsequent analysis. Time plot traces showing the effects of NA on normalised EPSC and IPSC amplitudes over time are of the fourth EPSC or IPSC response, as the low release probability the MF-CA3 synapse sometimes resulted in small and variable responses to the first pulse.

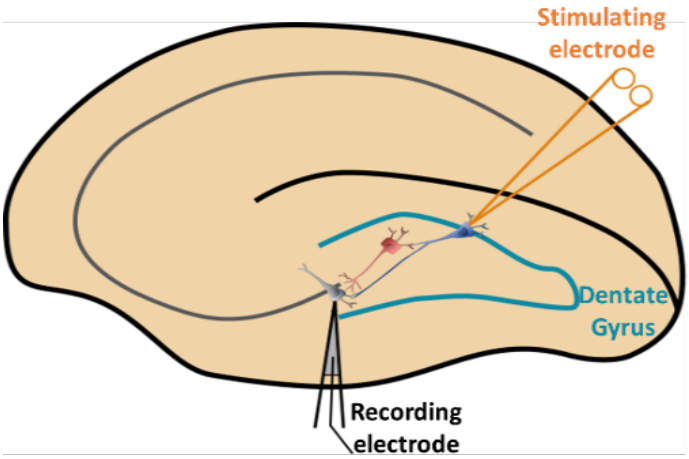

Figure 4.1: *Recording set-up for MF-CA3 recordings.*

4.2.3 Tsodyks-Markram model of short-term plasticity

For modelling the short-term plasticity of the MF-CA3 micro-circuit, the Tsodyks-Markram model (Tsodyks and Markram, 1997; Hennig, 2013) was utilised due to its widespread use, simplicity, and relation to biophysics. This model captures pre-synaptic release dynamics with two variables, a facilitating process (*f*) and a depressing process (*d*), that represent resources available to drive synaptic transmission. These evolve as follows:

$$\frac{df}{dt} = \frac{f_0 - f}{\tau_f} + a\,(1 - f)\,\sum_s \delta(t - t_s) \qquad \text{(Equation 1)}$$

$$\frac{dd}{dt} = \frac{1 - d}{\tau_d} - f\,d\,\sum_s \delta(t - t_s) \qquad \text{(Equation 2)}$$

The dynamics of f are governed by three parameters: f_o (baseline value of f), τ_f (decay time constant of f), and a (increment scaling factor with incoming spike at time t_s). This variable roughly represents the build-up of free Ca^{2+} ions in the pre-synaptic terminal that triggers exocytosis of neurotransmitter-containing vesicles into the synapse. Dynamics of d are governed by a single parameter τ_d, representing the availability of docked vesicles at release sites. Since these variables are bounded between 0 and 1, they convert into a conductance amplitude and are multiplied by a conductance scaling factor g, i.e:

$$\text{PSC Amplitude} = g\ f\ d \qquad \text{(Equation 3)}$$

Further details on the model can be found in Appendix I.

4.2.4 Drugs

DCG-IV was purchased from Tocris, and stock solutions were made up in dH_2O and stored at -20° C.

4.3 Results

4.3.1 MF-CA3 characterisation

We characterised the excitatory and inhibitory MF responses to CA3 neurons prior to their inclusion in subsequent analysis. In agreement with the literature, mono-synaptic EPSCs and di-synaptic feed-forward IPSCs showed an average latency (stimulation artefact to response onset) of 2.4 ± 0.3 ms and 5.4 ± 0.7 ms, respectively (n = 11 and 10, Figure 4.2A). This difference was significant ($p < 0.0001$, unpaired Student's t-test), indicative of the additional synapses traversed in feed-forward inhibition (Torborg *et al.*, 2010). Both excitatory and inhibitory inputs facilitated, showing fold increases of 7.2 ± 1.4 and 4.0 ± 1.0, respectively, that were not significantly different from one another ($p > 0.05$, Mann-Whitney test, n = 11 and 7, Figure 4.2B). Both excitatory and feed-forward inhibitory inputs also showed strong inhibition by the mGluR2/3 agonist, DCG-V (1 μM), which blocks glutamate release from mossy fibre terminals (90.1 ± 1.9% and 93.1 ± 2.2%, respectively, n = 11 and 10, Figure 4.2C).

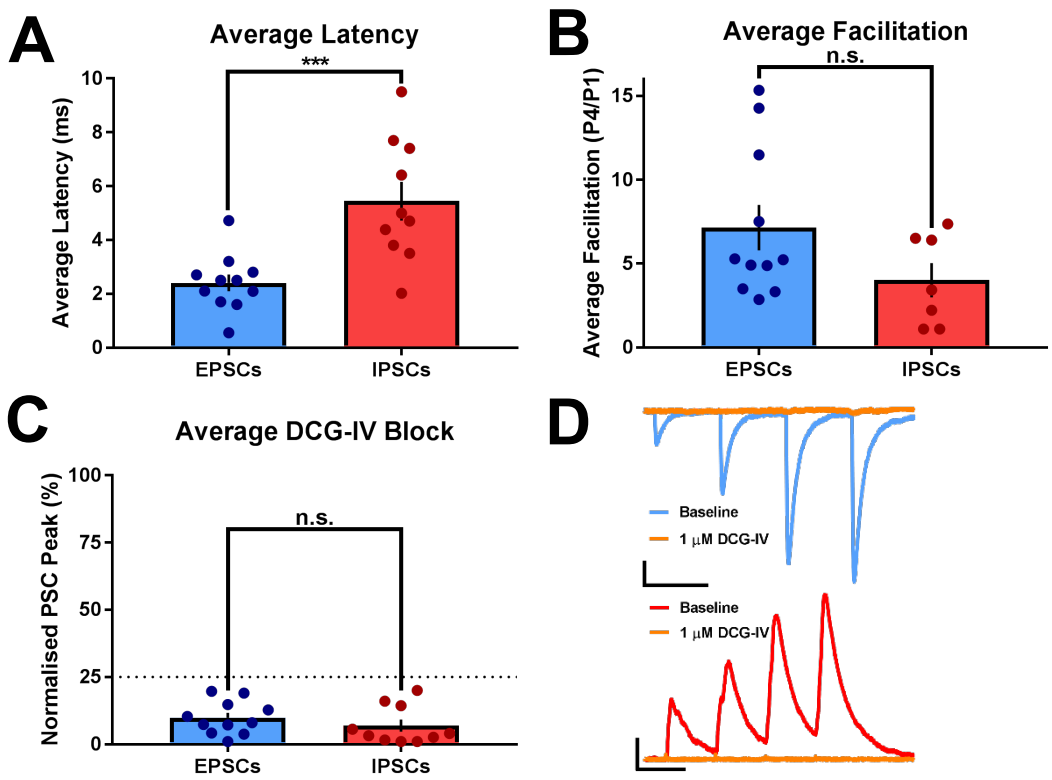

Figure 4.2: *MF characteristics. A) IPSCs showed significantly longer latencies than EPSCs, in line with their di-synaptic nature (n = 7 and 11, respectively). B) Both EPSCs and IPSCs showed an average facilitation (P4/P1) of at least 3-fold. C) Both EPSCs and IPSCs were strongly inhibited by the mGluR2/3 agonist DCG-V. D) Example traces showing baseline EPSCs (top) and IPSCs (bottom) and their inhibition by DCG-V. Scale bars = 50 pA and 50 ms (EPSCs), 100 pA and 50 ms (IPSCs).*

4.3.2 NA attenuates the mossy fibre feed-forward inhibition but spares excitatory inputs to CA3

We next examined how bath application of 20 μM NA affected mossy fibre excitatory inputs and feed-forward inhibition. Unlike in Chapters 2 and 3, four pulses at a fixed stimulation frequency of 20 Hz were used. There were two reasons for this: 1) to allow direct comparison with Dr. Luke Prince's experiments with the cholinergic receptor agonist, carbachol (CCh), and 2) the mossy fibre terminals are unreliable at low stimulation frequencies but can undergo substantive plasticity at high frequencies (Vyleta, Borges-Merjane and Jonas, 2016). Therefore, we used 20 Hz to induce short-term facilitation of synaptic responses that were sufficient for analysis but would avoid long-term plasticity changes. The computational model of the MF-CA3 was designed to simulate a single synapse, hence we used minimal stimulation with a monopolar electrode to evoke synaptic responses.

Bath application of 20 μM NA had no effect on the MF-CA3 EPSCs (fourth EPSC = 107.0 ± 12.1% of baseline, n = 15, $p > 0.05$, paired Student's *t*-test, Figure 4.3A-C), however the feed-forward IPSCs were attenuated (fourth IPSC = 68.0 ± 9.8 of baseline, n = 10, $p < 0.05$, Wilcoxon Matched-Pairs Signed Rank Test, Figure 4.3A, B and D). Using these

peak amplitudes to examine the effects of NA on the E/I balance, we found a significant shift toward excitation ($p < 0.05$, Mann-Whitney Test, Figure 4.3F). We also examined the PPR of excitatory transmission to see if there were any potential pre-synaptic changes induced by NA, however the PPR did not change (2.5 ± 0.3 at baseline compared to 2.3 ± 0.2 in the presence of NA, n = 14, $p > 0.05$, paired Student's *t*-test, Figure 4.3E).

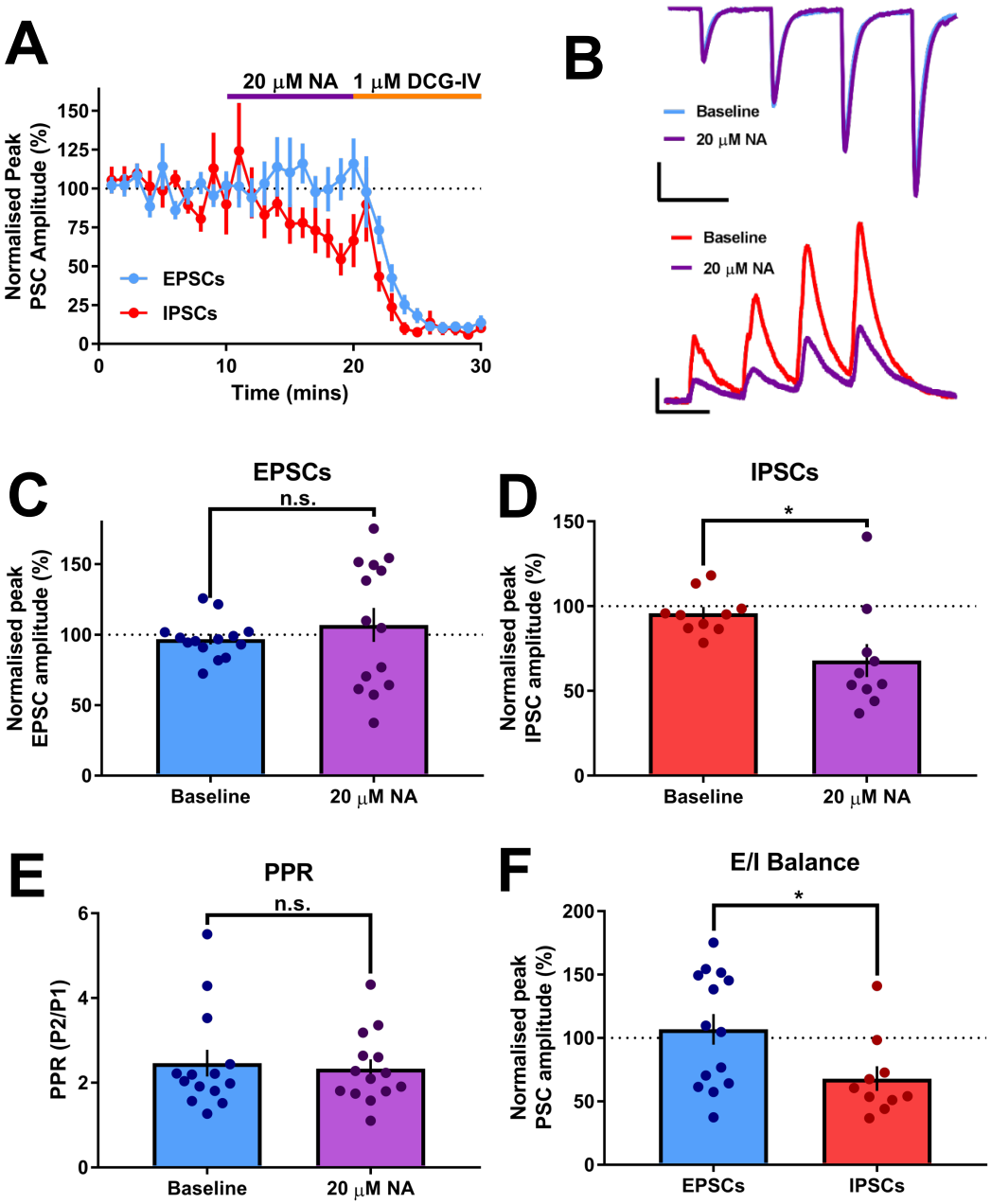

Figure 4.3: *Modulation of regular MF responses by NA. A) Time course trace showing the effects of NA on the fourth MF EPSCs (n = 15) and IPSCs (n = 10) in the train of pulses, and their subsequent inhibition by DCG-IV. B) Example traces of EPSCs (top) and IPSCs (bottom). Scale bars = 200 pA and 50 ms (EPSCs), 100 pA and 50 ms (IPSCs). C) Averaged data for EPSC amplitudes. D) As in C but for IPSCs. E) PPRs of EPSCs were unaffected by NA (n = 14). F) Comparison of peak EPSC and IPSC responses after application of NA showed a significant attenuation of IPSCs and therefore a potential shift in the E/I balance towards excitation.*

We also examined the individual synaptic responses to the 2nd and 3rd pulses of our regular stimulation protocol. Here we found that the third and fourth inhibitory responses were more strongly depressed than the second (2nd= 76.1 ± 27.3%, 3rd = 65.5 ± 11.5%, 68.0 ± 9.8%, Figure 4.4B), however there were no significant differences between the groups (p > 0.05, repeated measures Friedman ANOVA with Dunn's multiple comparison test, n = 10). Excitatory responses also showed no significant differences, although the second and third responses did show a minor increase from baseline (2nd = 122.3 ± 15.8%, 3rd = 122.3 ± 18.1%, 4th = 107.0 ± 12.1%, Figure 4.4A, p > 0.05, repeated measures Friedman ANOVA with Dunn's multiple comparison test, n = 14).

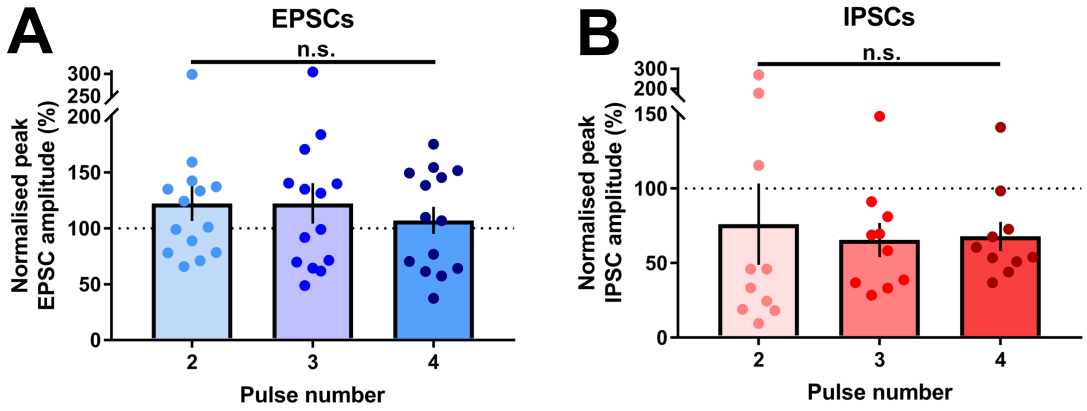

Figure 4.4: *Modulation of the nth synaptic response by NA. A) Average 2nd, 3rd and 4th EPSCs amplitudes in the presence of NA (n = 14). B) As in A but for IPSCs (n = 10).*

4.3.3 Carbachol attenuates the mossy fibre feed-forward inhibition but spares excitatory inputs to CA3

Unlike NA, 5 µM carbachol significantly attenuated MF-evoked EPSCs (66.2 ± 11.9%, n = 7, p < 0.05) and IPSCs were almost completely inhibited (29.3 ± 13.5%, n = 5, p < 0.05). These data were gathered by Dr. Luke Prince and presented here for comparative purposes (Figure 4.5). Further information can be found in Appendix I.

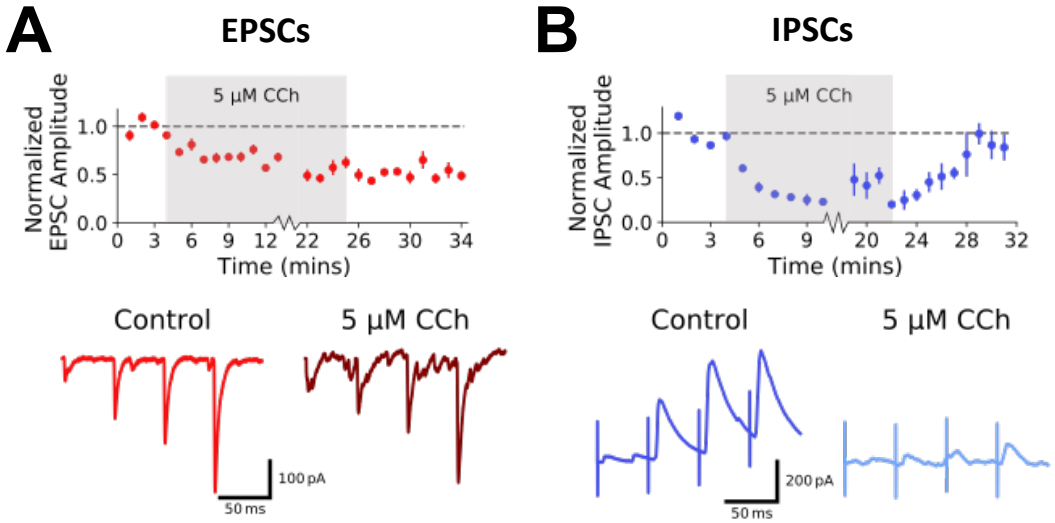

Figure 4.5: *Modulation of regular MF responses by carbachol (CCh). A) Time course trace showing the effects of NA on MF EPSCs (n = 7). Below are example traces. B) Time course trace showing the effects of NA on MF IPSCs (n = 5). Below are example traces. From Prince et al., 2017.*

4.3.4 NA has little effect on the MF-CA3 E/I balance at most frequencies

We next sought to examine how NA modulates the short-term plasticity of the MF-CA3 synapse at a range of physiologically relevant stimulation frequencies. To achieve this, we used an irregular stimulation protocol modelled on naturalistic granule cell spike patterns that were recorded *in vivo* during a spatial memory task (Figure 4.6A, left. These spike patterns showed a bi-modal inter-spike interval (ISI) distribution (Figure 4.6A, top right). This distribution was modelled as a doubly stochastic Cox process (Figure 4.6A, middle right) and a sample was drawn from this process in order to generate an irregular stimulation protocol (Figure 4.6A, bottom left and right). This process was carried out by Dr. Luke Prince, see Appendix I for more details.

Synaptic responses in whole-cell voltage-clamp using this protocol were then interleaved with the regular stimulation protocols, and the recordings analysed using a Tsodyks-Markram short-term plasticity model (Figure 4.6B and Figure 4.7). Several excitatory and inhibitory short-term plasticity models with varying levels of complexity for excitatory and inhibitory synaptic responses were assessed for fit to the experimental data (see Appendix I). Both models comprise several pre-synaptic components – facilitating (*f*) and depressing (*d*), with time constants (τ_f, τ_d) – and a post-synaptic scaling factor (*g*). Additional parameters in the inhibitory model include a_o and *b* (incremental scaling factors) and a time constant for *a* (τ_f). Further details regarding the model can be found in Appendix I.

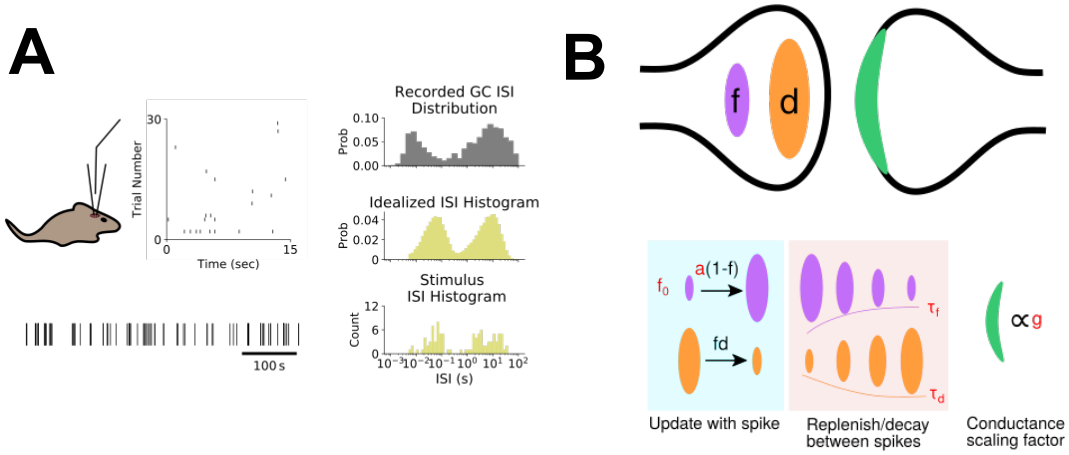

Figure 4.6: *Development of the irregular spike train protocol and outline of the Tsodyks-Markram model of short-term plasticity. A) In vivo recordings from mouse DG granule cells showed bi-modal distributions (top right) that could be modelled using a doubly stochastic process (middle right), a sample of which was used as a mossy fibre stimulation protocol in ex vivo slices (bottom). B) Outline of the short-term plasticity model including the pre-synaptic facilitating (f) and depressing (d) components alongside time constants (τf, τd) and the post-synaptic conductance scaling factor (g). From Prince et al., 2017.*

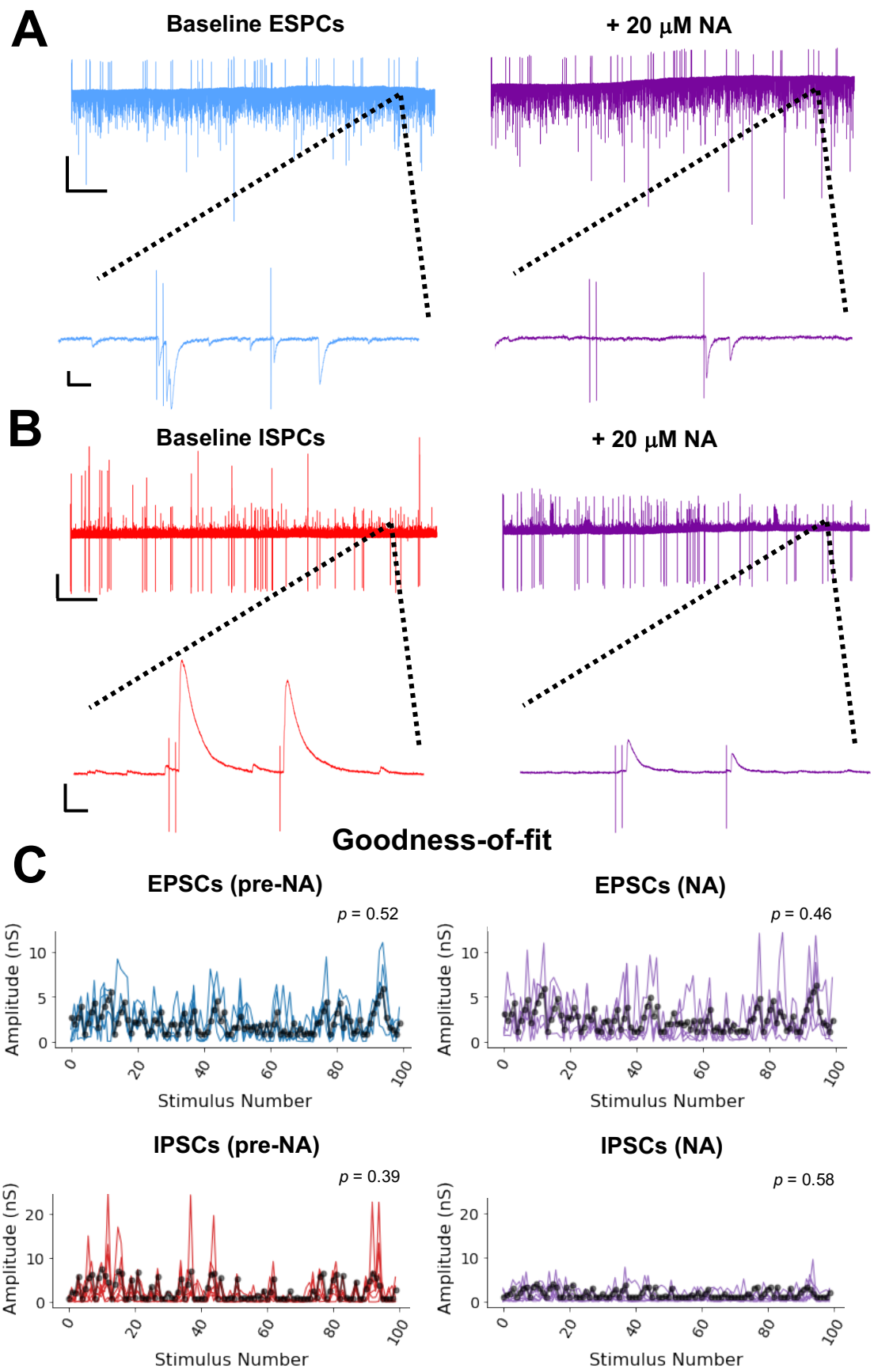

Figure 4.7: *CA3 synaptic responses to MF stimulation using the irregular spike train. A) Full length recordings of EPSCs at baseline (left) and in the presence of NA (right). Top scale bar = 1 min and 200 pA. Bottom scale bar = 125 ms and 100 pA. B) As in A except for IPSCs. Top scale bar = 1 min and 200 pA. Bottom scale bar = 125 ms and 200 pA. C) Goodness-of-fit for EPSC (left, n = 6) and IPSC (right, n = 6) short-term plasticity models before and after NA application were assessed by Bayesian posterior predictive p values. The blue, red and purple lines denote the observed data for all experiments, and the black dots indicate the expected values from the model. p values close to 0.5 indicate best fit.*

Fitting the MF responses to the irregular stimulation protocol using this Tsodyks-Markram model again showed a reduction in feed-forward IPSCs but no effect on EPSCs (Figure 4.7C, note: currents are expressed as conductance as part of the model fitting) and allowed us to examine which parameter changes (*maximum a posteriori*, MAP) best explain the results. For ACh, a decrease in the post-synaptic excitatory conductance (g, reduced by 49.8 ± 7.9%, n = 6, Kruskall-Wallis H test with Dunn's multiple comparison test) explained the attenuation of EPSCs; and a decrease in the post-synaptic inhibitory conductance alongside an increase in inhibitory baseline facilitation (f_o) explained the IPSC decrease (73.1 ± 27.9% decrease in g and 225.7 ± 160.1% increase in f_o, $n = 5$, one-way ANOVA with Bonferroni multiple comparisons test). For NA, the only significant parameter change was an increase in the inhibitory τ_d parameter (203.7 ± 46.7%, $p < 0.001$, n = 6, one-way ANOVA with Bonferroni multiple comparisons test), representing an increase in the time taken for interneurons to recover from short-term depression. These parameter changes are summarised in Figure 4.8.

Modelling excitatory and inhibitory responses and examining the E/I balance over a range of within-burst and between-burst intervals in the presence and absence of NA and ACh revealed striking differences between the two neuromodulators. In control conditions, excitation dominated over inhibition upon repeated stimulation due to the pronounced facilitation at MF synapses. The pre- and post-synaptic changes mediated by ACh strongly augmented this effect, permitting a pronounced domination of excitation over inhibition later in the stimulus train. NA, however, had only a minor effect on E/I balance, showing a slight shift towards excitation from the fourth pulse onwards at longer within-burst intervals (Figure 4.9). Interestingly, modelling the paired-pulse dynamics we found that – in agreement with our experimental results – there was no change in PPR.

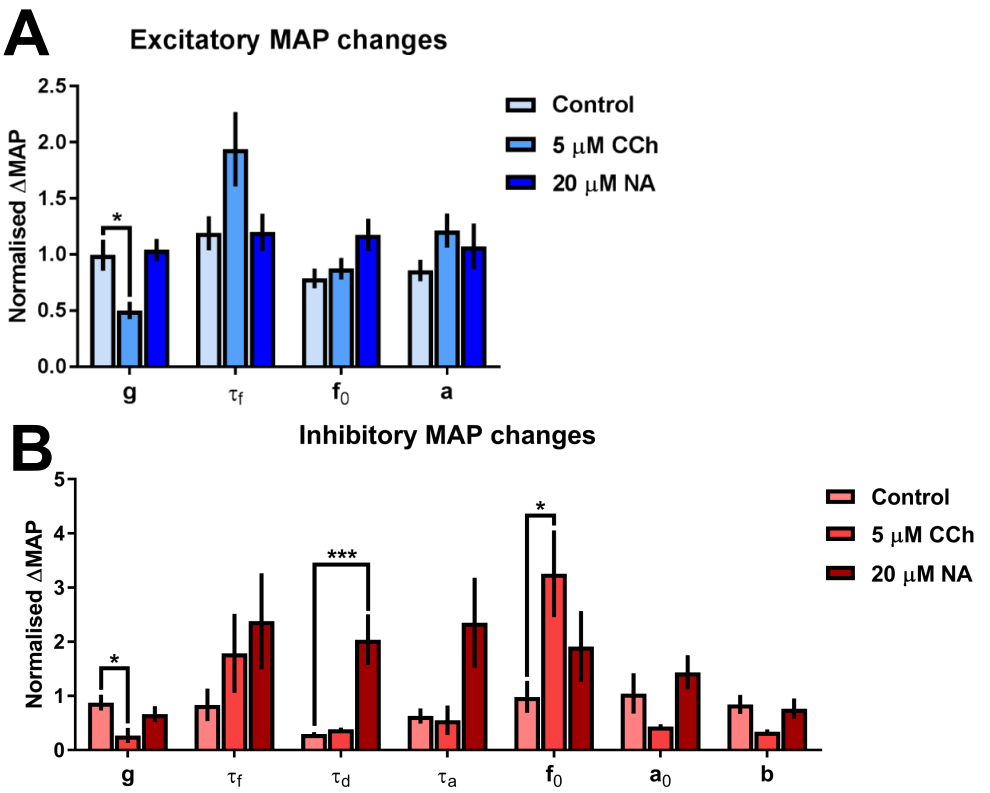

Figure 4.8: *Neuromodulatory effects of NA and CCh on EPSCs (top) and IPSCs (bottom) as assessed by their effects on parameter fits normalised to a time-matched control.*

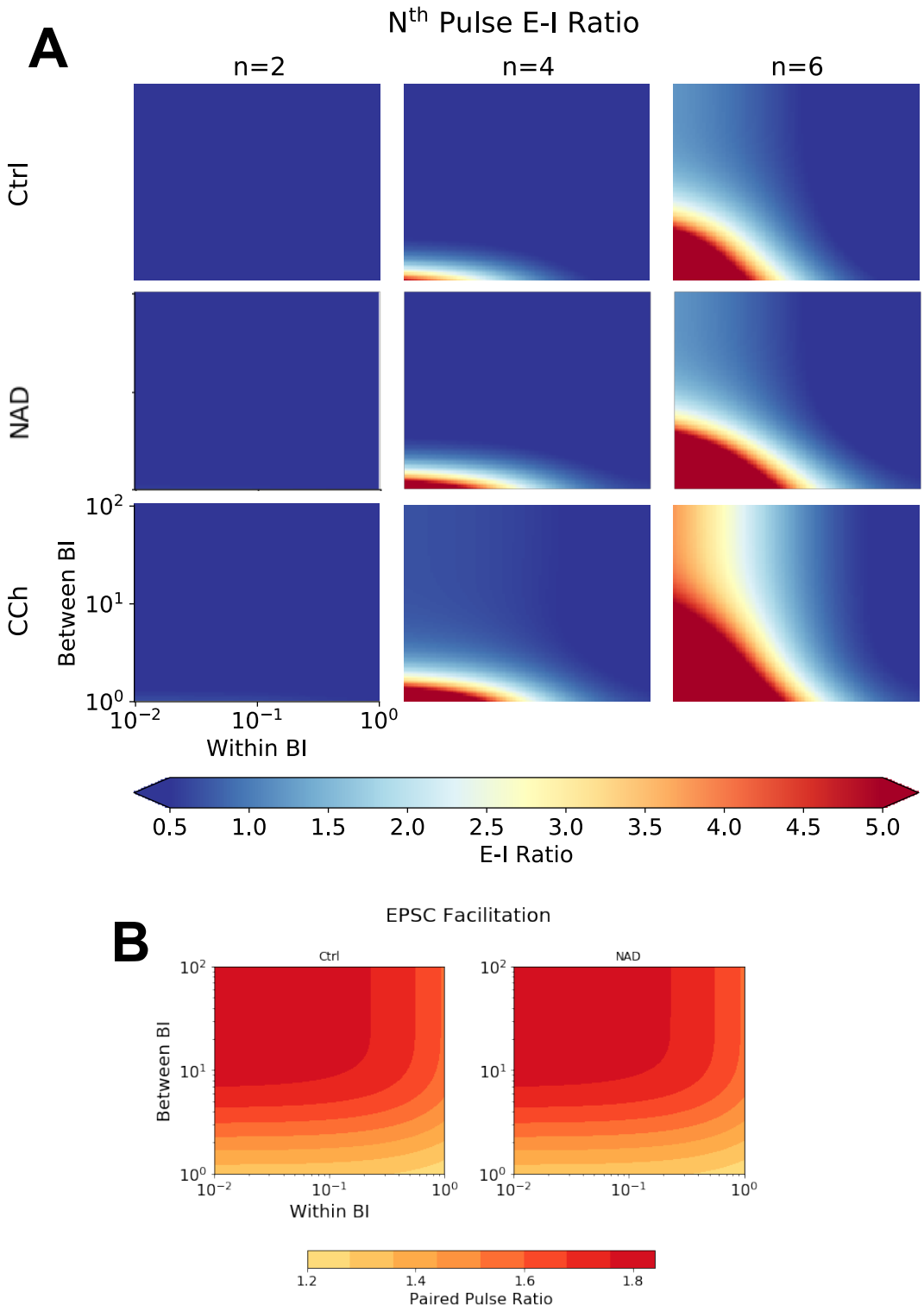

Figure 4.9: *Modulation of MF-CA3 E/I balance by NA and CCh across a range of stimulation frequencies. A) Development of the E/I balance across a range of within and between BIs in control, NA and CCh conditions, n = 2, 4 and 6 denote pulse numbers, illustrating the shift in E/I balance across a 6 pulse burst. B) The excitatory PPR across a range of stimulation frequencies was not affected by NA.*

4.4 Discussion

4.4.1 Noradrenergic modulation of MF-CA3 E/I balance is more modest than cholinergic modulation

We aimed to ascertain whether NA modulates the MF-CA3 feed-forward micro-circuit in a manner similar to that found with CCh (Appendix I). We found several differences between the neuromodulators using both regular stimulation and naturalistic stimulation protocols. Both neuromodulators attenuated feed-forward inhibition in response to a regular stimulation protocol, however this effect was much more pronounced with CCh. CCh also attenuated EPSCs (but to a lower magnitude than IPSCs), whereas NA did not appear to show any effect on EPSCs. Previous work found no effect on basal excitatory transmission with the specific β-AR agonist, isoproteronol, (Huang and Kandel, 1996), but in hippocampal cultures an α1-AR-mediated depression of EPSCs was found with 5 μM NA (Scanziani, Gähwiler and Thompson, 1993). It is our understanding that noradrenergic modulation of feed-forward inhibition in the CA3 has not been examined before, and so our findings regarding this appear to be novel, however noradrenergic suppression of feed-forward inhibition has been shown in feed-forward DG interneurons (Brown *et al.*, 2005). The effects on inhibitory attenuation in the present study appeared to be more pronounced later in the train, implying a use-dependent effect, even though the differences between the 2nd, 3rd and 4th responses were not significant. We therefore further examined the effects of NA on MF-CA3 neurotransmission using a naturalistic spike trains and a short-term plasticity model.

Similar to our regular stimulation, NA showed little effect on EPSCs but attenuated feed-forward IPSCs, however the mechanisms at play appear to differ from those observed with CCh. Fitting the irregular stimulation data with our Tsodyks-Markram short-term plasticity model suggested CCh exerted effects both pre- and post-synaptically, decreasing excitatory and inhibitory post-synaptic conductance and also decreasing the baseline facilitation of inhibitory synapses. NA, on the other hand appeared to increase the time taken for inhibitory synapses to recover from short-term depression (τ_d) at inhibitory synapses. This suggest that the IPSCs stay depleted over longer WB intervals because they cannot recover quickly enough and, given the shift towards excitation, NA would be expected to enhance spike output. Testing this hypothesis in current-clamp would therefore be of use in future work.

MF-CA3 IPSCs are di-synaptic, therefore interpreting how this parameter change results in alterations to synaptic transmission is not straightforward. The τ_d parameter loosely represents the availability of docked vesicles at release sites, however there are more components at play in the terminal than the vesicle recycling speed that is captured by τ_d, such as recruitment of additional vesicles from the recycling and reserve pools in

response to enhanced Ca^{2+} influx upon repetitive stimulation (Denker and Rizzoli, 2010). Despite this simplification, the alteration of this parameter does imply that NA may modulate the release machinery in CA3 interneurons, and one possible mechanism of this reduced vesicle recovery could be a reduced phosphorylation of synapsins. Synapsins 1 and 2 are synaptic phosphoproteins involved in vesicle release, and Rosahl *et al.* (1995) showed that genetic knock-out of synapsin 2 reduces synaptic facilitation and enhances vesicle depletion, even in low Ca^{2+} aCSF, in hippocampal neurons. Moreover, associated vesicle release proteins such synaptophysin 1 and synaptobrevin 2 were down-regulated by synapsin 1 and 2. Future work could investigate this parameter change by examining the effect of NA on the PPR of mono-synaptic inhibitory inputs (which could be isolated by including NBQX in the perfusing aCSF), as well as its effects on the facilitation of these responses with repeated stimulation, at different stimulation (i.e. within burst) frequencies.

In the DG, β-AR activation enhances the phosphorylation of the aforementioned vesicle release proteins, presumably by an increase in cAMP levels, leading to an increase in neurotransmitter release (Parfitt, Hoffer and Browing, 1991; Parfitt *et al.*, 1992). Therefore, local cAMP levels in the synaptic terminals of feed-forward interneurons could be decreased if α2-ARs are also activated in these cells, reducing their synapsin activation and slowing vesicle recovery. Indeed, α2-AR activation has been shown to reduce neurotransmitter release in the central amygdala via α2-ARs (Delaney, Crane and Sah, 2007) and in single hippocampal neurons grown on glial microislands (Boehm, 1999). However, in the latter study only glutamatergic currents were affected, with GABAergic currents spared. Boehm (1999) attributed this effect to an attenuation of VGCCs by NA. Therefore, rather than affecting interneurons, NA may decrease VGCC activity at the MF-interneuron synapse, reducing post-synaptic activation of interneurons and the downstream action potential-dependent GABA release.

Another possibility is that re-uptake of GABA (into interneurons) or glutamate (into the filopodia innervating these interneurons) is inhibited by NA, reducing the levels of these neurotransmitters available for release with repetitive stimulation. β-ARs are known to increase glutamate uptake in primary cultures of astrocytes, suggesting NA can modulate neurotransmitter re-uptake in at least one direction (Huang and Hertz, 1995). α2-ARs are present on CA3 glial neurons (Milner *et al.*, 1998), however the functional effect of these receptors remains to be explored.

4.5 Improvements and future work

4.5.1 Time-match control

Unlike previous experiments described in this thesis, no time-match control was obtained for the regular spike train experiments, therefore these recordings are

imperative to ensure none of the effects observed are due to run-up or run-down of the responses.

4.5.2 Paired granule-cell interneuron recordings

The modelling data suggests the effects of NA are mediated by a change in the interneuron's ability to recover from short-term depression. In addition to the aforementioned investigation of the noradrenergic modulation of mono-synaptic IPSC PPR, it would be of interest to examine how NA affects the intrinsic excitability of these neurons. This could be achieved by obtaining whole-cell recordings in a K^+-based internal solution. Moreover, an ideal configuration would be to make paired recordings between DG granule cell neurons and interneurons. This pairing is necessary to ensure the interneurons are feed-forward and not feed-back (Torborg *et al.*, 2010). Driving action potentials in the DG granule cells in the presence and absence of NA could then be used to examine whether interneuron firing is reduced. For instance, NA may hyperpolarise these neurons, making spiking more difficult, ultimately reducing VGCC Ca^{2+} influx at the axonal terminal and impairing GABA release onto CA3 neurons.

In the present study, the use of a Cs^+-based intracellular solution precluded analysis of membrane depolarisation/hyperpolarisation or input resistance, therefore in future it may be of benefit to analyse MF responses in current-clamp and examine changes in resting membrane potential and/or input resistance. Much like in CA1, β-AR depolarising and α2-AR hyperpolarising effects have been reported in CA3 pyramidal neuron and DG granule cells (Lacaille and Schwartzkroin, 1988; Ul Haq *et al.*, 2012). These effects were obtained using adrenoceptor subtype-specific agonists, but using the endogenous ligand may reveal distinct sub-populations of neurons that respond differentially to NA.

4.5.3 Noradrenergic modulation of non-MF inputs

Future work could examine recurrent A/C inputs to CA3, as previous work by Scanziani, Gähwiler and Thompson (1993) found an attenuation in both these recurrent inputs and excitatory MF inputs. The fact this study utilised organotypic slice cultures makes interpretation of their results problematic, particularly since MF terminals in cultured slices lose their restrictive targeting of CA3 thorny excrescences and expand to innervate the distal dendrites (Robain *et al.*, 1994). However, examining the effects of NA on both recurrent and MF inputs in the same neuron in acute slices may reveal interesting results regarding how NA prioritises incoming information in the CA3. For example, NA may exert little effect on MF inputs (as in the present study) but instead strongly attenuate A/C inputs, biasing CA3 input to novel information. Indeed, this has been shown in the piriform cortex (Hasselmo *et al.*, 1997), where NA attenuated recurrent layer 1b inputs much more strongly than afferent layer 1a inputs. Subsequently modelling this biasing

effect of NA towards novel inputs suggested that NA increased signal-to-noise, enhancing the influence of extrinsic input on cortical representations, thereby facilitating the formation of memories regarding the novel context of the environment.

In the CA3 this reduction in background recurrent activity may reduce overlapping activity between CA3 neurons, with MF and direct PP inputs still driving recurrent firing. Interestingly, direct excitatory PP inputs to CA3 are enhanced by LC stimulation and β-AR activation *in vivo* (Shen *et al.*, 2012). Therefore, if NA reduces inhibition and "background" recurrent CA3 network activity whilst sparing MF inputs and enhancing PP inputs, it is conceivable that NA could bias the network towards incoming cortical information. Moreover, the reduction in background activity may also improve the sparsification of the cortical signal during pattern separation by DG granule cells (McClelland and Goddard, 1996).

In support of this, mice in which the LC inputs specifically to CA3 (not DG or CA1) had been optogenetically silenced during exposure to a novel context showed no memory of the context upon re-exposure, exhibiting significantly more exploration than mice who had not had their LC inputs silenced (Wagatsuma *et al.*, 2018). Moreover, subsequent reactivation of engram cell ensembles in the CA3 and downstream in the CA1 upon re-exposure to the same context were reduced, implying impaired encoding in the CA3. Silencing LC inputs during retrieval (i.e. when the environment was now familiar) had no effect. These data suggest noradrenergic input to the CA3 is critical for one-trial learning and, since such learning is critically dependent upon NMDAR activation at recurrent CA3 synapses (Nakazawa *et al.*, 2002, 2003, 2004) a role for NA in modulating these synapses to prioritise and encode novel information is highly likely.

Although this prospect is indeed intriguing, some MF EPSCs in the present study also showed strong attenuation. Moreover, STDP between recurrent CA3 synapses requires both MF and recurrent CA3 inputs (Kobayashi and Poo, 2004), therefore if the latter responses are attenuated then driving plasticity at these synapses would be more difficult. A possible counter to this would be that since inhibition is lowered by NA, the threshold for STDP is effectively reduced (Meredith, Floyer-Lea and Paulsen, 2003), and since PP inputs are augmented by β-ARs then a strong drive for CA3 spiking and the associated action potential backpropagation required for STDP and ensemble formation would still exist in the presence of NA.

4.5.4 Model selection

The chosen Tsodyks-Markram model was selected for use based on the goodness-of-fit to cholinergic data. Although the model also appeared to fit the noradrenergic data well, several cells had to be discarded based on wide posterior parameter fits. It would therefore be of benefit to examine alternative models with additional parameters

underscoring the complex Ca^{2+} dynamics at the release terminal. For instance, models that incorporate Ca_{Res} dynamics (Dittman, Kreitzer and Regehr, 2000; Hennig, 2013).

It should also be mentioned that the data for ACh and NA were obtained on different electrophysiology rigs, and since the model was selected based on fitting to the cholinergic data, differences in rig characteristics may have affected the fitting (i.e. temperature, Bui and Glavinovic, 2014).

4.5.5 Lower concentrations or optogenetically evoked NA

Given the data presented in Chapters 2 and 3, it would be remiss not to suggest repeating the present experiments using a lower concentration of NA. The noradrenergic modulation of the MF-CA3 synapse is less well-characterised than the SC-CA1, and our results in Chapters 2 and 3 suggest NA may exert concentration-dependent effects. In addition, the absence of effect on EPSCs may be due to opposing actions of different adrenoceptors. For instance, α1-AR-dependent depotentiation of SC-CA1 LTP can be blocked by co-application with the β-AR agonist, isoproterenol (Katsuki, Izumi and Zorumski, 1997).

Moreover, given the possibility that CA3 neurons are synaptically targeted by the LC (Walling *et al.*, 2012) the spatiotemporal properties of optogenetically-evoked NA may reveal interesting neuromodulatory effects with different release patterns (i.e. tonic vs. phasic).

4.6 General conclusion

In summary, we have shown that neuromodulation of the MF-CA3 synapse by NA is less pronounced than ACh, and the modulation that does occur is mediated by a different mechanism. Further work is needed to clarify these effects, as well as to examine the effects of lower concentrations of NA and to analyse the data using more complex models that better account for the intricate Ca^{2+} dynamics in the synaptic terminal.

Chapter 5: Methods to detect optogenetically evoked NA in *ex vivo* slices

5.1 Introduction

In Chapters 2 and 3 we described a functional disparity between bath-applied and optogenetically-evoked NA release. A similar phenomenon has also been demonstrated for dopamine by Rosen, Cheung and Siegelbaum (2015). We found that part of this discrepancy could be explained by differences in concentration, with 600 nM recapitulating some of the effects we observed with endogenous NA. This agrees with the estimated release of NA from LC terminals in brainstem slices in response to electrical stimulation (~560 nM, Feng *et al.*, 2019), but the concentration of NA released in the hippocampus in response to our opto-stimulation protocols is still unknown. Differences in terminal density and NA re-uptake mechanisms between the two areas may mean this concentration is an over- or under-estimate with regards to release in the hippocampus.

Traditionally, NA release has been quantified using micro-dialysis or fast-scan cyclic voltammetry (FSCV) (Delgado *et al.*, 1972; Ewing *et al.*, 1983). Micro-dialysis involves the implantation of a cannula to collect neurotransmitter-containing extracellular fluid for subsequent analysis. A major drawback of this technique is its very low spatial and temporal resolution, with ≥1 minute collection times commonly required (Chefer *et al.*, 2009; Rodeberg *et al.*, 2017) from a sampling probe with a diameter of around 400 µm. Moreover, micro-dialysis estimates are based on whole tissue concentration and not on local release from terminals (Abercrombie, Keller and Zigmond, 1988).

FSCV, on the other hand, offers higher temporal and spatial resolution. It involves placing a carbon-fibre micro-electrode into a bath solution or brain tissue and applying rapid (typically >300 V/s) triangular voltage waves from ~-0.4 to +1.2 V across the electrode. Larger tip sizes yield greater oxidation currents (as there is more surface area available for electrochemical oxidation) but also generate larger background faradic currents (Pihel, Walker and Wightman, 1996). As the potential difference across the electrode increases and decreases, reactive chemical species (typically catecholamines such as NA and DA) undergo oxidation and reduction at specific voltages. Subtracting these currents from background faradic currents allows the generation of voltage vs. current plots for specific compounds. Unfortunately, due to the high structural similarity between NA and DA (differing by only a single hydroxyl group), FSCV is typically unable to distinguish between the two catecholamines (although the electrodes are slightly more sensitive for DA and produce larger currents, Robinson *et al.*, 2003; Park *et al.*, 2018). There are also additional species such as serotonin and DOPAC that can contaminate the

NA or DA response, particularly serotonin as its oxidation products are unstable and can break down into additional electroactive compounds (Robinson *et al.*, 2003). It is for this reason that FSCV is usually employed in brain regions only receiving either noradrenergic or dopaminergic innervation.

More recently, genetically encoded fluorescent sensors such as NA1m, DA1m and dLight (Patriarchi *et al.*, 2018; Sun *et al.*, 2018; Feng *et al.*, 2019) have shown nano-molar sensitivity and rapid kinetics in response to electrically or behaviourally evoked catecholamine release. Most relevant to the present work, the NA1m protein comprises the GFP module from GCamp6 coupled to the human α2-AR (Feng *et al.*, 2019). This fluorescent sensor is able to detect NA release in the sub-micromolar range, saturates at 50 μM and is ~350-fold more selective for NA than DA. Moreover, the human synapsin (hSyn) promoter controlling the NA1m protein expression allows the sensor to be widely expressed in neurons (Schoch, Cibelli and Thiel, 1996; Kügler, Kilic and Bähr, 2003; McLean *et al.*, 2014). To date, this sensor has been characterised *in vitro* and used *in vivo* to detect optically-evoked NA release from mice LC; *in vivo* NA release into the mouse hypothalamus in response to a range of behavioural assays including the forced swim test, tail suspension test, hand presentation test, and social interaction with an intruder; as well as *in vivo* midbrain NA release in zebrafish in response to visual looming stimuli (Feng *et al.*, 2019).

These interesting new tools offer high spatial resolution, with detection at the cellular level, and could therefore provide a way of estimating the concentrations of endogenous NA in *ex vivo* slices and thereby reconciling the data shown in Chapters 2 and 3.

Our key questions in this chapter were:

1) Can we detect NA release evoked from LC terminals using optogenetic stimulation?

2) What is the approximate concentration of this release?

3) Is there spatiotemporal patterning of this release?

We utilised several methods in an attempt to achieve this. We first used FSCV, but we found time-dependent oxidation signals in WT animals upon opto-stimulation that confounded our results. We then employed the recently developed genetically encoded fluorescent sensor, NA1m (Feng *et al.*, 2019). We found NA1m expressed well but gave variable results. Preliminary experiments with opto-stimulation of ChR2-expressing LC terminals in the hippocampus appeared to show a transient increase in fluorescence and then a consistent run-down, which is likely due to photobleaching.

The work in this chapter is exploratory and the FSCV experiments involving opto-stimulation of ChR2-expressing LC slices were carried out by an undergraduate summer student, Heng Wui Zhu, supervised by Travis Bacon. The 2-photon NA1m experiments were carried out by Travis Bacon under the supervision of Dr. Mascia Amici.

5.2 Materials and methods

5.2.1 Viral vector injections

Two viral vectors were used in the research described in this chapter: 1) CAV2-PRS-ChR2-mCherry, injected into the LC as outlined in Chapter 3; and 2) AAV9-hSyn-$GRAB_{NE1m}$, a fluorescent NA sensor for detecting bath-applied NA and optogenetically-evoked NA from LC hippocampal terminals (Feng *et al.*, 2019, referred to as NA1m, injected into the CA1 area of the dorsal hippocampus). In both cases, mice had acclimatised to the animal unit for at least a week prior to viral vector injections and were injected between P24 and P35. For all injections, mice were anesthetised for recovery surgery with an IP injection of a ketamine (70 mg/kg, Vetalar) and medetomidine (0.5 mg/kg, Domitor) cocktail and maintained on a heat pad throughout the surgery.

The CAV2-PRS-ChR2-mCherry injections to the right LC were the same as described in Chapter 3. For dorsal hippocampus injections of AAV9-hSyn-$GRAB_{NE1m}$, two burr holes (Ø 1.0 mm) were made in the right hemisphere at stereotaxic coordinates from bregma: 1) AP: 1.8 mm and ML: 1.5, 2) AP: 2.3 mm and ML: 2.5 mm. A glass micropipette (as described in Chapter 3) containing the viral vector was advanced directly downwards and two injections (250 µL each, at a speed of 125 µL/min) were executed at depths of 1.6 mm and then 1.8 mm for each burr hole.

Following injection, mice received an IP injection of atipamezole hydrochloride reversal agent (1 mg/kg, Anti-sedan) and a subcutaneous injection of buprenorphine hydrochloride (0.1 mg/kg) and were monitored until use in experiments >3 weeks later.

5.2.2 Ex vivo slice preparation

Coronal hippocampal slices and LC slices were prepared from injected male (P50-P70) C57BL/6J (>3 weeks post-injection) or age-matched controls. Following cervical dislocation, brains were immediately removed and immersed in ice-cold sucrose-based cutting solution containing the following (in mM): 205 sucrose, 10 glucose, 26 $NaHCO_3$, 2.5 KCl, 1.25 NaH_2PO_4, 0.5 $CaCl_2$, and 5 $MgSO_4$. Brains were mounted on agar and 400 µm coronal hippocampal or LC slices were cut using a VT1200 vibratome (Leica). Following dissection and slicing, slices were transferred to aCSF containing the following (in mM): 119 NaCl, 10 glucose, 26 $NaHCO_3$, 2.5 KCl, 1 NaH_2PO_4, 1.3 $MgSO_4$, and 2.5 $CaCl_2$, maintained at ~35°C for 30 min, and then stored at room temperature. Slices were left for a minimum of 1 h after dissection before recordings were made. All solutions were saturated with 95% O_2 and 5% CO_2 and all experiments were performed in

accordance with Home Office guidelines (UK Animal Scientific Procedures Act (1986)) as directed by the University of Bristol Home Office Licensing Team.

5.2.3 Fast-scan cyclic voltammetry

Carbon-fibre micro-electrodes (34 μm tip diameter, Kation Scientific) connected to an Intan RHD2000 amplifier headstage and Intan recording controller were placed freely into the aCSF perfused into the slice chamber. Triangular voltage ramps (-0.4 V to +1.2 V) were applied at a rate of 10 Hz by an Intan CLAMP controller at 250 V/s or 400 V/s using a custom-written .csv file imported into the Intan user interface software. Recordings were digitised at 30 kHz by the analog-to-digital converter present in the headstage and saved to a MATLAB format for offline analysis. Custom-written MATLAB scripts performed signal averaging, baseline subtraction and peak analysis for bath-applied NA and optically-evoked NA oxidation peaks.

For drug application experiments, the FSCV protocol consisted of 3 voltage cycles at 250 V/s repeated in triplicate for baseline and drug application recordings. Drug recordings were obtained 5 minutes after wash-in to allow the drug to equilibrate in the chamber. The 9 voltage ramps for each condition were then averaged to produce a single oxidation trace for subtraction from baseline. For evoked NA experiments, LC slices were perfused at 2-4 ml/min with aCSF (as above) at 31-32°C, heated via an inline heating system (TC-324, Warner Instruments). DIC optics were used to locate the LC and the carbon-fibre micro-electrode was gently inserted into the centre of this region and a glass cannula connected to a 473 nm LED (ThorLabs) via a fibre optic cable was positioned slightly above the LC. Voltage cycles were repeated continuously in 10 ramp sweeps at 250 V/s for 3 minutes, with a brief 18 Hz burst of 10 light pulses delivered at 30 seconds. The final 10 voltage ramps of each 30 second period were then averaged, and baseline subtracted from the pre-light average.

Figure 5.1A-B outlines the FSCV protocol and baseline subtraction used to obtain an oxidation peak for 100 μM NA. The Intan software/hardware combination utilised in this work required us to design our own triangular voltage cycles in an arbitrary waveform .csv file. The minimum time step resolution allowed was 20 μs and the minimum voltage step resolution was 5 mV, thus limiting our maximum voltage ramp speed to 250 V/s (with full voltage step size resolution). This is slightly slower than the 400 V/s used in typical FSCV experiments, however if we increased the voltage step size to 8 mV we could achieve this 400 V/s. With this protocol we observed NA peaks at the typical voltage (~ 0.65 V) however we also observed an increase in the width of the oxidation curve (Figure 1C). The Gaussian oxidation curve is effectively a probability distribution for NA oxidation at each voltage, therefore increasing the time spent at each voltage (i.e. by having smaller steps) increases the amount of NA oxidised, thus the level

of NA available for oxidation is more rapidly depleted (leading to a narrower and left shifted oxidation current). The optimisation of the FSCV was originally going to be used to distinguish between NA and DA release within *ex vivo* slices, and since these two catecholamines have almost identical oxidation peaks (Park *et al.*, 2018) we chose to use the 250 V/s protocol as it gave a narrower peak.

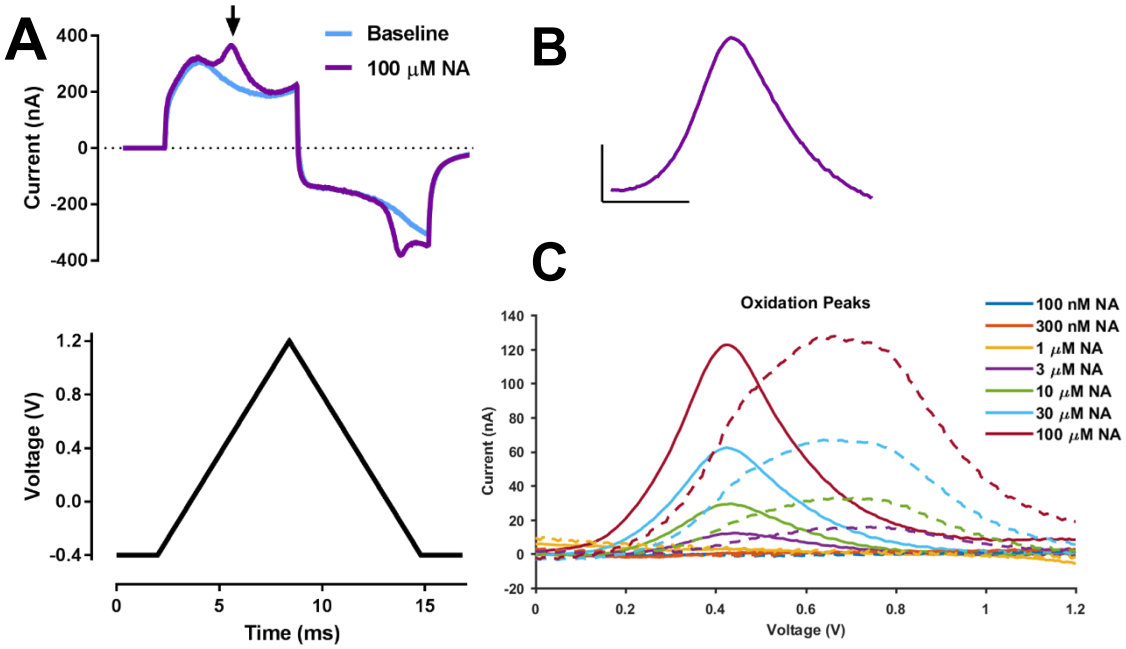

Figure 5.1: *FSCV schematic. A) Rapidly cycling the voltage across a carbon-fibre micro-electrode from -0.4 to 1.2 V (bottom) produces large amplitude faradic currents (top). B) Subtracting the currents produced in the presence of an oxidisable compound (i.e. NA) produces a smaller oxidisation current. Scale bars = 50 nA and 1 ms. C) The NA oxidation current shape produced is dependent upon the triangular waveform speed, due to the exhaustion of NA at slower speeds. Dotted lines denote 400 V/s, solid lines denote 250 V/s cycling speeds.*

5.2.4 NA1m fluorescent NA reporter experiments

Coronal hippocampal slices were mounted on cover slips coated with poly-D-lysine (Sigma) and placed in a custom-designed recording chamber under a 2-photon microscope (Dukker). Slices were perfused at 2-4 ml/min with aCSF (as above) at 31-32°C, heated via an inline heating system (TC-324, Warner Instruments). Hippocampal slices were initially visualised using Dodt Gradient Contrast (DGC) optics to find the injection site and estimate the region of highest NA1m expression. A higher resolution section of the slice (560 x 560 pixels) was then imaged using a 40x objective 2-photon optics (920 nm at 27 mW power, Mai Tai Sapphire Laser, SpectraPhysics). Images were acquired continuously at 0.25 Hz for time series experiments examining the change in NA1m fluorescence in response to bath application of NA and, subsequently, yohimbine (α2-AR antagonist, 100 μM). To examine the effects of opto-stimulation of hippocampal LC fibres, Z-stacks (20 images per stack covering a depth of 40 μm) were acquired every 2 minutes, with a tonic 1 Hz 473 LED stimulation protocol (2.3 mW, delivered via an ø200 μm, 0.20 NA fibre optic cannula (ThorLabs) positioned over the CA1 region) running between Z-stacks. Following this protocol, 2 phasic protocols (10 pulses then 60 pulses at 25 Hz) were acquired, with a Z-stack taken after each one.

5.2.5 Immunohistochemistry

For perfuse fixation, mice were given a terminal IP dose of sodium pentobarbital (100 mg/kg, Euthatal) and, after breathing had ceased and no response to foot pinch was found, the abdomen was opened and the heart exposed. The left ventricle was then injected with 20 ml of 0.01 M PBS and then 4% PFA. The mouse was then decapitated, the scalp cut along the midline and the cerebellum and brain stem were removed and stored in 4% PFA for >24 hours before transferring to 30% sucrose in PB at least 24 hours before slice preparation. The cortex was then mounted on a freezing cryotome (Leica) using Cryomatrix embedding resin (ThermoFisher Scientific) and 60 μm whole-brain coronal slices cut manually then stored in 0.1 M PB + 0.02% NaN_3.

Free-floating slices were washed in 0.1 M PB for 10 minutes (3x) before transfer to 50% alcohol in dH_2O for 30 minutes and washing again in 0.1 M PB for 10 minutes (3x). Slices were then incubated overnight in 0.1 M PB + 0.3% Triton X-100 containing 5% goat serum (Sigma-Aldrich) and rabbit anti-GFP (1:1000, Fisher Scientific). The following day, slices were washed in 0.1 M PB for 10 minutes (x3) and then incubated for >3 hours in 0.1 M PB + 0.3% Triton X-100 containing 2% goat serum and goat anti-rabbit Alexa-fluor 594 (1:1000, InVitrogen). Slices were mounted on glass slides and covered with rectangular glass slips using Fluorsave (Merck Millipore). Slides were stored in a fridge and imaged using a fluorescent microscope (Leica) and LASX imaging software (Leica).

5.2.6 Viral vectors and drugs

AAV9-hSyn-GRAB$_{NE1m}$ was purchased from ViGene Biosciences. Yohimbine was purchased from Tocris, and stock solutions were made up in fresh in dH_2O every day.

5.3 Results

5.3.1 Bath-applied NA concentration-response curve with FSCV

We first performed a concentration-response assay with bath-applied NA, increasing the concentration in half-log units from 100 nM to 100 μM. We found clear responses from 10 μM upwards (Figure 5.2A), but in some cases the signal was also above noise at 3 μM (Figure 5.2B). The maximum peak oxidation current (at 100 μM NA) was 143.1 ± 10.5 nA (n = 3).

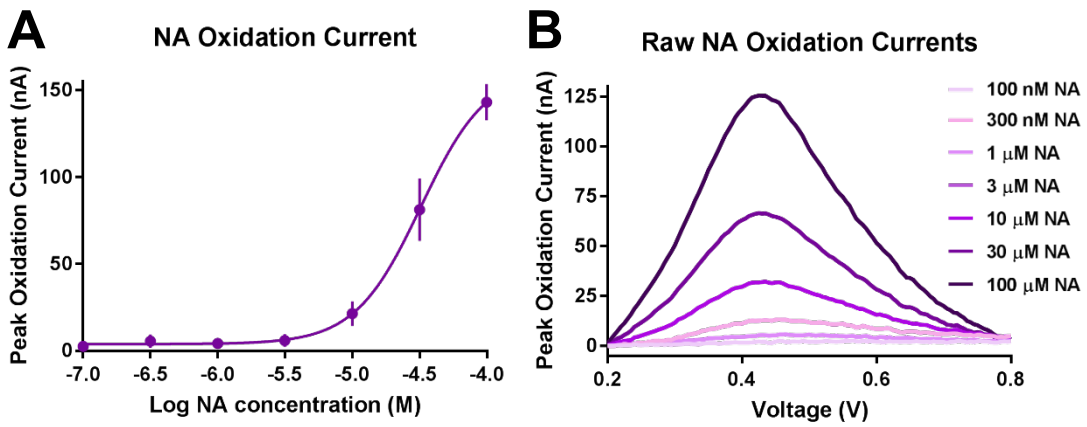

Figure 5.2: *FSCV concentration-response curve for NA. A) Concentration-response curve for the normalised peak oxidation currents of NA concentrations ranging from 100 nM to 100 μM (n = 3). B) Example trace of raw oxidation currents.*

5.3.2 Opto-evoked NA

We next examined whether optogenetic stimulation of LC slices containing ChR2-expressing neurons could release sufficient NA to be detectable using our FSCV set-up. >3 weeks after viral injection, we obtained acute brainstem slices showing clear LC mCherry fluorescence on our microscope (Nikon Eclipse E600FN). We positioned the carbon-fibre micro-electrode at the centre of fluorescence and applied a brief 18 Hz LED train (60 pulses) delivered via an optical fibre (Figure 5.3A). We also sampled using the triangular waveform every 30 seconds, in order to monitor the potential change in oxidation peak over time. We found that opto-stimulation did yield an oxidation peak from slices of both WT and ChR2-injected mice (Figure 5.3B-C). Both WT and ChR2-expressing slices exhibited an increasingly larger peak over time, with the maximum peak occurring 150 seconds after light stimulation (WT = 1.3 ± 0.2 nA, ChR2 = 1.5 ± 0.5 nA, n = 3 and 4, respectively, Figure 5.3C). These increases were not significantly different from one another ($p > 0.05$, unpaired Student's *t*-test on maximum oxidation

peaks at 150 seconds post light stimulation). There was also no difference in voltage at which the oxidation peak occurred (WT = 0.15 ± 0.01 V, ChR2 = 0.16 ± 0.05 V). However, in one ChR2-injected animal we observed an additional peak at ~0.3 V (Figure 5.3B, bottom), which was slightly closer to the oxidation peak we observed with bath-applied NA (~0.4 V). The time-course for the peak oxidation increase over time was also not significantly different between slices from WT and ChR2-injected mice ($p > 0.05$, two-way ANOVA with Sidak's multiple comparisons test).

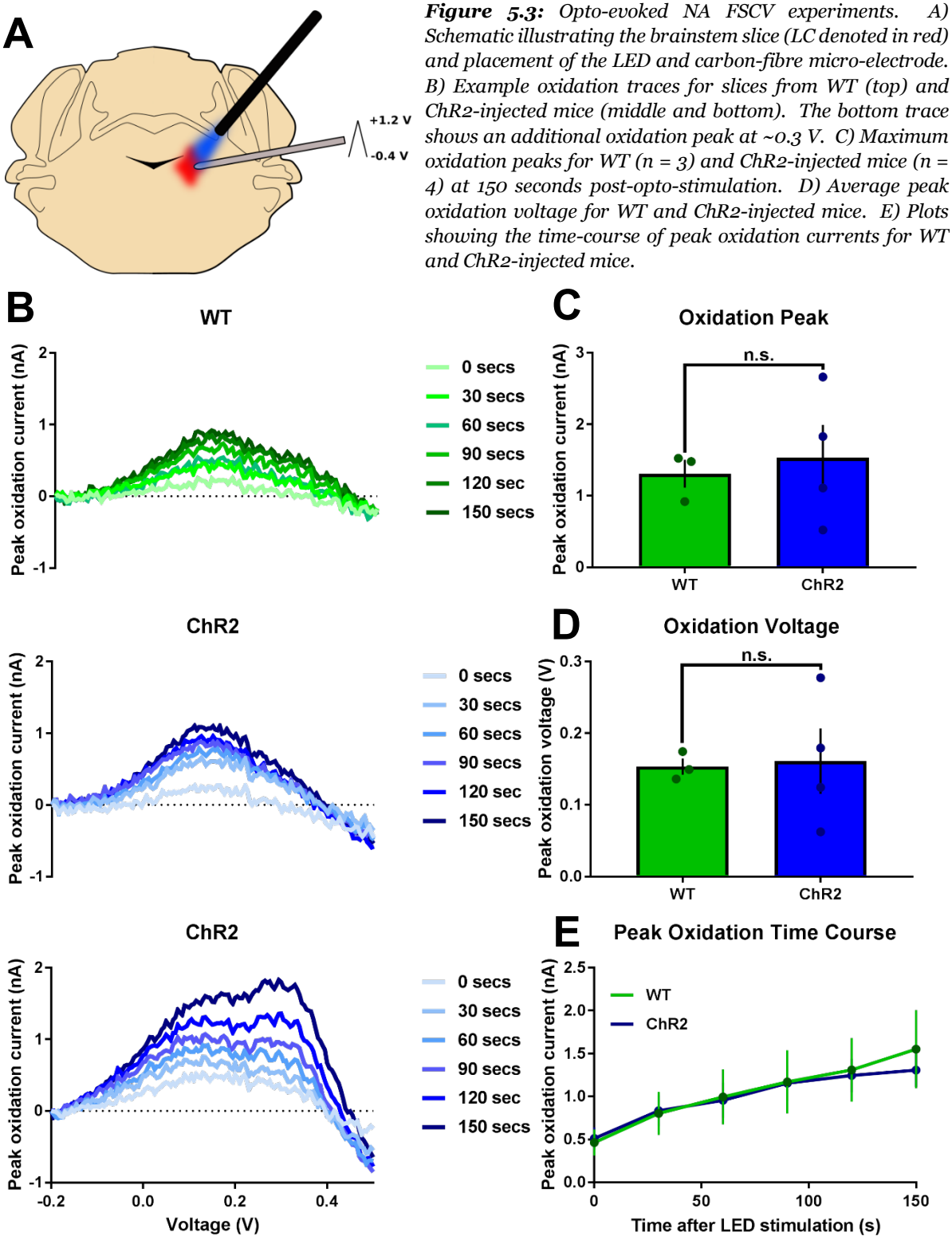

Figure 5.3: *Opto-evoked NA FSCV experiments. A) Schematic illustrating the brainstem slice (LC denoted in red) and placement of the LED and carbon-fibre micro-electrode. B) Example oxidation traces for slices from WT (top) and ChR2-injected mice (middle and bottom). The bottom trace shows an additional oxidation peak at ~0.3 V. C) Maximum oxidation peaks for WT (n = 3) and ChR2-injected mice (n = 4) at 150 seconds post-opto-stimulation. D) Average peak oxidation voltage for WT and ChR2-injected mice. E) Plots showing the time-course of peak oxidation currents for WT and ChR2-injected mice.*

5.4 NA1m expression

In light of a recent publication outlining a highly sensitive fluorescent sensor for NA1m (Feng *et al.*, 2019), we switched our approach. We unilaterally injected the AAV9-hSyn-GRAB$_{NE1m}$ viral vector into the dorsal hippocampus of naïve animals and allowed >3 weeks for sufficient expression. We chose to inject into the dorsal hippocampus rather than the LC for two reasons: 1) to obtain more slices per animal, due to the substantially larger size of the hippocampus compared to the LC, and 2) to avoid accidentally injecting the virus into the fourth ventricle, as happened on occasion with LC ChR2 injections. Mice that had already undergone a unilateral (right) LC injection of the CAV2-PRS-mCherry-ChR2 virus (performed by Dr Hiroki Ito) subsequently received an injection of AAV9-hSyn-GRAB$_{NE1m}$ viral vector into the right dorsal hippocampus.

Figure 5.4 shows two images of slices showing NA1m expression, in Figure 5.4A the slice had undergone immunohistochemical processing for GFP, which was much more abundant in the hippocampus than the surrounding cortex. Figure 5.4B is a wide-field fluorescent image of a hippocampal slice expressing NA1m, taken on a 4x objective on the 2-photon rig.

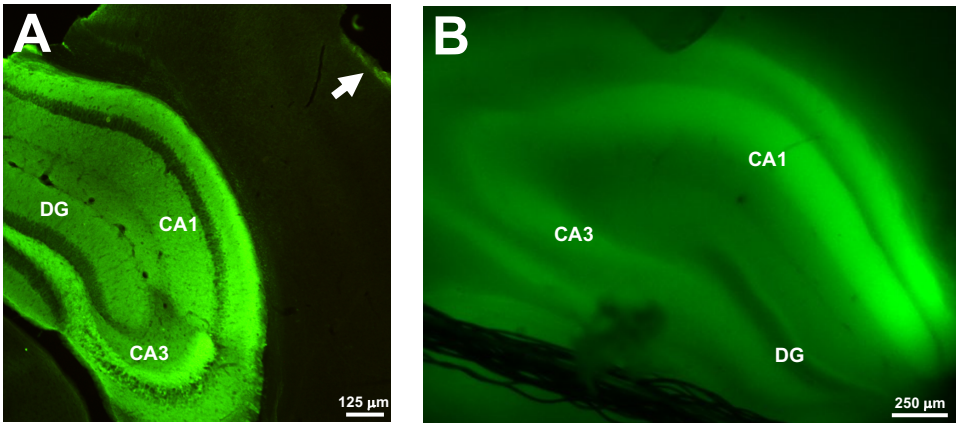

Figure 5.4: *Hippocampal NA1m expression. A) Coronal slice showing a GFP-expressing hippocampus (green) and the surrounding cortex following a GFP immunohistochemistry protocol (see materials and methods). The highest expression appears below the minor surface tissue damage caused during viral injection, indicated by a white arrow. B) Wide-field fluorescent image of a hippocampal slice showing NA1m GFP fluorescence.*

5.4.1 Functional characterisation of NA1m

We first maximally activated the NA1m sensor by perfusing 100 µM NA onto the slice. Our immunohistochemical analysis indicated that NA1m expression was greatest in the hippocampal region inferior to the cortex where minor tissue damage from surgery could be visualised (Figure 5.4A). Therefore, we used a wide-field view of the slice, under DGC optics, to determine the injection site and therefore where to focus our 2-photon laser. Using a 40x objective, we then obtained a magnified field of view comprising the cell body layer and dendrites. Despite consistent laser power (920 nm at 27 mW) the effects of NA perfusion were highly variable, with one slice showing an increase in fluorescence of >4-fold, whereas others increased by <0.5-fold. The average $\Delta F/F_0$ with 100 µM was

3.3 ± 0.7, and this was attenuated to 0.8 ± 0.1 following perfusion of the α2-AR antagonist, yohimbine (100 μM). These changes were not significant ($p > 0.05$, n = 5, repeated measure ANOVA with Dunnett's multiple comparison test). Figure 5.5A-B shows the time course for these fluorescent changes and the associated average $\Delta F/F_0$ values. Interestingly, fluorescent changes appeared most pronounced in the dendrites, with the cell body layer only showing an increase in one slice (Figure 5.5C).

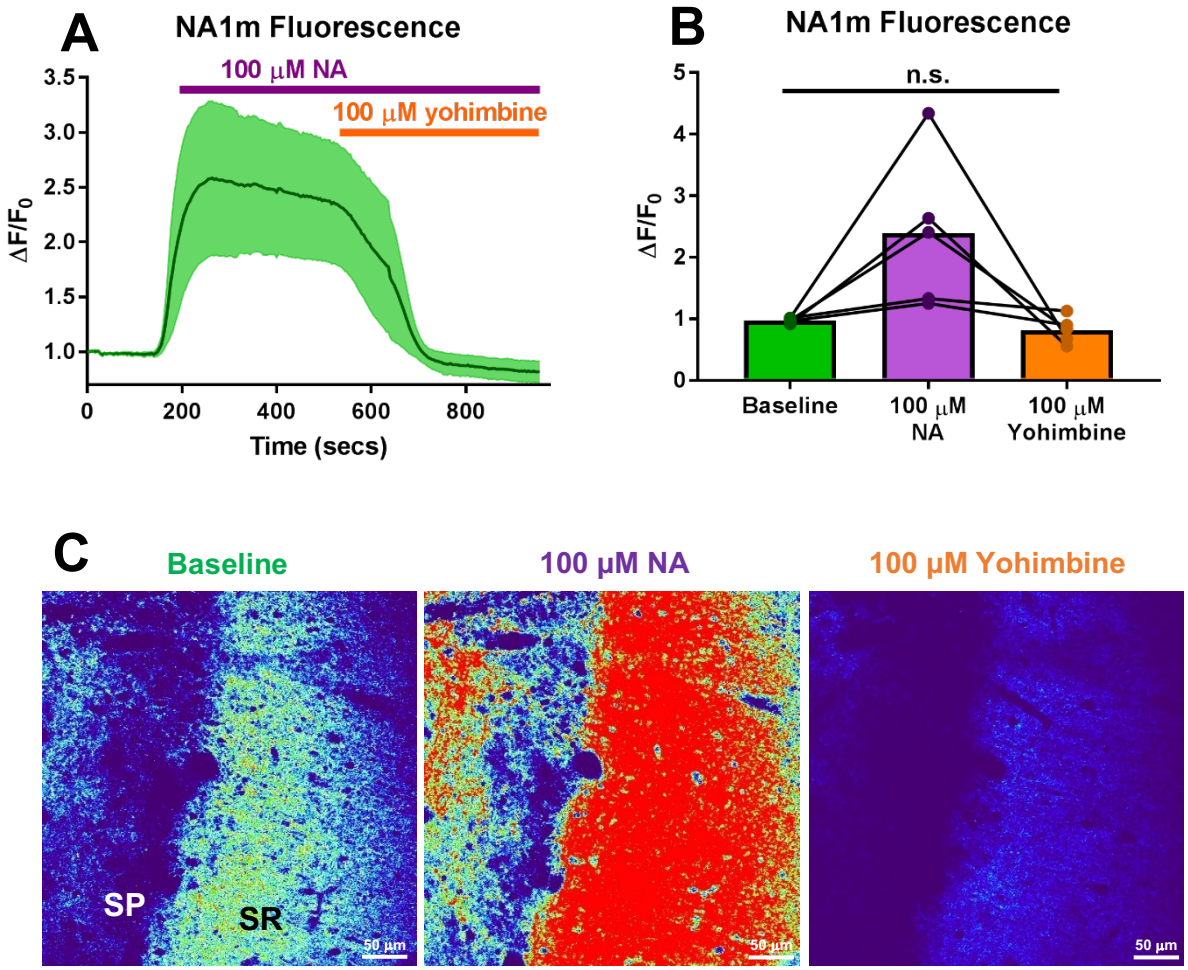

Figure 5.5: *Preliminary pharmacological characterisation of NA1m. A) Average time course trace showing the increase in NA1m fluorescence in response to NA and subsequent reduction by the α2-AR antagonist, yohimbine (n = 5). B) Averaged data for A. C) Example heat images for A, with the cell body stratum pyramidale (SP) and dendritic stratum radiatum (SR) layers labelled accordingly. Note the attenuation of basal fluorescence with yohimbine.*

5.4.2 NA1m concentration-response curve

We next performed a concentration-response assay to determine the sensitivity of NA1m to NA. Preliminary work optimised the imaging frame rate and laser duration required for a continuous 10 minute recording, however these initial attempts resulted in tissue damage and images that were not viable for subsequent analysis. We successfully obtained one concentration-response curve using 600 nM, 2 μM and 20 μM NA, however we only observed an increase in fluorescence of >3-fold with 20 μM NA (Figure 5.6).

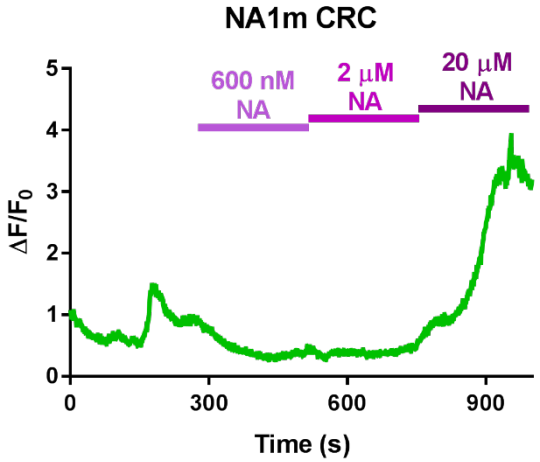

Figure 5.6: *NA concentration response curve for NA1m.*

5.4.3 Tonic opto-stimulation of hippocampal slices expressing NA1m

Unfortunately, due to time constraints, further optimisation was not possible. We next applied opto-stimulation protocols used in Chapter 3 to our dual-injected mice (ChR2 in LC and NA1m in hippocampus). We aimed to mimic the opto-stimulation protocols from Chapter 3, however a methodological issue arose for the tonic (1 Hz) protocol based on the fact that continuous blue light (5 ms pulses at 10 Hz for 10 minutes) was believed to be required to activate the ChR2-expressing LC fibres. This would saturate the photo-multiplier tube (PMT) on the 2-photon microscope and cause an automatic switch-off. To circumvent this issue, we continuously stimulated the slice with our tonic opto-stimulation protocol for 2 minutes, then rapidly acquire a Z-stack before restarting our tonic stimulation. This was repeated every 2 minutes. After the 10 minute tonic protocol was completed, two final phasic opto-stimulation protocols were applied to the slice: 10 pulses at 25 Hz and 60 pulses at 25 Hz. After each of these another Z-stack was acquired. This protocol is outlined in Figure 5.7A. Analysing the averaged Z-stack data for the tonic stimulation protocol revealed a small peak after 2 minutes which then declined over the subsequent 8 minutes ($p < 0.05$, n = 3, repeated measures ANOVA with Dunnett's multiple comparison test, Figure 5.7B). Neither of the 25 Hz protocols produced a significant change in $\Delta F/F_0$ ($p > 0.05$, one-sampled *t*-test, Figure 5.7C). Interestingly, there was a greater decrease following the 60 pulse protocol, however this was not

significantly different from the 10 pulse protocol ΔF/Fo ($p > 0.05$, paired Student's *t*-test, Figure 5.7C).

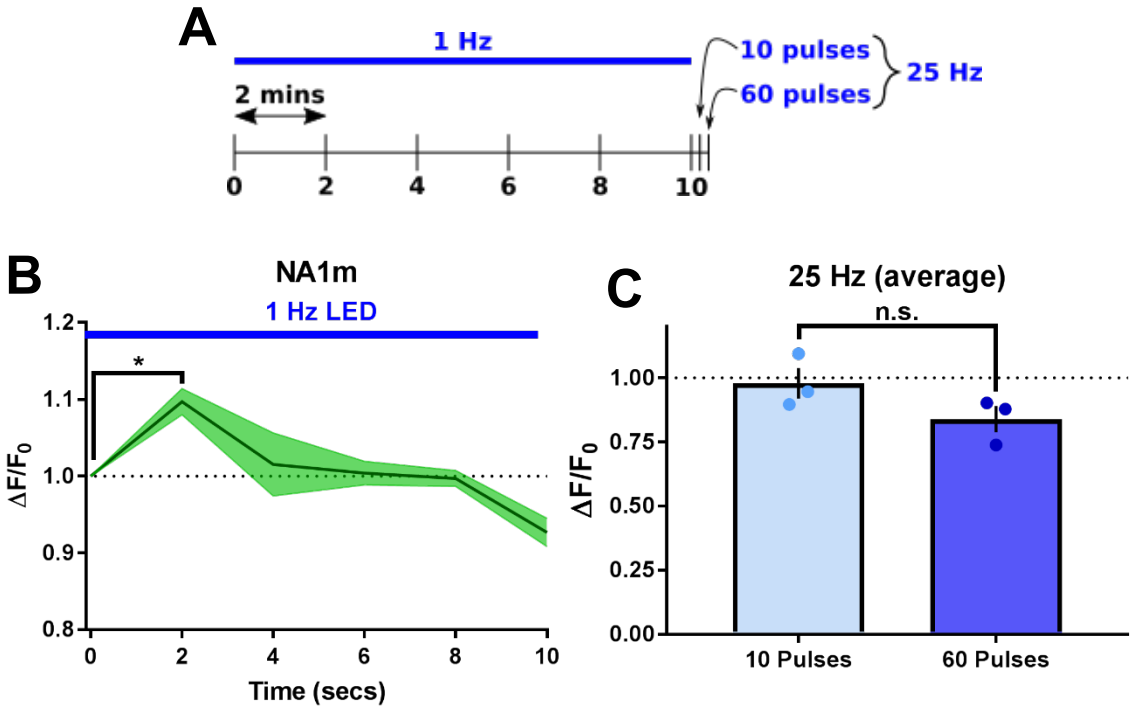

Figure 5.7: *Detection of optically-evoked NA using NA1m. A) Hippocampal slice opto-stimulation protocol, Z stacks were obtained every 2 minutes during the 1 Hz tonic stimulation protocol, and immediately after each 25 Hz phasic protocol. B) Average time course trace for the 1 Hz protocol showing the transient fluorescence increase in the first two minutes before a subsequent decrease (n = 3). C) Averaged fluorescence data for the 10 and 60 pulse phasic protocols (n = 3).*

5.5 Discussion

The results discussed in Chapters 2 and 3 imply that a concentration of ~600 nM NA is released upon opto-stimulation of hippocampal LC fibres. We therefore aimed to ascertain whether it is possible to detect such a concentration using two methods: a traditional FSCV assay and the novel genetically-encoded fluorescent sensor, NA1m. Both methods show putative responses to opto-stimulation but require further optimisation. One important point to note is that the minimum clear signals for bath-applied NA were ~10 μM for FSCV and 20 μM for NA1m. Since opto-stimulation gave putative signals that were clearly below this (particularly with NA1m), the conclusion could be drawn that 20 μM is not a physiological concentration of NA, a claim tentatively made in Chapter 3. However, it is important to note that both methods measure NA levels at a bulk level, therefore local terminal release may still be high but so transient in nature (i.e. due to rapid diffusion and re-uptake mechanisms) and spatially precise (i.e. below the microscope resolution) that we were still unable to capture it.

5.5.1 FSCV

Bath-applied NA FSCV experiments revealed a lower detection threshold for bath-applied NA (i.e. higher signal-to-noise) compared to NA1m, but only one slice showed a

possible optogenetically-evoked NA oxidation current. Increasing the voltage scan speed is one way to potentially improve the sensitivity of this assay. *In vivo* detection methods sometimes employ speeds of 2400 V/s, which can give clear catecholamine oxidation peaks at 1 μM (Keithley *et al.*, 2011). Moreover, incorporating a "sawhorse" scan pattern (holding the peak voltage for ~55 ms before cycling back down again) can improve signal-to-noise *in vivo* by 4-fold (Keithley *et al.*, 2011). Therefore, using an amplifier and analogue-to-digital converter able to run specially-designed FSCV scan waveforms at a high frequency could further improve NA detection in future work.

The left-shifted oxidation peaks we observed with slices from WT mice suggest that the rapid voltage changes applied across the carbon fibre micro-electrode during FSCV may induce the release of chemicals that can also undergo oxidation. However, given that the oxidation peaks for DA, 5-HT and adenosine all occur at voltages ≥0.6 V (Nguyen and Venton, 2015), it is unknown what the molecule associated with this peak may be. There is evidence of a serotonergic innervation of the LC (Kaehler, Singewald and Philippu, 1999; Pudovkina, Cremers and Westerink, 2002), and serotonin oxidation currents occur at lower voltages than NA and DA and have higher (~10-fold) amplitudes (Robinson *et al.*, 2003), suggesting serotonin (and/or its break-down products may have contaminated our signal.

Alternatively, the increasing peak over time may be indicative of an unstable faradic current. Background FSCV currents are known to be unstable over time (Heien *et al.*, 2005; Meunier, McCarty and Sombers, 2019). In future it would be of benefit to run several time-match controls before the light stimulation and subtract the post-light stimulation samples from these individual baselines for each time point, rather than subtracting from just one baseline at the start. This would help to ensure that the time-dependent oxidation currents are not a component of the faradic currents associated with longer FSCV recordings. In addition, changes to the protocol and subsequent analysis may help to more accurately subtract the fluctuating baseline. For instance, double-waveform partial-least-squares regression (DW-PLSR) is a FSCV protocol whereby a smaller triangular waveform (+0.3 to +0.8 V) precedes the standard triangular waveform (-0.4 to 1.2 V) (Meunier, McCarty and Sombers, 2019). The smaller waveform is insufficient to oxidise catecholamines and is instead used to capture information regarding the degree of electrochemical drift. This predicted drift is then subtracted from the subsequent standard triangular waveform.

5.5.2 NA1m

The NA1m experiments were carried out in the latter few months of this PhD and were therefore subject to tight time restrictions and a limited number of mice, with each mouse only yielding 2-3 NA1m-expressing slices. We also experienced a number of

initial problems during the optimisation, such as slices moving during the image acquisition process and tissue damage upon continuous image acquisition.

Despite this, we recorded a strong signal with both 20 μM and 100 μM NA, however lower concentrations of bath-applied NA showed no effect. This is somewhat disappointing, given that NA1m shows an EC_{50} values of ~83 nM, ~1 μM and ~1.9 μM for NA (in HEK293 cells, cultured neurons and acute LC slices, respectively, Feng *et al.*, 2019). The virus titres and incubation periods were similar between the present study and the previous characterisation of the sensor. Interestingly, the strongest fluorescent signal was observed in the dendrites, suggesting a strong trafficking of the sensor (which is based on the α2-AR membrane-bound protein) to the dendrites.

There was also a basal level of NA1m fluorescence in the hippocampal slices, as evidenced by the fluorescence observed on the slice pre-NA perfusion and also the fact that yohimbine often reduced fluorescence to levels lower than observed at baseline. This is not surprising, as LC inputs likely still spontaneously release NA even when not stimulated, with microdialysis research estimating basal hippocampal NA levels somewhere between ~14 nM and ~560 nM in freely-moving rats (Abercrombie, Keller and Zigmond, 1988; Huttunen, 1991).

The transient increase in fluorescent signal may reflect a biological signal, however the subsequent decrease is confounding and may be due to photobleaching. Indeed, the fact that a further decrease (although not significant) after the 25 Hz 60 pulse protocol seems to support this.

5.6 Improvements and future work

5.6.1 Alternative measures of detecting NA release

Prior to the development of NA1m, several other methods of detecting catecholamine release emerged that could be used to address our research questions. Cell-based neurotransmitter fluorescent-engineered reporters (CNiFERs) to detect NA and DA were recently developed by Muller *et al.* (2014) and Lacin *et al.* (2016). These tools utilise the α1-AR and D2-R GPCR specificity to discriminate nanomolar concentrations of NA and DA. In brief, HEK293 cells are genetically engineered to express α1-ARs and the fluorescence resonance energy transfer (FRET) based Ca^{2+} indicator, TN-XXL. Activation of the α1-AR by NA activates the downstream G_q G-protein, which in turn stimulates PLC leading to an increase in intracellular Ca^{2+} by inositol triphosphate (IP_3). This rise in intracellular Ca^{2+} is then detected by the TN-XXL Ca^{2+} sensor, which shifts its fluorescent emission wavelength from ~470 nm (cyan) to ~535 nm (yellow) when excited with a 2-photon laser (820 nm). The α1-CNiFER demonstrated nanomolar affinity for NA, with an EC_{50} of ~19 nM for NA, which was 100-fold more selective for NA

than DA. There are several methods that could be used to utilise this approach to answer our research question. One would be to culture HEK293 neurons onto acute slices immediately after they are obtained, or co-culture them on organotypic slices. This latter approach was used by Mosienko *et al.* (2018) to detect NA release from LC neurons in response to L-lactate. Consistent with Muller *et al.* (2014), the α1-CNiFERs cultured on organotypic slices exhibited nanomolar affinity for NA (EC_{50} = ~31 nM). Muller *et al.* (2014) used a variation of this approach, implanting and co-culturing populations of D2-CNiFER and α1-CNiFER HEK293 cells in the frontal cortices of mice to simultaneously detect NA and DA release during behavioural conditioning. Given that our research question concerns *ex vivo* LC terminal release in response to opto-stimulation, culturing the CNiFERs on acute slices would be an acceptable initial approach. Although it is unknown how effectively the CNiFERs would adhere to the slice and whether they would be stable enough for subsequent imaging. Co-culturing on organotypic slices would not be viable as, due to the axotomisation of LC fibres from their somas, these long-range inputs would likely be lost after several days in culture.

The cleanest alternative would be to genetically engineer mice to express the TN-XXL in hippocampal neurons, for instance using an adenovirus incorporating a widespread promoter such as hSyn (as in the present study). TN-XXL has been expressed in neurons and astrocytes of organotypic hippocampal cultures using a Semliki Forest virus vector (SFV, Mank *et al.*, 2008), however long-term (>5 days) expression using this vector is troublesome due to its excitotoxicity compared to lentiviral approaches (Ehrengruber *et al.*, 2001; Mank *et al.*, 2008). Therefore, a lentiviral approach would be preferable to generate acute slices. Activation of endogenous α1-ARs in response to opto-activation of LC inputs would then be expected to trigger the aforementioned signalling cascade to induce FRET responses in the TN-XXL-expressing hippocampal neurons. However, whether native α1-AR expression and activation would be high enough to induce a FRET response is not known. The technical difficulty regarding concurrent tonic optogenetic stimulation and imaging would also remain an issue. A TTL-triggered shutter to protect the PMT could be used to overcome this.

A non-imaging approach to determining NA release could utilise LC nucleated macro-patches, as in Courtney and Ford (2014). In this study, large, nucleated outside-out macro-patches of LC or VTA neurons – which endogenously express α2-AR and D2-R auto-receptors, respectively – were obtained using a patch pipette. Barrel perfusion of NA or DA elicited clear IPSCs mediated by α2-ARs and D2-Rs, respectively. Moreover, they held the LC isolated macropatches above LC slices and electrically stimulated the slice, and this elicited IPSCs with kinetics similar to IPSCs obtained in whole-cell patch-clamp neurons within the LC. In the future a similar approach could be used, whereby macropatches isolated from the LC contralateral to the ChR2-injected hemisphere could

be held above hippocampal slices expressing ChR2 in LC terminals. Opto-stimulation protocols could then be applied to see if α2-AR-mediated IPSCs could be elicited by endogenous NA release. A confound in this could be contralateral retrograde transport of the viral vector, subsequent ChR2 expression and IPSCs mediated by direct NA release from the macropatch.

5.6.2 Mutant NA1m sensor

We also obtained a mutant version of the NA1m virus in which the NA binding site is intact, but ligand binding does not induce GFP fluorescence (Feng *et al.*, 2019). Repeating the NA1m experiments – particularly those involving opto-stimulation of the hippocampus – are needed to ensure fluorescent changes aren't due to time-related effects.

5.7 General conclusion

In summary, we have undertaken preliminary work to explore methods of detecting optically-evoked NA release from LC terminals. Both methods were able to detect bath application of NA, however FSCV appeared to be more reliable and slightly more sensitive.

Both methods also showed putative NA-associated signals, but these were somewhat unreliable in their presence and inconsistent in amplitude. FSCV appears to suffer from a lack of sub-micromolar sensitivity due to software and hardware limitations, and current instability over time. Equipment changes to allow faster voltage ramps, coupled with improved background current subtraction methods, may be able to mitigate these problems in future work.

NA1m expression was clearly seen in the hippocampus, however the response to maximal NA application was variable. Longer incubation times may improve the reliability of the signal, coupled with – paradoxically – lower virus titres in an attempt to resolve individual cell/dendrite fluorescence. There is also a large scope for optimisation of the imaging optics to counteract potential photobleaching of the GFP and minimise tissue damage.

Concluding remarks

In summary, the results presented in this thesis highlight a number of interesting findings regarding the noradrenergic modulation of the SC-CA1 and MF-CA3 synapses in the hippocampus.

Bath application of NA at a typical concentration used in the literature (20 μM) differentially modulates synaptic transmission at SC-CA1 and MF-CA3 synapses. Specifically, NA attenuates both SC excitatory and feed-forward inhibitory inputs to CA1, maintaining an E/I balance at low frequencies that acts to suppress CA1 spike output. At high frequencies, however, the mono-synaptic excitatory input can overcome this attenuation and the E/I balance is shifted towards excitation. These novel results support the notion that NA improves signal-to-noise in cortical networks by imposing a high-pass filter on incoming information (Woodward *et al.*, 1979). It would be expected that under these conditions, CA1 spike output would increase, however this remains to be tested in current-clamp conditions. We also sought to examine whether modulation of SK channels could serve as a common signalling mechanism for increasing NMDAR function and STDP at the SC-CA1 synapse for NA and ACh. However, we found no effect of NA upon either of these parameters. SK channel regulation of NMDARs is more prominent in ventral slices (Babiec *et al.*, 2017). Given the focus on dorsal slices in the present study, future work could utilise ventral slices to determine whether this is the case across the whole dorso-ventral axis.

At the MF-CA3 synapse, excitatory transmission is unaffected by NA, but feed-forward inhibition is suppressed to a degree reminiscent of that seen in the CA1. Using a combination of naturalistic firing patterns and a computational model of the MF-CA3 synapse to examine the effects of NA on a wide range of mossy fibre input frequencies revealed that, compared to ACh, NA exerts only a modest effect on the E/I balance. Such a result highlights the diversity of neuromodulatory systems in modifying CA3 network activity and – given the importance of noradrenergic input on CA3-dependent memory performance – future work into additional pathways innervating CA3 pyramidal neurons (A/C fibres and/or cortical PP synapses) may find that NA exerts more notable effects at these inputs.

A major goal of this PhD was to ascertain whether any of the effects observed with bath application of NA could be recapitulated by optically evoking endogenous NA release from within the LC hippocampal terminals. Strikingly, we found that such release had contrasting effects to that observed using 20 μM NA, dramatically enhancing spike output via a β-AR mechanism that may involve the inhibition of transient voltage-gated K^+ channels. Further characterisation suggested that this functional distinction arises

due to differences in concentration and spatiotemporal release, as we were able to recapitulate a number of the effects using a sub-micromolar concentration of bath-applied NA that is close to recent estimates of NA release from LC terminals. However, the fact that this low concentration still exerted effects not seen using optically-evoked NA implies that the LC may target distinct CA1 pyramidal neuron compartments. In future it would be of benefit to examine optically-evoked NA on a range of opto-stimulation frequencies. Moreover, combining naturalistic SC stimulation patterns with optically-evoked patterns of behaviourally-related LC firing patterns (i.e. tonic opto-stimulation during low frequency SC inputs followed by phasic bursts of opto-stimulation during high frequency SC inputs) may reveal how the LC dynamically modulates the SC-CA1 synapse as an animal enters or leaves its place field.

Moreover, we found that tonic opto-stimulation of LC terminals produced a greater increase in spike output than a phasic-like protocol. The reason for this was not entirely clear but could be due to auto-inhibition of the LC terminals at high frequencies, rapid re-uptake via noradrenaline re-uptake transporters, an inability of the terminals to follow high-frequency opto-stimulation, or noradrenergic engagement with hippocampal inhibitory mechanisms that counteract β-AR effects. Such confounds make it difficult to relate the effects of phasic-like opto-stimulation with a functional role *in vivo*. However, at a functional level, the tonic optically-evoked release of NA may be analogous to a behaving mouse transitioning from disengaged wakefulness or sleep to a mode of explorative behaviour. The enhanced EPSP-spike coupling we have shown with optically-evoked NA would serve to improve communication between the CA3 and CA1 and support place field encoding and stability. In future, it is imperative to investigate the effects of optically-evoked NA on additional parameters such as NMDAR function, spontaneous release and plasticity at the SC-CA1, MF-CA3 and TA-CA1 synapses to build a more complete picture of the noradrenergic modulation of these micro-circuits.

Finally, our efforts to establish the concentration of NA released using opto-stimulation of hippocampal LC terminals showed promise but requires further optimisation. Despite the fact that we were unable to detect the actual concentration released, the results rule out the notion of 20 μM NA as a physiological concentration of NA and – in combination with the data from Rosen, Cheung and Siegelbaum (2015) – highlight the need for opto-genetic methods to be integrated into future *ex vivo* neuromodulator studies.

Appendix I

Acetylcholine disinhibits hippocampal circuits to enable rapid formation of overlapping memory ensembles

Luke Y. Prince[1,5], Krasimira Tsaneva-Atanasova[2,3], Claudia Clopath[4], and Jack R. Mellor[1]

[1] Centre for Synaptic Plasticity, School of Physiology Pharmacology, and Neuroscience, University of Bristol, BS8 1TD, UK

[2] Department of Mathematics and Living Systems Institute, University of Exeter, Exeter, EX4 4QF, UK

[3] EPRSC Centre for Predictive Modelling in Healthcare, University of Exeter, Exeter, EX4 4QJ, UK

[4] Bioengineering Department, Imperial College London, London, SW7 2AZ, UK

[5] Current address: Department of Biological Sciences, University of Toronto Scarborough, Toronto, ON, M1C 1A4, Canada

Correspondence: Jack.Mellor@Bristol.ac.uk

Keywords: acetylcholine, hippocampus, computational modelling, electrophysiology, neuronal ensembles, dentate gyrus, CA3.

Abstract

In the hippocampus, episodic memories are thought to be encoded by the formation of ensembles of synaptically coupled CA3 pyramidal cells driven by sparse but powerful mossy fiber inputs from dentate gyrus granule cells. Since CA3 network capacity is finite, a mechanism for enhancing memory encoding during important events would ensure greater efficiency. Acetylcholine is proposed as the salient signal that determines this memory selectivity filter but its actions on mossy fiber transmission are largely unknown. Here, we show experimentally that cholinergic receptor activation suppresses feedforward inhibition and enhances excitatory–inhibitory ratio. In modelled reconstructions of CA3 pyramidal cells with active dendrites, this disinhibition enables postsynaptic depolarization required for synaptic plasticity at CA3-CA3 recurrent synapses. We further show in a spiking neural network model of CA3 how a combination of disinhibited mossy fiber activity, enhanced cellular excitability and reduced recurrent synapse strength can drive rapid overlapping ensemble formation through CA3-CA3 recurrent synaptic plasticity. Thus, we propose a coordinated set of mechanisms by which acetylcholine release enables the selective encoding of salient high-density episodic memories in the hippocampus.

.

Introduction

The hippocampus plays a central role in the formation of episodic memories by processing information from the entorhinal cortex sequentially through the dentate gyrus, CA3 and CA1 regions. Anatomical, functional and theoretical considerations propose separate computational properties for each of these regions in support of memory processing (Marr, 1971; McClelland and Goddard, 1996; Kesner and Rolls, 2015). In particular, the CA3 region is characterized by a recurrently connected set of excitatory pyramidal neurons, which are believed to encode auto-associative memories by selectively strengthening recurrent synapses between ensembles of neurons that provide a neural representation of the memory (Nakazawa et al., 2002; Rebola et al., 2017). Configuring a recurrent network in this way is proposed to endow the network with attractor dynamics, in which the network is driven towards a stable state of ensemble formation (Marr, 1971; Hopfield, 1982; Kesner and Rolls, 2015). This process is related to memory retrieval, in which external sources of input will alter the state of the network by activating subsets of neurons and through recurrent dynamics will be driven towards these stable states in which all neurons in the ensemble are reactivated – a process also referred to as pattern completion (Gold and Kesner, 2005; Yassa and Stark, 2011). Within this framework, memory encoding is believed to be the procedure of altering the network through synaptic plasticity to create or change the position of attractor states (Treves and Rolls, 1994; Tsodyks, 1999). However, not all memories are stored, indicating that there may be a gate to select which experiences should be encoded, but it is unclear how such a filter might operate.

One potential filter mechanism is the release of neuromodulators such as acetylcholine that can rapidly reconfigure neuronal networks (Hasselmo, 2006; Prince et al., 2016). Acetylcholine is thought to promote encoding of new information by facilitating NMDA receptor function and induction of synaptic plasticity (Markram and Segal, 1992; Marino et al., 1998; Buchanan et al., 2010; Fernandez de Sevilla and Buno, 2010; Gu and Yakel, 2011; Dennis et al., 2016; Papouin et al., 2017) and selectively suppressing recurrent activity representing previously stored information in favour of feed-forward activity representing novel information (Hasselmo et al., 1995; Hummos et al., 2014). These properties are predicted to facilitate the encoding of new memories and allow greater overlap between representations (Hasselmo et al., 1995; Hasselmo, 2006). Commensurate with the concept of acetylcholine being important for encoding new information, acetylcholine release in the hippocampus and neocortex is associated with reward and arousal during periods of behavioural activity when it is beneficial to learn associated information in the environment to gain future rewards (Hangya et al., 2015; Teles-Grilo Ruivo et al., 2017). An alternative way to conceptualize the role of acetylcholine is as a signal for

uncertainty, which may be resolved by familiarization through learning (Yu and Dayan, 2005). In either scenario, salience is indicated by increasing the release of acetylcholine in the hippocampus and other brain areas.

The dentate gyrus receives excitatory glutamatergic input from layer II of the medial entorhinal cortex, and sparsifies this signal by suppressing the activity of most dentate gyrus granule cells through lateral inhibition while dramatically increasing the firing rate of a select few granule cells (O'Reilly and McClelland, 1994; Leutgeb et al., 2007). By this mechanism granule cells detect salient, novel information and accentuate minor contextual details related to familiar information (a process often referred to as pattern separation). Individual granule cells provide a strong, sparse, facilitating input to a small number of CA3 pyramidal cells that can be sufficiently powerful to engage 1:1 spike transfer after multiple spikes in a granule cell burst (Acsady et al., 1998; Henze et al., 2002; Sachidhanandam et al., 2009; Vyleta et al., 2016). This focal excitation by mossy fibers drives synchronisation between subsets of CA3 pyramidal cells potentially allowing recurrent CA3-CA3 synapses to engage Hebbian plasticity mechanisms to create ensembles of strongly coupled CA3 cells thereby initiating the storage of new information (O'Reilly and McClelland, 1994; Treves and Rolls, 1994; Kobayashi and Poo, 2004; Brandalise and Gerber, 2014; Guzman et al., 2016; Mishra et al., 2016). Mossy fibers also excite a broad and diverse set of inhibitory interneurons that provide a widespread 'blanket' of feed-forward inhibition over a large population of CA3 pyramidal cells (Acsady et al., 1998; Toth et al., 2000; Mori et al., 2007; Szabadics and Soltesz, 2009). This feed-forward inhibition prevents runaway excitation and ensures tight spike timing for spike transfer (Torborg et al., 2010; Restivo et al., 2015; Zucca et al., 2017), while also enhancing memory precision (Ruediger et al., 2011) but it is not known what impact it may have on synaptic plasticity within the CA3 recurrent network.

Here we investigate the modulation by acetylcholine of ensemble creation and therefore memory encoding within the hippocampal CA3 network. Using slice electrophysiology and a hierarchy of experimentally constrained computational models of mossy fiber synaptic transmission and CA3 network activity, we demonstrate that acetylcholine suppresses feed-forward inhibition enabling plasticity at recurrent CA3-CA3 synapses and the formation of ensembles within the CA3 network. Furthermore, we show that acetylcholine increases the density of stable ensembles by enhancing permissible overlap between ensembles.

Results

Acetylcholine regulates CA3-CA3 recurrent synaptic inputs and cellular excitability (Hasselmo et al., 1995; Vogt and Regehr, 2001; Dasari and Gulledge, 2011) which are both likely to be important for the creation of CA3 ensembles (Hasselmo et al., 1992). An additional critical feature of ensemble formation in CA3 is the mossy fiber input from dentate gyrus. However, the cumulative effects of acetylcholine on the mossy fiber projection incorporating both excitatory and inhibitory synaptic transmission are not known. Therefore, we first recorded experimentally the effect of acetylcholine on combined feed-forward excitatory and inhibitory synaptic transmission in the mossy fiber pathway of mouse hippocampal slices. Minimal stimulation of granule cells resulted in EPSCs and IPSCs that were individually isolated by setting the membrane potential to -70mV and +10mV respectively in accordance with experimentally determined reversal potentials for inhibitory and excitatory transmission respectively (Supplementary Fig. 1). Mossy fibers were stimulated with trains of 4 pulses at 20 Hz every 20 s. Application of the group II mGluR agonist DCG-IV (1 µM) reduced EPSC amplitudes by >90% (Fig. 1B) indicating selective activation of the mossy fiber pathway (Kamiya et al., 1996). The EPSC rise times (20-80%), latencies, and jitter were 0.57 ± 0.11 ms, 2.1 ± 0.49 ms and 0.53 ± 0.27 ms respectively (Supplementary Fig. 1) characteristic of mossy fiber synapses and confirming their monosynaptic origin (Nicoll and Schmitz, 2005). DCG-IV also reduced IPSC amplitudes by >90% and the rise times, latencies and jitter were 3.52 ± 1.08 ms, 6.20 ± 1.82 ms and 0.73 ± 0.25 ms respectively (Supplementary Fig. 1) indicating that IPSCs were mediated by disynaptic feed-forward inhibitory transmission in the mossy fiber pathway (Torborg et al., 2010). Both EPSCs and IPSCs exhibited pronounced facilitation in response to a train of 4 stimuli at 20 Hz as previously shown for mossy fiber feed-forward excitatory and inhibitory pathways (Torborg et al., 2010).

Acetylcholine reduces feed-forward inhibition in the mossy fiber pathway

The impact of acetylcholine on information transfer between the dentate gyrus and CA3 will depend on its effects on both excitatory and inhibitory pathways. To assess the effect of acetylcholine on both pathways we used the broad-spectrum cholinergic receptor agonist carbachol (CCh). Application of 5 µM CCh depressed EPSC amplitudes by ~25% (Fig. 1C; 75.6 ± 17.0% and 66.2 ± 11.9% of baseline measured at 1st and 4th pulses, n = 7, $p < 0.05$) without altering facilitation ratios (Fig. 1C; $p = 0.509$; Measured at 1st to 4th pulse). This depression did not recover on washout of CCh. The use of minimal stimulation meant that responses to the first stimuli were highly variable and often very small or absent due to the low basal probability of

release at mossy fiber synapses (Nicoll and Schmitz, 2005; Sachidhanandam et al., 2009; Torborg et al., 2010). This was particularly true for IPSC recordings resulting in very large facilitation ratios and a highly variable effect of CCh on the first IPSC in a train. In contrast to the effect on EPSCs, 5 µM CCh had no consistent effect on the 1st IPSC in a train but depressed subsequent IPSC amplitudes reversibly and to a much greater degree (Fig. 1D; 121.5 ± 19.5% and 29.3 ± 13.5% of baseline measured at 1st and 4th pulses; n = 6, p = 0.012 measured at 4th pulse) and at the same time reduced facilitation ratios (Fig 1D; p = 0.012; measured at 1st to 4th pulse). Because the larger IPSCs were greatly reduced by CCh this represents a substantial reduction in feed-forward inhibition across the 4 pulse stimulus train. CCh also enhances the excitability of neurons in the CA3 network (Hasselmo et al., 1995; Vogt and Regehr, 2001; Dasari and Gulledge, 2011) but this effect was absent at a cellular level in our recordings because of the inclusion of cesium in the pipette solution. Elevated network excitability was evident from a general increase in the frequency of spontaneous EPSCs and IPSCs (Supplementary Fig. 1). At lower concentrations, 1 µM CCh had limited effect on IPSC amplitudes whereas at higher concentrations 10 µM CCh had similar effects to 5 µM CCh with a substantial depression of IPSC amplitudes (Supplementary Fig. 1). These results indicate that acetylcholine causes a small irreversible depression of excitatory transmission at mossy fiber synapses whereas feed-forward inhibitory transmission is substantially depressed. Overall, this indicates a substantial net enhancement of Excitatory-Inhibitory ratio in the mossy fiber pathway in the presence of acetylcholine.

Effects of acetylcholine on short-term plasticity at the mossy fiber synapse

Information transfer between the dentate gyrus and CA3 network depends on bursts of high frequency activity in dentate granule cells leading to pronounced frequency facilitation of excitatory synaptic input (Henze et al., 2002; Vyleta et al., 2016; Zucca et al., 2017). This is balanced by frequency-dependent facilitation of inhibitory synaptic input (Torborg et al., 2010) but variations in the short-term plasticity dynamics between the excitatory and inhibitory pathways will lead to windows within the frequency domain when excitation dominates and action potentials are triggered in CA3 pyramidal cells (Mori et al., 2004). However, these temporal windows have not been fully characterized and, furthermore, the effect of acetylcholine on Excitatory-Inhibitory ratio over a range of mossy fiber stimulation patterns is not known. To investigate the patterns of activity that trigger action potentials under conditions of presence and absence of acetylcholine we adapted a Tsodyks-Markram based model of short-term plasticity dynamics in both excitatory and inhibitory pathways (see Methods).

Short-term plasticity models are difficult to constrain with responses evoked by regular stimulation protocols (Costa et al., 2013). Therefore, we constrained the model using responses to a stimulation pattern resembling the natural spike statistics of dentate gyrus granule cells which incorporate a broad range of inter-stimulus intervals (ISIs) (Fig. 2A) (Wiebe and Staubli, 2001; Mistry et al., 2011). Similar to the regular stimulation pattern of 4 stimuli at 20Hz, CCh depressed EPSCs and IPSCs in response to the irregular stimulation pattern across the range of ISIs but the depression was much more pronounced for IPSCs (Fig. 2B). Several short-term plasticity models of increasing level of complexity for both excitatory and inhibitory synaptic responses were assessed for fit to the experimental data (see Methods for detailed description of these models). The basic form of these models included a facilitation and a depression variable, here represented as *f* and *d* respectively. Dynamics for these variables are governed by parameters for degree (*a*) and timecourse of facilitation (τ_f) and depression (τ_d) as well as baseline of release (f_0) and synaptic conductance (*g*) (Fig. 2B). Parameter inference for the short-term plasticity models was carried out and the best fitting models were selected by comparing the Akaike and Bayesian Information Criteria (AIC and BIC respectively) weights. These weights represent a normalisation of AIC and BIC values calculated by dividing the AIC and BIC values by the sum of these values across all models (log-likelihood of model given data punished for increasing complexity in two different ways). This is convenient as it allows these values to be transformed into a probability space and hence comparable across samples {Wagenmakers, 2004 #3194}. The model with the highest weight explains the data best. For excitatory mossy fiber synaptic transmission, a model containing a single facilitating variable with an exponent of 2 (f^2) (Equations 1 and 2) best explained the experimental data (Fig. 2D).

$$\text{EPSC amplitude} = g_E^{max}\, f^2\, (V_{mem} - E_{GLUT}) \quad \text{(Equation 3)}$$

$$\frac{df}{dt} = \frac{f_0 - f}{\tau_f} + a\,(1 - f)\sum_s \delta(t - t_s) \quad \text{(Equation 4)}$$

where V_{mem} is the holding voltage of the cell in voltage clamp, g_E^{max} is the maximum excitatory conductance, E_{GLUT} is the reversal potential of glutamatergic transmission, and t_s is the timing of the s^{th} spike (or pulse). Explanation of other parameters for the short-term plasticity model is given in the Methods section.

It is noticeable that AIC and BIC weights disagree on which model best explains the data. The f^2 model had only the second highest AIC weight, but had the highest BIC weight, whereas the more complex *af* model had a higher AIC weight. However, the evidence ratio for BIC points

favours the f^2 model (P(f^2 |Data)/P(af |Data) = 8.92 (see (Kass and Raftery, 1995)), whereas the evidence ratio for AIC indicates little evidence in favour of the *af* model (P(*af* |Data)/P(f^2 |Data) = 1.51). Together this indicates that the f^2 model best explains the data.

For inhibitory feed-forward mossy fiber synaptic transmission, a complex model with facilitation (*f*), depression (*d*), and additional facilitation over the increment parameter *a* (*afd*) produced the best fit (Fig. 2E and Equations 3, 4, 5 and 6) with both AIC and BIC weights convincingly pointing to the *afd* model as most appropriate to describe the data. Additional parameters in this model included a time course for facilitation of *a* (τ_a), an increment scaling factor for *a* (*b*), and baseline (a_0).

$$\text{IPSC amplitude} = g_I^{MAX}\ f\ d\ (\mathrm{V}_{mem} - E_{GABA}) \quad \text{(Equation 5)}$$

$$\frac{df}{dt} = \frac{f_0 - f}{\tau_f} + a\,(1-f)\sum_s \delta(t - t_s) \quad \text{(Equation 6)}$$

$$\frac{dd}{dt} = \frac{1-d}{\tau_d} - f\ d\sum_s \delta(t - t_s) \quad \text{(Equation 7)}$$

$$\frac{da}{dt} = \frac{a_0 - a}{\tau_a} + b\,(1-a)\sum_s \delta(t - t_s) \quad \text{(Equation 8)}$$

where g_I^{max} is maximum inhibitory conductance and E_{GABA} is the reversal potential of GABAergic transmission. See Methods for detailed explanation of the above equations.

Discrepancies between samples drawn from posterior-predictive distributions of these models indicated good fit for both models (Supplementary Fig. 2).

Using these models for the activity-dependent progression of excitatory and inhibitory synaptic weights we were then able to investigate the effect of acetylcholine on short-term plasticity by comparing normalized parameter estimates to time matched controls. Since posterior distributions for EPSC data were narrow and unimodal, maximum a posteriori (MAP) estimates were used, whereas mean parameter estimates were used for IPSC data since posterior distributions were wide and bimodal in some cases (Supplementary Fig. 2). This analysis revealed the small decrease in EPSC amplitude caused by CCh resulted from a reduction in the conductance scaling parameter '*g*' (Fig. 2D; 49.9 ± 17.6%) in agreement with the data in Fig. 1C and indicating a postsynaptic mechanism. The substantial decrease in IPSC amplitude caused by

CCh resulted from a large reduction in the conductance scaling parameter '*g*', and an increase in the baseline parameter 'f_0' which also had the effect of reducing facilitation (Fig. 2E; 73.1 ± 27.9% decrease in 'g'; 225.7 ± 160.1 % increase in 'p_0'). Since IPSCs are disynaptic, it is not straightforward to interpret how these parameter changes reflect biophysical changes to synaptic transmission, but the most likely explanation is a combination of increased feed-forward interneuron excitability and spike rate, coupled with a strong depression of GABA release. These results indicate the mechanisms underlying the effects of CCh on mossy fiber synaptic transmission and enable investigation of the granule cell spike patterns that favor excitation over inhibition.

Enhancement of mossy fiber Excitatory-Inhibitory balance by acetylcholine

Feed-forward inhibition dominates excitation in the mossy fiber pathway for the majority of spike patterns (Mori et al., 2004; Torborg et al., 2010). Since acetylcholine depresses inhibitory transmission more than excitatory transmission (Figs 1 and 2) it is expected that the Excitatory-Inhibitory balance will be shifted towards excitation but the precise spike patterns that this occurs for are unclear. To examine how Excitatory-Inhibitory balance is affected by carbachol with different spike patterns we first tested the dependence of short-term synaptic dynamics on background firing rate using the model for short-term plasticity dynamics. Spike patterns were described by two parameters: a between burst interval $\Delta t_{between}$ describing a background firing rate, and a within burst interval Δt_{within} describing the time between spikes in a burst. The steady state value of *f*, *d*, and *a* given $\Delta t_{between}$ were then used to replace their baseline values ($a_0 \rightarrow a_\infty$; $f_0 \rightarrow f_\infty$; $d_0 = 1 \rightarrow d_\infty$) to set their initial values at the beginning of a burst, i.e.,

$$a_\infty = \frac{a_0 exp(\Delta t_{between}/\tau_a) - a_0 + b}{\exp(\Delta t_{between}/\tau_a) - 1 + b} \qquad \text{(Equation 9)}$$

$$f_\infty = \frac{f_0 \exp(\Delta t_{between}/\tau_f) - f_0 + a_\infty}{\exp(\Delta t_{between}/\tau_f) - 1 + a_\infty} \qquad \text{(Equation 10)}$$

$$d_\infty = \frac{1 - \exp(-\Delta t_{between}/\tau_d)}{1 + (1 - f_\infty)\exp(-\Delta t_{between}/\tau_d)} \qquad \text{(Equation 11)}$$

By systematically varying the between and within burst intervals for both excitatory and inhibitory synaptic input we were able to simulate EPSCs and IPSCs in the presence and absence of acetylcholine (Fig. 3A). The amplitudes of these responses were then used to explore the

effects of acetylcholine on within burst facilitation ratios and Excitatory-Inhibitory balance across a wide range of between and within burst intervals.

Experimental data shows that mossy fiber EPSCs are exquisitely sensitive to between burst interval with facilitation revealed as between burst interval is decreased. Furthermore, it has been shown that shortening the between burst interval decreases within burst facilitation (Salin et al., 1996). Our simulations replicated this interdependence of between and within burst interval with respect to EPSC facilitation with values closely associated with the experimental data in the literature (Salin et al., 1996; Toth et al., 2000) (Fig. 3B). Since the CCh induced depression of EPSCs was mediated by a reduction in synaptic conductance it did not alter either between or within burst synaptic facilitation.

The situation for inhibitory synaptic transmission was more complex. Over the course of a burst synaptic amplitude facilitation was greatest when between and within burst intervals were largest. As between and within burst intervals reduced the facilitation morphed into a depression towards the end of the burst resulting in limited inhibition at the end of high frequency bursts (Fig. 3C). CCh dramatically reduced both the initial IPSC amplitude and subsequent facilitation within bursts at all between and within burst intervals (Fig. 3C).

We then combined the results from excitatory and inhibitory facilitation to predict EPSC-IPSC amplitude ratios over the course of a burst. In control conditions, excitation dominates over inhibition only after multiple spikes in a burst and when bursts occur at shorter between and within burst intervals (Fig. 3E) (Mori et al., 2004; Torborg et al., 2010; Zucca et al., 2017). However, in the presence of CCh, excitation dominates over inhibition at earlier stimuli within the burst, and over longer between and within burst intervals meaning cholinergic receptor activation allows excitation to dominate over inhibition for a broader range of stimulus patterns.

We next investigated the biophysical effects of the acetylcholine-induced reduction in feed-forward inhibitory synaptic transmission at mossy fiber synapses. In particular, the modulation of back-propagating action potentials and EPSPs in CA3 pyramidal cells that are critical for the induction of long-term potentiation (LTP) at recurrent CA3-CA3 synapses and therefore the formation of CA3 ensembles (Brandalise and Gerber, 2014; Guzman et al., 2016; Mishra et al., 2016). Mossy fibers provide powerful excitatory drive to the soma of CA3 pyramidal cells and have been referred to as ‘conditional detonator’ synapses because a single synapse can trigger postsynaptic action potentials in response to high frequency bursts of presynaptic action potentials but not single action potentials (Henze et al., 2002; Sachidhanandam et al., 2009;

Vyleta et al., 2016). We hypothesized that feed-forward inhibitory synaptic transmission reduces back-propagating action potentials and mossy fiber evoked EPSPs which will inhibit or prevent the induction of LTP (Tsubokawa and Ross, 1996; Mullner et al., 2015; Wilmes et al., 2016), and that acetylcholine will relieve this inhibition by reducing feed-forward inhibition. To test this, we used a well characterized multi-compartment biophysical model of a CA3 pyramidal cell (Henze et al., 1996; Hemond et al., 2008) with 15 different reconstructed morphologies selected from Neuromorpho.org (Ishizuka et al., 1995; Ascoli et al., 2007). Our model incorporated mossy fiber excitatory synaptic input on the very proximal portion of the apical dendrite and feed-forward inhibitory synapses distributed across both somatic and dendritic compartments (Fig. 4A) (Szabadics and Soltesz, 2009). Membrane potential and the resultant intracellular calcium concentration were simulated across multiple somatic and dendritic compartments of a reconstructed CA3 pyramidal cell incorporating the thin oblique dendrites in stratum radiatum where the majority of CA3-CA3 recurrent synapses are located (Major et al., 1994). With feed-forward inhibition intact, action potentials and EPSPs back-propagate into the principal dendritic shafts without much change in amplitude but are rapidly attenuated on entering the thin oblique dendrites (Fig. 4B and C). This leads to minimal calcium influx through voltage-gated calcium channels at these dendritic sites (Fig. 4B). However, when feed-forward inhibition is reduced by acetylcholine, attenuation of action potentials and EPSPs is greatly reduced allowing substantial calcium influx (Fig. 4B-F). The relief of action potential and EPSP attenuation by acetylcholine was selective for the oblique dendrites in stratum radiatum, was consistent for multiple different CA3 pyramidal cell morphologies (Fig. 4C and supplementary Fig. 3) and resulted in increases in both the amplitude and probability of action potential backpropagation (Fig. 4D-F). The disinhibition of mossy fiber feed-forward inhibition by acetylcholine has major implications for synaptic plasticity at CA3-CA3 recurrent synapses, since spike timing-dependent plasticity is dependent on the back-propagation of action potentials and EPSPs, postsynaptic calcium accumulation and activation of calcium-dependent signalling pathways (Brandalise and Gerber, 2014; Mishra et al., 2016). Our simulations indicate that disinhibition by acetylcholine is a requirement for reliable induction of synaptic plasticity between CA3 pyramidal cells when CA3 ensembles are activated by mossy fiber inputs.

Ensemble formation in CA3 driven by mossy fiber input

To investigate the effects of acetylcholine on the creation of CA3 ensembles by mossy fiber input we next turned to a spiking network model of CA3. This network was comprised of point neurons with Izhikevich-type dynamics (Izhikevich, 2003) parameterized to reproduce spiking patterns

for excitatory CA3 pyramidal cells and inhibitory fast spiking interneurons (Hummos et al., 2014) connected in an all-to-all fashion. Subsets of pyramidal cells were driven by excitatory mossy fiber input with short-term facilitation dictated by the model determined in Fig. 2. CA3-CA3 recurrent synaptic connections were subject to an experimentally determined symmetric spike timing-dependent plasticity (STDP) rule (Fig. 5A) with no short-term plasticity (Mishra et al., 2016). To maintain constant overall network spiking dynamics, the symmetric STDP rule was modified to allow for depression dependent on the postsynaptic firing rate through synaptic scaling. At low firing rates, potentiation is induced with small differences in pre- and post-synaptic spike times. As the postsynaptic firing rates increase, large differences in pre- and post-synaptic spike times cause depression. At a maximum firing rate, no potentiation is possible.

Within this network we first characterized the speed and stability of ensemble creation where an ensemble was defined as being formed when all synapses between cells within the same ensemble had reached their maximum weight, and all synapses between cells not within the same ensemble had decreased to zero. In addition, the properties of mossy fiber input were studied in comparison with a more generic input reminiscent of perforant path activity during direct information transfer between entorhinal cortex and CA3 to see how they compared in their ability to drive ensemble formation via synchronous spiking in a small population of cells (Fig. 5B). Mossy fiber spike patterns were modelled as a Poisson process with brief (200 ms every 20 seconds) high intensity (50 Hz) firing rates on a very low basal firing rate (0.2 Hz), and were connected to pyramidal cells by a strong facilitating synapse (3.0 nS). This firing pattern represents a strongly separated, sparse firing pattern in a single presynaptic cell, which is expected in dentate gyrus granule cells. Perforant path spike patterns were modelled as a population of presynaptic entorhinal cells in the synchronous irregular state modelled as 120 homogeneous Poisson processes firing at 10 Hz with a correlation coefficient of 0.9 and static, weak synapses fixed at 0.1 nS, which broadly reflects entorhinal activity in a freely behaving rat (Chrobak and Buzsaki, 1998).

We initially built up the network model sequentially to investigate which components were necessary for the speed and stability of ensemble creation. At first, two CA3 pyramidal cells were connected and driven with only excitatory input. For both mossy fiber and perforant path inputs the cells quickly became connected (Fig. 5B, top row). Increasing ensemble size to 10 excitatory cells destabilized the ensemble formation process (Fig. 5B, middle row). The destabilization resulted from unbalanced potentiation of recurrent excitation that caused a large increase in the firing rate leading to strong depression or ‘resetting’ of the synaptic weight with further spiking as a result of synaptic scaling. The addition of 5 feedback inhibitory cells stabilized

ensemble formation in the case of mossy fiber input, but not for perforant path input (Fig. 5B, bottom row). This was because the perforant path input provided a colored noise signal amplified by recurrent excitation that caused excitatory cells to fire at high rates too often and feedback inhibition was insufficient to counter this amplification. Mossy fiber input is driven only briefly at sparse intervals, meaning there was little opportunity to exceed target firing rate, and when there was, feedback inhibition was sufficient to contain it. These results show that mossy fiber-like sparse inputs and feedback inhibition within the CA3 recurrent network are important for rapid and stable formation of CA3 ensembles.

The advantages of short-term facilitation were also explored. To model how input from multiple granule cells is transmitted to a single pyramidal cell, a single excitatory input layer network to one excitatory cell was constructed (Fig. 5C). Inputs followed an inhomogeneous Poisson process, each of which was connected to the cell with a facilitating mossy fiber synapse, or with a synapse with a fixed conductance at half the maximum weight of the facilitating synapse. Inhomogeneous rates were defined by a winner take all process (Fukai and Tanaka, 1997) with adaptation (see methods). For good transmission of a separated (winner) pattern, the postsynaptic cell should only spike (Fig. 5C; red trace) when the winning input is the only input with a non-zero weight i.e., once the winner has been selected (Fig. 5C; grey traces). The efficacy of transmission is defined as the rate of the winning input r_N at the time of the postsynaptic spike t_{spike} divided by the sum of rates r of all inputs at the time of the postsynaptic spike, i.e.,

$$efficacy = \frac{\sum_{t_{spike}} r_N(t)\delta(t - t_{spike})}{\sum_i \sum_{t_{spike}} r_i(t)\delta(t - t_{spike})} \qquad \text{(Equation 12)}$$

The population of input rates were defined by two parameters: scale and separation, where the scale parameter is a scaling factor that multiplies each rate in the population by the same amount, whereas the separation parameter controls the difference in input to the population of rates, determining how much the winner wins by. Increasing both the scales and separation of input rates produced a sharper transition between no transmission (efficacy = 0) and perfect transmission (efficacy = 1) when synapses were facilitating (Fig. 5C). However, when synaptic conductance was fixed, there was a smoother transition from no transmission to perfect transmission. This indicates that short-term facilitation supports robust transmission of separated patterns, as weakly separated patterns can still be transmitted perfectly. In contrast, weakly separated patterns transmit more ambiguously when input is of fixed conductance. This is because facilitating synapses place very low weight on signals at the start of a winner-take-all

process, but much greater weight at the end making spiking more likely once the winner has been chosen, whereas constant synapses place too much weight before a winner has been selected and can cause postsynaptic cells to fire too early.

Acetylcholine facilitates mossy-fiber driven ensemble formation in CA3

We next examined how acetylcholine affects the CA3 network's ability to form ensembles. In addition to facilitating plasticity at CA3-CA3 recurrent synapses by control of feed-forward inhibition, two well established effects of acetycholine in CA3 are to increase cellular excitability and reduce the overall conductance of CA3-CA3 recurrent synapses by reducing the probability of glutamate release (Hasselmo et al., 1995; Vogt and Regehr, 2001; Dasari and Gulledge, 2011). These cholinergic actions are predicted to increase the number of stored associations within an autoassociative network (Hasselmo et al., 1992; Hasselmo et al., 1995). We implemented these effects of acetylcholine within the spiking network model by depolarizing the resting membrane potential for excitatory and inhibitory cells to -70 mV and -63 mV respectively and halved the CA3-CA3 excitatory synaptic conductance (Hummos et al., 2014). Networks contained 64 excitatory and 16 inhibitory cells with excitatory cells grouped into 8 ensembles consisting of 8 cells each (Fig. 6A). Each cell within a single ensemble received the same mossy fiber input, which followed Poisson process with a low firing rate of 0.2 Hz punctuated by bursts for 250 ms every 20 s at varying frequency and short-term plasticity dynamics dictated by the model determined in Fig. 2. No two ensembles received bursts at the same time and spike timing-dependent plasticity rules were implemented regardless of the presence of acetylcholine.

Without acetylcholine, bursts at a frequency of 30 Hz formed discrete ensembles, but these were almost completely abolished when burst frequency was reduced to 20 Hz (Fig. 6B, Supplementary Fig. 5). Remarkably, acetylcholine rescued ensemble formation at the lower burst frequency. To quantify network ensemble formation performance and the impact of acetylcholine in greater detail, we used an error metric (*WME*) defined as the summed absolute difference between target and actual weight matrix (W_{ij}^{actual}), where the target weight matrix (W_{ij}^{target}) is maximum synaptic weights between cells *i* and *j* in the same ensemble, and zero weight otherwise, i.e.,

$$WME = \sum_{ij} |W_{ij}^{actual} - W_{ij}^{target}| \qquad \text{(Equation 13)}$$

This analysis revealed that acetylcholine lowers the frequency and increases the speed at which ensembles form (Fig. 6C). To test which effects of acetylcholine were critical for these aspects of ensemble formation we removed each parameter change in turn. This revealed that the key factor was the increase in cellular excitability, as removing the parameter changes to cellular excitability abolished the effect of acetylcholine but removing reductions in CA3-CA3 recurrent connections did not (Fig. 6C and Supplementary Fig. 4).

Within the CA3 network multiple often highly overlapping ensembles may be encoded. Theoretically this increases the capacity of information encoding but reduces the fidelity of retrieval with a necessary trade-off between these two parameters. Therefore, we investigated the impact of acetylcholine on the ability of the CA3 network to reliably encode overlapping ensembles. To incorporate overlap between ensembles the total network size was made variable whilst still containing 8 ensembles of 8 cells each and overlap was introduced by having a subset of excitatory cells receive input from two sources rather than one. Overlap was arranged in a ringed fashion such that each ensemble shared a certain number of cells with their adjacent 'neighbour' (Fig. 7A). Retrieval was studied by comparing the population rates of each ensemble, with a smaller difference in rates meaning lower discrimination and more difficult retrieval.

Without acetylcholine present, stable ensembles could be formed when the degree of overlap was low but discrete ensembles could not be formed with levels of overlap >1 (Fig. 7B and C, Supplementary Fig. 6). In contrast, in the presence of acetylcholine the network could safely support an overlap of 3 cells between discrete ensembles (Fig. 7B and C, Supplementary Fig. 6). To test which effects of acetylcholine mediated the enhanced discrimination between overlapping ensembles we removed each parameter change in turn. This revealed that the key factor was the reduction in CA3-CA3 recurrent synapse efficacy since removing this parameter change abolished the ability for acetylcholine to allow greater ensemble overlap. In contrast, removing the increase in cellular excitability only increased the time taken to form stable ensembles without affecting the final degree of overlap supported (Fig. 7C and Supplementary Fig. 4). Interestingly, the increase in stable ensembles with significant overlap was associated with a decrease in the discrimination between ensembles during retrieval of information as more overlap produced less separation of population rates between ensembles (Fig. 7D). Taken together these data indicate that acetylcholine increases the number of discrete ensembles that may be contained within a finite CA3 network but that this comes at a cost of reduced retrieval fidelity.

Discussion

In this study, we investigated the effects of acetylcholine on the ability of mossy fiber input from dentate granule cells to form ensembles within the CA3 recurrent network. Experimentally, we discovered that acetylcholine dramatically reduces feed-forward inhibition in the mossy fiber pathway whilst having limited effect on mossy fiber excitatory transmission (Figs 1&2). This disinhibition causes a strong positive shift in the Excitatory-Inhibitory balance (Fig. 3) resulting in a greatly enhanced potential for LTP at recurrent CA3-CA3 synapses and therefore ensemble formation (Fig. 4). In addition, in a computational spiking network model, the separate effects of acetylcholine on cellular excitability and basal CA3-CA3 synaptic strength were found respectively to enhance the robustness of ensemble formation (Fig. 6) and the amount of allowable overlap between ensembles (Fig. 7). Together, these findings indicate a central role for acetylcholine in gating and facilitating memory formation in the CA3 network and suggest that cholinergic activity may provide an important salience cue to signal when new ensembles may be formed and therefore which information to encode.

The three separate mechanisms we identify as important for ensemble formation are likely supported by different cholinergic receptors at distinct cellular and subcellular locations. In contrast to the presynaptic actions of cholinergic receptors at other hippocampal synapses (Dasari and Gulledge, 2011), our experimental data show only a small effect of cholinergic agonists at excitatory mossy fiber synapses onto CA3 pyramidal cells indicating a limited direct synaptic modulation by muscarinic or nicotinic receptors mediated by postsynaptic changes (Williams and Johnston, 1990; Vogt and Regehr, 2001; Dickinson et al., 2009). The lack of presynaptic changes indicates no indirect mechanism via enhancement of interneuron spiking and activation of presynaptic GABAB receptors by GABA spillover (Scanziani, 2000; Vogt and Regehr, 2001). For similar reasons, our data do not support a role for presynaptic nicotinic receptors ((Cheng and Yakel, 2014) but see (Vogt and Regehr, 2001)) or an increase in dentate granule cell spike frequency (Vogt and Regehr, 2001) since both would be expected to cause an increase in EPSC amplitude by presynaptic mechanisms. The large depression in feed-forward inhibitory mossy fiber transmission by cholinergic activity most likely results from a combination of an increase in feed-forward interneuron excitability and spike rate, mediated by a combination of muscarinic M1 and M3 receptors and nicotinic receptors (Vogt and Regehr, 2001; Cea-del Rio et al., 2010; Dasari and Gulledge, 2011), coupled with a strong depression of GABA release, mediated by presynaptic M2 receptors present on interneuron terminals (Szabo et al., 2010). This potentially accounts for the observed increase in basal synaptic release to initial stimulation but overall large reduction in synaptic conductance and release over the

course of a burst of stimuli seen in our experimental data and short-term plasticity model. Finally, the depression in basal CA3-CA3 recurrent synaptic strength is reported to result from the activation of presynaptic M4 receptors (Dasari and Gulledge, 2011). These mechanistic conclusions predict that M2 muscarinic receptors on interneuron terminals are important for disinhibition of mossy fiber feed-forward inhibition necessary for ensemble formation, M4 muscarinic receptors on CA3-CA3 recurrent axon terminals are important for increasing the amount of permissible overlap between ensembles and M1 muscarinic receptors on CA3 pyramidal cells facilitate the rapid and stable formation of ensembles.

Feed-forward inhibition dominates excitatory transmission in the mossy fiber pathway but unlike other examples of feed-forward inhibition, such as that occurring in the neocortex or CA1 region of the hippocampus, interneurons engaged with mossy fiber feed-forward inhibition target the dendritic compartments of CA3 pyramidal cells as much if not more than the perisomatic areas (Toth et al., 2000; Pelkey et al., 2005; Szabadics and Soltesz, 2009; Torborg et al., 2010). This means that mossy fiber feed-forward inhibition strongly inhibits recurrent CA3-CA3 inputs in stratum radiatum rather than excitatory mossy fiber inputs (Miles et al., 1996; Pouille and Scanziani, 2001). We show that inhibitory input to dendritic domains in stratum radiatum strongly attenuates the back-propagation of action potentials and EPSPs originating from the somatic compartment into the thin radial oblique dendrites where most of the recurrent CA3-CA3 synapses occur (Fig. 4). Since these back-propagating signals are necessary for the induction of LTP at recurrent CA3-CA3 synapses (Brandalise and Gerber, 2014; Mishra et al., 2016), this indicates that mossy fiber feed-forward inhibition is well placed to control the induction of LTP at these synapses. The dominance of mossy fiber feed-forward inhibition may be partially reduced with high frequency burst stimulation where feed-forward inhibition does not facilitate as strongly as excitation enabling excitation to dominate (Mori et al., 2004) (Fig. 3) although this is not the case during development of the mossy fiber pathway (Torborg et al., 2010). Here, the remarkable finding is that cholinergic activation reduces mossy fiber feed-forward inhibition by >70% (Fig. 1&2) removing the attenuation of back-propagating action potentials and EPSPs (Fig. 4), which therefore enables LTP at CA3-CA3 recurrent synapses.

Further investigation revealed that not only does acetylcholine enable ensemble formation by reducing mossy fiber feed-forward inhibition, but it also alters the properties of the CA3 network to allow ensemble formation to occur rapidly and robustly with a high degree of overlap between ensembles. This supports findings in similar models of piriform cortex and CA3 attractor networks (Hasselmo et al., 1992; Hasselmo et al., 1995). Enhancing cellular excitability within an attractor network such as the recurrent CA3 network increases the speed and

robustness of synaptic plasticity due to increased spiking during ensemble activity (Fig. 6). For stable ensemble formation and network configuration the increased excitability must be regulated by feedback inhibition (Fig. 5). Theoretically, the reduction in CA3-CA3 synaptic efficacy caused by acetylcholine (Hasselmo et al., 1995) might be predicted to reduce the efficiency of ensemble formation but our results show this is not the case (Fig. 6) likely because of reduced interference between ensembles (Hasselmo et al., 1992). Furthermore, we found that this effect of acetylcholine enabled a greater overlap between ensembles whilst still maintaining their discrete identity (Fig. 7). This is important for a couple of reasons: i) it allows an increased density of discrete ensembles to be encoded which in a finite network will increase its capacity to store information, and ii) an increase in overlap between ensembles has been suggested to facilitate memory consolidation and generalization during reactivation of ensembles that occurs during sleep (O'Donnell and Sejnowski, 2014). Interestingly, our model used a method to limit synaptic strengthening based on recently described STDP rules (Mishra et al., 2016) coupled with a rate-based scaling factor, whereas previous models of similar autoassociative networks have used an LTP only rule with a saturation function (Hasselmo et al., 1992; Hasselmo et al., 1995). Remarkably, both these methods produced very similar outcomes indicating that the effects of acetylcholine on the rate and degree of overlap for ensemble creation are independent of different plasticity rules. A more important factor may be non-linear dendritic conductances which increase the storage capacity for similar or overlapping memories within the CA3 network (Kaifosh and Losonczy, 2016). Future studies may determine how the mechanisms engaged by acetylcholine and non-linear conductances interact and combine within the hippocampal CA3 network.

A core symptom of Alzheimer's disease is deteriorating episodic memory, which may be ameliorated by treatment with cholinesterase inhibitors. However, the mechanisms by which increasing the availability of acetylcholine in the brain provides this cognitive benefit remain obscure. At the behavioral level, our findings predict that cholinesterase treatment facilitates the formation of memory ensembles within the hippocampus and increases the storage capacity for separate memory representations. It is widely reported that cholinesterase inhibitors provide cognitive enhancement (McGleenon et al., 1999) but the specific cognitive domains affected are less well characterized. At a network level, our findings predict that interventions to deprive the hippocampus of cholinergic innervation will prevent the update of ensemble configurations in CA3 (Atri et al., 2004) and, furthermore, that stimulation of acetylcholine release at specific locations will bias ensemble formation towards the incorporation of place cells representing those locations. Manipulations of acetylcholine release in the hippocampus have largely focussed on the effects on oscillatory activity where acetylcholine has been found

to promote theta activity and suppress sharp wave ripples (Vandecasteele et al., 2014). However, in support of our predictions, cholinergic activation has also been found to increase the number of neurons incorporated into ensembles measured by their activity during sharp wave ripples (Zylla et al., 2013).

Acetylcholine release within the central nervous system has classically been portrayed as a signal for arousal and attention and is strongly associated with learning (McGaughy et al., 2000; Parikh et al., 2007; Hasselmo and Sarter, 2011). This model has been adapted to propose that acetylcholine is released in response to environments where the outcome is uncertain or not as predicted by internal representations (Yu and Dayan, 2005). In such a scenario new information needs to be incorporated into the internal representation to make the environment more familiar and the outcomes more predictable (Hasselmo and Sarter, 2011). Acetylcholine supports this process by enabling the updating of internal representations of the environment (episodic memories). Our data support such a model where acetylcholine reconfigures the dentate gyrus and CA3 microcircuit to enable the formation of memory ensembles within the recurrent CA3 network.

Materials and Methods

Ethical approval

All experiments were performed in accordance with the UK Animal Scientific Procedures Act (1986) and local guidance from the Home Office Licensing Team at the University of Bristol. The protocol was approved by the Animal Welfare and Ethics Review Board at the University of Bristol.

Slice Preparation

500 µm thick transverse slices of the hippocampus were prepared from 4-6 week old C57/BL6 mice. After cervical dislocation, brains were removed and submerged in ice-cold cutting solution saturated with oxygen (in mM: 85 NaCl, 75 Sucrose, 2.5 KCl, 25 Glucose, 1.25 NaH_2PO_4, 4 $MgCl_2$, 0.5 $CaCl_2$, 24 $NaHCO_3$). Each hippocampus was dissected out and mounted onto a cube of agar then glued to the slicing plate such that hippocampi were positioned vertically and cut using a Leica VT1200 vibratome. Slices were then transferred

to a holding chamber with oxygenated aCSF (in mM: 119 NaCl, 2.5 KCl, 11 Glucose, 1 NaH2PO4, 26.5 NaHCO3, 1.3 MgSO4, 2.5 CaCl2), incubated for 30 mins at 35°C and left to rest for a further 30 minutes – 5 hours at room temperature.

Electrophysiology

Slices recordings were made in a submerged recording chamber at 33-35°C. CA3 pyramidal cells were visually identified using infra-red differential interference contrast on an Olympus BX-51W1 microscope. Recording pipettes with resistance 2-4 MΩ were pulled from borosilicate filamented glass capillaries and filled with a caesium-based intracellular solution (in mM: 130 CsMeSO3, 4 NaCl, 10 HEPES, 0.5 EGTA, 10 TEA, 1 QX-314 chloride, 2 MgATP, 0.5 NaGTP). Series resistances were continuously monitored and recordings discarded if series resistance > 25 MΩ or changed by >50%. Recordings were collected using a Multiclamp 700A amplifier (Molecular Devices) filtered at 4 kHz and sampled at 10 or 25 kHz using Signal or Spike2 acquisition software, and a CED Power 1401 data acquisition board.

Postsynaptic currents were evoked by placing monopolar stimulation electrodes in the granular layer of the dentate gyrus and applying 200μs pulses driven by a Digitimer DS2A Isolated stimulator. Stimulating the granular layer avoids the risk of contamination from perforant path inputs, associational/commissurals, or monosynaptic inhibitory synapses. Excitatory currents were obtained by holding the cell in voltage-clamp mode at -70 mV, while inhibitory currents were obtained by holding at +10 mV. Candidate mossy fiber driven responses were chosen based on their latency (2-3 ms for excitatory, 5-10 ms for inhibitory). Excitatory currents were also selected based on kinetics (< 1 ms 20-80% rise time) and short-term facilitation in response to 4 pulses at 20 Hz. Stimulation strength was calibrated to the minimum strength that evoked a response (minimal stimulation). Excitatory and inhibitory responses were blocked > 80% by 1 μM DCG-IV in 100% cases (Fig. 1; n=9 MF-EPSCs, n=6 MF-IPSCs), therefore it can be inferred that this approach reliably stimulated mossy fibers (Kamiya et al., 1996). Carbachol (CCh) was bath applied for 5-10 minutes before measuring effect on

synaptic transmission. Effects of carbachol were normalised to control values taken in first 3 minutes of the experiment.

Short-Term Plasticity Model

The Tsodyks-Markram model (Tsodyks and Markram, 1997; Hennig, 2013) was adopted due to its widespread use, simplicity, and relation to biophysics. This model captures pre-synaptic release dynamics with two variables, a facilitating process *f* and a depressing process *d*, that represent 'resources' available to drive synaptic transmission. These evolve as follows:

$$\frac{df}{dt} = \frac{f_0 - f}{\tau_f} + a\,(1-f)\,\sum_s \delta(t - t_s) \qquad \text{(Equation 14)}$$

$$\frac{dd}{dt} = \frac{1-d}{\tau_d} - f\,d\,\sum_s \delta(t - t_s) \qquad \text{(Equation 15)}$$

The dynamics of *f* are governed by three parameters: f_0 (baseline value of *f*), τ_f (decay time constant of *f*), and *a* (increment scaling factor with incoming spike at time t_s). This variable loosely represents the build-up of free calcium ions in the presynaptic terminal that triggers exocytosis of neurotransmitter-containing vesicles into the synaptic cleft. Dynamics of *d* is governed by a single parameter τ_d, and loosely represents the availability of docked vesicles at release sites. Since these variables are bounded between 0 and 1, the convert into a conductance amplitude these are multiplied by a conductance scaling factor *g*, i.e.,

$$\text{PSC Amplitude} = g\,f\,d \qquad \text{(Equation 16)}$$

This basic model can be extended to more complex facilitation models for example by making parameters f_0 and *a* time dependent (Hennig, 2013), i.e.,

$$\frac{df_0}{dt} = \frac{\widetilde{f_0} - f_0}{\tau_{f_0}} + b_{f_0}\,(1-f_0)\,\sum_s \delta(t - t_s) \qquad \text{(Equation 17)}$$

$$\frac{da}{dt} = \frac{a_0 - a}{\tau_a} + b_a\,(1-a)\,\sum_s \delta(t - t_s) \qquad \text{(Equation 18)}$$

where $\widetilde{f_0}$ is a baseline for f_0, a_0 is the baseline for *a*, τ_{f_0} is the time constant for f_0, τ_a is the time constant for *a*, b_{f_0} is the increment scaling factor for f_0, and b_a is the increment scaling factor for

a. It can also be reduced by making *f* or *d* constant. Since the mossy fiber synapse is well known for its large pool of readily releasable vesicles that can be quickly replenished, a simple reduction is to keep *d* constant at 1, which is true when τ_d << min(*ISI*). Further complexity can be incorporated by allowing multiple independent depressing variables, or by having a time dependent scaling factor

$$\frac{dg}{dt} = -g/\tau_g + k \sum_s \delta(t - t_s) \qquad \text{(Equation 19)}$$

where τ_g is the time constant for short-term changes in conductance, and *k* is an increment scaling factor that can take positive values for facilitation, or negative values for depression.

Naturalistic stimulation patterns

Previous research has shown that short-term facilitation models are difficult to constrain with responses evoked by regular stimulation protocols (Costa et al., 2013), and that irregular or naturalistic stimulus trains allowed much better fits to data due to sampling across a broader range of inter-stimulus intervals (ISI) (Gundlfinger et al., 2007; Costa et al., 2013). Dentate gyrus granule cells in vivo have been shown to have bimodal ISI distributions, with long periods of quiescence punctuated by short bursts of action potential firing (Jung and McNaughton, 1993; Mistry et al., 2011). This bimodal ISI distribution was modelled as a doubly stochastic Cox process to allow generation of stimuli resembling natural spike patterns (Dayan and Abbott, 2001). Each Cox process *i* is defined by a rate parameter λ_{ii}, and a refractoriness parameter σ_i. These two processes are then mixed with responsibility π i.e.,

$$\mathrm{P(ISI)} = \pi\, q_1 + (1 - \pi)\, q_2 \qquad \text{(Equation 20)}$$

$$\mathrm{q}_i = r_i \quad \text{if} \quad r_i > x_i \quad \text{else} = 0 \qquad \text{(Equation 21)}$$

$$\mathrm{x}_i \sim \mathcal{N}(\mu_i, \sigma_i^2) \qquad \text{(Equation 22)}$$

$$\mathrm{r}_i \sim \mathrm{Exp}(\lambda_i) \qquad \text{(Equation 23)}$$

$$\pi \sim \mathrm{Ber}(p) \qquad \text{(Equation 24)}$$

In brief, ISIs were generated by sampling from two exponential distributions with parameters λ_i, which were rejected if they were less than a sample from a normal distribution with standard deviation σ_i. These candidate ISIs were then accepted according to a Bernoulli distribution with probability π. These parameters were set as λ_1 = 3.0, λ_2 = 0.25, σ_1 = 0.12, σ_2 = 0.01, π = 0.55. Ninety-nine ISIs were sampled to provide 100 spike times for a stimulation protocol lasting 525 seconds.

Model Fitting

The Bayesian parameter inference procedure used by (Costa et al., 2013) was used to fit parameters to the model. Each model was converted into an iterative form, integrating *f* and *d* over each ISI Δt_s between the n^{th} and $n+1^{th}$ spike to output a normalised post-synaptic conductance amplitude for the n^{th} spike in the sequence, i.e.,

$$f_{n+1} = f_0 - (f_0 - f_+)\ \exp(-\Delta t_s/\tau_f). \quad f_+ = f_n + a\,(1 - f_n)$$

(Equation 25)

$$d_{n+1} = 1 - (1 - d_+)\ \exp(-\Delta t_s/\tau_d), \quad d_+ = d_n - f_n\,d_n$$

(Equation 26)

from the original Tsodyks-Markram formalism, however for more complex models in which *a* and f_0 are time dependent

$$f_{0,n+1} = \widetilde{f_0} - (\widetilde{f_0} - f_{0,+})\ \exp\left(-\Delta t_s/\tau_{f_0}\right), \quad f_{0,+} = f_{0,n} + b_{f_0}\,(1 - f_{0,n})$$

(Equation 27)

$$a_{n+1} = a_0 - (a_0 - a_+)\ \exp\left(-\Delta t_s/\tau_a\right), \quad a_+ = a_n + b_a\,(1 - a_n)$$

(Equation 28)

Additionally, when f_0 is time-dependent, Equation 22 becomes

$$f_{n+1} = \frac{1}{\tau_{f_0} - \tau_f}\,(-\tau_{f_0}\ \tilde{f}_0\ \exp\left(-\Delta t/\tau_{f_0}\right) + \tau_f\ \tilde{f}_0\ \exp\left(-\Delta t/\tau_f\right) - \tau_f\ \tilde{f}_0 + \tau_{f_0}\ \tilde{f}_0 - \tau_f\ f_+\ \exp\left(-\Delta t/\tau_f\right) + \tau_{f_0}\ f_{0+}\ \exp\left(-\Delta t/\tau_{f_0}\right) + \tau_{f_0}\ f_+\ \exp\left(-\Delta t/\tau_f\right) - \tau_{f_0}\ f_{0+}\ \exp\left(-\Delta t/\tau_f\right))$$

(Equation 29)

These were then compared to PSC amplitude estimated by the difference between response peak and a baseline taken just before stimulus onset.

Since these equations are deterministic, a likelihood model was constructed where the amplitude was used as parameters for a normal distribution, i.e.,

$$P(D|\theta) = \mathcal{N}(A, A/2)$$ (Equation 30)

where *A* is PSC amplitude (Equation 14).

Exponential priors were used for conductance scaling parameters, beta priors for baseline and increment parameters, and uniform priors for time constants. This was to bias conductances towards smaller values and keep baselines low as would be expected from facilitating synapses. Posterior distributions were estimated using Markov Chain Monte Carlo sampling via the Metropolis-Hastings algorithm using the pymc python module.

Model selection was conducted using AIC and BIC weights (Wagenmakers and Farrell, 2004), a transformation of AIC and BIC values into a probability space, with best model having the highest weight. This made it possible to compare the best fitting model over the population when fitted for each individual sample. For the information criterion of a model for a given sampleC_n^m this is defined as

$$w(C) = \frac{\exp(-0.5\Delta_i(C))}{\sum_{k=1}^{K}\exp(-0.5\Delta_k(C))} \qquad \text{(Equation 31)}$$

where

$$\Delta(C) = \frac{1}{N}\sum_n[C_n - \mathrm{argmin}_m(C^m)] \qquad \text{(Equation 32)}$$

Goodness-of-fit for the best fitting model was assessed by estimating Bayesian poster-predictive *p*-values, where samples are drawn from the posterior-predictive distribution and discrepancies $D(x|\vartheta)$ to expected values *e* from the model x_{sim} and to the data x_{obs} are compared (Gelman et al., 1996), i.e.,

$$p = Pr[D(x_{sim}|\theta) > D(x_{obs}|\theta)] \qquad \text{(Equation 33)}$$

where

$$D(x|\theta) = \sum_j(\sqrt{x_j} - \sqrt{e_j})^2 \qquad \text{(Equation 34)}$$

If discrepancies were similar, i.e., $p > 0.025$ or < 0.975, then the model is assessed to fit well. This quantifies how easy it is to discriminate between posterior samples and actual data.

Compartmental Modelling

A 943 compartment reconstruction of a CA3 pyramidal cell with active dendrites (Henze et al., 1996; Hemond et al., 2008) was used to study whether mossy fiber feed-forward inhibition could regulate action potential backpropagation, which would be necessary for feed-forward inhibition to regulate plasticity between recurrent synapses. Simulations were carried out using NEURON.

Active conductances included voltage-gated sodium (Na_V), voltage-activated potassium conductance including delayed rectifier (K_{DR}), M-current (K_M), fast-inactivating A-type (K_A), calcium conductances including N-type (Ca_N), T-type (Ca_T), and L-type (Ca_L), calcium-activated potassium conductances (K_C and K_{AHP}). Calcium extrusion was modelled as a 100ms decay to a resting Ca^{2+} of 50 nM. Channel kinetics were similar to those used in other hippocampal pyramidal neuron models (Migliore et al., 1999).

Somatic compartments contained all conductances, dendritic compartments contained all except K_M, and the axonal compartment contained only Na_V, K_{DR}, and K_A. For action potential generation, sodium conductance was five times higher in the axon than the rest of the neuron. Conductances were set as (in $\mu S/cm^2$): $gNa_V = 0.022$, $gK_{DR} = 0.005$, $gK_M = 0.017$, $gK_A = 0.02$, $gCa_N = 0.00001$, $gCa_T = 0.00001$, $gCa_L = 0.00001$, $gK_C = 0.00005$, $gK_{AHP} = 0.0001$.

Dendritic compartments along the apical dendrite were subdivided according to distance (in microns from soma) into those within stratum lucidum (≤ 150), stratum radiatum (>150 or ≤400), and stratum lacunosum moleculare (>400). Mossy fiber synapses were targeted towards compartments in stratum lucidum. Feed-forward inhibition was targeted towards somatic compartments (50%) and dendritic compartments in stratum lucidum and stratum radiatum (50%) reflecting the diversity of interneuron subtypes and their targets (Szabadics and Soltesz, 2009).

Synaptic input was modelled using bi-exponential kinetics and short-term plasticity dynamics fit to experimental data. The effect of carbachol was modelled as a three-fold reduction in feed-forward inhibitory conductance.

CA3 Network Modelling

The hippocampal CA3 region was modelled as a small all-to-all recurrent network comprised of excitatory and inhibitory point neurons with adaptive quadratic-integrate-and-fire dynamics with parameters to reflect the firing patterns in response to current injection of CA3 pyramidal

cells and fast-spiking basket cells respectively (Izhikevich, 2003; Hummos et al., 2014). Continuous membrane dynamics for neuron *i* is described by two equations:

$$C_m \frac{dv_i}{dt} = k\,(v_i - v_r)\,(v_i - v_t) - u - g_E\,(v_i - v_E) - g_I\,(v_i - v_I)$$

(Equation 35)

$$\frac{du_i}{dt} = a[b(v_i - v_r) - u_i] \qquad \text{(Equation 36)}$$

where v_i describes membrane potential, and u_i is a slow adaptation variable. Parameters for excitatory cells were: C_m = 24 pF, k = 1.5 pA/mV^2, a= 10 Hz, b = 2 nS, c = -63 mV, d = 60 pA, v_r = -75, v_t = -58 mV, v_{peak} = 29 mV. Parameters for inhibitory cells were: C_m = 16 pF, k = 1.5 nS/mV, a = 900 Hz, b = 2 nS, c = -80 mV, d = 400 pA, v_r = -65 mV, v_t = -50 mV, v_{peak} = 28 mV.
Synaptic reversal potentials were set as v_E = 10 mV, and v_I = -80 mV. When $v_i \geq v_{peak}$, v_i and u_i were reset to

$$v_i \leftarrow c \qquad \text{(Equation 37)}$$

$$u_i \leftarrow u_i + d \qquad \text{(Equation 38)}$$

Excitatory and inhibitory cells were connected through four types of synapses: excitatory to excitatory cell (EE) synapses, excitatory to inhibitory cell synapses (EI), inhibitory to excitatory cell synapses (IE), and inhibitory to inhibitory cell (II) synapses. Kinetics were modelled as exponential synapses such that the synaptic conductance g_{syn} evolved according to:

$$\frac{dg_{syn}}{dt} = -g_{syn}/\tau_g + \widetilde{g_{syn}} w \sum_{t_s} \delta(t - t_s) \qquad \text{(Equation 39)}$$

where $g_{\widetilde{syn}}$ is the maximum synaptic conductance, and τ_g = 10 ms for EE and EI synapses and 20 ms for IE and II synapses. Maximum excitatory synapse conductance was 0.5 nS, and 1.0 nS for inhibitory synapses. Cholinergic modulation was implemented by changing a subset of network parameters (See Table 1).

EE and IE synapses were subject to spike timing-dependent plasticity of the form

$$\Delta w = \eta[\exp(-|t_{pre} - t_{post}|) - z] \qquad \text{(Equation 40)}$$

where η is a learning rate, and z is a scaling factor. This provides a symmetric STDP rule used previously as a homeostatic means to balance excitation and inhibition through inhibitory plasticity, (Vogels et al., 2011) and has also recently been shown to operate at CA3 associated commissural synapses (Mishra et al., 2016). In the case of IE synapses, η and z are fixed, however in the case of EE synapses these evolve according to

$$\frac{d\eta}{dt} = -\eta/\tau_\eta + \xi \sum_{t_{post}} \delta(t - t_{post}) \qquad \text{(Equation 41)}$$

$$\frac{dz}{dt} = -z/\tau_z + \rho_{max}^{-1} \sum_{t_{post}} \delta(t - t_{post}) \qquad \text{(Equation 42)}$$

This makes η and z track the postsynaptic firing rate for two different purposes, and on different time scales since τ_η = 100 ms, and τ_z = 1 second; η becomes a burst detector that increases the learning rate by a factor ξ meaning STDP requires multiple post-synaptic spikes to be activated, and z scales STDP such that the postsynaptic firing rate reaches a maximum ρ_{max}, more pre- and post-synaptic spike pairs cause depression, preventing STDP from inducing unrealistically high firing rates in an excitatory recurrent network. Additionally, STDP was bounded between 0 and the maximum conductance of the synapse.

Synaptic input to cells was comprised of recurrent and feed-forward inputs, i.e.,

$$g_E^i = \sum_{ij} g_{EY}^{ij} + \sum_{ik} g_{FF}^{ik} \qquad \text{(Equation 43)}$$

$$g_I^i = \sum_{ij} g_{IY}^{ij} \qquad \text{(Equation 44)}$$

where g_{FF} is the conductance of feed-forward input, g_{EY} is excitatory recurrent input, and g_{IY} is recurrent inhibition. Feed-forward input was given only to excitatory cells. CA3 Network architecture and feed-forward dynamics varied according to each simulation.

Granule cell spiking was modelled as an inhomegenous Poisson process. For most simulations, it was modelled low spike rate of 0.2 Hz, punctuated by jumps to a much higher burst frequency every 20 seconds for 250 ms. In one set of simulations, a small granule cell population (N = 50) was modelled as a set of Poisson processes rates defined by winner-take-all dynamics with adaptation (Fukai and Tanaka, 1997)

$$\frac{dy_i}{dt} = y(\sum_j (y_j - 50\alpha_j) + \kappa_i)/10 \qquad \text{(Equation 45)}$$

$$\frac{d\alpha_i}{dt} = -(\alpha_i - y_i)/5000 \quad \text{(Equation 46)}$$

$$\kappa_i = h + (i/N)\sigma \quad \text{(Equation 47)}$$

where *y* are granule cell rates following winner-take-all dynamics, *α* is rate-adaptation taking place over a longer time scale, and *κ* is the input to each granule cell determined by *h* and *σ,* which define the scale and separation of rates respectively, where the scale parameter is a scaling factor that multiples each rate in the population by the same amount, whereas the separation parameter controls the difference in input to the population of rates, determining how much the winner wins by. The winner granule cell receives input *κ = h + σ.*

Network retrieval performance is measured by a discrimination index that imagines that ensemble population rates are read by a downstream neuron. The greater the difference in ensemble population rates, the easier it is to differentiate between ensembles and retrieval is more precise. The discrimination index *D* is defined as

$$\mathrm{D} = \frac{\int \nu_{\gamma}(t)dt}{\sum_{\iota=\{-1,0,+1\}} \int \nu_{\gamma+\iota}(t)dt} \quad \text{(Equation 48)}$$

$$\nu(t) = \frac{\int K(\tau) \sum_i S_i(t-\tau)d\tau}{\int K(\tau)d\tau} \quad \text{(Equation 49)}$$

$$\mathrm{S(t)} = \sum_s \delta(t - t_s) \quad \text{(Equation 50)}$$

where $v_\gamma(t)$ is the population rate *v* of ensemble *γ*, $S_i(t)$ is the spike train *S(t)* of neuron *i*, *K(t)* is a kernel averaging the spike train over a defined window, and $\delta(t\text{-}t_s)$ is the delta function modelling a spike at time t_s. This discrimination index essentially calculates the ratio *signal/(signal + noise)* where the signal is the population rate of the ensemble representing the memory being retrieved, and the noise is the population rate of ensembles representing memories that should not be retrieved and are interfering with the retrieval process. As such, when *D* is smaller the interference from neighbouring neurons is higher.

Acknowledgements

We thank members of the Mellor lab for helpful discussion and C. O'Donnell and M. Ashby for comments on previous versions of the manuscript. LYP, CC and JRM funded by the Wellcome Trust. The project was also supported by an IBRO & Simons fund through Grant ID # isiCNI2017.

KTA gratefully acknowledges the financial support of the EPSRC via grant EP/N014391/1. The authors confirm no conflict of interest.

Author Contributions

Conceptualization, L.Y.P. and J.R.M.; Methodology, L.Y.P., K.T.-A. and C.C.; Investigation and Analysis, L.Y.P.; Writing, L.Y.P., K. T.-A., C.C. and J.R.M.; Supervision, K.T.-A., C.C. and J.R.M.

References

Acsady L, Kamondi A, Sik A, Freund T, Buzsaki G (1998) GABAergic cells are the major postsynaptic targets of mossy fibers in the rat hippocampus. J Neurosci 18:3386-3403.

Ascoli GA, Donohue DE, Halavi M (2007) NeuroMorpho.Org: a central resource for neuronal morphologies. J Neurosci 27:9247-9251.

Atri A, Sherman S, Norman KA, Kirchhoff BA, Nicolas MM, Greicius MD, Cramer SC, Breiter HC, Hasselmo ME, Stern CE (2004) Blockade of central cholinergic receptors impairs new learning and increases proactive interference in a word paired-associate memory task. Behav Neurosci 118:223-236.

Brandalise F, Gerber U (2014) Mossy fiber-evoked subthreshold responses induce timing-dependent plasticity at hippocampal CA3 recurrent synapses. Proc Natl Acad Sci U S A 111:4303-4308.

Buchanan KA, Petrovic MM, Chamberlain SE, Marrion NV, Mellor JR (2010) Facilitation of long-term potentiation by muscarinic M(1) receptors is mediated by inhibition of SK channels. Neuron 68:948-963.

Cea-del Rio CA, Lawrence JJ, Tricoire L, Erdelyi F, Szabo G, McBain CJ (2010) M3 muscarinic acetylcholine receptor expression confers differential cholinergic modulation to neurochemically distinct hippocampal basket cell subtypes. J Neurosci 30:6011-6024.

Cheng Q, Yakel JL (2014) Presynaptic alpha7 nicotinic acetylcholine receptors enhance hippocampal mossy fiber glutamatergic transmission via PKA activation. J Neurosci 34:124-133.

Chrobak JJ, Buzsaki G (1998) Gamma oscillations in the entorhinal cortex of the freely behaving rat. J Neurosci 18:388-398.

Costa RP, Sjostrom PJ, van Rossum MC (2013) Probabilistic inference of short-term synaptic plasticity in neocortical microcircuits. Frontiers in computational neuroscience 7:75.

Dasari S, Gulledge AT (2011) M1 and M4 receptors modulate hippocampal pyramidal neurons. J Neurophysiol 105:779-792.

Dayan P, Abbott LF (2001) Theoretical Neuroscience: Computational and Mathematical Modeling of Neural Systems. : MIT press.

Dennis SH, Pasqui F, Colvin EM, Sanger H, Mogg AJ, Felder CC, Broad LM, Fitzjohn SM, Isaac JT, Mellor JR (2016) Activation of Muscarinic M1 Acetylcholine Receptors Induces Long-Term Potentiation in the Hippocampus. Cereb Cortex 26:414-426.

Dickinson BA, Jo J, Seok H, Son GH, Whitcomb DJ, Davies CH, Sheng M, Collingridge GL, Cho K (2009) A novel mechanism of hippocampal LTD involving muscarinic receptor-triggered interactions between AMPARs, GRIP and liprin-alpha. Molecular brain 2:18.

Fernandez de Sevilla D, Buno W (2010) The muscarinic long-term enhancement of NMDA and AMPA receptor-mediated transmission at Schaffer collateral synapses develop through different intracellular mechanisms. J Neurosci 30:11032-11042.

Fukai T, Tanaka S (1997) A simple neural network exhibiting selective activation of neuronal ensembles: from winner-take-all to winners-share-all. Neural Comput 9:77-97.

Gelman A, Meng XL, Stern H (1996) Posterior predictive assessment of model fitness via realized discrepancies. Stat Sinica 6:733-760.

Gold AE, Kesner RP (2005) The role of the CA3 subregion of the dorsal hippocampus in spatial pattern completion in the rat. Hippocampus 15:808-814.
Gu Z, Yakel JL (2011) Timing-dependent septal cholinergic induction of dynamic hippocampal synaptic plasticity. Neuron 71:155-165.
Gundlfinger A, Leibold C, Gebert K, Moisel M, Schmitz D, Kempter R (2007) Differential modulation of short-term synaptic dynamics by long-term potentiation at mouse hippocampal mossy fibre synapses. J Physiol 585:853-865.
Guzman SJ, Schlogl A, Frotscher M, Jonas P (2016) Synaptic mechanisms of pattern completion in the hippocampal CA3 network. Science 353:1117-1123.
Hangya B, Ranade SP, Lorenc M, Kepecs A (2015) Central Cholinergic Neurons Are Rapidly Recruited by Reinforcement Feedback. Cell 162:1155-1168.
Hasselmo ME (2006) The role of acetylcholine in learning and memory. Curr Opin Neurobiol 16:710-715.
Hasselmo ME, Sarter M (2011) Modes and models of forebrain cholinergic neuromodulation of cognition. Neuropsychopharmacology 36:52-73.
Hasselmo ME, Anderson BP, Bower JM (1992) Cholinergic modulation of cortical associative memory function. J Neurophysiol 67:1230-1246.
Hasselmo ME, Schnell E, Barkai E (1995) Dynamics of learning and recall at excitatory recurrent synapses and cholinergic modulation in rat hippocampal region CA3. J Neurosci 15:5249-5262.
Hemond P, Epstein D, Boley A, Migliore M, Ascoli GA, Jaffe DB (2008) Distinct classes of pyramidal cells exhibit mutually exclusive firing patterns in hippocampal area CA3b. Hippocampus 18:411-424.
Hennig MH (2013) Theoretical models of synaptic short term plasticity. Frontiers in computational neuroscience 7:154.
Henze DA, Cameron WE, Barrionuevo G (1996) Dendritic morphology and its effects on the amplitude and rise-time of synaptic signals in hippocampal CA3 pyramidal cells. J Comp Neurol 369:331-344.
Henze DA, Wittner L, Buzsaki G (2002) Single granule cells reliably discharge targets in the hippocampal CA3 network in vivo. Nat Neurosci 5:790-795.
Hopfield JJ (1982) Neural networks and physical systems with emergent collective computational abilities. Proc Natl Acad Sci U S A 79:2554-2558.
Hummos A, Franklin CC, Nair SS (2014) Intrinsic mechanisms stabilize encoding and retrieval circuits differentially in a hippocampal network model. Hippocampus 24:1430-1448.
Ishizuka N, Cowan WM, Amaral DG (1995) A quantitative analysis of the dendritic organization of pyramidal cells in the rat hippocampus. J Comp Neurol 362:17-45.
Izhikevich EM (2003) Simple model of spiking neurons. Ieee T Neural Networ 14:1569-1572.
Jung MW, McNaughton BL (1993) Spatial selectivity of unit activity in the hippocampal granular layer. Hippocampus 3:165-182.
Kaifosh P, Losonczy A (2016) Mnemonic Functions for Nonlinear Dendritic Integration in Hippocampal Pyramidal Circuits. Neuron 90:622-634.
Kamiya H, Shinozaki H, Yamamoto C (1996) Activation of metabotropic glutamate receptor type 2/3 suppresses transmission at rat hippocampal mossy fibre synapses. J Physiol (Lond) 493:447-455.

Kass RE, Raftery AE (1995) Bayes Factors. J Am Stat Assoc 90:773-795.
Kesner RP, Rolls ET (2015) A computational theory of hippocampal function, and tests of the theory: new developments. Neurosci Biobehav Rev 48:92-147.
Kobayashi K, Poo MM (2004) Spike train timing-dependent associative modification of hippocampal CA3 recurrent synapses by mossy fibers. Neuron 41:445-454.
Leutgeb JK, Leutgeb S, Moser MB, Moser EI (2007) Pattern separation in the dentate gyrus and CA3 of the hippocampus. Science 315:961-966.
Major G, Larkman AU, Jonas P, Sakmann B, Jack JJ (1994) Detailed passive cable models of whole-cell recorded CA3 pyramidal neurons in rat hippocampal slices. Journal of Neuroscience 14:4613-4638.
Marino MJ, Rouse ST, Levey AI, Potter LT, Conn PJ (1998) Activation of the genetically defined m1 muscarinic receptor potentiates N-methyl-D-aspartate (NMDA) receptor currents in hippocampal pyramidal cells. P Natl Acad Sci USA 95:11465-11470.
Markram H, Segal M (1992) The inositol 1,4,5-trisphosphate pathway mediates cholinergic potentiation of rat hippocampal neuronal responses to NMDA. J Physiol 447:513-533.
Marr D (1971) Simple memory: a theory for archicortex. Philos Trans R Soc Lond B Biol Sci 262:23-81.
McClelland JL, Goddard NH (1996) Considerations arising from a complementary learning systems perspective on hippocampus and neocortex. Hippocampus 6:654-665.
McGaughy J, Everitt BJ, Robbins TW, Sarter M (2000) The role of cortical cholinergic afferent projections in cognition: impact of new selective immunotoxins. Behav Brain Res 115:251-263.
McGleenon BM, Dynan KB, Passmore AP (1999) Acetylcholinesterase inhibitors in Alzheimer's disease. British journal of clinical pharmacology 48:471-480.
Migliore M, Hoffman DA, Magee JC, Johnston D (1999) Role of an A-type K+ conductance in the back-propagation of action potentials in the dendrites of hippocampal pyramidal neurons. J Comput Neurosci 7:5-15.
Miles R, Toth K, Gulyas AI, Hajos N, Freund TF (1996) Differences between somatic and dendritic inhibition in the hippocampus. Neuron 16:815-823.
Mishra RK, Kim S, Guzman SJ, Jonas P (2016) Symmetric spike timing-dependent plasticity at CA3-CA3 synapses optimizes storage and recall in autoassociative networks. Nature communications 7:11552.
Mistry R, Dennis S, Frerking M, Mellor JR (2011) Dentate gyrus granule cell firing patterns can induce mossy fiber long-term potentiation in vitro. Hippocampus 21:1157-1168.
Mori M, Gahwiler BH, Gerber U (2007) Recruitment of an inhibitory hippocampal network after bursting in a single granule cell. Proc Natl Acad Sci U S A 104:7640-7645.
Mori M, Abegg MH, Gahwiler BH, Gerber U (2004) A frequency-dependent switch from inhibition to excitation in a hippocampal unitary circuit. Nature 431:453-456.
Mullner FE, Wierenga CJ, Bonhoeffer T (2015) Precision of Inhibition: Dendritic Inhibition by Individual GABAergic Synapses on Hippocampal Pyramidal Cells Is Confined in Space and Time. Neuron 87:576-589.
Nakazawa K, Quirk MC, Chitwood RA, Watanabe M, Yeckel MF, Sun LD, Kato A, Carr CA, Johnston D, Wilson MA, Tonegawa S (2002) Requirement

for hippocampal CA3 NMDA receptors in associative memory recall. Science 297:211-218.
Nicoll RA, Schmitz D (2005) Synaptic plasticity at hippocampal mossy fibre synapses. Nat Rev Neurosci 6:863-876.
O'Donnell C, Sejnowski TJ (2014) Selective memory generalization by spatial patterning of protein synthesis. Neuron 82:398-412.
O'Reilly RC, McClelland JL (1994) Hippocampal conjunctive encoding, storage, and recall: avoiding a trade-off. Hippocampus 4:661-682.
Papouin T, Dunphy JM, Tolman M, Dineley KT, Haydon PG (2017) Septal Cholinergic Neuromodulation Tunes the Astrocyte-Dependent Gating of Hippocampal NMDA Receptors to Wakefulness. Neuron 94:840-854 e847.
Parikh V, Kozak R, Martinez V, Sarter M (2007) Prefrontal acetylcholine release controls cue detection on multiple timescales. Neuron 56:141-154.
Pelkey KA, Lavezzari G, Racca C, Roche KW, McBain CJ (2005) mGluR7 is a metaplastic switch controlling bidirectional plasticity of feedforward inhibition. Neuron 46:89-102.
Pouille F, Scanziani M (2001) Enforcement of temporal fidelity in pyramidal cells by somatic feed-forward inhibition. Science 293:1159-1163.
Prince LY, Bacon TJ, Tigaret CM, Mellor JR (2016) Neuromodulation of the Feedforward Dentate Gyrus-CA3 Microcircuit. Front Synaptic Neurosci 8:32.
Rebola N, Carta M, Mulle C (2017) Operation and plasticity of hippocampal CA3 circuits: implications for memory encoding. Nat Rev Neurosci 18:208-220.
Restivo L, Niibori Y, Mercaldo V, Josselyn SA, Frankland PW (2015) Development of Adult-Generated Cell Connectivity with Excitatory and Inhibitory Cell Populations in the Hippocampus. J Neurosci 35:10600-10612.
Ruediger S, Vittori C, Bednarek E, Genoud C, Strata P, Sacchetti B, Caroni P (2011) Learning-related feedforward inhibitory connectivity growth required for memory precision. Nature 473:514-518.
Sachidhanandam S, Blanchet C, Jeantet Y, Cho YH, Mulle C (2009) Kainate receptors act as conditional amplifiers of spike transmission at hippocampal mossy fiber synapses. J Neurosci 29:5000-5008.
Salin PA, Scanziani M, Malenka RC, Nicoll RA (1996) Distinct short-term plasticity at two excitatory synapses in the hippocampus. P Natl Acad Sci USA 93:13304-13309.
Scanziani M (2000) GABA spillover activates postsynaptic GABA(B) receptors to control rhythmic hippocampal activity. Neuron 25:673-681.
Szabadics J, Soltesz I (2009) Functional specificity of mossy fiber innervation of GABAergic cells in the hippocampus. J Neurosci 29:4239-4251.
Szabo GG, Holderith N, Gulyas AI, Freund TF, Hajos N (2010) Distinct synaptic properties of perisomatic inhibitory cell types and their different modulation by cholinergic receptor activation in the CA3 region of the mouse hippocampus. Eur J Neurosci 31:2234-2246.
Teles-Grilo Ruivo LM, Baker KL, Conway MW, Kinsley PJ, Gilmour G, Phillips KG, Isaac JT, Lowry JP, Mellor JR (2017) Coordinated Acetylcholine Release in Prefrontal Cortex and Hippocampus Is Associated with Arousal and Reward on Distinct Timescales. Cell reports 18:905-917.

Torborg CL, Nakashiba T, Tonegawa S, McBain CJ (2010) Control of CA3 output by feedforward inhibition despite developmental changes in the excitation-inhibition balance. J Neurosci 30:15628-15637.
Toth K, Suares G, Lawrence JJ, Philips-Tansey E, McBain CJ (2000) Differential mechanisms of transmission at three types of mossy fiber synapse. J Neurosci 20:8279-8289.
Treves A, Rolls ET (1994) Computational analysis of the role of the hippocampus in memory. Hippocampus 4:374-391.
Tsodyks M (1999) Attractor neural network models of spatial maps in hippocampus. Hippocampus 9:481-489.
Tsodyks MV, Markram H (1997) The neural code between neocortical pyramidal neurons depends on neurotransmitter release probability. Proc Natl Acad Sci U S A 94:719-723.
Tsubokawa H, Ross WN (1996) IPSPs modulate spike backpropagation and associated [Ca2+]i changes in the dendrites of hippocampal CA1 pyramidal neurons. J Neurophysiol 76:2896-2906.
Vandecasteele M, Varga V, Berenyi A, Papp E, Bartho P, Venance L, Freund TF, Buzsaki G (2014) Optogenetic activation of septal cholinergic neurons suppresses sharp wave ripples and enhances theta oscillations in the hippocampus. Proc Natl Acad Sci U S A 111:13535-13540.
Vogels TP, Sprekeler H, Zenke F, Clopath C, Gerstner W (2011) Inhibitory plasticity balances excitation and inhibition in sensory pathways and memory networks. Science 334:1569-1573.
Vogt KE, Regehr WG (2001) Cholinergic modulation of excitatory synaptic transmission in the CA3 area of the hippocampus. J Neurosci 21:75-83.
Vyleta NP, Borges-Merjane C, Jonas P (2016) Plasticity-dependent, full detonation at hippocampal mossy fiber-CA3 pyramidal neuron synapses. Elife 5.
Wagenmakers EJ, Farrell S (2004) AIC model selection using Akaike weights. Psychon Bull Rev 11:192-196.
Wiebe SP, Staubli UV (2001) Recognition memory correlates of hippocampal theta cells. J Neurosci 21:3955-3967.
Williams S, Johnston D (1990) Muscarinic depression of synaptic transmission at the hippocampal mossy fiber synapse. J Neurophysiol 64:1089-1097.
Wilmes KA, Sprekeler H, Schreiber S (2016) Inhibition as a Binary Switch for Excitatory Plasticity in Pyramidal Neurons. PLoS computational biology 12:e1004768.
Yassa MA, Stark CE (2011) Pattern separation in the hippocampus. Trends Neurosci 34:515-525.
Yu AJ, Dayan P (2005) Uncertainty, neuromodulation, and attention. Neuron 46:681-692.
Zucca S, Griguoli M, Malezieux M, Grosjean N, Carta M, Mulle C (2017) Control of Spike Transfer at Hippocampal Mossy Fiber Synapses In Vivo by GABAA and GABAB Receptor-Mediated Inhibition. J Neurosci 37:587-598.
Zylla MM, Zhang X, Reichinnek S, Draguhn A, Both M (2013) Cholinergic plasticity of oscillating neuronal assemblies in mouse hippocampal slices. PLoS ONE 8:e80718.

Figure legends

Figure 1: **The effects of carbachol on feed-forward excitatory and inhibitory transmission in the mossy fiber pathway.** A) Left: Experimental setup indicating the location of stimulation and recording electrodes within a hippocampal slice. Right: Schema of feed-forward mossy fiber circuit. B) EPSCs and IPSCs evoked by granule cells stimulation were blocked by 1 µM DCG-IV, confirming responses were driven by mossy fiber activation. Top: Example traces of DCG-IV block (black) of EPSCs (red) and IPSCs (blue). Bottom: Time course of DCG-IV block of 4th EPSC (red, n = 9) and IPSC (blue, n = 6). C) 5 µM CCh mildly suppresses mossy fiber EPSCs. Top left: Example traces before and after bath application of 5 µM CCh. Bottom Left: Time course of CCh effect, and washout (n = 7). Top Right: Effect of CCh on response amplitudes for each pulse. Bottom Right: Effect of CCh on nth/1st Pulse Ratio. D) 5 µM CCh substantially reduces disynaptic mossy fiber driven IPSC amplitudes. Top left: Example traces before and after bath application of 5 µM CCh. Bottom Left: Time course of CCh effect, and washout (n = 5). Top Right: Effect of CCh on response amplitudes for each pulse. Bottom Right: Effect of CCh on nth/1st Pulse Ratio.

Figure 2: The mechanism of carbachol action on excitatory and inhibitory feed-forward mossy fiber transmission determined by short-term plasticity models. A) Irregular stimulation protocol modelled on naturalistic granule cell spike patterns. GC spike patterns recorded *in vivo* during a spatial memory task, with a bimodal inter-spike interval (ISI) distribution (top right). Bimodal ISI distribution modelled as a doubly stochastic Cox process (middle right), with irregular stimulation protocol a sample drawn from this process (bottom right). B-C) Experimentally recorded EPSCs and IPSCs evoked by irregular stimulation protocol in hippocampal slices. Evoked peaks highlighted by white dots. An example burst is shown on expanded timescale. D) Tsodyks-Markram short-term plasticity model schematic illustrating facilitating (*f*) and depressing (*d*) presynaptic components with time constants (τ_f, τ_d) and postsynaptic scaling factor (*g*). E-F) Model selection and fitting for EPSCs (E) and IPSCs (F). Top: AIC and BIC weights for each fitted model. Model selection by highest AIC and BIC weights and evidence ratios. Bottom: Modulation of CCh assessed by effect on parameter fits normalized by time-matched control. * denotes significant parameter change.

Figure 3: Carbachol alters the Excitatory-Inhibitory ratio within the feed-forward mossy fiber pathway in a frequency-dependent manner. A) Simplification of bursting spike trains into two parameter spaces: between burst interval (BI) describing interval between bursts in a spike train, and within BI describing interval between spikes within a burst. B) Example synaptic waveforms of expected mossy fiber EPSCs and IPSCs generated by the short-term plasticity models given

short-term plasticity dynamics at three pairs of within and between burst intervals (20ms and 2s, 20ms and 50s, 500ms and 50s respectively). C) Expected short-term plasticity of EPSCs across a wide range of within and between BIs. Light blue, dark blue and black crosses shown in C denote within and between BIs used in the examples shown in B. Data in the presence of CCh not shown since CCh does not change the facilitation of EPSCs. D) Expected short-term plasticity of IPSCs across a wide range of within and between BIs and in the presence and absence of CCh. Pulse ratios for 2^{nd}, 4^{th} and 6^{th} pulses compared to the 1^{st} are shown to illustrate change in facilitation across a 6 pulse burst. E) Progression of Excitatory-Inhibitory ratio across the range of within and between BIs and in the presence and absence of CCh. Pulse ratios for 2^{nd}, 4^{th} and 6^{th} pulses compared to the 1^{st} are shown to illustrate change in E-I ratio across a 6 pulse burst.

Figure 4: Acetylcholine-mediated disinhibition facilitates back-propagation of EPSPs and action potentials into the dendrites of CA3 pyramidal cells. A) Sketch of CA3 pyramidal cell and positioning within the layers of the hippocampus. Synaptic inputs are shown with location of contact (red - recurrent CA3-CA3 synapse, blue - feed-forward inhibitory synapse, gray - mossy fiber synapse). SLM – stratum lacunosum moleculare, SR – stratum radiatum, SL – stratum lucidum, SP – stratum pyramidale, SO – stratum oriens. B) Example traces produced by the biophysical CA3 neuron model of action potentials generated at the soma from summated mossy fiber EPSPs presented at 20 Hz (top), back-propagation into the radial oblique dendrites (middle), and dendritic calcium influx (bottom), with and without acetylcholine-mediated disinhibition of feed-forward inhibition. C) Back-propagating action potential amplitude before (left) and after (middle) cholinergic modulation, and the difference in amplitude (right) distributed across an example CA3 pyramidal cell. D) Histogram of differences in back-propagating action potential amplitudes with and without acetylcholine disinhibition in stratum radiatum oblique dendritic compartments (< 1 μm diameter) from 15 cells. E) Distribution of back-propagating action potential amplitudes in stratum radiatum oblique dendrites for a range of excitation-inhibition ratios in 15 cells. In our simulations the effect of acetylcholine was modelled as a change in this ratio (the absence of acetylcholine, gI/gE = 3; in the presence of acetylcholine, gI/gE = 1). F) The probability of successful action potential back-propagation (bAP amplitude > 40 mV) in oblique dendrites in 15 cells as a function of excitation-inhibition ratio.

Figure 5: Facilitating mossy fiber inputs generate rapid and stable ensemble formation. A) Schematic showing the network properties of the spiking network model and long-term plasticity rules. Left: A population of excitatory (red) and inhibitory (blue) cells with all-to-all connectivity and mossy fiber input (gray). Right: Recurrent excitatory CA3-CA3 spike timing-dependent plasticity rule with a symmetric window that shifted from potentiation for correlated

spiking at low rates (Ppost = 0), to depression for uncorrelated spiking near the maximum postsynaptic firing rate (Ppost = Pmax). B) Comparison of mossy fiber to irregular 'perforant path' input. Synaptic weight evolution with time for CA3-CA3 recurrent connections (red) and inhibitory to excitatory connections (blue) for a two cell excitatory population (top), a 10 cell excitatory population (middle) and a population including 10 excitatory and 5 inhibitory cells (bottom). C) Top Left: Network setup - 50 feed-forward inputs to a single granule cell. Top Right: Example of winner-take-all rates and postsynaptic spiking (red) for the population of inputs (gray). This instance shows strong efficacy since postsynaptic spiking occurs once all but one input rates have decreased to near zero. Bottom: Efficacy of winner granule cell to CA3 pyramidal cell coupling with facilitating and constant synaptic input

Figure 6: Acetylcholine speeds up ensemble formation and lowers input frequency requirement by increasing cellular excitability. A) Network setup: A population of excitatory and inhibitory cells connected in all-to-all fashion. Subpopulations of excitatory cells receive independent feed-forward input that drives ensemble formation. B) Example weight matrix driven by input with 30 Hz, 20 Hz or 20 Hz bursts with CA3 acetylcholine effects. Stronger weights indicate robust ensemble formation. C) Evolution of ensemble formation illustrated by the weight matrix error reduction over time for different input burst frequencies. Triangles denote which effects of acetylcholine on the CA3 network were included in each set of simulations.

Figure 7: Acetylcholine enables a CA3 network to form stable overlapping ensembles by reducing the strength of recurrent excitatory CA3-CA3 synapses. A) Network setup: A population of excitatory and inhibitory cells connected in all-to-all fashion. Subpopulations of excitatory cells receive overlapping feed-forward input that drives ensemble formation. B) Example weight matrix driven by input with increasing degrees of overlap between ensembles [0, 2, 4 cells]. C) Evolution of ensemble formation illustrated by the weight matrix error over time for different degrees of overlap between ensembles. Triangles denote which effects of acetylcholine were included in the simulation. D) Effect of increasing overlap between ensembles on the ability to discriminate between ensembles defined as the difference in ensemble population spiking rates.

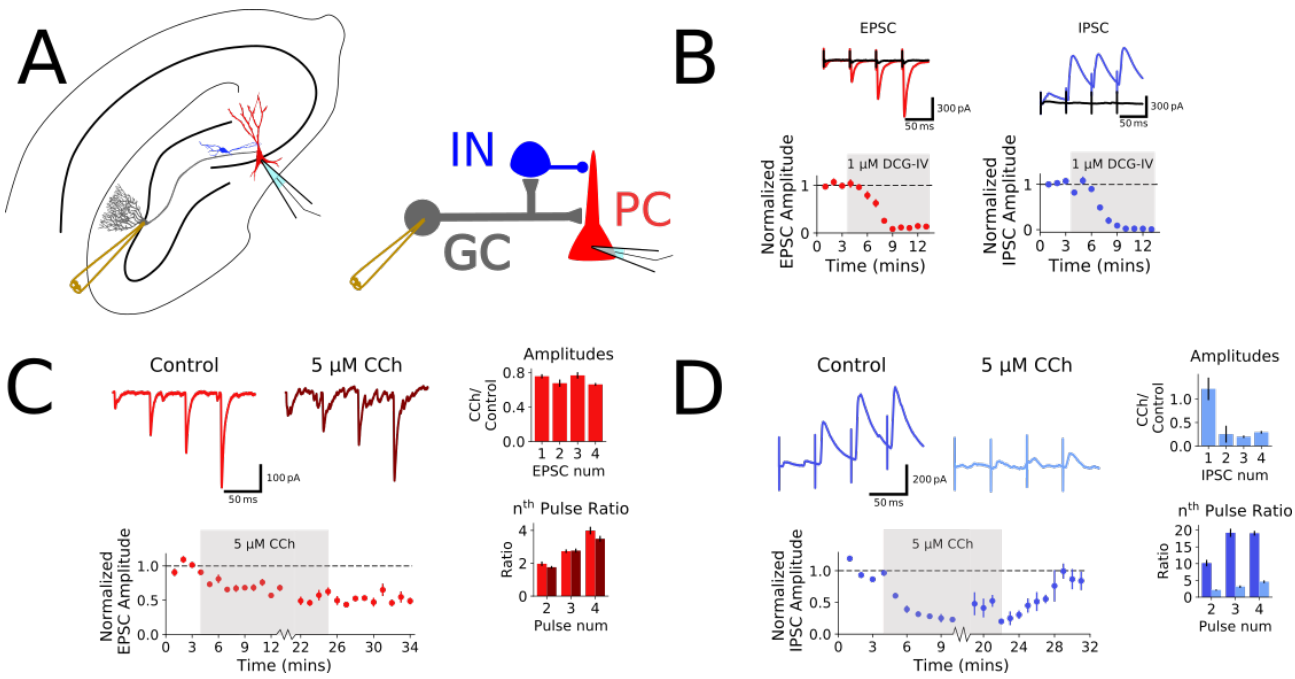

Figure 1: **The effects of carbachol on feed-forward excitatory and inhibitory transmission in the mossy fiber pathway.** A) Left: Experimental setup indicating the location of stimulation and recording electrodes within a hippocampal slice. Right: Schema of feed-forward mossy fiber circuit. B) EPSCs and IPSCs evoked by granule cells stimulation were blocked by 1 µM DCG-IV, confirming responses were driven by mossy fiber activation. Top: Example traces of DCG-IV block (black) of EPSCs (red) and IPSCs (blue). Bottom: Time course of DCG-IV block of 4th EPSC (red, n = 9) and IPSC (blue, n = 6). C) 5 µM CCh mildly suppresses mossy fiber EPSCs. Top left: Example traces before and after bath application of 5 µM CCh. Bottom Left: Time course of CCh effect, and washout (n = 7). Top Right: Effect of CCh on response amplitudes for each pulse. Bottom Right: Effect of CCh on nth/1st Pulse Ratio. D) 5 µM CCh substantially reduces disynaptic mossy fiber driven IPSC amplitudes. Top left: Example traces before and after bath application of 5 µM CCh. Bottom Left: Time course of CCh effect, and washout (n = 5). Top Right: Effect of CCh on response amplitudes for each pulse. Bottom Right: Effect of CCh on nth/1st Pulse Ratio.

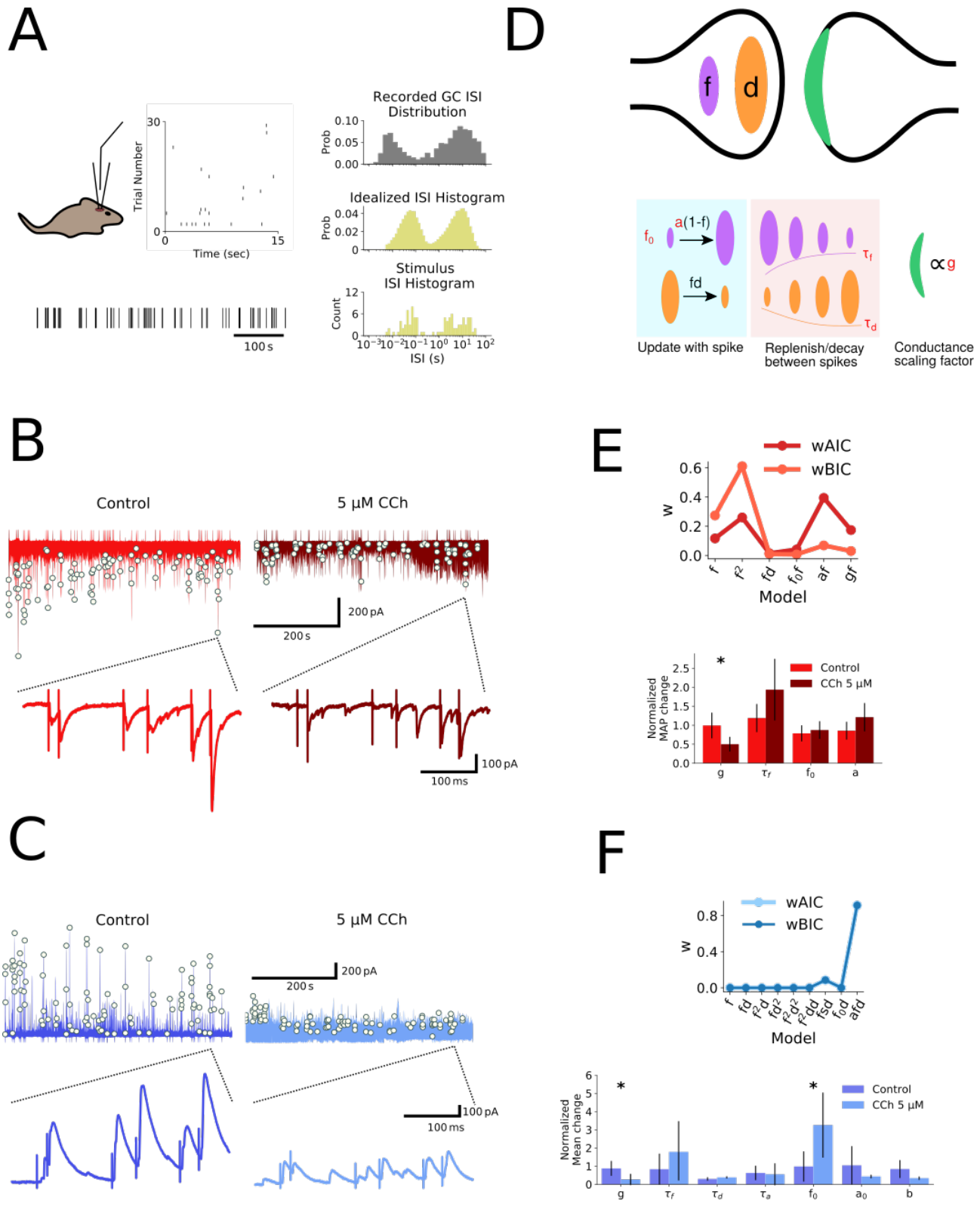

Figure 2: The mechanism of carbachol action on excitatory and inhibitory feed-forward mossy fiber transmission determined by short-term plasticity models. A) Irregular stimulation protocol modelled on naturalistic granule cell spike patterns. GC spike patterns recorded *in vivo* during a spatial memory task, with a bimodal inter-spike interval (ISI) distribution (top right). Bimodal ISI distribution modelled as a doubly stochastic Cox process (middle right), with irregular stimulation protocol a sample drawn from this process (bottom right). B-C) Experimentally recorded EPSCs and IPSCs evoked by irregular stimulation protocol in hippocampal slices. Evoked peaks highlighted by white dots. An example burst is shown on expanded timescale. D) Tsodyks-Markram short-term plasticity model schematic illustrating

facilitating (*f*) and depressing (*d*) presynaptic components with time constants (τ_f, τ_d) and postsynaptic scaling factor (*g*). E-F) Model selection and fitting for EPSCs (E) and IPSCs (F). Top: AIC and BIC weights for each fitted model. Model selection by highest AIC and BIC weights and evidence ratios. Bottom: Modulation of CCh assessed by effect on parameter fits normalized by time-matched control. * denotes significant parameter change.

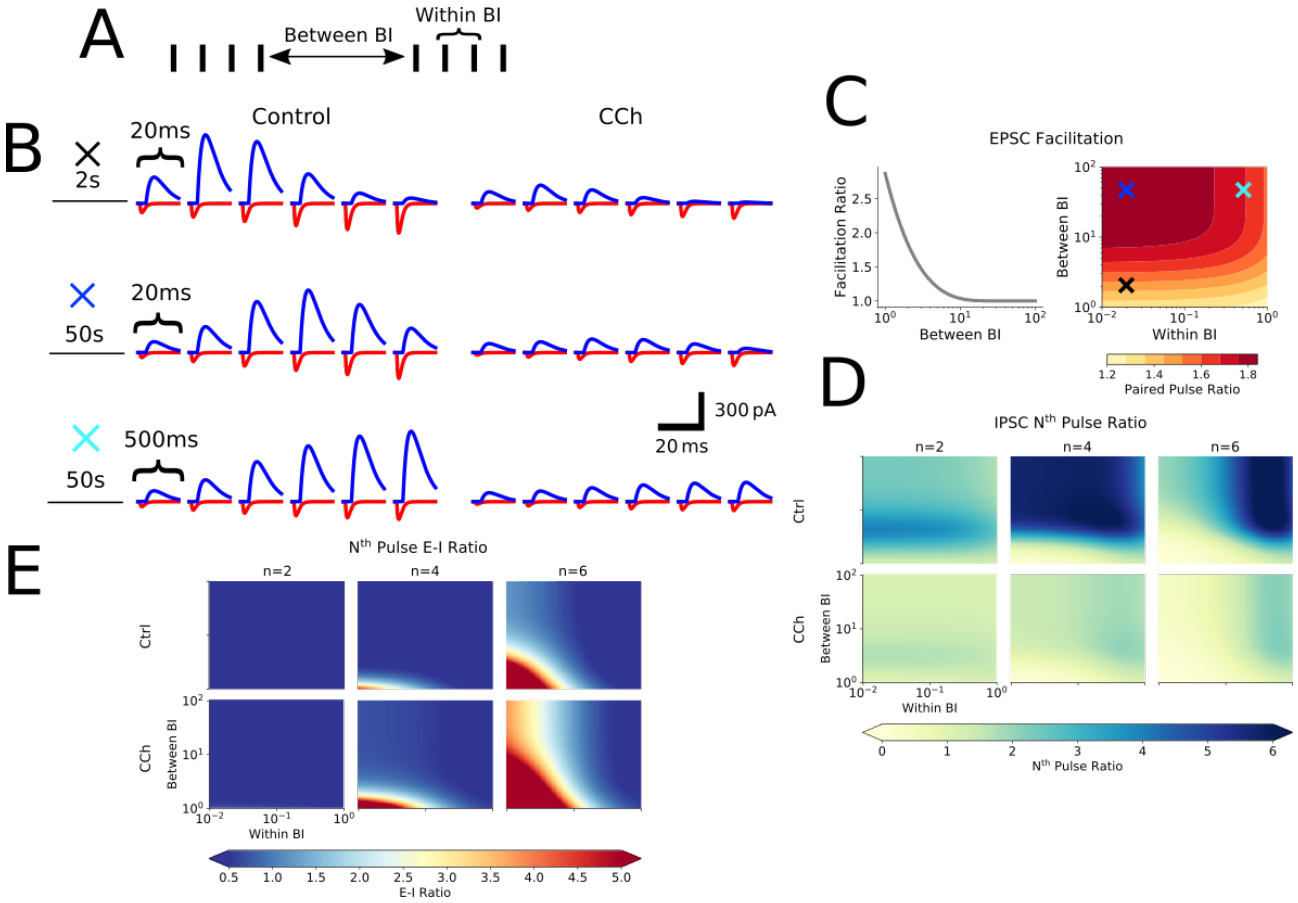

Figure 3: Carbachol alters the Excitatory-Inhibitory ratio within the feed-forward mossy fiber pathway in a frequency-dependent manner. A) Simplification of bursting spike trains into two parameter spaces: between burst interval (BI) describing interval between bursts in a spike train, and within BI describing interval between spikes within a burst. B) Example synaptic waveforms of expected mossy fiber EPSCs and IPSCs generated by the short-term plasticity models given short-term plasticity dynamics at three pairs of within and between burst intervals (20ms and 2s, 20ms and 50s, 500ms and 50s respectively). C) Expected short-term plasticity of EPSCs across a wide range of within and between BIs. Light blue, dark blue and black crosses shown in C denote within and between BIs used in the examples shown in B. Data in the presence of CCh not shown since CCh does not change the facilitation of EPSCs. D) Expected short-term plasticity of IPSCs across a wide range of within and between BIs and in the presence and absence of CCh. Pulse ratios for 2nd, 4th and 6th pulses compared to the 1st are shown to illustrate change in facilitation across a 6 pulse burst. E) Progression of Excitatory-Inhibitory ratio across the range of within and between BIs and in the presence and absence of CCh. Pulse ratios for 2nd, 4th and 6th pulses compared to the 1st are shown to illustrate change in E-I ratio across a 6 pulse burst.

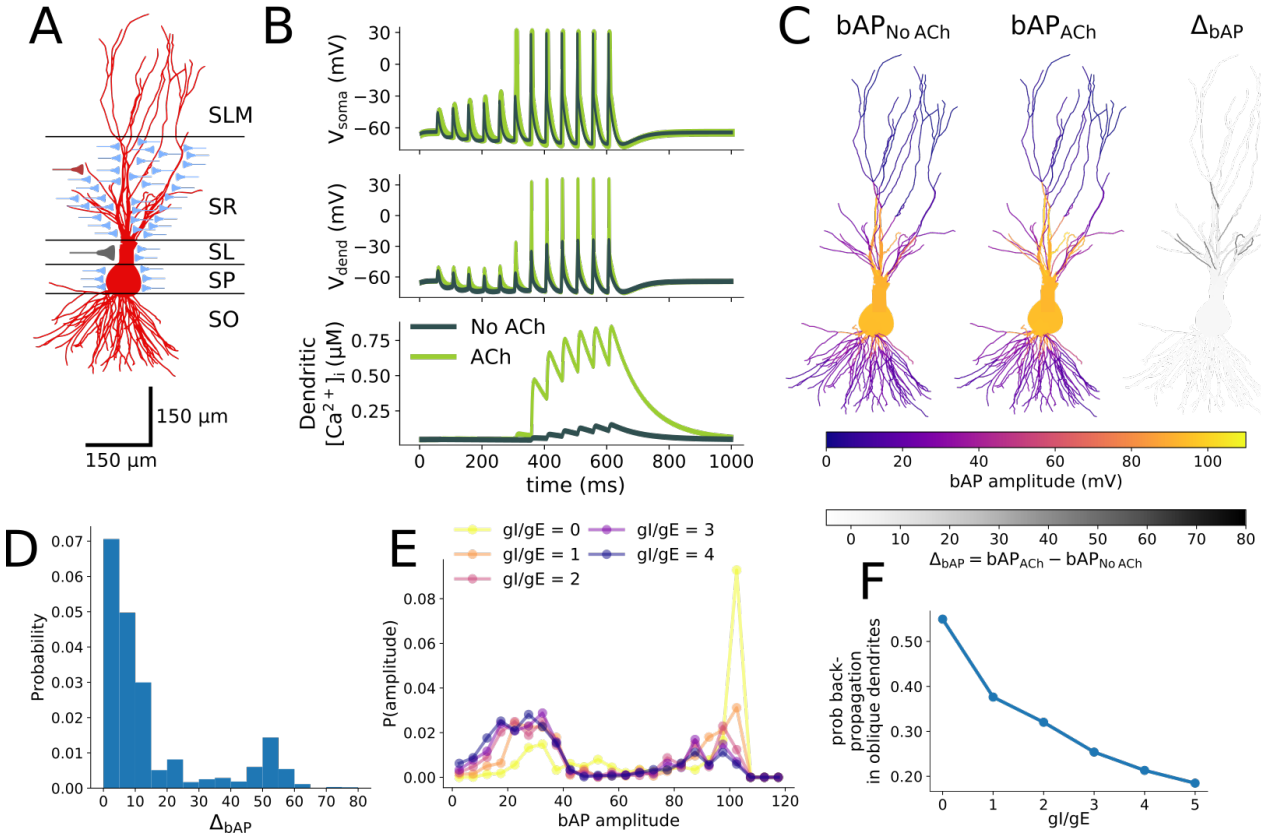

Figure 4: Acetylcholine-mediated disinhibition facilitates back-propagation of EPSPs and action potentials into the dendrites of CA3 pyramidal cells. A) Sketch of CA3 pyramidal cell and positioning within the layers of the hippocampus. Synaptic inputs are shown with location of contact (red - recurrent CA3-CA3 synapse, blue - feed-forward inhibitory synapse, gray - mossy fiber synapse). SLM – stratum lacunosum moleculare, SR – stratum radiatum, SL – stratum lucidum, SP – stratum pyramidale, SO – stratum oriens. B) Example traces produced by the biophysical CA3 neuron model of action potentials generated at the soma from summated mossy fiber EPSPs presented at 20 Hz (top), back-propagation into the radial oblique dendrites (middle), and dendritic calcium influx (bottom), with and without acetylcholine-mediated disinhibition of feed-forward inhibition. C) Back-propagating action potential amplitude before (left) and after (middle) cholinergic modulation, and the difference in amplitude (right) distributed across an example CA3 pyramidal cell. D) Histogram of differences in back-propagating action potential amplitudes with and without acetylcholine disinhibition in stratum radiatum oblique dendritic compartments (< 1 µm diameter) from 15 cells. E) Distribution of back-propagating action potential amplitudes in stratum radiatum oblique dendrites for a range of excitation-inhibition ratios in 15 cells. In our simulations the effect of acetylcholine was modelled as a change in this ratio (the absence of acetylcholine, gI/gE = 3; in the presence of acetylcholine, gI/gE = 1). F) The probability of successful action potential back-propagation (bAP amplitude > 40 mV) in oblique dendrites in 15 cells as a function of excitation-inhibition ratio.

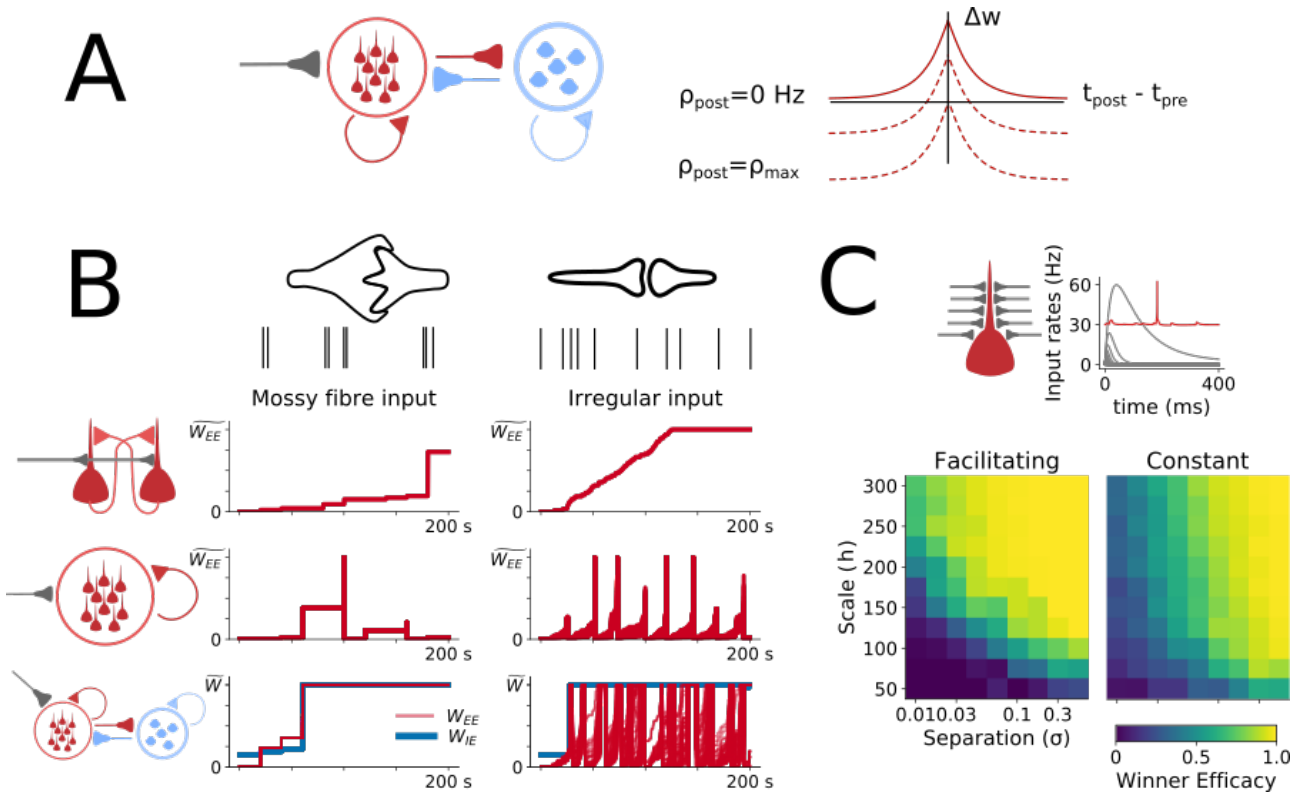

Figure 5: Facilitating mossy fiber inputs generate rapid and stable ensemble formation. A) Schematic showing the network properties of the spiking network model and long-term plasticity rules. Left: A population of excitatory (red) and inhibitory (blue) cells with all-to-all connectivity and mossy fiber input (gray). Right: Recurrent excitatory CA3-CA3 spike timing-dependent plasticity rule with a symmetric window that shifted from potentiation for correlated spiking at low rates (Ppost = 0), to depression for uncorrelated spiking near the maximum postsynaptic firing rate (Ppost = Pmax). B) Comparison of mossy fiber to irregular 'perforant path' input. Synaptic weight evolution with time for CA3-CA3 recurrent connections (red) and inhibitory to excitatory connections (blue) for a two cell excitatory population (top), a 10 cell excitatory population (middle) and a population including 10 excitatory and 5 inhibitory cells (bottom). C) Top Left: Network setup - 50 feed-forward inputs to a single granule cell. Top Right: Example of winner-take-all rates for population of inputs (gray) and postsynaptic spiking (red). This instance shows strong efficacy since postsynaptic spiking occurs once all but one input rates have decreased to near zero. Bottom: Efficacy of winner granule cell to CA3 pyramidal cell coupling with facilitating and constant synaptic input

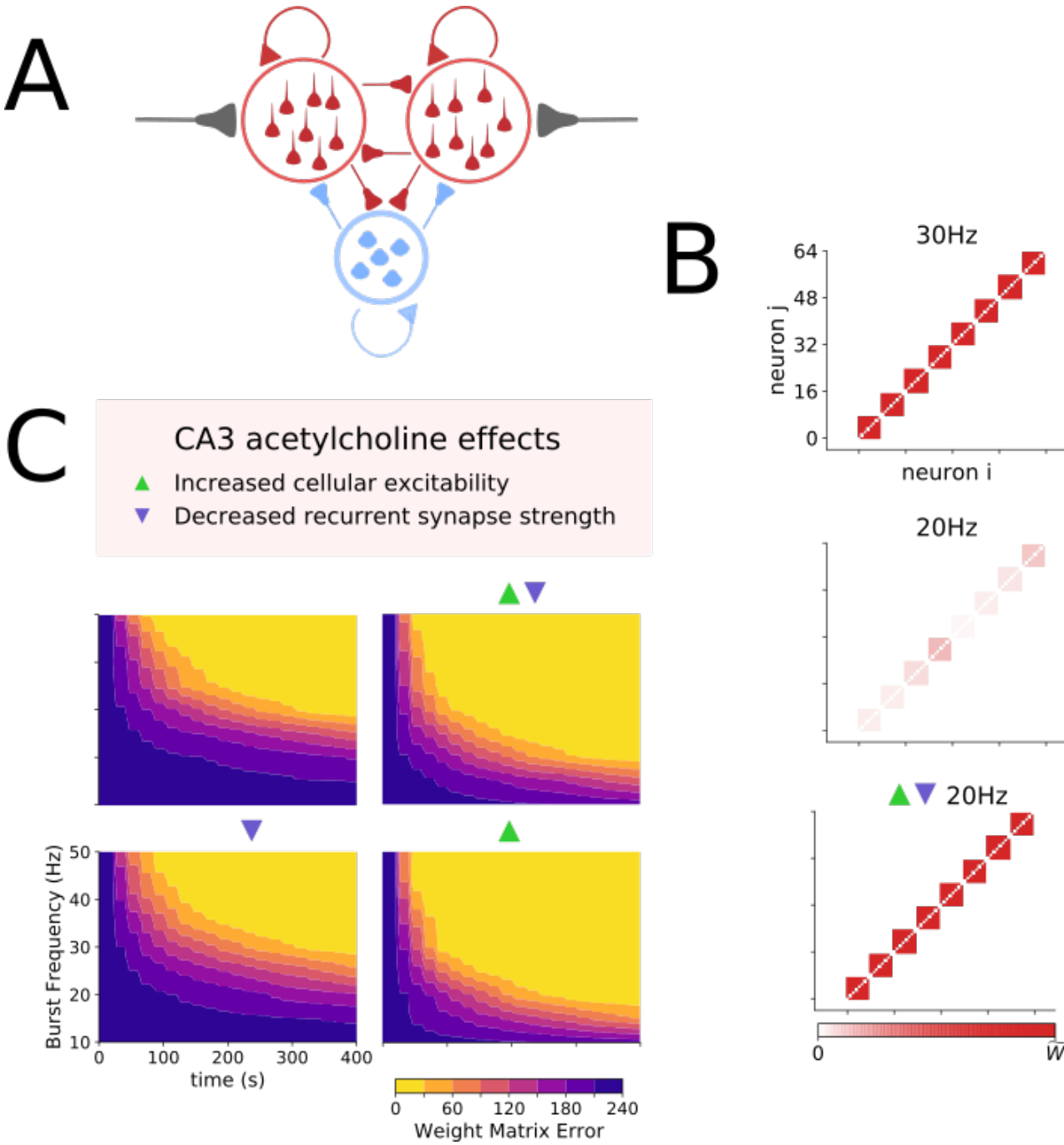

Figure 6: Acetylcholine speeds up ensemble formation and lowers input frequency requirement by increasing cellular excitability. A) Network setup: A population of excitatory and inhibitory cells connected in all-to-all fashion. Subpopulations of excitatory cells receive independent feed-forward input that drives ensemble formation. B) Example weight matrix driven by input with 30 Hz, 20 Hz or 20 Hz bursts with CA3 acetylcholine effects. Stronger weights indicate robust ensemble formation. C) Evolution of ensemble formation illustrated by the weight matrix error reduction over time for different input burst frequencies. Triangles denote which effects of acetylcholine on the CA3 network were included in each set of simulations.

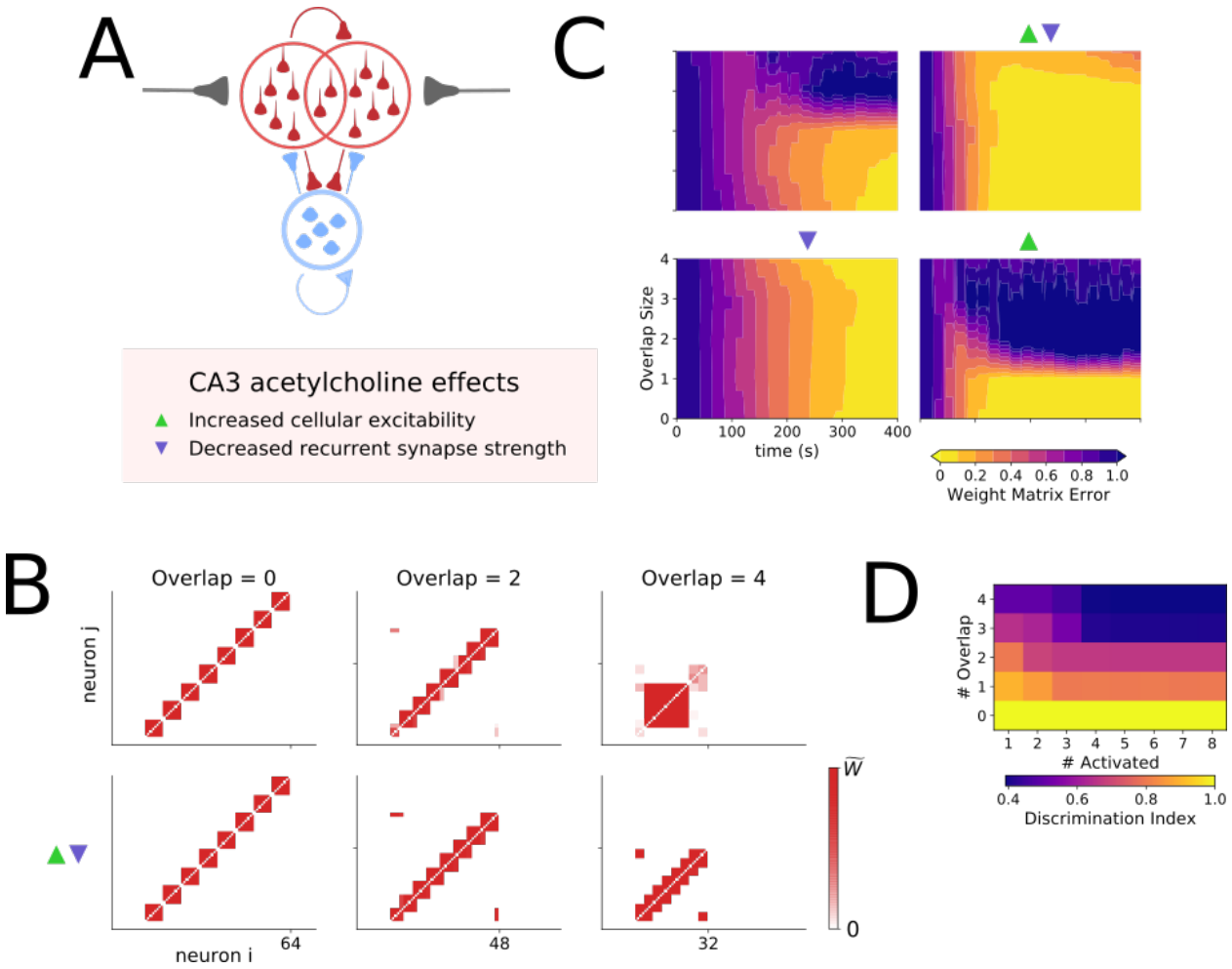

Figure 7: Acetylcholine enables a CA3 network to form stable overlapping ensembles by reducing the strength of recurrent excitatory CA3-CA3 synapses. A) Network setup: A population of excitatory and inhibitory cells connected in all-to-all fashion. Subpopulations of excitatory cells receive overlapping feed-forward input that drives ensemble formation. B) Example weight matrix driven by input with increasing degrees of overlap between ensembles [0, 2, 4 cells]. C) Evolution of ensemble formation illustrated by the weight matrix error over time for different degrees of overlap between ensembles. Triangles denote which effects of acetylcholine were included in the simulation. D) Effect of increasing overlap between ensembles on the ability to discriminate between ensembles defined as the difference in ensemble population spiking rates.

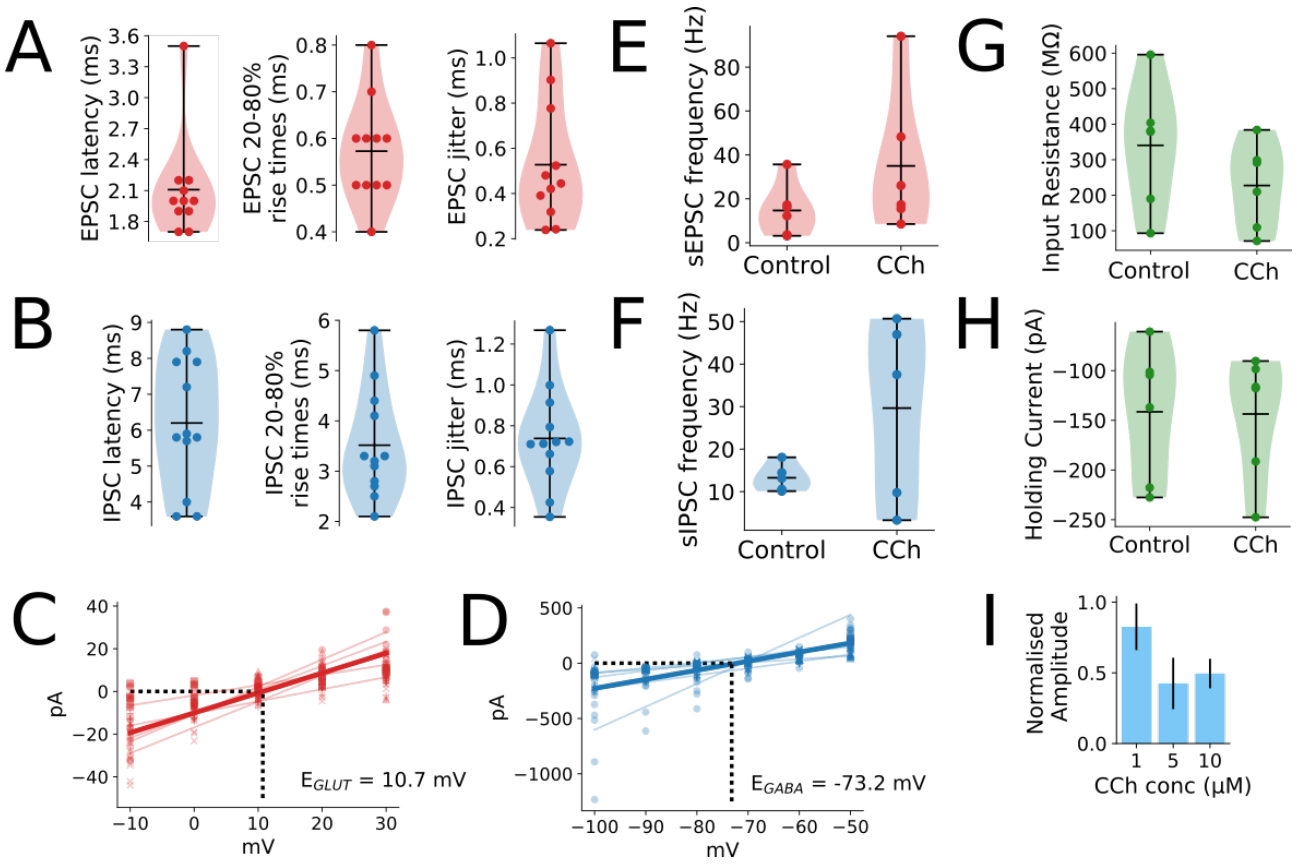

Supplementary Figure 1: A-B) Latency, rise times, and jitter of mossy fiber driven EPSCs (n = 11) (A) and IPSCs (n = 12) (B). C-D) Reversal potential estimation of glutamatergic (n = 5) (C) and GABAergic (n = 6) (D) transmission at CA3 pyramidal cells. E-F) Spontaneous EPSC (n = 6) (E) and IPSC (n = 5) (F) frequency recorded before and after carbachol application. G-H) CA3 pyramidal cell input resistance (n = 5) (G) and holding current at -70 mV (n = 5) (H) before and after carbachol application. I) Dose-response of carbachol effect on IPSC amplitudes (n = 3).

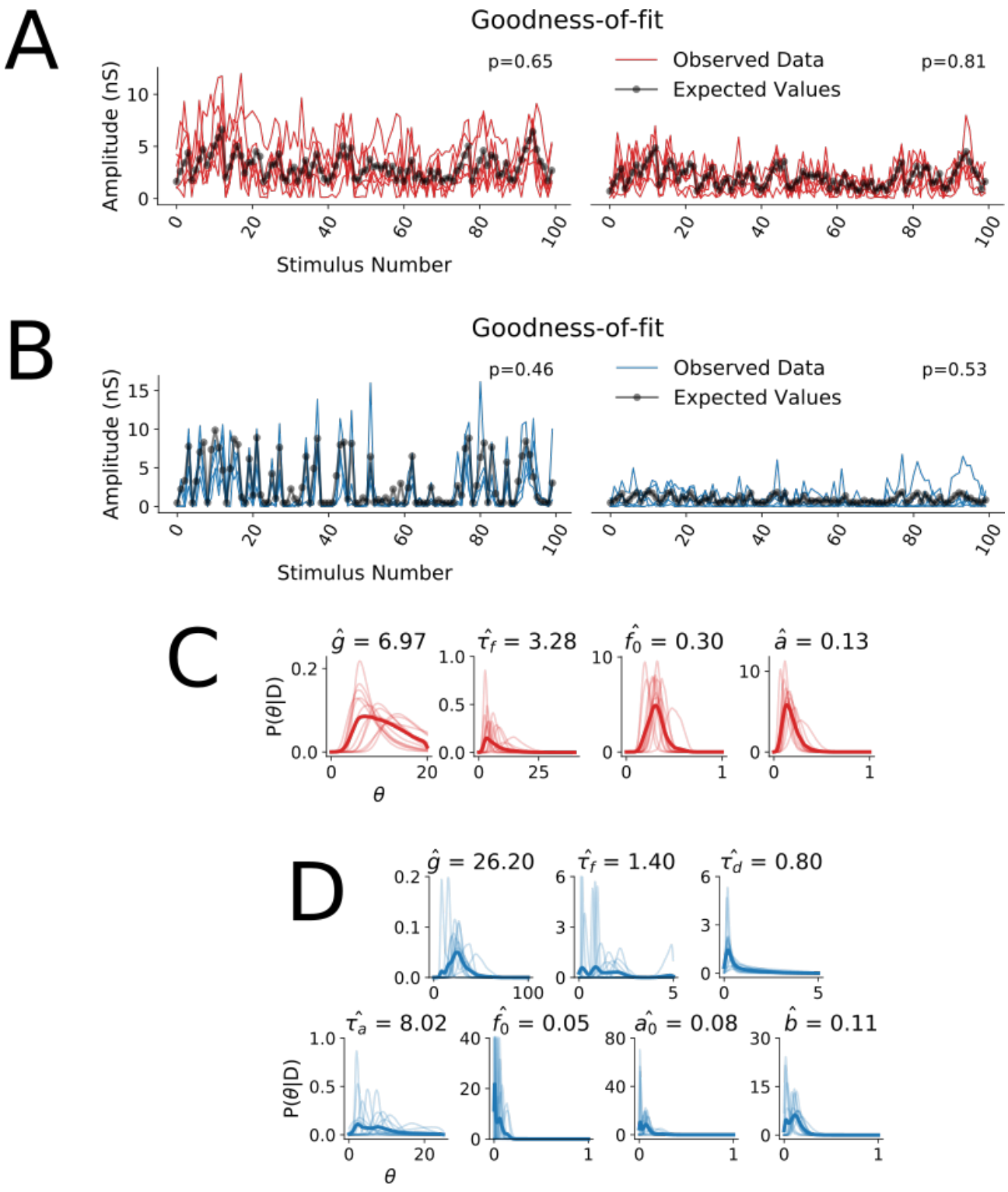

Supplementary Figure 2: A-B) Goodness-of-fit for EPSC (A) and IPSC (B) short-term plasticity models assessed by Bayesian posterior predictive *p*-values. Plots show the observed data for all experiments (EPSCs and IPSCs respectively) together with the expected values from the model before and after the application of 5 μM carbachol. *p*-values close to 0.5 indicate best fit. C-D) Posterior distributions for parameters of best fitting models given data for EPSCs (C) and IPSCs (D).

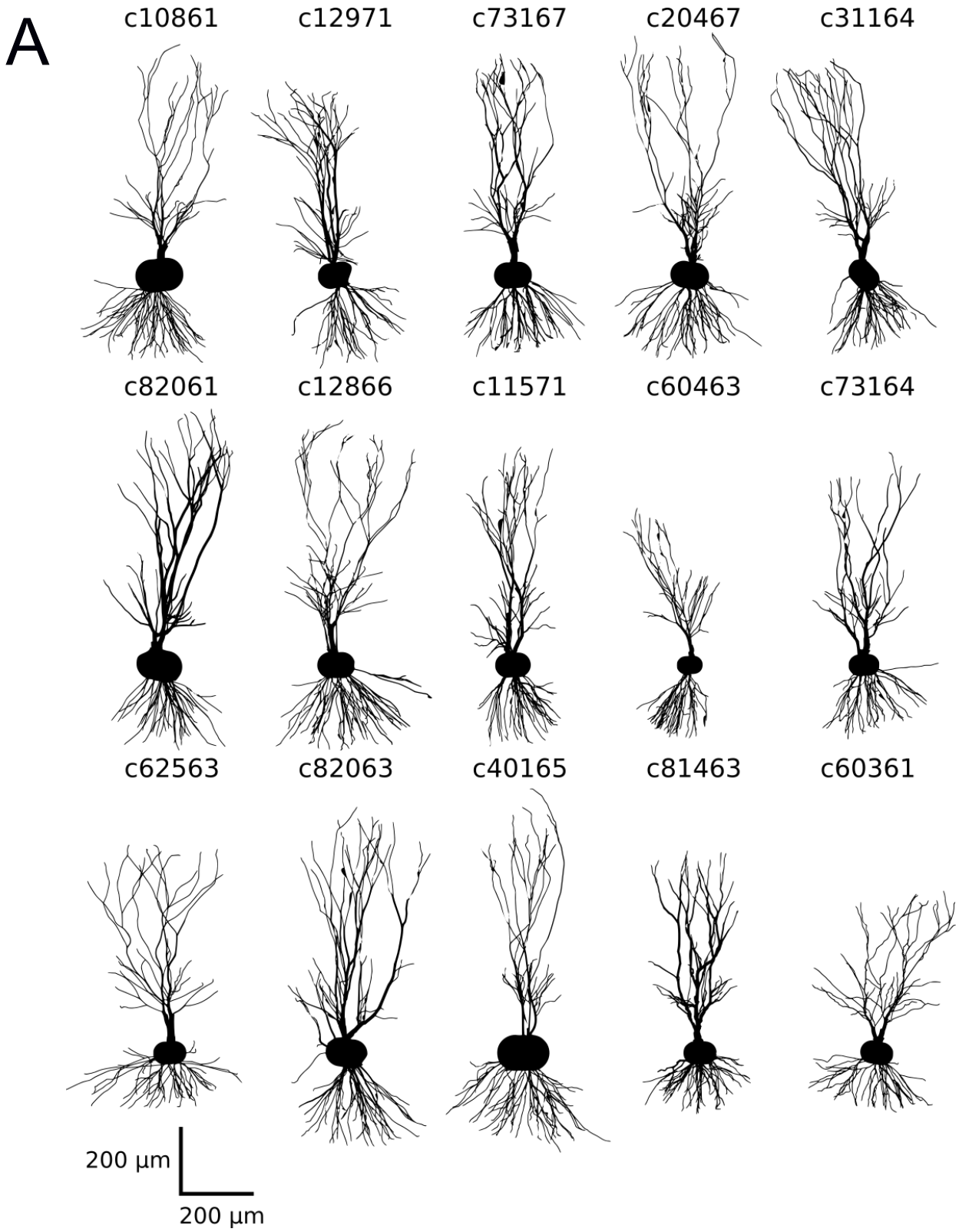
A
c10861
c12971
c73167
c20467
c31164
c82061
c12866
c11571
c60463
c73164
c62563
c82063
c40165
c81463
c60361
200 µm
200 µm

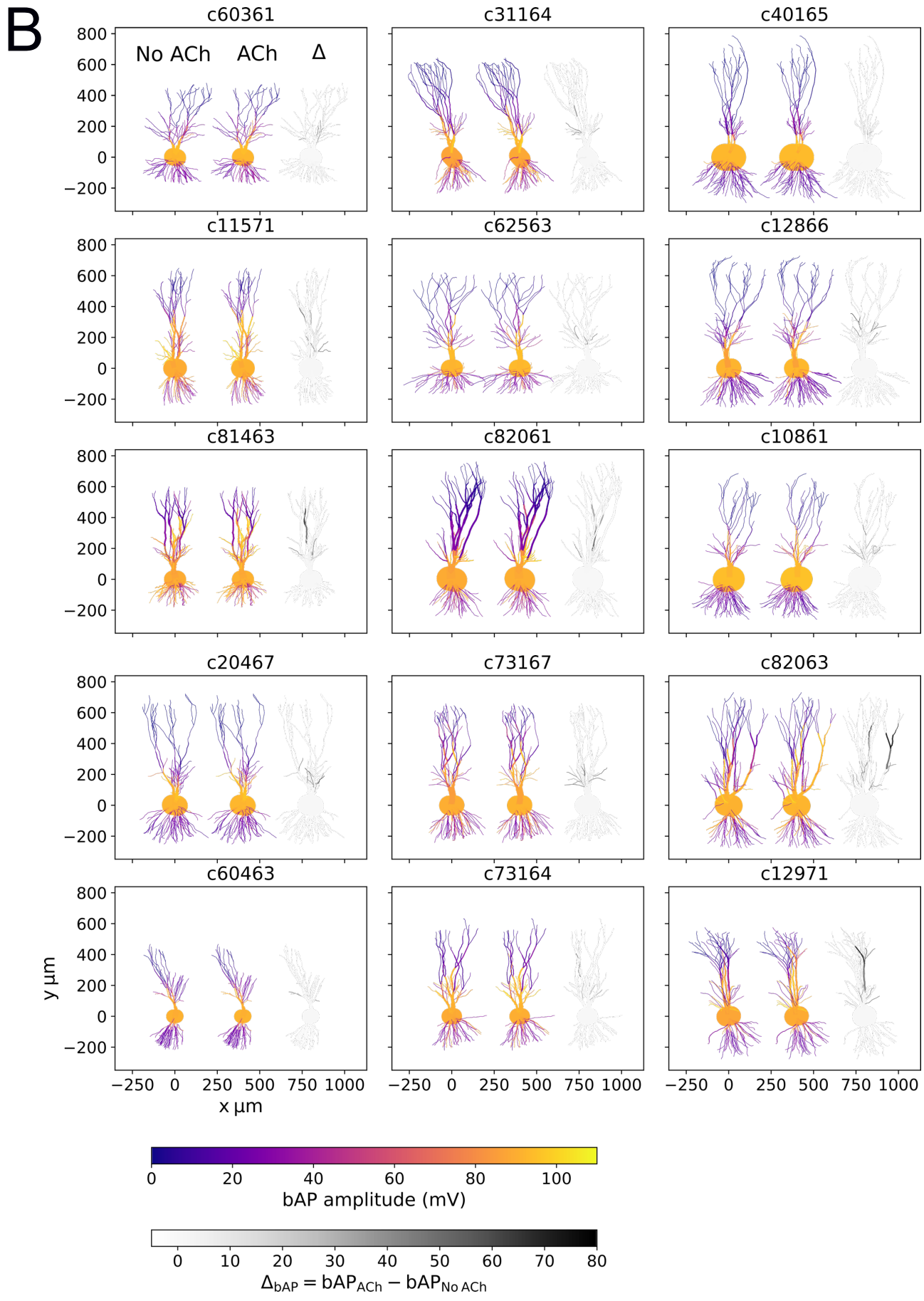
B
c60361
c31164
c40165
c11571
c62563
c12866
c81463
c82061
c10861
c20467
c73167
c82063
c60463
c73164
c12971
No ACh
ACh
Δ
y µm
x µm
bAP amplitude (mV)
$\Delta_{bAP} = bAP_{ACh} - bAP_{No\ ACh}$

Supplementary Figure 3: CA3 pyramidal cell morphologies used for biophysical modelling. A) All 15 cell morphologies plotted from NEURON spatial information. B) For each cell morphology, back-propagating action potential amplitude before (left) and after (middle) cholinergic modulation, and the difference in amplitude (right) are shown distributed across each CA3 pyramidal cell.

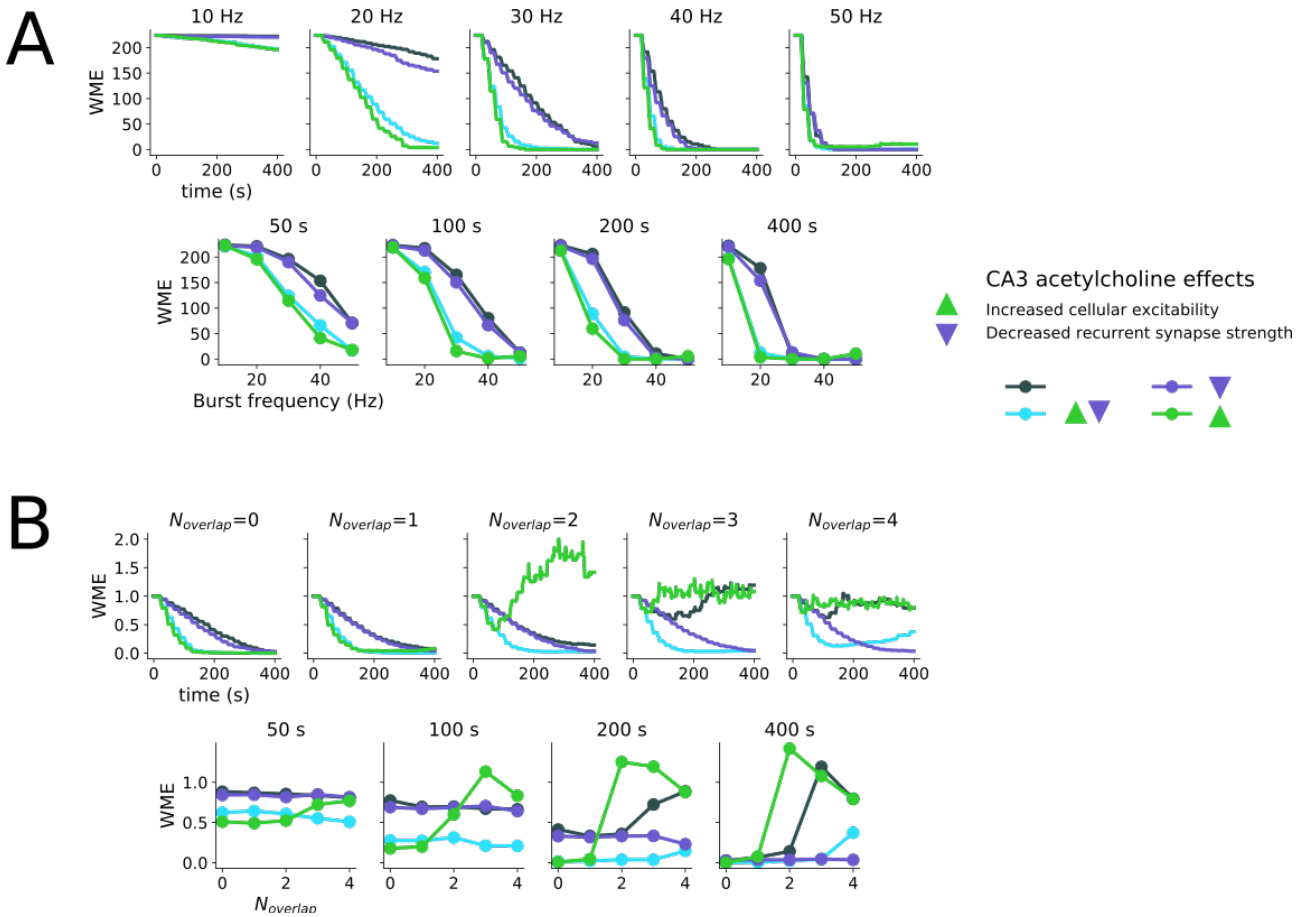

Supplementary Figure 4: A) Slices of data shown in Figure 6C along frequency (top) and time (bottom) axes. B) Slices of data shown in Figure 7C along overlap (top) and time (bottom) axes. Colour coding for plots is indicated in the legend representing inclusion of different effects of acetylcholine in CA3.

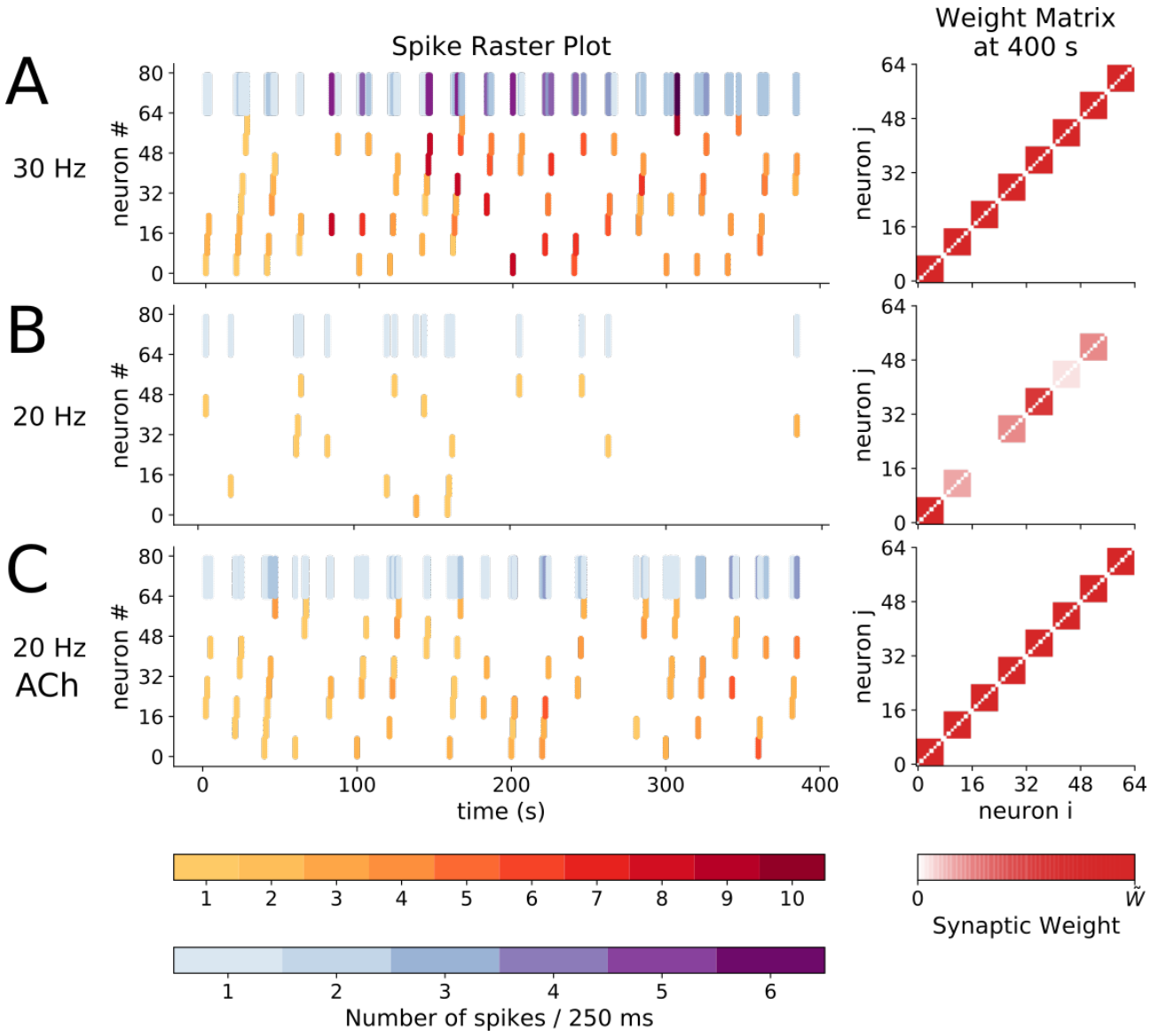

Supplementary Figure 5: Model CA3 spiking activity (left) and resulting pyramidal cell weight matrix (right) with mossy fibre bursting at 30 Hz (A), 20 Hz (B), and 20 Hz with cholinergic modulation (C).

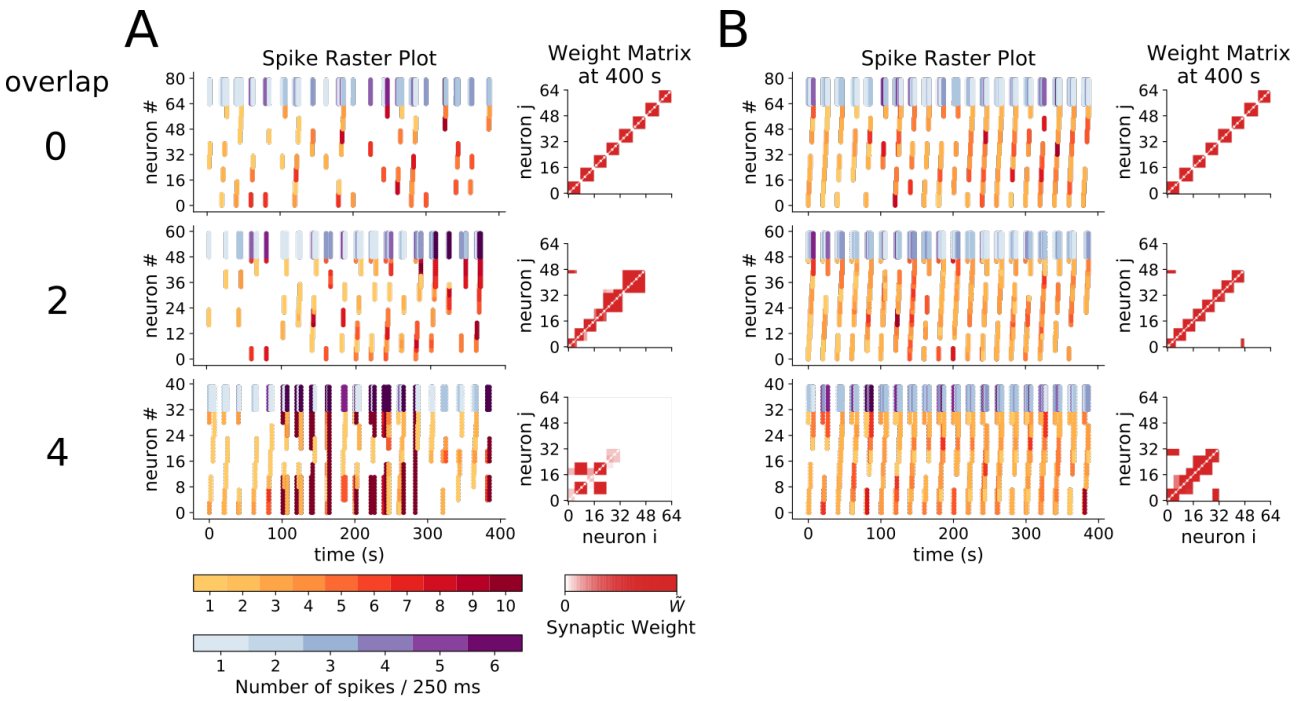

Supplementary Figure 6: Model CA3 spiking activity and resulting weight matrix without cholinergic modulation (A) and with cholinergic modulation (B) with 0 (top), 2 (middle), and 4 (top) cells overlapping between ensembles.

Parameter	Type	Normal	ACh
c	E cell	-63 mV	-61 mV
d	E cell	60 pA	50 pA
v_{rest}	E cell	-75 mV	-70 mV
v_{rest}	I cell	-65 mV	-63 mV
$g_{\widetilde{syn}}$	EE syn	0.5 nS	0.25 nS

Table 1: CA3 network parameter changes to model cholinergic modulation of CA3

References

Abbott, L. F. and Regehr, W. G. (2004). Synaptic computation. *Nature*, **431**(7010), pp. 796–803.

Abercrombie, E. D., Keller, R. W. J. and Zigmond, M. J. (1988). Characterization of hippocampal norepinephrine release as measured by microdialysis perfusion: pharmacological and behavioral studies. *Neuroscience*, **27**(3), pp. 897–904.

Abraham, W. C. (2003). How long will long-term potentiation last? *Philosophical Transactions Of The Royal Society Of London. Series B, Biological Sciences*, **358**(1432), pp. 735–744.

Acsady, L. *et al.* (1998). GABAergic cells are the major postsynaptic targets of mossy fibers in the rat hippocampus. *The Journal of Neuroscience*, **18**(9), pp. 3386–3403.

Adamantidis, A. R. *et al.* (2007). Neural substrates of awakening probed with optogenetic control of hypocretin neurons. *Nature*, **450**(November), pp. 1–6.

Afroz, S. *et al.* (2016). Synaptic pruning in the female hippocampus is triggered at puberty by extrasynaptic $GABA_A$ receptors on dendritic spines. *ELife*, **5**(May 2016), pp. 1–23.

Ahmed, M. S. and Siegelbaum, S. A. (2009). Recruitment of N-type ca^{2+} channels during LTP enhances low release efficacy of hippocampal CA1 perforant path synapses. *Neuron*. **63**(3), pp. 372–385.

Aksoy-Aksel, A. and Manahan-Vaughan, D. (2013). The temporoammonic input to the hippocampal CA1 region displays distinctly different synaptic plasticity compared to the Schaffer collateral input in vivo: Significance for synaptic information processing. *Frontiers In Synaptic Neuroscience*, **5**(1), pp. 1–12.

Ali, A. B. and Thomson, A. M. (1998). Facilitating pyramid to horizontal oriens-alveus interneurone inputs: dual intracellular recordings in slices of rat hippocampus. *The Journal of Physiology*. **507**(1), pp. 185–199.

Allen, D. *et al.* (2007). Organization and regulation of small conductance Ca^{2+}-activated K^+ channel multiprotein complexes. *The Journal of Neuroscience*. **27**(9), pp. 2369–2376.

Allen, P. B. *et al.* (2000). Protein phosphatase-1 regulation in the induction of long-term potentiation: heterogeneous molecular mechanisms. *The Journal of Neuroscience*, **20**(10), pp. 3537–3543.

Amaral, D. G., Ishizuka, N. and Claiborne, B. (1990). Neurons, numbers and the

hippocampal network. *Progress in Brain Research*, **83**, pp. 1–11.

Amaral, D. G. and Witter, M. P. (1989). The three-dimensional organization of the hippocampal formation: a review of anatomical data. *Neuroscience*, **31**(3), pp. 571–591.

Anagnostaras, S. G., Gale, G. D. and Fanselow, M. S. (2001). Hippocampus and contextual fear conditioning: recent controversies and advances. *Hippocampus*, **11**(1), pp. 8–17.

Andersen, P. *et al.* (1977). Specific long-lasting potentiation of synaptic transmission in hippocampal slices. *Nature*, **266**(5604), pp. 736–737.

Andersen, P. Morris, R., Amaral, D. (eds.), and Bliss, T., and O'Keefe, J. (ed.) (2007). *The Hippocampus Book*. Oxford: Oxford University Press.

Andrade, R., Foehring, R. C. and Tzingounis, A. V. (2012). The calcium-activated slow AHP: cutting through the Gordian knot. *Frontiers In Cellular Neuroscience*, **6**(October), p. 47.

Andrasfalvy, B. K. and Magee, J. C. (2004). Changes in AMPA receptor currents following LTP induction on rat CA1 pyramidal neurones. *The Journal of Physiology*, **559**(Pt 2), pp. 543–554.

Ang, C. W., Carlson, G. C. and Coulter, D. A. (2005). Hippocampal CA1 circuitry dynamically gates direct cortical inputs preferentially at theta frequencies. *The Journal of Neuroscience*, **25**(42), pp. 9567–9580.

Apostol, G. and Creutzfeldt, O. D. (1974). Crosscorrelation between the activity of septal units and hippocampal EEG during arousal. *Brain Research*. **67**(1), pp. 65–75.

Apostolides, P. F. *et al.* (2016). Axonal filtering allows reliable output during dendritic plateau-driven complex spiking in CA1 neurons. *Neuron*, **89**(4), pp. 770–783.

Araki, C. (1947). Konsui senshi ni tuite (in Japanese) (Puncture of the coma). *Saishin Igaku*, **2**, pp. 357–366.

Arnsten, A. F. T. and Dudley, A. G. (2005). Methylphenidate improves prefrontal cortical cognitive function through α2 adrenoceptor and dopamine D1 receptor actions: Relevance to therapeutic effects in Attention Deficit Hyperactivity Disorder. *Behavioural and Brain Functions*. **9**, pp. 1–9.

Ascoli, G. A., Donohue, D. E. and Halavi, M. (2007). NeuroMorpho.Org: a central resource for neuronal morphologies. *The Journal of Neuroscience*, **27**(35), pp. 9247–9251.

Aston-Jones, G. *et al.* (1994). Locus coeruleus neurons in monkey are selectively

activated by attended cues in a vigilance task. *The Journal of Neuroscience*, **14**(7), pp. 4467–4480.

Aston-Jones, G. *et al.* (1996). Role of the locus coeruleus in emotional activation. *Progress in Brain Research*, **107**, pp. 379–402.

Aston-Jones, Gary and Bloom, F. E. (1981). Activity of norepinephrine-containing locus coeruleus neurons in behaving rats anticipates fluctuations in the sleep-wake cycle. *The Journal of Neuroscience*, **1**(8), pp. 876–886.

Aston-Jones, G and Bloom, F. E. (1981). Norepinephrine-containing locus coeruleus neurons in behaving rats exhibit pronounced responses to non-noxious environmental stimuli. *The Journal of Neuroscience*, **1**(8), pp. 887–900.

Aston-Jones, G. and Cohen, J. D. (2005a). Adaptive gain and the role of the locus coeruleus – norepinephrine system in optimal performance. *The Journal of Comparative Neurology*, **110**(May), pp. 99–110.

Aston-Jones, G. and Cohen, J. D. (2005b). An integrative theory of locus coeruleus-norepinephrine function: adaptive gain and optimal performance. *Annual Review of Neuroscience*, **28**, pp. 403–450.

Aston-Jones, G., Rajkowski, J. and Kubiak, P. (1997). Conditioned responses of monkey locus coeruleus neurons anticipate acquisition of discriminative behavior in a vigilance task. *Neuroscience*, **80**(3), pp. 697–715.

Aston-Jones, G. and Waterhouse, B. (2016). Locus coeruleus: From global projection system to adaptive regulation of behavior. *Brain Research*, **1645**, pp. 75–78.

Atzori, M. *et al.* (2016). Locus ceruleus norepinephrine release: a central regulator of CNS. *Frontiers in Synaptic Neuroscience*, **8**(August), pp. 1–25.

Avery, M. C. and Krichmar, J. L. (2017). Neuromodulatory systems and their interactions: a review of models, theories, and experiments. *Frontiers In Neural CIrcuits*, **11**, p. 1–18.

Babiec, X. W. E. *et al.* (2017). Differential regulation of NMDA receptor-mediated transmission by SK channels underlies dorsal-ventral differences in dynamics of Schaffer Collateral synaptic function. *The Journal of Neuroscience*, **37**(7), pp. 1950–1964.

Bailhache, T. and Balthazart, J. (1993). The catecholaminergic system of the quail brain: Immunocytochemical studies of dopamine β-hydroxylase and tyrosine hydroxylase. *Journal of Comparative Neurology*, **329**(2), pp. 230–256.

Barker, G. R. I. and Warburton, E. C. (2011). When is the hippocampus involved in recognition memory? *The Journal of Neuroscience*, **31**(29), pp. 10721–10731.

Barnes, C. A. *et al.* (1990). Comparison of spatial and temporal characteristics of neuronal activity in sequential stages of hippocampal processing. *In:* Storm-Mathisen, J., Zimmer, J. and Ottersen O. P., (eds.). *Understanding the brain through the hippocampus the hippocampal region as a model for studying brain structure and function* (*Progress in Brain Research*, vol. **83)**. Oxford: Elsevier, pp. 287–300.

Barria, A. and Malinow, R. (2005). NMDA receptor subunit composition controls synaptic plasticity by regulating binding to CaMKII. *Neuron*, **48**(2), pp. 289–301.

Barrionuevo, G. and Brown, T. H. (1983). Associative long-term potentiation in hippocampal slices. *Proceedings of The National Academy of Sciences of The United States of America*, **80**(December), pp. 7347–7351.

Barrionuevo, G., Schottler, F. and Lynch, G. (1980). The effects of repetitive low frequency stimulation on control and 'potentiated' synaptic responses in the hippocampus. *Life Sciences*, **27**(24), pp. 2385–2391.

Barry, P. H. (1994). JPCalc, a software package for calculating liquid-junction potential corrections in patch-clamp, intracellular, epithelial and bilayer measurements and for correcting junction potential measurements. *Journal of Neuroscience Methods*, **51**(1), pp. 107–116.

Barth, A. M. I. *et al.* (2008). A2-adrenergic receptors modify dendritic spike generation via HCN channels in the prefrontal cortex. *Journal of Neurophysiology*, **99**(1), pp. 394–401.

Bartley, A. F. and Dobrunz, L. E. (2015). Short-term plasticity regulates the excitation/inhibition ratio and the temporal window for spike integration in CA1 pyramidal cells. *The European Journal of Neuroscience*, **41**(11), pp. 1402–1415.

Bashir, Z. I. and Collingridge, G. L. (1994). An investigation of depotentiation of long-term potentiation in the CA1 region of the hippocampus. *Experimental Brain Research*, **100**(3), pp. 437–443.

Bayley, P. J. *et al.* (2005). The neuroanatomy of remote memory. *Neuron*, **46**(5), pp. 799–810.

Beattie, E. C. *et al.* (2000). Regulation of AMPA receptor endocytosis by a signaling mechanism shared with LTD. *Nature Neuroscience*, **3**(12), pp. 1291–1300.

Beaulieu, J.-M. and Gainetdinov, R. R. (2011). The physiology, signaling, and pharmacology of dopamine receptors. *Pharmacological Reviews*, **63**(1), pp. 182–217.

Behr, J. and Heinemann, U. (1996). Low Mg^{2+} induced epileptiform activity in the subiculum before and after disconnection from rat hippocampal and entorhinal cortex

slices. *Neuroscience Letters*, **205**(1), pp. 25–28.

Ben-Ari, Y. *et al.* (1989). Giant synaptic potentials in immature rat CA3 hippocampal neurones. *The Journal of Physiology*, **416**(1), pp. 303–325.

Benardo, L. S. and Prince, D. A. (1982). Dopamine action on hippocampal pyramidal cells. *The Journal of Neuroscience*, **2**(4), pp. 415–423.

Benke, T. A. *et al.* (1998). Modulation of AMPA receptor unitary conductance by synaptic activity. *Nature*, **393**(6687), pp. 793–797.

Benson, D. A. *et al.* (2012). GenBank. *Nucleic Acids Research*, **40**(Database issue), pp. 48-53.

Bergles, D. E. *et al.* (1996). Excitatory actions of norepinephrine on multiple classes of hippocampal CA1 interneurons. *The Journal of Neuroscience*, **16**(2), pp. 572–585.

Bergmann, E. *et al.* (2016). The organization of mouse and human cortico-hippocampal networks estimated by intrinsic functional connectivity. *Cerebral Cortex*, **26**(12), pp. 4497–4512.

Berlucchi, G. and Buchtel, H. A. (2009). Neuronal plasticity: Historical roots and evolution of meaning. *Experimental Brain Research*, **192**(3), pp. 307–319.

Berndt, A. *et al.* (2011). High-efficiency channelrhodopsins for fast neuronal stimulation at low light levels. *Proceedings of The National Academy of Sciences of The United States of America,* **108**(3), pp. 7595–7600.

Berridge, C. W. and Waterhouse, B. D. (2003). The locus coeruleus – noradrenergic system : modulation of behavioral state and state-dependent cognitive processes. *Brain Research Reviews*, **42**(1), pp. 33–84.

Bijak, M. and Misgeld, U. (1995). Adrenergic modulation of hilar neuron activity and granule cell inhibition in the guinea-pig hippocampal slice. *Neuroscience*, **67**(3), pp. 541–550.

Bildl, W. *et al.* (2004). Protein kinase CK2 is coassembled with small conductance $Ca^{(2+)}$-activated K^+ channels and regulates channel gating. *Neuron*, **43**(6), pp. 847–858.

Bird, C. M. and Burgess, N. (2008). The hippocampus and memory: Insights from spatial processing. *Nature Reviews Neuroscience*, **9**(3), pp. 182–194.

Biscoe, T. J. and Straughan, D. W. (1966). Micro-electrophoretic studies of neurones in the cat hippocampus. *The Journal of Physiology*, **183**(2), pp. 341–359.

Bittner, K. C. *et al.* (2015). Conjunctive input processing drives feature selectivity in hippocampal CA1 neurons. *Nature Neuroscience*, **18**(8), pp. 1133–1142.

Blackstad, T. W. *et al.* (1970). Distribution of hippocampal mossy fibers in the rat. An experimental study with silver impregnation methods. *The Journal of Comparative Neurology*, **138**(4), pp. 433–449.

Bland, B. H. (1986). The physiology and pharmacology of hippocampal formation theta rhythms. *Progress In Neurobiology*, **26**(1), pp. 1–54.

Bland, B. H. and Colom, L. V. (1989). Preliminary observations on the physiology and pharmacology of hippocampal theta-off cells. *Brain Research*, **505**(2), pp. 333–336.

Bliss, T. V and Collingridge, G. L. (1993). A synaptic model of memory: long-term potentiation in the hippocampus. *Nature*, **361**(6407), pp. 31–39.

Bliss, T. V and Lomo, T. (1973). Long-lasting potentiation of synaptic transmission in the dentate area of the anaesthetized rabbit following stimulation of the perforant path. *The Journal of Physiology*, **232**(2), pp. 331–356.

Bloodgood, B. L. and Sabatini, B. L. (2007). $Ca^{(2+)}$ signaling in dendritic spines. *Current Opinion In Neurobiology*, **17**(3), pp. 345–351.

Boehm, S. (1999). Presynaptic a2-adrenoceptors control excitatory, but not inhibitory, transmission at rat hippocampal synapses. *The Journal of Physiology*, **519**(2), pp. 439–449.

Boehringer, R. *et al.* (2017). Chronic loss of CA2 transmission leads to hippocampal hyperexcitability. *Neuron*, **94**(3), pp. 642-655.

Bond, C. T. *et al.* (2004). Small conductance Ca^{2+}-activated K^{+} channel knock-out mice reveal the identity of calcium-dependent afterhyperpolarization currents. *The Journal of Neuroscience*, **24**(23), pp. 5301–5306.

Boss, B. D. *et al.* (1987). On the numbers of neurons on fields CA1 and CA3 of the hippocampus of Sprague-Dawley and Wistar rats. *Brain Research*, **406**(1-2), pp. 280–287.

Boyden, E. S. *et al.* (2005). Millisecond-timescale, genetically targeted optical control of neural activity. *Nature Neuroscience*, **8**(9), pp. 1263–1268.

Bradford, H. F. (1995). Glutamate, GABA and epilepsy. *Progress In Neurobiology*, **47**(6), pp. 477–511.

Breustedt, J. *et al.* (2003). A1E-Containing Ca^{2+} channels are involved in synaptic plasticity. *Proceedings of The National Academy of Sciences of The United States of America*, **100**(21), pp. 12450–12455.

Brew, H. M. *et al.* (2007). Seizures and reduced life span in mice lacking the potassium

channel subunit Kv1.2, but hypoexcitability and enlarged Kv1 currents in auditory neurons. *The Journal of Neurophysiology*, **98**(3), pp. 1501–1525.

Brew, H. M., Hallows, J. L. and Tempel, B. L. (2003). Hyperexcitability reduced low threshold potassium currents auditory neurons of mice lacking the channel subunit Kv1.1. *The Journal of Physiology*, **548**(1), pp. 1–20.

Britt, J. P., McDevitt, R. A. and Bonci, A. (2012). Use of channelrhodopsin for activation of CNS neurons. *Current Protocols In Neuroscience*. **58**(1), pp. 1–25.

Brivanlou, I. H. *et al.* (2004). Topographic specificity of functional connections from hippocampal CA3 to CA1. *Proceedings of The National Academy of Sciences of The United States of America*, **101**(8), pp. 2560–2565.

Brown, R. A. M. *et al.* (2005). Locus ceruleus activation suppresses feedforward interneurons and reduces β–γ electroencephalogram frequencies while it enhances θ frequencies in rat dentate gyrus. *The Journal of Neuroscience*, **25**(8), pp. 1985–1991.

Bru, T., Salinas, S. and Kremer, E. J. (2010). An update on canine adenovirus type 2 and its vectors. *Viruses*, **2**(9), pp. 2134–2153.

Buchanan, K. A. *et al.* (2010). Facilitation of long-term potentiation by muscarinic m 1 receptors is mediated by inhibition of SK channels. *Neuron*, **68**(5), pp. 948–963.

Buchanan, K. A. and Mellor, J. R. (2007). The development of synaptic plasticity induction rules and the requirement for postsynaptic spikes in rat hippocampal CA1 pyramidal neurones. *The Journal of Physiology*, **585**(2), pp. 429–445.

Bui, L. and Glavinovic, M. I. (2014). Temperature dependence of vesicular dynamics at excitatory synapses of rat hippocampus. *Cognitive Neurodynamics*, **8**(4), pp. 277–286.

Buzsaki, G. (1980). Long-term potentiation of the commissural path-CA1 pyramidal cell synapse in the hippocampus of the freely moving rat. *Neuroscience Letters*, **19**(3), pp. 293–296.

Buzsaki, G. and Eidelberg, E. (1983). Phase relations of hippocampal projection cells and interneurons to theta activity in the anesthetized rat. *Brain Research*, **266**(2), pp. 334–339.

Buzsáki, G. and Moser, E. I. (2013). Memory, navigation and theta rhythm in the hippocampal-entorhinal system. *Nature Neuroscience*, **16**(2), pp. 130–138.

Campanac, E. and Debanne, D. (2008). Spike timing-dependent plasticity: A learning rule for dendritic integration in rat CA1 pyramidal neurons. *The Journal of Physiology*, **586**(3), pp. 779–793.

Campbell, E. J. and Marchant, N. J. (2018). The use of chemogenetics in behavioural neuroscience: receptor variants, targeting approaches and caveats. *British Journal of Pharmacology*, **175**(7), pp. 994–1003.

Canteras, N. S., Simerly, R. B. and Swanson, L. W. (1992). Connections of the posterior nucleus of the amygdala. *The Journal of Comparative Neurology*, **324**(2), pp. 143–179.

Carey, M. R. and Regehr, W. G. (2009). Noradrenergic control of associative synaptic plasticity by selective modulation of instructive signals. *Neuron*, **62**(1), pp. 112–122.

Carter, M. E. *et al.* (2010). Tuning arousal with optogenetic modulation of locus coeruleus neurons. *Nature Neuroscience*, **13**(12), pp. 1526–1533.

Cassel, J. C. *et al.* (2013). The reuniens and rhomboid nuclei: Neuroanatomy, electrophysiological characteristics and behavioral implications. *Progress In Neurobiology*, **111**, pp. 34–52.

Castillo, P. E., Weisskopf, M. G. and Nicoll, R. A. (1994). The role of Ca^{2+} channels in hippocampal mossy fiber synaptic transmission and long-term potentiation. *Neuron*, **12**(2), pp. 261–269.

Cenquizca, L. A. and Swanson, L. W. (2007). Spatial organization of direct hippocampal field CA1 axonal projections to the rest of the cerebral cortex. *Brain Research Reviews*, **56**(1), pp. 1–26.

Chandler, D. J., Gao, W. and Waterhouse, B. D. (2014). Heterogeneous organization of the locus coeruleus projections to prefrontal and motor cortices. *Proceedings of The National Academy of Sciences of The United States of America*, **111**(18), pp. 6816–6821.

Chattarji, S., Stanton, P. K. and Sejnowski, T. J. (1989). Commissural synapses, but not mossy fiber synapses, in hippocampal field CA3 exhibit associative long-term potentiation and depression. *Brain Research*, **495**(1), pp. 145–150.

Chechik, G., Meilijson, I. and Ruppin, E. (1999). Neuronal regulation: A mechanism for synaptic pruning during brain maturation. *Neural Computation*, **11**(8), pp. 2061–2080.

Chefer, V. I. *et al.* (2009). Overview of brain microdialysis. *Current Protocols In Neuroscience*, **7**(1), pp. 1–35.

Chen, X. and Johnston, D. (2004). Properties of single voltage-dependent K^+ channels in dendrites of CA1 pyramidal neurones of rat hippocampus. *The Journal of Physiology*, **559**(Pt 1), pp. 187–203.

Chicurel, M. E. and Harris, K. M. (1992). Three-dimensional analysis of the structure and composition of CA3 branched dendritic spines and their synaptic relationships with mossy fiber boutons in the rat hippocampus. *The Journal of Comparative Neurology*,

325(2), pp. 169–182.

Choi, D. W. (1988). Glutamate neurotoxicity and diseases of the nervous system. *Neuron*, **1**(8), pp. 623–634.

Chung, S., Li, X. and Nelson, S. B. (2002). Short-term depression at thalamocortical synapses contributes to rapid adaptation of cortical sensory responses *in vivo*. *Neuron*, **34**(3), pp. 437–446.

Citri, A. and Malenka, R. C. (2008). Synaptic plasticity: multiple forms, functions, and mechanisms. *Neuropsychopharmacology*, **33**(1), pp. 18–41.

Claiborne, B. J., Amaral, D. G. and Cowan, W. M. (1986). A light and electron microscopic analysis of the mossy fibers of the rat dentate gyrus. *The Journal of Comparative Neurology*, **246**(4), pp. 435–458.

Clark, B. D., Goldberg, E. M. and Rudy, B. (2009). Electrogenic tuning of the axon initial segment. *The Neuroscientist*, **15**(6), pp. 651–668.

Clark, R. E. and Squire, L. R. (2013). Similarity in form and function of the hippocampus in rodents, monkeys, and humans. *Proceedings of The National Academy of Sciences of The United States of America*, **110**(Suppl. 2), pp. 10365–10370.

Clayton, E. C. *et al.* (2004). Phasic activation of monkey locus ceruleus neurons by simple decisions in a forced-choice task, **24**(44), pp. 9914–9920.

Cobb, S. R. *et al.* (1995). Synchronization of neuronal activity in hippocampus by individual GABAergic interneurons. *Nature*, **378**, pp. 75–78.

Colgin, L. L. (2016). Rhythms of the hippocampal network. *Nature Reviews Neuroscience*, **17**(4), pp. 239–249.

Collingridge, G. L., Kehl, S. J. and McLennan, H. (1983). Excitatory amino acids in synaptic transmission in the Schaffer collateral-commissural pathway of the rat hippocampus. *The Journal of Physiology*, **334**(1), pp. 33–46.

Collingridge, G L, Kehl, S. J. and McLennan, H. (1983). The antagonism of amino acid-induced excitations of rat hippocampal CA1 neurones *in vitro*. *The Journal of Physiology*, **334**, pp. 19–31.

Compton, D. M. *et al.* (1995). Spatial and non-spatial learning in the rat following lesions to the nucleus locus coeruleus. *Neuroreport*, **7**(1), pp. 177–182.

Cooper, A. *et al.* (2012). Trisomy of the G protein-coupled K^+ channel gene, *Kcnj6*, affects reward mechanisms, cognitive functions, and synaptic plasticity in mice. *Proceedings of The National Academy of Sciences of The United States of America,* **109**(7), pp. 2642–

2647.

Cooper, S. J. (2005). Donald O. Hebb's synapse and learning rule: A history and commentary. *Neuroscience and Biobehavioral Reviews*, **28**(8), pp. 851–874.

Cornil, C. A. and Ball, G. F. (2008). Interplay among catecholamine systems: Dopamine binds to α2-adrenergic receptors in birds and mammals. *Journal of Comparative Neurology*, **511**(5), pp. 610–627.

Courtney, N. A. and Ford, C. P. (2014). The timing of dopamine- and noradrenaline-mediated transmission reflects underlying differences in the extent of spillover and pooling. *The Journal of Neuroscience*, **34**(22), pp. 7645–7656.

Cowan, W. M. and Kandel, E. R. (2001). Prospects for neurology and psychiatry. *The Journal of the American Medical Association*, **285**(5), pp. 594–600.

Cox, D. J., Racca, C. and LeBeau, F. E. N. (2008). β-Adrenergic Receptors Are Differentially Expressed in Distinct Interneuron Subtypes in the Rat Hippocampus. *Journal of Comparative Neurology*, **509**(6), pp. 551–565.

Cummings, J. A. *et al.* (1996). Ca^{2+} signaling requirements for long-term depression in the hippocampus. *Neuron*, **16**(4), pp. 825–833.

Curet, O. and de Montigny, C. (1988). Electrophysiological characterization of adrenoceptors in the rat dorsal hippocampus. II. Receptors mediating the effect of synaptically released norepinephrine. *Brain Research*, **475**(1), pp. 47–57.

Daoudal, G. and Debanne, D. (2003). Long-term plasticity of intrinsic excitability: learning rules and mechanisms. *Learning and Memory*, **10**(6), pp. 456–465.

Davidson, T. J., Kloosterman, F. and Wilson, M. A. (2009). Hippocampal replay of extended experience. *Neuron*, **63**(4), pp. 497–507.

Davis, H. P. and Squire, L. R. (1984). Protein synthesis and memory: A review. *Psychological Bulletin*, **96**(3), pp. 518–559.

Debanne, D. *et al.* (1996). Paired-pulse facilitation and depression at unitary synapses in rat hippocampus: quantal fluctuation affects subsequent release. *The Journal of Physiology,* **491**(Pt 1), pp. 163–176.

Debanne, D., Gähwiler, B. H. and Thompson, S. M. (1998). Long-term synaptic plasticity between pairs of individual CA3 pyramidal cells in rat hippocampal slice cultures. *The Journal of Physiology*, **507**(1), pp. 237–247.

Deisseroth, K. (2011). Optogenetics. *Nature Methods*, **8**(1), pp. 26–29.

Delaney, A. J., Crane, J. W. and Sah, P. (2007). Noradrenaline modulates transmission

at a central synapse by a presynaptic mechanism. *Neuron*, **6**(5), pp. 880–892.

Delgado, J. M. *et al.* (1972). Dialytrode for long term intracerebral perfusion in awake monkeys. *Archives Internationales De Pharmacodynamie Et De Therapie*, **198**(1), pp. 9–21.

Denker, A. and Rizzoli, S. O. (2010). Synaptic vesicle pools: an update. *Frontiers In Synaptic Neuroscience*, **2**(135), pp. 1–12.

Dere, E., Easton A., Nadel, L. and Huston J. (eds.) (2008). *Handbook of Episodic Memory, Volume 18*. Oxford: Elsevier.

Derkach, V., Barria, A. and Soderling, T. R. (1999). Ca^{2+}/calmodulin-kinase II enhances channel conductance of α-amino-3-hydroxy-5-methyl-4-isoxazolepropionate type glutamate receptors. *Proceedings of The National Academy of Sciences of The United States of America*, **96**(6), pp. 3269–3274.

Desai, N. S., Rutherford, L. C. and Turrigiano, G. G. (1999). Plasticity in the intrinsic excitability of cortical pyramidal neurons. *Nature Neuroscience*, **2**(6), pp. 515–520.

Devilbiss, D. M., Page, M. E. and Waterhouse, B. D. (2006). Locus ceruleus regulates sensory encoding by neurons and networks in waking animals. *The Journal of Neuroscience*, **26**(39), pp. 9860–9872.

Devilbiss, D. M. and Waterhouse, B. D. (2000). Norepinephrine exhibits two distinct profiles of action on sensory cortical neuron responses to excitatory synaptic stimuli. *Synapse*, **37**(4), pp. 273–282.

Devilbiss, D. M. and Waterhouse, B. D. (2004). The effects of tonic locus ceruleus output on sensory- evoked responses of ventral posterior medial thalamic and barrel field cortical neurons in the awake rat. *The Journal of Neuroscience*, **24**(48), pp. 10773–10785.

Devilbiss, D. M. and Waterhouse, B. D. (2011). Phasic and tonic patterns of locus coeruleus output differentially modulate sensory network function in the awake rat. *The Journal of Neurophysiology*, **105**(1), pp. 69–87.

Diamond, J. S. (2001). Neuronal glutamate transporters limit activation of NMDA receptors by neurotransmitter spillover on CA1 pyramidal cells. *The Journal of Neuroscience*, **21**(21), pp. 8328–8338.

Dittman, J. S., Kreitzer, A. C. and Regehr, W. G. (2000). Interplay between facilitation, depression, and residual calcium at three presynaptic terminals. *The Journal of Neuroscience*, **20**(4), pp. 1374–1385.

Dobrunz, L. E., Huang, E. P. and Stevens, C. F. (1997). Very short-term plasticity in

hippocampal synapses. *Proceedings of The National Academy of Sciences of The United States of America*, **94**(26), pp. 14843–14847.

Dodson, P. D., Barker, M. C. and Forsythe, I. D. (2002). Two heteromeric Kv1 potassium channels differentially regulate action potential firing. *The Journal of Neuroscience*, **22**(16), pp. 6953–6961.

Doller, H. J. and Weight, F. F. (1985). Perforant pathway-evoked long-term potentiation of CA1 neurons in the hippocampal slice preparation. *Brain Research*, **333**(2), pp. 305–310.

Dong, H. W. *et al.* (2009). Genomic-anatomic evidence for distinct functional domains in hippocampal field CA1. *Proceedings of The National Academy of Sciences of The United States of America*, **106**(28), pp. 11794–11799.

Dorrn, A. L. *et al.* (2010). Developmental sensory experience balances cortical excitation and inhibition. *Nature*, **465**(7300), pp. 932–936.

Doze, V. A., Cohen, G. A. and Madison, D. V. (1991). Synaptic localization of adrenergic disinhibition in the rat hippocampus. *Neuron*, **6**(6), pp. 889–900.

Druckmann, S. *et al.* (2014). Structured synaptic connectivity between hippocampal regions. *Neuron*, **81**(3), pp. 629–640.

Dudek, S. M. and Bear, M. F. (1992). Homosynaptic long-term depression in area CA1 of hippocampus and effects of N-methyl-D-aspartate receptor blockade. *Proceedings of The National Academy of Sciences of The United States of America*, **89**, pp. 4363–4367.

Dunwiddie, T. *et al.* (1992). Long-term increases in excitability in the CA1 region of rat hippocampus induced by beta-adrenergic stimulation: possible mediation by cAMP. *The Journal of Neuroscience*, **12**(2), pp. 506–517.

Duszkiewicz, A. J. *et al.* (2019). Novelty and dopaminergic modulation of memory persistence: A tale of two systems. *Trends In Neurosciences*, **42**(2), pp. 102–114.

Dutar, P. and Nicoll, R. A. (1988). Pre- and postsynaptic $GABA_B$ receptors in the hippocampus have different pharmacological properties. *Neuron*, **1**(7), pp. 585–591.

Edelmann, E. and Lessmann, V. (2011). Dopamine modulates spike timing-dependent plasticity and action potential properties in CA1 pyramidal neurons of acute rat hippocampal slices. *Frontiers In Synaptic Neuroscience*, **3**(Nov), pp. 1–16.

Ehrengruber, M. U. *et al.* (2001). Gene transfer into neurons from hippocampal slices: comparison of recombinant Semliki Forest Virus, adenovirus, adeno-associated virus, lentivirus, and measles virus. *Molecular and Cellular Neurosciences*, **17**(5), pp. 855–871.

Eichenbaum, H. *et al.* (1987). Cue-sampling and goal-approach correlates of hippocampal unit activity in rats performing an odor-discrimination task. *The Journal of Neuroscience*, **7**(3), pp. 716–732.

Eichenbaum, H. (2017). Prefrontal–hippocampal interactions in episodic memory. *Nature Reviews Neuroscience*, **18**(9), pp. 547–558.

Ekström, P., Honkanen, T. and Borg, B. (1992). Development of tyrosine hydroxylase-, dopamine- and dopamine β-hydroxylase-immunoreactive neurons in a teleost, the three-spined stickleback. *Journal of Chemical Neuroanatomy*, **5**(6), pp. 481–501.

Emptage, N. J. *et al.* (2003). Optical quantal analysis reveals a presynaptic component of LTP at hippocampal Schaffer-Associational synapses, **38**(5), pp. 797–804.

Epsztein, J. *et al.* (2010). Impact of spikelets on hippocampal CA1 pyramidal cell activity during spatial exploration. *Science*, **327**(5964), pp. 474–477.

Erdtsieck-Ernste, B. H., Feenstra, M. G. and Boer, G. J. (1991). Pre- and postnatal developmental changes of adrenoceptor subtypes in rat brain. *Journal of Neurochemistry*, **57**(3), pp. 897–903.

Espinoza, C. *et al.* (2018). Parvalbumin+ interneurons obey unique connectivity rules and establish a powerful lateral-inhibition microcircuit in dentate gyrus. *Nature Communications*, **9**(4605), pp. 1–10.

Evstratova, A. and Toth, K. (2014). Information processing and synaptic plasticity at hippocampal mossy fiber terminals. *Frontiers In Cellular Neuroscience*, **8**(28), pp. 1–12.

Ewing, A. G. *et al.* (1983). Simultaneous electrochemical and unit recording measurements: characterization of the effects of D-amphetamine and ascorbic acid on neostriatal neurons. *Brain Research*, **261**(1), pp. 101–108.

Faber, E. S. L. *et al.* (2008). Modulation of SK channel trafficking by beta adrenoceptors enhances excitatory synaptic transmission and plasticity in the amygdala. *The Journal of Neuroscience*, **28**(43), pp. 10803–10813.

Fanselow, M. S. and Dong, H.-W. (2010). Are the dorsal and ventral hippocampus functionally distinct structures? *Neuron*, **65**(1), pp. 7–19.

Fastenrath, M. *et al.* (2014). Dynamic modulation of amygdala–hippocampal connectivity by emotional arousal. *The Journal of Neuroscience*, **34**(42), pp. 13935–13947.

Feder, R. and Ranck, J. B. J. (1973). Studies on single neurons in dorsal hippocampal formation and septum in unrestrained rats. II. Hippocampal slow waves and theta cell

firing during bar pressing and other behaviors. *Experimental Neurology*, **41**(2), pp. 532–555.

Feng, J. *et al.* (2019). A genetically encoded fluorescent sensor for rapid and specific in vivo detection of norepinephrine. *Neuron*, **102**(4), pp. 745-761.

Fenno, L., Yizhar, O. and Deisseroth, K. (2011). The development and application of optogenetics. *Annual Review of Neuroscience*, **34**, pp. 389–412.

Fisher, S. A., Fischer, T. M. and Carew, T. J. (1997). Multiple overlapping processes underlying short-term synaptic enhancement. *Trends In Neurosciences*, **20**(4), pp. 170–177.

Florin-Lechner, S. M. *et al.* (1996). Enhanced norepinephrine release in prefrontal cortex with burst stimulation of the locus coeruleus. *Brain Research*, **742**(1-2), pp. 89–97.

Fogelson, A. L. and Zucker, R. S. (1985). Presynaptic calcium diffusion from various arrays of single channels. Implications for transmitter release and synaptic facilitation. *Biophysical Journal*, **48**(6), pp. 1003–1017.

Foote, S. L., Aston-Jones, G. and Bloom, F. E. (1980). Impulse activity of locus coeruleus neurons in awake rats and monkeys is a function of sensory stimulation and arousal Neurobiology : *Proceedings of The National Academy of Sciences of The United States of America*, **77**(5), pp. 3033–3037.

Frerking, M. *et al.* (2001). Kainate receptors depress excitatory synaptic transmission at CA3-CA1 synapses in the hippocampus via a direct presynaptic action. *The Journal of Neuroscience*, **21**(9), pp. 2958–2966.

Freund, T. F. and Antal, M. (1988). GABA-containing neurons in the septum control inhibitory interneurons in the hippocampus. *Nature*, **336**(6195), pp. 170–173.

Frotscher, M. and Leranth, C. (1985). Cholinergic innervation of the rat hippocampus as revealed by choline acetyltransferase immunocytochemistry: a combined light and electron microscopic study. *The Journal of Comparative Neurology*, **239**(2), pp. 237–246.

Fuenzalida, M., Fernandez de Sevilla, D. and Buno, W. (2007). Changes of the EPSP waveform regulate the temporal window for spike-timing-dependent plasticity. *The Journal of Neuroscience*, **27**(44), pp. 11940–11948.

Fyhn, M. *et al.* (2004). Spatial representation in the entorhinal cortex. *Science*, **305**(5688), pp. 1258–1264.

Gage, F. H., Thompson, R. G. and Valdes, J. J. (1978). Endogenous norepinephrine and serotonin within the hippocampal formation during development and recovery from

septal hyperactivity. *Pharmacology, Biochemistry and Behavior*, **9**(3), pp. 359–367.

Gainetdinov, R. R. *et al.* (2004). Desensitization of G protein-coupled receptors and neuronal functions. *Annual Review of Neuroscience*, **27**, pp. 107–144.

Gangadharan, G. *et al.* (2016). Medial septal GABAergic projection neurons promote object exploration behavior and type 2 theta rhythm. *Proceedings of The National Academy of Sciences of The United States of America*, **113**(23), pp. 6550–6555.

Gassmann, M. and Bettler, B. (2012). Regulation of neuronal $GABA_B$ receptor functions by subunit composition. *Nature Reviews Neuroscience*, **13**(6), pp. 380–394.

Geiger, R. P. and Jonas, P. (2000). Dynamic control of presynaptic Ca^{2+} inflow by fast-inactivating K^+ channels in hippocampal mossy fiber boutons. *Neuron*, **28**(3), pp. 927–939.

Gelinas, J. N. *et al.* (2007). ERK and mTOR signaling couple beta-adrenergic receptors to translation initiation machinery to gate induction of protein synthesis-dependent long-term potentiation. *The Journal of Biological Chemistry*, **282**(37), pp. 27527–27535.

Gelinas, J. N. and Nguyen, P. V. (2005). B-adrenergic receptor activation facilitates induction of a protein synthesis-dependent late phase of long-term potentiation. *The Journal of Neuroscience*, **25**(13), pp. 3294–3303.

Gewirtz, J. C., McNish, K. A. and Davis, M. (2000). Is the hippocampus necessary for contextual fear conditioning? *Behavioural Brain Research*, **110**(1–2), pp. 83–95.

Gilzenrat, M. S. *et al.* (2010). Pupil diameter tracks changes in control state predicted by the adaptive gain theory of locus coeruleus function. *Cognitive, Affective and Behavioral Neuroscience*, **10**(2), pp. 252–269.

Girault, J. A. and Greengard, P. (2004). The neurobiology of dopamine signaling. *Archives Of Neurology*, **61**(5), pp. 641–644.

Goh, J. J. and Manahan-Vaughan, D. (2013). Hippocampal long-term depression in freely behaving mice requires the activation of beta-adrenergic receptors. *Hippocampus*, **23**(12), pp. 1299–1308.

Goldberg, E. M. *et al.* (2008). K^+ channels at the axon initial segment dampen near-threshold excitability of neocortical fast-spiking GABAergic interneurons. *Neuron*, **58**(3), pp. 387–400.

Goldenstein, B. L. *et al.* (2009). Regulator of G protein signaling protein suppression of Gαo protein-mediated α2A adrenergic receptor inhibition of mouse hippocampal CA3 epileptiform activity. *Molecular Pharmacology*, **75**(5), pp. 1222–1230.

Goldman, M. S., Maldonado, P. and Abbott, L. F. (2002). Redundancy reduction and sustained firing with stochastic depressing synapses. *The Journal of Neuroscience*, **22**(2), pp. 584–591.

Gonzalez, J. *et al.* (2016). Long-term potentiation at temporoammonic path-CA1 synapses in freely moving rats. *Frontiers in Neural Circuits*, **10**(2), pp. 1–13.

Gray, R. and Johnston, D. (1987). Noradrenaline and β-adrenoceptor agonists increase activity of voltage-dependent calcium channels in hippocampal neurons. *Nature*, **327**, pp. 620–622.

Grella, S. L. *et al.* (2019). Locus coeruleus phasic, but not tonic, activation initiates global remapping in a familiar environment. *The Journal of Neuroscience*, **39**(3), pp. 445–455.

Van Groen, T. and Wyss, J. M. (1990). Extrinsic projections from area CA1 of the rat hippocampus: Olfactory, cortical, subcortical, and bilateral hippocampal formation projections. *The Journal of Comparative Neurology*, **302**(3), pp. 515–528.

Grosse, G. *et al.* (2000). Expression of Kv1 potassium channels in mouse hippocampal primary cultures: development and activity-dependent regulation. *The Journal of Neuroscience*, **20**(5), pp. 1869–82.

Grzelka, K. *et al.* (2017). Noradrenaline modulates the membrane potential and holding current of medial prefrontal cortex pyramidal neurons via β1-adrenergic receptors and HCN channels. *Frontiers In Cellular Neuroscience*, **11**(341), pp. 1–22.

Guan, D. *et al.* (2006). Expression and biophysical properties of Kv1 channels in supragranular neocortical pyramidal neurones. *The Journal of Physiology*, **571**(2), pp. 371–389.

Gundlfinger, A. *et al.* (2007). Adenosine modulates transmission at the hippocampal mossy fibre synapse via direct inhibition of presynaptic calcium channels. *The Journal of Physiology*, **582**(1), pp. 263–277.

Gundlfinger, A. *et al.* (2010). Natural spike trains trigger short- and long-lasting dynamics at hippocampal mossy fiber synapses in rodents. *PloS ONE*, **5**(4), pp. 1–9.

Guo, N.-N. and Li, B.-M. (2007). Cellular and subcellular distributions of β1- and β2-Adrenoceptors in the CA1 and CA3 regions of the rat hippocampus. *Neuroscience*, **146**(1), pp. 298–305.

Guzman, S. J. *et al.* (2016). Synaptic mechanisms of pattern completion in the hippocampal CA3 network. *Science*, **353**(6304), pp. 1117–1123.

Haas, H. L. and Konnerth, A. (1983). Histamine and noradrenaline decrease calcium-activated potassium conductance in hippocampal pyramidal cells. *Nature*, 302, pp. 432–

434.

Haas, H. L. and Rose, G. M. (1987). Noradrenaline blocks potassium conductance in rat dentate gyrus cells in vitro. *Neuroscience Letters*, **78**(2), pp. 171–174.

Hafting, T. *et al.* (2005). Microstructure of a spatial map in the entorhinal cortex. *Nature*, **436**(7052), pp. 801–806.

Hagena, H., Hansen, N. and Manahan-Vaughan, D. (2016). β-adrenergic control of hippocampal function: Subserving the choreography of synaptic information storage and memory. *Cerebral Cortex*, **26**, pp. 1349–1364.

Hagena, H. and Manahan-Vaughan, D. (2011). Learning-facilitated synaptic plasticity at CA3 mossy fiber and commissural-associational synapses reveals different roles in information processing. *Cerebral Cortex*, **21**(11), pp. 2442–2449.

Hagena, H. and Manahan-Vaughan, D. (2012). Learning-facilitated long-term depression and long-term potentiation at mossy fiber-CA3 synapses requires activation of β-adrenergic receptors. *Frontiers In Integrative Neuroscience*, **6**(23), pp. 1–11.

Hammond, R. S. *et al.* (2006). Small-conductance Ca^{2+}-activated K^{+} channel type 2 (SK2) modulates hippocampal learning, memory, and synaptic plasticity. *The Journal of Neuroscience*, **26**(6), pp. 1844–1853.

Harris, E. W. and Cotman, C. W. (1986). Long-term potentiation of guinea pig mossy fiber responses is not blocked by N-methyl D-aspartate antagonists. *Neuroscience Letters*, **70**(1), pp. 132–137.

Harris, E. W., Ganong, A. H. and Cotman, C. W. (1984). Long-term potentiation in the hippocampus involves activation of N-methyl-D-aspartate receptors. *Brain Research*, **323**(1), pp. 132–137.

Hasselmo, M. E. *et al.* (1997). Noradrenergic suppression of synaptic transmission may influence cortical signal-to-noise ratio. *The Journal of Neurophysiology*, **77**(6), pp. 3326–3339.

Hausdorff, W. P., Caron, M. G. and Lefkowitz, R. J. (2019). Turning off the signal: desensitization of B-adrenergic receptor function. *The FASEB Journal*, **4**(11), pp. 2881–2889.

Hayat, H. *et al.* (2019). Locus-coeruleus norepinephrine activity gates sensory-evoked awakenings from sleep. *BioRxiv Neuroscience*.

Hebb, D. O. (1949). *The organization of behaviour: A neuropsychological theory*. New York: Wiley.

Heginbotham, L. and Dunwiddie, T. (1991). Long-term increases in the evoked population spike in the CA1 region of rat hippocampus induced by beta-adrenergic receptor activation. *The Journal of Neuroscience*, **11**(8), pp. 2519–2527.

Heien, M. L. A. V *et al.* (2005). Real-time measurement of dopamine fluctuations after cocaine in the brain of behaving rats. *Proceedings of The National Academy of Sciences of The United States of America*, **102**(29), pp. 10023–10028.

Henke, P. G. (1990). Hippocampal pathway to the amygdala and stress ulcer development. *Brain Research Bulletin*, **25**(5), pp. 691–695.

Hennig, M. H. (2013). Theoretical models of synaptic short term plasticity. *Frontiers In Computational Neuroscience*, **7**(45), pp. 1–10.

Henze, D. A., Wittner, L. and Buzsáki, G. (2002). Single granule cells reliably discharge targets in the hippocampal CA3 network *in vivo*. *Nature Neuroscience*, **5**(8), pp. 790–795.

Hernandez, R. V *et al.* (2005). Differences in the magnitude of long-term potentiation produced by theta burst and high frequency stimulation protocols matched in stimulus number. *Brain Research Protocols*, **15**(1), pp. 6–13.

Hillman, K. L. *et al.* (2005). Adrenergic receptor characterization of CA1 hippocampal neurons using real time single cell RT-PCR. *Molecular Brain Research*, **139**(2), pp. 267–276.

Hillman, K. L. *et al.* (2009). Alpha-1A adrenergic receptor activation increases inhibitory tone in CA1 hippocampus. *Epilepsy Research*, **84**(2–3), pp. 97–109.

Hillman, K. L., Doze, V. A. and Porter, J. E. (2005). Functional characterization of the beta-adrenergic receptor subtypes expressed by CA1 pyramidal cells in the rat hippocampus. *The Journal of Pharmacology and Experimental Therapeutics*, **314**(2), pp. 561–567.

Hillman, K. L., Doze, V. A. and Porter, J. E. (2007). α1A-adrenergic receptors are functionally expressed by a subpopulation of Cornu Ammonis 1 interneurons in rat hippocampus. *The Journal of Pharmacology and Experimental Therapeutics,* **321**(3), pp. 1062–1068.

Hiratani, N. and Fukai, T. (2014a). Interplay between short- and long-term plasticity in cell-assembly formation. *PloS ONE*, **9**(7), pp. 1–16.

Hirschberg, S. *et al.* (2017). Functional dichotomy in spinal- vs prefrontal-projecting locus coeruleus modules splits descending noradrenergic analgesia from ascending aversion and anxiety in rats. *eLife*, **6**, pp. 1–26.

Hjorth-Simonsen, A. and Jeune, B. (1972). Origin and termination of the hippocampal perforant path in the rat studied by silver impregnation. *The Journal of Comparative Neurology*, **144**(2), pp. 215–232.

Hladuvka, J. and Grôller, E. (2002). Exploiting the Hessian matrix for content-based retrieval of volume-data features. *The Visual Computer*, **18**(4), pp. 207–217.

Hock, B. J. J. and Bunsey, M. D. (1998). Differential effects of dorsal and ventral hippocampal lesions. *The Journal of Neuroscience*, **18**(17), pp. 7027–7032.

Hoffman, D. A. *et al.* (1997). K^+ channel regulation of signal propagation in dendrites of hippocampal pyramidal neurons. *Nature*, **387**(6636), pp. 869–875.

Holets, V. R. *et al.* (1988). Locus coeruleus neurons in the rat containing neuropeptide Y, tyrosine hydroxylase or galanin and their efferent projections to the spinal cord, cerebral cortex and hypothalamus. *Neuroscience*, **24**(3), pp. 893–906.

Hoover, W. B. and Vertes, R. P. (2007). Anatomical analysis of afferent projections to the medial prefrontal cortex in the rat. *Brain Structure and Function*, **212**(2), pp. 149–179.

Hopkins, W. F. and Johnston, D. (1984). Frequency-dependent noradrenergic modulation of long-term potentiation in the hippocampus. *Science*, **226**(4672), pp. 350–352.

Hopkins, W. F. and Johnston, D. (1988). Noradrenergic enhancement of long-term potentiation at mossy fiber synapses in the hippocampus. *The Journal of Neurophysiology*, **59**(2), pp. 667–687.

Houghton, C. (2016). The dentate gyrus and the hilar revised. *Behavioral and Brain Sciences*, **39**, pp. 1–6.

Howorth, P. W., Teschemacher, A. G. and Pickering, A. E. (2009). Retrograde adenoviral vector targeting of nociresponsive pontospinal noradrenergic neurons in the rat *in vivo*. *The Journal of Comparative Neurology*, **512**(2), pp. 141–157.

Hu, H. *et al.* (2007). Emotion enhances learning via norepinephrine regulation of AMPA-receptor trafficking. *Cell*, **131**(1), pp. 160–173.

Hu, H., Gan, J. and Jonas, P. (2014). Interneurons. Fast-spiking, parvalbumin(+) GABAergic interneurons: from cellular design to microcircuit function. *Science*, **345**(6196), pp. 1–15.

Huang, H. P. *et al.* (2012). Physiology of quantal norepinephrine release from somatodendritic sites of neurons in locus coeruleus. *Frontiers In Molecular Neuroscience*, **5**(29), pp. 1–5.

Huang, H. Bin *et al.* (1999). Characterization of the inhibition of protein phosphatase-1 by DARPP-32 and inhibitor-2. *The Journal of Biological Chemistry*, **274**(12), pp. 7870–7878.

Huang, R. and Hertz, L. (1995). Noradrenaline-induced stimulation of glutamine metabolism in primary cultures of astrocytes. *Journal of Neuroscience Research*, **41**(5), pp. 677–683.

Huang, Y. Y. and Kandel, E. R. (1996). Modulation of both the early and the late phase of mossy fiber LTP by the activation of β-adrenergic receptors. *Neuron*, **16**(3), pp. 611–617.

Huang, Y. Y., Li, X. C. and Kandel, E. R. (1994). CAMP Contributes to mossy fiber LTP by initiating both a covalently mediated early phase and macromolecular synthesis-dependent late phase. *Cell*, **79**(1), pp. 69–79.

Huerta, P. T. and Lisman, J. E. (1995). Bidirectional synaptic plasticity induced by a single burst during cholinergic theta oscillation in CA1 in vitro. *Neuron*, **15**(5), pp. 1053–1063.

Hughes, K. R. (1965). Dorsal and ventral hippocampus lesions and maze learning: influence of preoperative environment. *Canadian Journal of Psychology*, **19**(4), pp. 325–332.

Humpel, C. (2015). Neuroscience forefront review organotypic brain slice cultures: A review. *Neuroscience*, **305**, pp. 86–98.

Hurley, L. M., Devilbiss, D. M. and Waterhouse, B. D. (2004). A matter of focus: monoaminergic modulation of stimulus coding in mammalian sensory networks. *Current Opinion In Neurobiology*, **14**(4), pp. 488–495.

Huttunen, P. (1991). Microdialysis of extracellular noradrenaline in the hippocampus of the rat after long-term alcohol intake. *Brain Research*, **560**(1–2), pp. 225–228.

Hwang, D. Y. *et al.* (2001). A high-efficiency synthetic promoter that drives transgene expression selectively in noradrenergic neurons. *Human Gene Therapy*, **12**(14), pp. 1731–1740.

Insel, P. A. *et al.* (1983). Time-dependent decreases in binding affinity of agonists for beta-adrenergic receptors of intact S49 lymphoma cells. A mechanism of desensitization. *Journal of Biological Chemistry*, **258**(22), pp. 13597–13605.

Isaac, J. T. R., Nicoll, R. A. and Malenka, R. C. (1995). Evidence for silent synapses: Implications for the expression of LTP. *Neuron*, **15**, pp. 427–434.

Ishizuka, N., Cowan, W. M. and Amaral, D. G. (1995). A quantitative analysis of the

dendritic organization of pyramidal cells in the rat hippocampus. *The Journal of Comparative Neurology*, **362**(1), pp. 17–45.

Ishizuka, N., Weber, J. and Amaral, D. G. (1990). Organization of intrahippocampal projections originating from CA3 pyramidal cells in the rat. *The Journal of Comparative Neurology*, **295**(4), pp. 580–623.

Ito, H. T. and Schuman, E. M. (2007). Frequency-dependent gating of synaptic transmission and plasticity by dopamine. *Frontiers In Neural Circuits*, **1**(1), pp. 1–13.

Ito, H. T. and Schuman, E. M. (2012). Functional division of hippocampal area CA1 via modulatory gating of entorhinal cortical inputs. *Hippocampus*, **22**(2), pp. 372–387.

Jackman, S. L. *et al.* (2016). The calcium sensor synaptotagmin 7 is required for synaptic facilitation. *Nature*, **529**(7584), pp. 88–91.

Jackman, S. L. and Regehr, W. G. (2017). The mechanisms and functions of synaptic facilitation. *Neuron*, **94**(3), pp. 447–464.

Jay, T. M., Glowinski, J. and Thierry, A. M. (1989). Selectivity of the hippocampal projection to the prelimbic area of the prefrontal cortex in the rat. *Brain Research*, **505**(2), pp. 337–340.

Jay, T. M. and Witter, M. P. (1991). Distribution of hippocampal CA1 and subicular efferents in the prefrontal cortex of the rat studied by means of anterograde transport of Phaseolus vulgaris-leucoagglutinin. *The Journal of Comparative Neurology*, **313**(4), pp. 574–586.

Jędrzejewska-Szmek, J. *et al.* (2017). β-adrenergic signaling broadly contributes to LTP induction. *PLoS Computational Biology*, **13**(7), pp. 1–32.

Ji, J., Zhang, X. and Li, B. (2003). Deficient spatial memory induced by blockade of beta-adrenoceptors in the hippocampal CA1 region, **117**(6), pp. 1378–1384.

Jiang, X. *et al.* (2015). Principles of connectivity among morphologically defined cell types in adult neocortex. *Science*, **350**(6264), pp. 1–12.

Jin, J. and Maren, S. (2015). Prefrontal-hippocampal interactions in memory and emotion. *Frontiers In Systems Neuroscience*, **9**(170), pp. 1–8.

Jing, M. *et al.* (2018). A genetically encoded fluorescent acetylcholine indicator for in vitro and in vivo studies. *Nature Biotechnology*, **36**(8), pp. 726–737.

Johnston D. and Amaral, D. G. (1998). *Hippocampus*. In: Shepherd G.M., (ed.). *The synaptic organization of the brain*. New York: Oxford University Press, pp. 417–458

Jones, M. W. and Wilson, M. A. (2005). Theta rhythms coordinate hippocampal-

prefrontal interactions in a spatial memory task. *PLoS Biology*, **3**(12), pp. 1–13.

Jung, M. W. and McNaughton, B. L. (1993). Spatial selectivity of unit activity in the hippocampal granular layer. *Hippocampus*, **3**(2), pp. 165–182.

Jung, M. W., Wiener, S. I. and McNaughton, B. L. (1994). Comparison of spatial firing characteristics of units in dorsal and ventral hippocampus of the rat. *The Journal of Neuroscience*, **14**(12), pp. 7347–7356.

Jurgens, Chris W. D. *et al.* (2005). Adrenergic receptor modulation of hippocampal CA3 network activity. *Epilepsy Research*, **66**, pp. 117–128.

Jurgens, Chris W. D. *et al.* (2005). B1 adrenergic receptor-mediated enhancement of hippocampal CA3 network activity. *The Journal of Pharmacology and Experimental Therapeutics*, **314**(2), pp. 552–560.

Jurgens, Chris W. D. *et al.* (2007). Alpha2A adrenergic receptor activation inhibits epileptiform activity in the rat hippocampal CA3 region. *Molecular Pharmacology*, **71**(6), pp. 1572–81.

Kaehler, S. T., Singewald, N. and Philippu, A. (1999). Dependence of serotonin release in the locus coeruleus on dorsal raphe neuronal activity. *Naunyn-Schmiedeberg's Archives of Pharmacology*, **359**(5), pp. 386–393.

Kajiwara, R. *et al.* (2008). Convergence of entorhinal and CA3 inputs onto pyramidal neurons and interneurons in hippocampal area CA1-an anatomical study in the rat. *Hippocampus*, **18**(3), pp. 266–280.

Kandel, E. R. and Spencer, W. A. (1961). Electrophysiology of hippocampal neurons. II. After-potentials and repetitive firing. *The Journal of Neurophysiology*, **24**, pp. 243–259.

Kane, G. A. *et al.* (2017). Increased locus coeruleus tonic activity causes disengagement from a patch-foraging task. *Cognitive, Affective and Behavioral Neuroscience*, **17**(6), pp. 1073–1083.

Kaski, S. and Kohonen, T. (1994). Winner-take-all networks for physiological models of competitive learning. *Neural Networks*, **7**(6–7), pp. 973–984.

Katagiri, H., Tanaka, K. and Manabe, T. (2001). Requirement of appropriate glutamate concentrations in the synaptic cleft for hippocampal LTP induction. *European Journal of Neuroscience*, **14**(3), pp. 547–553.

Katsuki, H., Izumi, Y. and Zorumski, C. F. (1997). Noradrenergic regulation of synaptic plasticity in the hippocampal CA1 region. *The Journal of Neurophysiology*, **77**(6), pp. 3013–3020.

Kebschull, J. M. *et al.* (2016). High-throughput mapping of single-neuron projections by sequencing of barcoded RNA. *Neuron*, **91**(5), pp. 975–987.

Keithley, R. B. *et al.* (2011). Higher sensitivity dopamine measurements with faster-scan cyclic voltammetry. *Analytical Chemistry*, **83**(9), pp. 3563–3571.

Kemp, A. and Manahan-Vaughan, D. (2004). Hippocampal long-term depression and long-term potentiation encode different aspects of novelty acquisition. *Proceedings of The National Academy of Sciences of The United States of America*, **101**(21), pp. 8192–8197.

Kemp, A. and Manahan-Vaughan, D. (2008). The hippocampal CA1 region and dentate gyrus differentiate between environmental and spatial feature encoding through long-term depression. *Cerebral Cortex*, **18**(4), pp. 968–977.

Kempadoo, K. A. *et al.* (2016). Dopamine release from the locus coeruleus to the dorsal hippocampus promotes spatial learning and memory. *Proceedings of The National Academy of Sciences of The United States of America*, **113**(51), pp. 14835–14840.

Kennedy, P. J. and Shapiro, M. L. (2004). Retrieving Memories via Internal Context Requires the Hippocampus. *The Journal of Neuroscience*, **24**(31), pp. 6979–6985.

Kesner, R. P. (2007). Behavioral functions of the CA3 subregion of the hippocampus. *Learning and Memory*, **14**(11), pp. 771–781.

King, B. *et al.* (2015). IKCa channels are a critical determinant of the slow AHP in CA1 pyramidal neurons. *Cell Reports*, **11**(2), pp. 175–182.

Kinnavane, L. *et al.* (2016). Detecting and discriminating novel objects: The impact of perirhinal cortex disconnection on hippocampal activity patterns, **26**(11), pp. 1393–1413.

von Kitzing, E., Jonas, P. and Sakmann, B. (1994). Quantal analysis of excitatory postsynaptic currents at the hippocampal mossy fiber-CA3 pyramidal cell synapse. *Advances in Second Messenger and Phosphoprotein Research*, **29**, pp. 235–260.

Kjelstrup, K. B. *et al.* (2008). Finite scale of spatial representation in the hippocampus. *Science*, **321**(5885), pp. 140–143.

Klausberger, T. *et al.* (2003). Brain-state- and cell-type-specific firing of hippocampal interneurons *in vivo*. *Nature*, **421**(6925), pp. 844–848.

Klausberger, T. *et al.* (2004). Spike timing of dendrite-targeting bistratified cells during hippocampal network oscillations *in vivo*. *Nature Neuroscience*, **7**(1), pp. 41–47.

Klausberger, T. and Somogyi, P. (2008). Neuronal diversity and temporal dynamics : the unity of hippocampal circuit operations. *Science*, **321**(5885), pp. 53–57.

Knierim, J. J., Lee, I. and Hargreaves, E. L. (2006). Hippocampal place cells: Parallel input streams, subregional processing, and implications for episodic memory. *Hippocampus*, **16**(9), pp. 755–764.

Kobayashi, K. and Poo, M. (2004). Spike train timing-dependent associative modification of hippocampal CA3 recurrent synapses by mossy fibers. *Neuron*, **41**(3), pp. 445–454.

Kohara, K. *et al.* (2014). Cell type-specific genetic and optogenetic tools reveal hippocampal CA2 circuits. *Nature Neuroscience*, **17**(2):269–279.

Kole, M. H. P. *et al.* (2008). Action potential generation requires a high sodium channel density in the axon initial segment. *Nature Neuroscience*, **11**(2), pp. 178–186.

Konnerth, A. *et al.* (1990). Voltage sensitivity of NMDA-receptor mediated postsynaptic currents. *Experimental Brain Research*, **81**(1), pp. 209–212.

Kowalski, J. *et al.* (2016). Intrinsic membrane properties determine hippocampal differential firing pattern *in vivo* in anesthetized rats, **26**(5), pp. 668–682.

Kubota, D. *et al.* (2003). Endogenous waves in hippocampal slices. *The Journal of Neurophysiology*, **89**(1), pp. 81–89.

Kügler, S., Kilic, E. and Bähr, M. (2003). Human synapsin 1 gene promoter confers highly neuron-specific long-term transgene expression from an adenoviral vector in the adult rat brain depending on the transduced area. *Gene Therapy*, **10**(4), pp. 337–347.

Kupfermann, I. (1979). Modulatory actions of neurotransmitters. *Annual Review of Neuroscience*, **2**, pp. 447–465.

Kuzhikandathil, E. V, Oxford, G. S. and Carolina, N. (2002). Classic D1 dopamine receptor antagonist r-(+)-7-chloro-8-benzazepine hydrochloride (SCH23390) directly inhibits G Protein-coupled inwardly rectifying potassium channels, **62**(1), pp. 119–126.

Kwon, O. *et al.* (2018). Schaffer collateral inputs to CA1 excitatory and inhibitory neurons follow different connectivity rules. *The Journal of Neuroscience*, **38**(22), pp. 5140–5152.

Lacaille, J. C. and Schwartzkroin, P. A. (1988). Intracellular responses of rat hippocampal granule cells *in vitro* to discrete applications of norepinephrine. *Neuroscience Letters*, **89**(2), pp. 176–181.

Lacin, E. *et al.* (2016). Construction of cell-based neurotransmitter fluorescent engineered reporters (CNiFERs) for optical detection of neurotransmitters *in vivo*. *The Journal of Visualized Experiments*, **111**, pp. 1–13.

Lancaster, B. *et al.* (2001). Interaction between synaptic excitation and slow

afterhyperpolarization current in rat hippocampal pyramidal cells. *The Journal of Physiology*, **536**(3), pp. 809–823.

Larson, J. and Lynch, G. (1986). Induction of synaptic potentiation in hippocampus by patterned stimulation involves two events. *Science*, **232**(4753), pp. 985–988.

Latuske, P. *et al.* (2017). Hippocampal remapping and its entorhinal origin. *Frontiers In Behavioral Neuroscience*, **11**(253), pp. 1–13.

Lazarov, E. *et al.* (2018). An axon initial segment is required for temporal precision in action potential encoding by neuronal populations. *Science Advances*, **4**(11), pp. 1–14.

Leão, R. M. and Von Gersdorff, H. (2002). Noradrenaline increases high-frequency firing at the calyx of Held synapse during development by inhibiting glutamate release. *Journal of Neurophysiology*, **87**(5), pp. 2297–2306.

Lee, A. K. and Wilson, M. A. (2002). Memory of sequential experience in the hippocampus during slow wave sleep. *Neuron*, **36**(6), pp. 1183–1194.

Lee, I. *et al.* (2004). Comparison of population coherence of place cells in hippocampal subfields CA1 and CA3. *Nature*, **430**(6998), pp. 456–459.

Lemon, N. *et al.* (2009). Locus coeruleus activation facilitates memory encoding and induces hippocampal LTD that depends on β-Adrenergic receptor activation. *Cerebral Cortex*, **19**(12), pp. 2827–2837.

Leterrier, C. (2018). The axon initial segment: An updated viewpoint. *The Journal of Neuroscience*, **38**(9), pp. 2135–2145.

Leutgeb, J. K. *et al.* (2007). Pattern separation in the dentate gyrus and CA3 of the hippocampus. *Science*, **315**(5814), pp. 961–966.

Leutgeb, S. *et al.* (2005). Independent codes for spatial and episodic memory in hippocampal neuronal ensembles. *Science*, **309**(5734), pp. 619–623.

Leutgeb, S. and Leutgeb, J. K. (2007). Pattern separation, pattern completion, and new neuronal codes within a continuous CA3 map. *Learning and Memory*, **14**, pp. 745–757.

Li, X. G. *et al.* (1992). Axonal and dendritic arborization of an intracellularly labeled chandelier cell in the CA1 region of rat hippocampus. *Experimental Brain Research*. Germany, **90**(3), pp. 519–525.

Li, X. G. *et al.* (1994). The hippocampal CA3 network: an *in vivo* intracellular labeling study. *The Journal of Comparative Neurology*, **339**(2), pp. 181–208.

Li, Y. *et al.* (2016). Retrograde optogenetic characterization of the pontospinal module of the locus coeruleus with a canine adenoviral vector. *Brain Research*, **1641**, pp. 274–

290.

Liggett, S. B. *et al.* (1993). Structural basis for receptor subtype-specific regulation revealed by a chimeric β3/β2-adrenergic receptor. *Proceedings of The National Academy of Sciences of The United States of America*, **90**(8), pp. 3665–3669.

Lin, J. Y. *et al.* (2009). Characterization of engineered channelrhodopsin variants with improved properties and kinetics. *Biophysical Journal*, **96**(5), pp. 1803–1814.

Lin, J. Y. (2011). A user's guide to channelrhodopsin variants: features, limitations and future developments. *Experimental Physiology*, **96**(1), pp. 19–25.

Lin, M. T. *et al.* (2008). SK2 channel plasticity contributes to LTP at Schaffer collateral-CA1 synapses. *Nature Neuroscience*, **11**(2), pp. 170–177.

Lin, M. T. *et al.* (2010). Coupled activity-dependent trafficking of synaptic SK2 channels and AMPA receptors. *The Journal of Neuroscience*, **30**(35), pp. 11726–11734.

Lin, Y. W. *et al.* (2003). Enhancement of associative long-term potentiation by activation of β-adrenergic receptors at CA1 synapses in rat hippocampal slices. *The Journal of Neuroscience*, **23**(10), pp. 4173–4181.

Lisman, J. (1989). A mechanism for the Hebb and the anti-Hebb processes underlying learning and memory. *Proceedings of The National Academy of Sciences of The United States of America*, **86**(23), pp. 9574–9578.

Lisman, J. E. (1997). Bursts as a unit of neural information: making unreliable synapses reliable. *Trends In Neurosciences*, **20**(1), pp. 38–43.

Lisman, J. E. (1999). Relating hippocampal circuitry to function: recall of memory sequences by reciprocal dentate-CA3 interactions. *Neuron*, **22**(2), pp. 233–242.

Lisman, J. E. and Grace, A. A. (2005). The hippocampal-VTA loop: Controlling the entry of information into long-term memory. *Neuron*, **46**(5), pp. 703–713.

Lisman, J. E. and Idiart, M. A. P. (1995). Storage of 7 +/- 2 short-term memories in oscillatory subcycles. *Science*, **267**(5203), pp. 1512–1515.

Lisman, J., Schulman, H. and Cline, H. (2002). The molecular basis of CaMKII function in synaptic and behavioural memory. *Nature Reviews Neuroscience*, **3**(3), pp. 175–190.

Liu, Y. *et al.* (2017). Adrenergic Gate Release for Spike Timing- Dependent Synaptic Potentiation. *Neuron*, **93**(2), pp. 394–408.

Lodato, S. and Arlotta, P. (2015). Generating neuronal diversity in the mammalian cerebral cortex. *Annual Review of Cell and Developmental Biology*, **31**, pp. 699–720.

Lohse, J. *et al.* (1990). Pathways of rapid receptor desensitization their contributions. *Biological Chemistry*, **265**(6), pp. 3202–3209.

Lohse, M. J. *et al.* (1996). Mechanisms of beta-adrenergic receptor desensitization: From molecular biology to heart failure. *Basic Research In Cardiology*, **91**(2), pp. 29–34.

Lorente de Nó, R. (1949). *Cerebral cortex: architecture, intracortical connections, motor projections. In:* J. F. Fulton, (ed).. *Physiology of the Nervous System*. New York: Oxford University Press, pp. 288–312.

Lossi, L. *et al.* (2009). Cell death and proliferation in acute slices and organotypic cultures of mammalian CNS. *Progress in Neurobiology*, **88**(4), pp. 221–245.

Lossi, L. and Merighi, A. (2018). The use of *ex vivo* rodent platforms in neuroscience translational research with attention to the 3Rs philosophy. *Frontiers in Veterinary Science*, **5**(164), pp. 1–14.

Loughlin, S. E., Foote, S. L. and Bloom, F. E. (1986). Efferent projections of nucleus locus coeruleus: Topographic organization of cells of origin demonstrated three-dimensional reconstruction. *Neuroscience*, **18**(2), pp. 291–306.

Loy, R. *et al.* (1980). Noradrenergic innervation of the adult rat hippocampal formation. Journal of Comparative Neurology, **186**(4), pp. 699–710.

Lugaro, E. (1898). Le resistenze nell'evoluzione della vita. *Rivista Moderna Di Cultura*, **1**, pp. 29–60.

Lugaro, E. (1906). *I problemi odierni della psichiatria*. Milan: Sandron.

Lugaro, E. (1909). *Modern problems in psychiatry*. (Translated by Orr, D. and Rows, R. G .). Manchester: The University Press.

Luján, R., Maylie, J. and Adelman, J. P. (2009). New sites of action for GIRK and SK channels. *Nature Reviews Neuroscience*, **10**(7), pp. 475–480.

Lüscher, C. *et al.* (1997). G protein-coupled inwardly rectifying K^+ channels (GIRKs) mediate postsynaptic but not presynaptic transmitter actions in hippocampal neurons. *Neuron*, **19**(3), pp. 687–695.

Lüscher, C. and Slesinger, P. A. (2010). Emerging roles for G protein-gated inwardly rectifying potassium (GIRK) channels in health and disease. *Nature Reviews Neuroscience*, **11**(5), p. 301–315.

Lynch, G. *et al.* (1983). Intracellular injections of EGTA block induction of hippocampal long-term potentiation. *Nature*, 305(5936), pp. 719–721.

Lynch, M. A. and Bliss, T. V. P. (1986). Noradrenaline modulates the release of

[14C]glutamate from dentate but not from CA1/CA3 slices of rat hippocampus. *Neuropharmacology*, **25**(5), pp. 493–498.

Ma, P. M. (1994). Catecholaminergic systems in the zebrafish. II. Projection pathways and pattern of termination of the locus coeruleus. *The Journal of Comparative Neurology*, **344**(2), pp. 256–269.

MacVicar, B. A. and Dudek, F. E. (1979). Intracellular recordings from hippocampal CA3 pyramidal cells during repetitive activation of the mossy fibers *in vitro*. *Brain Research*. Netherlands, **168**(2), pp. 377–381.

Madison, D. V and Nicoll, R. A. (1982). Noradrenaline blocks accommodation of pyramidal cell discharge in the hippocampus. *Nature*, **299**(5884), pp. 636–638.

Madison, D. V and Nicoll, R. A. (1986). Actions of noradrenaline recorded intracellularly in rat hippocampal CA1 pyramidal neurones, *in vitro*. *The Journal of Physiology*, **372**, pp. 221–244.

Madison, D. V and Nicoll, R. A. (1988). Norepinephrine decreases synaptic inhibition in the rat hippocampus. *Brain Research*, **442**(1), pp. 131–138.

Maeda, T. and Shimizu, N. (1972). Projections ascendantes du locus coeruleus et d'autres neurones aminergiques pontiques au niveau du prosencephale du rat. *Brain Research*, **36**(1), pp. 9–35.

Magee, J. C. *et al.* (1995). Subthreshold synaptic activation of voltage-gated Ca^{2+} channels mediates a localized Ca^{2+} influx into the dendrites of hippocampal pyramidal neurons. *The Journal of Neurophysiology*, **74**(3), pp. 1335–1342.

Magee, J. C. (1998). Dendritic hyperpolarization-activated currents modify the integrative properties of hippocampal CA1 pyramidal neurons. *The Journal of Neuroscience*, **18**(19), pp. 7613–7624.

Magee, J. C. and Carruth, M. (1999). Dendritic voltage-gated ion channels regulate the action potential firing mode of hippocampal CA1 pyramidal neurons. *The Journal of Neurophysiology*, **82**(4), pp. 1895–1901.

Magee, J. C. and Johnston, D. (1995). Synaptic activation of voltage-gated channels in the dendrites of hippocampal pyramidal neurons. *Science*, **268**(5208), pp. 301–304.

Magee, J. C. and Johnston, D. (1997). A synaptically controlled , associative signal for Hebbian plasticity in hippocampal neurons. *Science*, **275**(5297), pp. 209–214.

Maingret, F. *et al.* (2008). Neurotransmitter modulation of small-conductance Ca^{2+}-activated K^+ channels by regulation of Ca^{2+} gating. *Neuron*, **59**(3), pp. 439–449.

Maity, S. *et al.* (2015). Norepinephrine triggers metaplasticity of LTP by increasing translation of specific mRNAs. *Learning and Memory*, **22**(10), pp. 499–508.

Maity, S. *et al.* (2016). Noradrenaline goes nuclear: epigenetic modifications during long-lasting synaptic potentiation triggered by activation of β-adrenergic receptors. *Neuroscience*, **594**(4), pp. 863–881.

Makino, Y. *et al.* (2011). Enhanced synaptic plasticity in mice with phosphomimetic mutation of the GluA1 AMPA receptor. *Proceedings of The National Academy of Sciences of The United States of America*, **108**(20), pp. 8450–8455.

Maletic-Savatic, M., Lenn, N. J. and Trimmer, J. S. (1995). Differential spatiotemporal expression of K^+ channel polypeptides in rat hippocampal neurons developing *in situ* and *in vitro*. *The Journal of Neuroscience*, **15**(5), pp. 3840–3851.

Mank, M. *et al.* (2008). A genetically encoded calcium indicator for chronic *in vivo* two-photon imaging. *Nature*, **5**(9), pp. 805–811.

Marder, E. (2012). Neuromodulation of neuronal circuits: Back to the future. *Neuron*, **76**(1), pp. 1–11.

Markram, H. *et al.* (1997). Regulation of synaptic efficacy by coincidence of postsynaptic APs and EPSPs. *Science*, **275**(5297), pp. 213–215.

Martin, S. J., Grimwood, P. D. and Morris, R. G. (2000). Synaptic plasticity and memory: an evaluation of the hypothesis. *Annual Review of Neuroscience*, **23**, pp. 649–711.

Martinez, C. O. *et al.* (2002). Associative long-term potentiation (LTP) among extrinsic afferents of the hippocampal CA3 region *in vivo*. *Brain Research*, **940**(1–2), pp. 86–94.

Marzo, A., Bai, J. and Otani, S. (2009). Neuroplasticity regulation by noradrenaline in mammalian brain. *Current Neuropharmacology*, **7**(4), pp. 286–295.

Masukawa, L. M., Benardo, L. S. and Prince, D. A. (1982). Variations in electrophysiological properties of hippocampal neurons in different subfields. *Brain Research*, **242**(2), pp. 341–344.

Matsuzaki, M. *et al.* (2004). Structural basis of long-term potentiation in single dendritic spines. *Nature*, **429**, pp. 761–766.

Mattis, J. *et al.* (2011). Principles for applying optogenetic tools derived from direct comparative analysis of microbial opsins. *Nature Methods*, **9**(2), p. 159–172.

Mayer, M. L., Westbrook, G. L. and Guthrie, P. B. (1984). Voltage-dependent block by Mg2+ of NMDA responses in spinal cord neurones. *Nature*, **309**(5965), pp. 261–263.

McClelland, J. L. and Goddard, N. H. (1996). Considerations arising from a

complementary learning systems perspective on hippocampus and neocortex. *Hippocampus*, **6**(6), pp. 654–665.

McClelland, J. L., McNaughton, B. L. and O'Reilly, R. C. (1995). Why there are complementary learning systems in the hippocampus and neocortex: insights from the successes and failures of connectionist models of learning and memory. *Psychological Review*, **102**(3), pp. 419–457.

McDonald, A. J. (1998). Cortical pathways to the mammalian amygdala. *Progress In Neurobiology*, **55**(3), pp. 257–332.

McEchron, M. D. *et al.* (1998). Hippocampectomy disrupts auditory trace fear conditioning and contextual fear conditioning in the rat. *Hippocampus*, **8**(6), pp. 638–646.

McGraw, D. W. *et al.* (1998). Role of βARK in long-term agonist-promoted desensitisation of the β2-adrenergic receptor. *Cellular Signalling*, **10**(3), pp. 197–204.

McHugh, T. J. and Tonegawa, S. (2009). CA3 NMDA receptors are required for the rapid formation of a salient contextual representation. *Hippocampus*, **19**(12), pp. 1153–1158.

McLean, J. R. *et al.* (2014). Widespread neuron-specific transgene expression in brain and spinal cord following synapsin promoter-driven AAV9 neonatal intracerebroventricular injection. *Neuroscience Letters*, **576**, pp. 73–78.

McMahon, D. B. T. and Barrionuevo, G. (2002). Short- and long-term plasticity of the perforant path synapse in hippocampal area CA3. *The Journal of Neurophysiology*, **88**(1), pp. 528–533.

Mcnaughton, B. L. and Morris, R. G. M. (1987). Hippocampal synaptic enhancement and information storage within a distributed memory system. *Trends In Neurosciences*, **10**(10), pp. 408–415.

Meeks, J. P. and Mennerick, S. (2007). Action potential initiation and propagation in CA3 pyramidal axons. *The Journal of Neurophysiology*, **97**(5), pp. 3460–3472.

Megias, M. *et al.* (2001). Total number and distribution of inhibitory and excitatory synapses on hippocampal CA1 pyramidal cells. *Neuroscience*, **102**(3), pp. 527–540.

Meijering, E. (2003). FeatureJ: A Java Package for Image Feature Extraction.

Meredith, R. M., Floyer-Lea, A. M. and Paulsen, O. (2003). Maturation of long-term potentiation induction rules in rodent hippocampus: Role of GABAergic inhibition. *The Journal of Neuroscience*, **23**(35), pp. 11142–11146.

Meunier, C. J., McCarty, G. S. and Sombers, L. A. (2019). Drift subtraction for fast-scan

cyclic voltammetry using double-waveform partial-least-squares regression. *Analytical Chemistry*, **91**(11), pp. 7319–7327.

Miles, R. (1990). Synaptic excitation of inhibitory cells by single CA3 hippocampal pyramidal cells of the guinea-pig *in vitro*. *The Journal of Physiology*, **428**, pp. 61–77.

Millan, M. J. (2002). Descending control of pain. *Progress In Neurobiology*, **66**(6), pp. 355–474.

Miller, R. (1989). Cortico-hippocampal interplay: Self-organizing phase-locked loops for indexing memory. *Psychobiology*, **17**(2), pp. 115–128.

Milner, B., Squire, L. R. and Kandel, E. R. (1998). Cognitive neuroscience and the study of memory. *Neuron*, **20**(3), pp. 445–468.

Milner, P. M. (1957). The cell ensemble: Mark 2. *Psychological Review*, **64**(4), pp. 242–252.

Milner, T. A. *et al.* (1998). Hippocampal alpha2a-adrenergic receptors are located predominantly presynaptically but are also found postsynaptically and in selective astrocytes. *The Journal of Comparative Neurology*, **395**(3), pp. 310–327.

Milner, T. A. and Bacon, C. E. (1989). Ultrastructural localization of tyrosine hydroxylase-like immunoreactivity in the rat hippocampal formation. *The Journal of Comparative Neurology*, **281**(3), pp. 479–495.

Milner, T. A., Shah, P. and Pierce, J. P. (2000). β-adrenergic receptors primarily are located on the dendrites of granule cells and interneurons but also are found on astrocytes and a few presynaptic profiles in the rat dentate gyrus. *Synapse*, **36**(3), pp. 178–193.

Milner, T. A. and Veznedaroglu, E. (1989). Ultrastructural localization of neuropeptide Y-like immunoreactivity in the rat hippocampal formation. *Hippocampus*, **2**(2), pp. 107–125.

Milstein, A. D., Bloss, E. B., Apostolides, P. F., Vaidya, S. P., Dilly, G. A., Zemelman, B. V., Magee, J. C., *et al.* (2015). Inhibitory gating of input comparison in the CA1 Microcircuit. *Neuron*, **87**(6), pp. 1274–1289.

Minneman, P., Theroux, L. and Esbenshade, A. (1994). Selectivity subtypes of agonists for cloned alpha1-adrenergic receptor. *Molecular Pharmacology*, **46**(5), pp. 929–936.

Mishra, R. K. *et al.* (2016). Symmetric spike timing-dependent plasticity at CA3-CA3 synapses optimizes storage and recall in autoassociative networks. *Nature Communications*, **7**(11552), pp. 1–11.

Mo, A. *et al.* (2015). Epigenomic Signatures of Neuronal Diversity in the Mammalian Brain. *Neuron*, **86**(6), pp. 1369–1384.

Monday, H. R., Younts, T. J. and Castillo, P. E. (2018). Long-term plasticity of neurotransmitter release: Emerging mechanisms and contributions to brain function and disease. *Annual Review of Neuroscience*, **41**, pp. 299–322.

Moons, L. *et al.* (1995). Noradrenergic system in the chicken brain: Immunocytochemical study with antibodies to noradrenaline and dopamine-β-hydroxylase. *The Journal of Comparative Neurology*, **360**(2), pp. 331–348.

Moore, R. Y. and Bloom, F. E. (1979). Central catecholamine neuron systems: anatomy and physiology of the norepinephrine and epinephrine systems. *Annual Review of Neuroscience*, **2**, pp. 113–168.

Mori, M. *et al.* (2004). A frequency-dependent switch from inhibition to excitation in a hippocampal unitary circuit. *Nature*, **431**(7007), pp. 453–456.

Morris, R. G. *et al.* (1982). Place navigation impaired in rats with hippocampal lesions. *Nature*, **297**(5868), pp. 681–683.

Morris, R. G. M. *et al.* (1986). Selective impairment of learning and blockade of long-term potentiation by an N-methyl-D-aspartate receptor antagonist, AP5. *Nature*, **319**(6056), pp. 774–776.

Moser, E. I., Kropff, E. and Moser, M.-B. (2008). Place cells, grid cells, and the brain's spatial representation system. *Annual Review of Neuroscience*, **31**, pp. 69–89.

Moser, E., Moser, M.-B. and Andersen, P. (1993). Spatial learning impairment parallels the magnitude of dorsal hippocampal lesions, but is hardly present following ventral lesions. *The Journal of Neuroscience*, **13**(9), pp. 3916–3925.

Moser, M.-B., Rowland, D. C. and Moser, E. I. (2015). Place cells, grid cells, and memory. *Cold Spring Harbor Perspectives In Biology*, **7**(2), pp. 1–15.

Moser, M.-B. *et al.* (1995). Spatial learning with a minislab in the dorsal hippocampus. *Proceedings of The National Academy of Sciences of The United States of America*, **92**(21), pp. 9697–9701.

Moser, M.-B. and Moser, E. I. (1998). Functional differentiation in the hippocampus. *Hippocampus*, **8**(6), pp. 608–619.

Mosienko, V. *et al.* (2018). Putative receptors underpinning L-lactate signalling in locus coeruleus. *Neuroglia*, **1**, pp. 365–380.

Moyer, J. R., Thompson, L. T. and Disterhoft, J. F. (1996). Trace eyeblink conditioning

increases CA1 excitability in a transient and learning-specific manner. *The Journal of Neuroscience*, **16**(17), pp. 5536–5546.

Mueller, A. L. *et al.* (1982). Hippocampal noradrenergic responses *in vivo* and *in vitro* - Characterization of alpha and beta components. *Naunyn-Schmiedeberg's Archives Of Pharmacology*, **318**(4), pp. 259–266.

Mueller, A. L., Hoffer, B. J. and Dunwiddie, T. V. (1981). Noradrenergic responses in rat hippocampus: evidence for mediation by α and β receptors in the *in vitro* slice. *Brain Research*, **214**(1), pp. 113–126.

Mulkey, R. M. *et al.* (1994). Involvement of a calcineurin/inhibitor-1 phosphatase cascade in hippocampal long-term depression. *Nature*, **369**, pp. 486–488.

Mulkey, R. M. and Malenka, R. C. (1992). Mechanisms underlying induction of homosynaptic long-term depression in area CA1 of the hippocampus. *Neuron*, **9**(5), pp. 967–975.

Muller, A. *et al.* (2014). Cell-based reporters reveal *in vivo* dynamics of dopamine and norepinephrine release in murine cortex. *Nature Methods*, **11**(12), pp. 1245–1252.

Murchison, C. F. *et al.* (2004). A distinct role for norephinephrine in memory retrieval. *Cell*, **117**(1), pp. 131–142.

Murchison, C. F. *et al.* (2011). Norepinephrine and β1-adrenergic signaling facilitate activation of hippocampal CA1 pyramidal neurons during contextual memory retrieval. *Neuroscience*, **181**, pp. 109–116.

Murphy, J. A. *et al.* (2014). Phosphorylation of Ser1166 on GluN2B by PKA is critical to synaptic NMDA receptor function and Ca^{2+} signaling in spines. *The Journal of Neuroscience*, **34**(3), pp. 869–879.

Nabavi, S. *et al.* (2014). Engineering a memory with LTD and LTP. *Nature*, **511**(7509), pp. 348–352.

Nádasdy, Z. *et al.* (1999). Replay and time compression of recurring spike sequences in the hippocampus. *The Journal of Neuroscience*, **19**(21), pp. 9497–9507.

Nadel, L. and Moscovitsh, M. (1997). Memory consolidation, retrograde amnesia and the hippocampal complex. *Current Opinion In Neurobiology*, **7**(2), pp. 217–227.

Nadler, J. V *et al.* (1976). Aspartate and glutamate as possible transmitters of excitatory hippocampal afferents. *Nature*, **260**(5551), pp. 538–540.

Nagel, G. *et al.* (2003). Channelrhodopsin-2, a directly light-gated cation-selective membrane channel. *Proceedings of The National Academy of Sciences of The United*

States of America, **100**(24), pp. 13940–13945.

Nakashiba, T. *et al.* (2009). Hippocampal CA3 output is crucial for ripple-associated reactivation and consolidation of memory. *Neuron*, **62**(6), pp. 781–787.

Nakazawa, K. *et al.* (2002). Requirement for hippocampal CA3 NMDA receptors in associative memory recall. *Science*, **297**(5579), pp. 211–218.

Nakazawa, K. *et al.* (2003). Hippocampal CA3 NMDA receptors are crucial for memory acquisition of one-time experience. *Neuron*, **38**(2), pp. 305–315.

Nakazawa, K. *et al.* (2004). NMDA receptors, place cells and hippocampal spatial memory. *Nature Reviews Neuroscience*, **5**(5), pp. 361–372.

Nanou, E., Yan, J., *et al.* (2016). Altered short-term synaptic plasticity and reduced muscle strength in mice with impaired regulation of presynaptic CaV 2.1 Ca^{2+} channels. *Proceedings of The National Academy of Sciences of The United States of America*, **113**(4), pp. 1068–1073.

Nanou, E., Sullivan, J. M., *et al.* (2016). Calcium sensor regulation of the CaV 2.1 Ca^{2+} channel contributes to short-term synaptic plasticity in hippocampal neurons. *Proceedings of The National Academy of Sciences of The United States of America*, **113**(4), pp. 1062–1067.

Nanou, E., Scheuer, T. and Catterall, W. A. (2016). Calcium sensor regulation of the CaV2.1 Ca^{2+} channel contributes to long-term potentiation and spatial learning. *Proceedings of The National Academy of Sciences of The United States of America*, **113**(46), pp. 13209–13214.

Ngo-Anh, T. J. *et al.* (2005). SK channels and NMDA receptors form a Ca^{2+}-mediated feedback loop in dendritic spines. *Nature Neuroscience*, **8**(5), pp. 642–649.

Nguyen, M. D. and Venton, B. J. (2015). Fast-scan cyclic voltammetry for the characterization of rapid adenosine release. *Computational and Structural Biotechnology Journal*, **13**, pp. 47–54.

Nicoll, R. A. (2017). A brief history of long-term potentiation. *Neuron*, **93**(2), pp. 281–290.

Nicoll, R. A. and Malenka, R. C. (1995). Contrasting properties of two forms of long-term potentiation in the hippocampus. *Nature*, **377**(6545), pp. 115–118.

Nicoll, R. A. and Schmitz, D. (2005). Synaptic plasticity at hippocampal mossy fibre synapses. *Nature Reviews Neuroscience*, **6**(11), pp. 863–876.

Nishiyama, M. *et al.* (2000). Calcium stores regulate the polarity and input specificity of

synaptic modification. *Nature*, **408**(6812), pp. 584–588.

Nolan, M. F. *et al.* (2005). A behavioral role for dendritic integration. *Cell*, **120**(1), pp. 151–152.

Nowak, L. *et al.* (1984). Magnesium gates glutamate-activated channels in mouse central neurones. *Nature*, **307**(5950), pp. 462–465.

Ntamati, N. R. and Lüscher, C. (2016). VTA projection neurons releasing GABA and glutamate in the dentate gyrus, **3**(4), pp. 1–12.

O'Dell, T. J. *et al.* (2010). Viagra for your synapses: Enhancement of hippocampal long-term potentiation by activation of beta-adrenergic receptors. *Cellular Signalling*, **22**(5), pp. 728–736.

O'Dell, T. J. *et al.* (2015). B-Adrenergic receptor signaling and modulation of long-term potentiation in the mammalian hippocampus. *Cold Spring Harbor Laboratory Press*, **22**(9), pp. 461–471.

O'Donnell, J. *et al.* (2012). Norepinephrine: A neuromodulator that boosts the function of multiple cell types to optimize CNS performance. *Neurochemical Research*, **37**(11), pp. 2496–2512.

O'Keefe, J. (1976). Place units in the hippocampus of the freely moving rat. *Experimental Neurology*, **51**(1), pp. 78–109.

O'Keefe, J. and Conway, D. H. (1978). Hippocampal place units in the freely moving rat: why they fire where they fire. *Experimental Brain Research*, **31**(4), pp. 573–590.

O'Keefe, J. and Dostrovsky, J. (1971). The hippocampus as a spatial map. Preliminary evidence from unit activity in the freely-moving rat. *Brain Research*, **34**(1), pp. 171–175.

O'Keefe, J. and Recce, M. L. (1993). Phase relationship between hippocampal place units and the EEG theta rhythm. *Hippocampus*, **3**(3), pp. 317–330.

O'Mara, S. M. *et al.* (2001). The subiculum: a review of form, physiology and function. *Progress In Neurobiology*, **64**(2), pp. 129–155.

O'Mara, S. M. *et al.* (2009). Roles for the subiculum in spatial information processing, memory, motivation and the temporal control of behaviour. *Progress In Neuro-Psychopharmacology and Biological Psychiatry*, **33**(5), pp. 782–790.

O'Rourke, M. F. *et al.* (1994). Characterization of [3H]RX821002 binding to alpha-2 adrenergic receptor subtypes. *The Journal of Pharmacology and Experimental Therapeutics*, **268**(3), pp. 1362–1367.

Oh, M. M. *et al.* (2006). Watermaze learning enhances excitability of CA1 pyramidal

neurons. *The Journal of Neurophysiology*, **90**(4), pp. 2171–2179.

Oleskevich, S., Descarries, L. and Lacaille, J. (1989). Quantified distribution of the noradrenaline hippocampus of adult rat innervation in the hippocampus of adult rat. *The Journal of Neuroscience*, **9**(11), pp. 3803–3815.

Otmakhova, N. A. and Lisman, J. E. (1998). Dopamine selectively inhibits the direct cortical pathway to the CA1 hippocampal region. *The Journal of Neuroscience*, **19**(4), pp. 1437–1445.

Pacholczyk, T., Blakely, R. D. and Amara, S. G. (1991). Expression cloning of a cocaine- and antidepressant-sensitive human noradrenaline transporter. *Nature*, **350**(6316), pp. 350–354.

Palacios-Filardo, J. and Mellor, J. R. (2019). Neuromodulation of hippocampal long-term synaptic plasticity. *Current Opinion In Neurobiology*, **54**, pp. 37–43.

Pang, K. and Rose, G. M. (1987). Differential effects of norepinephrine on hippocampal complex-spike and theta-neurons. *Brain Research*, **425**(1), pp. 146–158.

Panuccio, G., Vicini, S. and Avoli, M. (2012). Cell type-specific properties of subicular GABAergic currents shape hippocampal output firing mode. *PloS ONE*, **7**(12), pp. 1–9.

Papay, R. *et al.* (2006). Localization of the mouse alpha1A-adrenergic receptor (AR) in the brain: alpha1AAR is expressed in neurons, GABAergic interneurons, and NG2 oligodendrocyte progenitors. *The Journal of Comparative Neurology*, **497**(2), pp. 209–222.

Parfitt, K. D. *et al.* (1992). Isoproterenol increases the phosphorylation of the synapsins and increases synaptic transmission in dentate gyrus, but not in area CA1, of the hippocampus. *Hippocampus*, **2**(1), pp. 59–64.

Parfitt, K. D., Hoffer, B. J. and Browing, M. D. (1991). Norepinephrine and isoproterenol increase the phosphorylation of synapsin I and synapsin II in dentate slices of young but not aged Fisher 344 rats. *Proceedings of The National Academy of Sciences of The United States of America*, **88**(6), pp. 2361–2365.

Park, C. *et al.* (2018). Fast cyclic square-wave voltammetry to enhance neurotransmitter selectivity and sensitivity. *Analytical Chemistry*, **90**(22), pp. 13348–13355.

Patriarchi, T. *et al.* (2018). Ultrafast neuronal imaging of dopamine dynamics with designed genetically encoded sensors. *Science*, **360**(6396).

Pawlak, V. *et al.* (2010). Timing is not everything: neuromodulation opens the STDP gate. *Frontiers In Synaptic Neuroscience*, **2**(146), pp. 1–14.

Pertovaara, A. (2006). Noradrenergic pain modulation. *Progress In Neurobiology*, **80**(2), pp. 53–83.

Petroff, O. A. C. (2002). GABA and glutamate in the human brain. *The Neuroscientist*, **8**(6), pp. 562–573.

Petsche, H. and Stumpf, C. (1962). The origin of theta-rhytm in the rabbit hippocampus. *Wiener Klinische Wochenschrift*, **74**, pp. 696–700.

Pihel, K., Walker, Q. D. and Wightman, R. M. (1996). Overoxidized polypyrrole-coated carbon fiber microelectrodes for dopamine measurements with fast-scan cyclic voltammetry. *Analytical Chemistry*, **68**(13), pp. 2084–2089.

Pikkarainen, M. *et al.* (1999). Projections from the lateral, basal, and accessory basal nuclei of the amygdala to the hippocampal formation in rat. *The Journal of Comparative Neurology*, **403**(2), pp. 229–260.

Pitkänen, A. *et al.* (2000). Reciprocal connections between the amygdala and the hippocampal formation, perirhinal cortex, and postrhinal cortex in rat. A review. *Annals Of The New York Academy Of Sciences*, **911**, pp. 369–391.

Pockett, S. (1985). Dopamine changes the shape of action potentials in hippocampal pyramidal cells. *Brain Research*, **342**(2), pp. 386–390.

Pouille, F. and Scanziani, M. (2001). Enforcement of temporal fidelity in pyramidal cells by somatic feed-forward inhibition. *Science*, **293**(5532), pp. 1159–1163.

Pouille, F. and Scanziani, M. (2004). Routing of spike series by dynamic circuits in the hippocampus. *Nature*, **429**(6993), pp. 717–723.

Power, J. M. *et al.* (2011). Location and function of the slow afterhyperpolarization channels in the basolateral amygdala. *The Journal of Neuroscience*, **31**(2), pp. 526–537.

Power, J. M. *et al.* (2018). Age-related enhancement of the slow outward calcium-activated potassium current in hippocampal ca1 pyramidal neurons *in vitro*. *The Journal of Neuroscience*, **22**(16), pp. 7234–7243.

Preston, A. R. and Eichenbaum, H. (2013). Interplay of hippocampus and prefrontal cortex in memory. *Current Biology*, **23**(17), pp. 764–773.

Prince, L. Y. *et al.* (2016). Neuromodulation of the feedforward dentate gyrus-CA3 microcircuit. *Frontiers In Synaptic Neuroscience*, **8**(32), pp. 1–16.

Prince, L. Y. *et al.* (2017). Acetylcholine disinhibits hippocampal circuits to enable rapid formation of overlapping memory ensembles. *BioRxiv Neuroscience*.

Pudovkina, O. L., Cremers, T. I. F. H. and Westerink, B. H. C. (2002). The interaction

between the locus coeruleus and dorsal raphe nucleus studied with dual-probe microdialysis. *European Journal of Pharmacology*, **445**(1–2), pp. 37–42.

Purves, D., Augustine, G. J. and Fitzpatrick, D. (eds.) *et al.* (2001). *Neuroscience (2nd Edition)*. Sunderland (MA): Sinauer Associates.

Qian, H. *et al.* (2012). β_2 -Adrenergic receptor supports prolonged theta tetanus-induced LTP. *The Journal of Neurophysiology*, **107**(10), pp. 2703–2712.

Quirk, G. J. *et al.* (1992). The positional firing properties of medial entorhinal neurons: Description and comparison with hippocampal place cells. *The Journal of Neuroscience*, **12**(5), pp. 1945–1963.

Rajasethupathy, P. *et al.* (2015). Projections from neocortex mediate top-down control of memory retrieval. *Nature*, **526**(7575), pp. 653–659.

Rajkowski, J., Kubiak, P. and Aston-Jones, G. (1993). Correlations between locus coeruleus (LC) neural activity, pupil diameter and behavior in monkey support a role of LC in attention. *Abstracts - Society for Neuroscience*, **19**, p. 974.

Rajkowski, J., Kubiak, P. and Aston-Jones, G. (1994). Locus coeruleus activity in monkey: phasic and tonic changes are associated with altered vigilance. *Brain Research Bulletin*, **35**(5–6), pp. 607–616.

Raman, I. M., Tong, G. and Jahr, C. E. (1996). Beta-adrenergic regulation of synaptic NMDA receptors by cAMP-dependent protein kinase. *Neuron*, **16**(2), pp. 415–421.

Ramón y Cajal, S. (1894). La fine structure des centres nerveux. *Proceedings of The Royal Society London*, **55**, pp. 444–468.

Ramón y Cajal, S. (1899). *Comparative study of the sensory areas of the human cortex.*

Ramos, B. P. and Arnsten, A. F. T. (2007). Adrenergic pharmacology and cognition: Focus on the prefrontal cortex, **113**(3), pp. 523–536.

Ranck, J. B. (1973). Studies on single neurons in dorsal hippocampal formation and septum in unrestrained rats. Part I. Behavioral correlates and firing repertoires. *Experimental Neurology*, **41**(2), pp. 462–531.

Regehr, W. G. (2012). Short-term presynaptic plasticity. *Cold Spring Harbor Perspectives In Biology*, **4**(7), pp. 1–19.

Reid, C. A. *et al.* (2004). Optical quantal analysis indicates that long-term potentiation at single hippocampal mossy fiber synapses is expressed through increased release probability, recruitment of new release sites, and activation of silent synapses. *The Journal of Neuroscience*, **24**(14), pp. 3618–3626.

Remondes, M. and Schuman, E. M. (2003). Molecular mechanisms contributing to long-lasting synaptic plasticity at the temporoammonic–CA1 synapse. *Learning and Memory*, **10**(4), pp. 247–252.

Remondes, M. and Schuman, E. M. (2004). Role for a cortical input to hippocampal area CA1 in the consolidation of a long-term memory, **431**(7009), pp. 699–703.

Remy, S. and Spruston, N. (2007). Dendritic spikes induce single-burst long-term potentiation. *Proceedings of The National Academy of Sciences of The United States of America*, **104**(43), pp. 17192–17197.

Repina, N. A. *et al.* (2017). At light speed: Advances in optogenetic systems for regulating cell signaling and behavior. *Annual Review of Chemical and Biomolecular Engineering*, **8**, pp. 13–39.

Rich, P. D., Liaw, H. and Lee, A. K. (2014). Large environments reveal the statistical structure governing hippocampal representations. *Science*, **345**(6198), pp. 15–18.

Richer, F. and Beatty, J. (1987). Contrasting effects of response uncertainty on the task-evoked pupillary response and reaction time. *Psychophysiology*, **24**(3), pp. 258–262.

Richter-Levin, G. and Akirav, I. (2001). Amygdala-hippocampus dynamic interaction in relation to memory. *Molecular Neurobiology*, **22**(1–3), pp. 11–20.

Robain, O. *et al.* (1994). Development of mossy fiber synapses in hippocampal slice culture. *Developmental Brain Research*, **80**(1–2), pp. 244–250.

Robbins, C. A. and Tempel, B. L. (2012). Kv1.1 and Kv1.2: similar channels, different seizure models. *Epilepsia*, **53**(Suppl 1), pp. 134–141.

Robertson, S. D. *et al.* (2013). Developmental origins of central norepinephrine neuron diversity. *Nature Neuroscience*, **16**(8), pp. 1016–1023.

Robinson, D. L. *et al.* (2003). Detecting subsecond dopamine release with fast-scan cyclic voltammetry *in vivo*. *Clinical Chemistry*, **49**(10), pp. 1763–1773.

Robinson, R. B. and Siegelbaum, S. A. (2003). Hyperpolarization-activated cation currents: From molecules to physiological function. *Annual Review of Physiology*, **65**, pp. 453–480.

Rodeberg, N. T. *et al.* (2017). Hitchhiker's Guide to Voltammetry: Acute and chronic electrodes for *in vivo* fast-scan cyclic voltammetry. *ACS Chemical Neuroscience*, **8**(2), pp. 221–234.

Rodríguez-Moreno, A. and Lerma, J. (1998). Kainate receptor modulation of GABA release involves a metabotropic function. *Neuron*, **20**(6), pp. 1211–1218.

Rollenhagen, A. *et al.* (2007). Structural determinants of transmission at large hippocampal mossy fiber synapses. *The Journal of Neuroscience*, **27**(39), pp. 10434–10444.

Rolls, E. T. (2013). The mechanisms for pattern completion and pattern separation in the hippocampus. *Frontiers In Systems Neuroscience*, **7**(74), pp. 1–21.

Rosahl, T. W. *et al.* (1995). Essential functions of synapsins I and II in synaptic vesicle regulation. *Nature*, **375**(6531), pp. 488–493.

Rose, G. M. and Dunwiddie, T. V. (1986). Induction of hippocampal long-term potentiation using physiologically patterned stimulation. *Neuroscience Letters*, **69**(3), pp. 244–248.

Rosen, Z. B., Cheung, S. and Siegelbaum, S. A. (2015). Midbrain dopamine neurons bidirectionally regulate CA3-CA1 synaptic drive. *Nature Neuroscience*, **18**(12), pp. 1763–1771.

Roussel, B. *et al.* (1967). Locus ceruleus, paradoxal sleep, and cerebral noradrenaline. *Comptes Rendus Des Seances De La Societe De Biologie Et De Ses Filiales*, **161**(12), pp. 2537–2541.

Rowland, D. C. *et al.* (2016). Ten years of grid cells. *Annual Review of Neuroscience*, **39**, pp. 19–40.

Royer, S. *et al.* (2012). Control of timing, rate and bursts of hippocampal place cells by dendritic and somatic inhibition. *Nature Neuroscience*, **15**(5), pp. 769–775.

Rubenstein, J. L. R. and Merzenich, M. M. (2003). Model of autism: increased ratio of excitation/inhibition in key neural systems. *Genes, Brain, and Behavior*, **2**(5), pp. 255–267.

Russell, G. V. (1955). The nucleus locus coeruleus (dorsolateralis tegmenti). *Texas Reports on Biology and Medicine*, **13**(4), pp. 939–988.

Saenz, L. *et al.* (2008). Distribution and Neurochemical Characterization of Neurons Expressing GIRK Channels in the Rat Brain, **510**(6), pp. 581–606.

Sah, P. and Bekkers, J. M. (1996). Apical dendritic location of slow afterhyperpolarization current in hippocampal pyramidal neurons: Implications for the integration of long-term potentiation. *The Journal of Neuroscience*, **16**(15), pp. 4537–4542.

Sah, P. and Isaacson, J. S. (1995). Channels underlying the slow afterhyperpolarization in hippocampal pyramidal neurons: neurotransmitters modulate the open probability. *Neuron*, **15**(2), pp. 435–441.

Sakaba, T. and Neher, E. (2003). Direct modulation of synaptic vesicle priming by GABA(B) receptor activation at a glutamatergic synapse. *Nature*, **424**(6950), pp. 775–778.

Sales, A. C. *et al.* (2019). Locus coeruleus tracking of prediction errors optimises cognitive flexibility: An active inference model. *PLoS Computational Biology*, **15**(1), pp. 1–24.

Salgado, H., Köhr, G. and Treviño, M. (2012). Noradrenergic 'tone' determines dichotomous control of cortical spike-timing-dependent plasticity. *Scientific Reports*, **2**(417), pp. 1–7.

Salin, P. A. *et al.* (1996). Distinct short-term plasticity at two excitatory synapses in the hippocampus. *Proceedings of The National Academy of Sciences of The United States of America*, **93**(23), pp. 13304–13309.

Samuels, E. R. and Szabadi, E. (2008). Functional neuroanatomy of the noradrenergic locus coeruleus: Its roles in the regulation of arousal and autonomic function part I: principles of functional organisation. *Current Neuropharmacology*, **6**(3), pp. 235–253.

Sánchez-Ponce, D. *et al.* (2012). Developmental expression of Kv potassium channels at the axon initial segment of cultured hippocampal neurons. *PloS ONE*, **7**(10), pp. 1–14.

Sánchez-rodríguez, I. *et al.* (2017). Activation of G-protein-gated inwardly rectifying potassium (Kir3/GirK) channels rescues hippocampal functions in a mouse model of early amyloid-β pathology. Scientific Reports, **7**(14658), pp. 1–13.

Sano, F. (1941). Honyurui no seihankaku ni kansuru hikaku kaibou- gakuteki kenkyu (in Japanese) (Eine vergleichend-anatomische Studie uber den Nucleus loci caerulei der Saugetiere). *Kaibogaku Zassi*, **18**, pp. 149–175.

Sara, S. J. (2009). The locus coeruleus and noradrenergic modulation of cognition. *Nature Reviews Neuroscience*, **10**(3), pp. 211–223.

Sara, S. J. and Bouret, S. (2012). Review orienting and reorienting: The locus coeruleus mediates cognition through arousal. *Neuron*, **76**(1), pp. 130–141.

Sara, S. J., Vankov, A. and Herve, A. (1994). Locus coeruleus-evoked responses in behaving rats: A clue to the role of noradrenaline in memory. *Brain Research Bulletin*, **35**(5–6), pp. 457–465.

Sathyanesan, A., Ogura, T. and Lin, W. (2012). Automated measurement of nerve fiber density using line intensity scan analysis. *Journal of Neuroscience Methods*, **206**(2), pp. 165–175.

Sato, Y. *et al.* (1998). Three-dimensional multi-scale line filter for segmentation and

visualization of curvilinear structures in medical images. *Medical Image Analysis*, **2**(2), pp. 143–168.

Save, E., Nerad, L. and Poucet, B. (2000). Contribution of multiple sensory information to place field stability in hippocampal place cells. *Hippocampus*, **10**(1), pp. 64–76.

Scanziani, M., Gähwiler, B. H. and Thompson, S. M. (1993). Presynaptic inhibition of excitatory synaptic transmission mediated by α adrenergic receptors in area CA3 of the rat hippocampus *in vitro*. *The Journal of Neuroscience*, **13**(12), pp. 5393–5401.

Schacter, D. L., Chiu, C.-Y. P. and Ochsner, K. N. (1993). Implicit Memory: A selective review. *Annual Review of Neuroscience*, **16**, pp. 159–182.

Schaffer, K. (1892). Beitrag zur Histologie der Ammonshornformation. *Arch Mikroskop Anatomie*, **39**, pp. 611–632.

Scharfman, H. E. (2007). The CA3 'backprojection' to the dentate gyrus. *Progress in Brain Research*, 163, pp. 627–637.

Schlingloff, D. *et al.* (2014). Mechanisms of sharp wave initiation and ripple generation. *The Journal of Neuroscience*, **34**(34), pp. 11385–11398.

Schmitz, D., Mellor, J. and Nicoll, R. A. (2001). Presynaptic kainate receptor mediation of frequency facilitation at hippocampal mossy fiber synapses. *Science*, **291**(5510), pp. 1972–1976.

Schoch, S., Cibelli, G. and Thiel, G. (1996). Neuron-specific gene expression of synapsin I: Major role of a negative regulatory mechanism. *The Journal of Biological Chemistry*, **271**(6), pp. 3317–3323.

Schwartzkroin, P. A. and Wester, K. (1975). Long-lasting facilitation of a synaptic potential following tetanization in the *in vitro* hippocampal slice. *Brain Research*, **89**(1), pp. 107–119.

Schwarz, L. A. *et al.* (2015). Viral-genetic tracing of the input-output organization of a central noradrenaline circuit. *Nature*, **524**(7563), pp. 88–92.

Scimemi, A., Tian, H. and Diamond, J. S. (2009). Neuronal transporters regulate glutamate clearance, NMDA receptor activation, and synaptic plasticity in the hippocampus. *The Journal of Neuroscience*, **29**(46), pp. 14581–14595.

Scoville, W. B. and Milner, B. (1957). Loss of recent memory after bilateral hippocampal lesions. *The Journal of Neurology, Neurosurgery, and Psychiatry*, **20**(1), pp. 11–21.

Selten, M., Bokhoven, H. Van and Kasri, N. N. (2018). Inhibitory control of the excitatory/inhibitory balance in psychiatric disorders. *F1000Research*, **7**(23), pp. 1–16.

Senzai, Y. and Buzsaki, G. (2017). Physiological properties and behavioral correlates of hippocampal granule cells and mossy cells. *Neuron*, **93**(3), pp. 691-704.

Shah, M. M. (2014). Cortical HCN channels: Function, trafficking and plasticity. *The Journal of Physiology*, **592**(13), pp. 2711–2719.

Sharma, Y. *et al.* (2010). Comparative anatomy of the locus coeruleus in humans and nonhuman primates. *The Journal of Comparative Neurology*, **518**(7), pp. 963–971.

Shen, H. *et al.* (2012). Vagus nerve stimulation enhances perforant path-CA3 synaptic transmission via the activation of β-adrenergic receptors and the locus coeruleus. *International Journal of Neuropsychopharmacology*, **15**(4), pp. 523–530.

Shields, S. M., Ingebritsen, T. S. and Kelly, P. T. (1985). Identification of protein phosphatase 1 in synaptic junctions: Dephosphorylation of endogenous calmodulin-dependent kinase II and synapse-enriched phosphoproteins. *The Journal of Neuroscience*, **5**(12), pp. 3414–3422.

Shinohara, Y. *et al.* (2012). Hippocampal CA3 and CA2 have distinct bilateral innervation patterns to CA1 in rodents. *The European Journal of Neuroscience*, **35**(5), pp. 702–710.

Siapas, A. G. and Wilson, M. A. (1998). Coordinated interactions between hippocampal ripples and cortical spindles during slow-wave sleep. *Neuron*, **21**(5), pp. 1123–1128.

Siegelbaum, S. A. and Kandel, E. R. (1991). Learning-related synaptic plasticity: LTP and LTD. *Current Opinion In Neurobiology*, **1**(1), pp. 113–120.

Sigel, E. and Steinmann, M. E. (2012). Structure, function, and modulation of $GABA_A$ receptors. *The Journal of Biological Chemistry*, **287**(48), pp. 40224–40231.

Sigurdsson, T. and Duvarci, S. (2016). Hippocampal-prefrontal interactions in cognition, behavior and psychiatric disease. *Frontiers In Systems Neuroscience*, **9**(190), pp. 1–18.

Silberberg, G. *et al.* (2005). Synaptic pathways in neural microcircuits. *Trends In Neurosciences*, **28**(10), pp. 541–551.

Sirota, A. *et al.* (2003). Communication between neocortex and hippocampus during sleep in rodents. *Proceedings of The National Academy of Sciences of The United States of America*, **100**(4), pp. 2065–2069.

Siuda, E. R. *et al.* (2015). Optodynamic simulation of β-adrenergic receptor signalling. *Nature Communications*, **6**(8480), p p. 1–13.

Skou, J. C. (1957). The influence of some cations on an adenosine triphosphatase from peripheral nerves. *Biochimica Et Biophysica Acta*, **23**(2), pp. 394–401.

Smart, S. L. *et al.* (1998). Deletion of the K(V)1.1 potassium channel causes epilepsy in

mice. *Neuron*, **20**(4), pp. 809–819.

Smith, C. C. and Greene, R. W. (2012). CNS dopamine transmission mediated by noradrenergic innervation. *The Journal of Neuroscience*, **32**(18), pp. 6072–6080.

Spruston, N. (2008). Pyramidal neurons: Dendritic structure and synaptic integration. *Nature Reviews Neuroscience*, **9**(3), pp. 206–221.

Squire, L. R. (1986). Mechanisms of memory. *Science*, **232**(4758), pp. 1612–1619.

Squire, L. R. (1992). Memory and the hippocampus: A synthesis from findings with rats, monkeys, and humans. *Psychological Review*, **99**(2), pp. 195–231.

Squire, L. R. *et al.* (1993). The structure and organisation of memory. *Annual Review of Neuroscience*, **44**, pp. 493–495.

Stanzione, P. *et al.* (1984). Dopamine modulates CA1 hippocampal neurons by elevating the threshold for spike generation: An *in vitro* study. *Neuroscience*, **13**(4), pp. 1105–1116.

Starke, K. and Montel, H. (1973). Involvement of α-receptors in clonidine-induced inhibition of transmitter release from central monoamine neurones. *Neuropharmacology*, **12**(11), pp. 1073–1080.

Sternson, S. M. and Roth, B. L. (2014). Chemogenetic tools to interrogate brain functions. *Annual Review of Neuroscience*, **37**, pp. 387–407.

Stevens, C. F. (1998). A million dollar question: does LTP = memory? *Neuron*, **20**(1), pp. 1–2.

Steward, O. and Scoville, S. A. (1976). Cells of origin of entorhinal cortical afferents to the hippocampus and fascia dentata of the rat. *The Journal of Comparative Neurology*, **169**(3), pp. 347–370.

Stewart, M. and Fox, S. E. (1990). Firing relations of lateral septal neurons to the hippocampal theta rhythm in urethane anesthetized rats. *Experimental Brain Research*, **79**(1), pp. 92–96.

Sugita, S. *et al.* (2001). Synaptotagmin VII as a Plasma Membrane Ca^{2+} Sensor in Exocytosis. *Neuron*, **30**(2), pp. 459–473.

Sun, F. *et al.* (2018). A genetically encoded fluorescent sensor enables rapid and specific detection of dopamine in flies, fish, and mice. *Cell*, **174**(2), pp. 481–496.

Sun, H. Y., Lyons, S. A. and Dobrunz, L. E. (2005). Mechanisms of target-cell specific short-term plasticity at Schaffer collateral synapses onto interneurones versus pyramidal cells in juvenile rats, **568**(3), pp. 815–840.

Sun, Y., Nguyen, Amanda Q, *et al.* (2014). Cell-type-specific circuit connectivity of hippocampal CA1 revealed through Cre-dependent rabies tracing. *Cell Reports*, **7**(1), pp. 269–280.

Sun, Y., Nguyen, Amanda Q., *et al.* (2014). Cell-type-specific circuit connectivity of hippocampal CA1 revealed through cre-dependent rabies tracing. *Cell Reports*, **7**(1), pp. 269–280.

Sun, Y. J. *et al.* (2010). Fine-tuning of pre-balanced excitation and inhibition during auditory cortical development. *Nature*, **465**(7300), pp. 927–931.

Suzuki, S. S. and Smith, G. K. (1985). Burst characteristics of hippocampal complex spike cells in the awake rat. *Experimental Neurology*, **89**(1), pp. 90–95.

Swedenborg, E. (1887). *The Brain: considered anatomically, physiologically and phylosopically*. (Translated and edited by Tafel, R, L). London: James Speirs.

Sweeney, J. E., Lamour, Y. and Bassant, M. H. (1992). Arousal-dependent properties of medial septal neurons in the unanesthetized rat. *Neuroscience*, **48**(2), pp. 353–362.

Swift, K. M. *et al.* (2018). Abnormal locus coeruleus sleep activity alters sleep signatures of memory consolidation and impairs place cell stability and spatial memory. *Current Biology*, **28**(22), pp. 3599–3609.

Takahashi, H. and Magee, J. C. (2009). Pathway interactions and synaptic plasticity in the dendritic tuft regions of CA1 pyramidal neurons. *Neuron*, **62**(1), pp. 102–111.

Takahashi, K. *et al.* (2010). Locus coeruleus neuronal activity during the sleep-waking cycle in mice. *Neuroscience*, **169**(3), pp. 1115–1126.

Takeuchi, T. *et al.* (2016). Locus coeruleus and dopaminergic consolidation of everyday memory. *Nature*, **537**(7620), pp. 357–362.

Talley, E. M. *et al.* (1999). Differential distribution of three members of a gene family encoding low voltage-activated (T-type) calcium channels. *The Journal of Neuroscience*, **19**(6), pp. 1895–1911.

Tamamaki, N. and Nojyo, Y. (1993). Projection of the entorhinal layer II neurons in the rat as revealed by intracellular pressure-injection of neurobiotin. *Hippocampus*, **3**(4), pp. 471–480.

Tanzi, E. (1893). I fatti e le induzioni dell'odierna istologia del sistema nervoso. *Riv Sper Fren Med Leg*, **19**, pp. 419–472.

Taube, J. S. (1993). Electrophysiological properties of neurons in the rat subiculum in vitro. *Experimental Brain Research*, **96**(2), pp. 304–318.

Thomson, A. M. (1997). Activity-dependent properties of synaptic transmission at two classes of connections made by rat neocortical pyramidal axons *in vitro*, **502**(1), pp. 131–147.

Tigaret, C. M. *et al.* (2016). Coordinated activation of distinct Ca^{2+} sources and metabotropic glutamate receptors encodes Hebbian synaptic plasticity. *Nature Communications*, **7**(10289), pp. 1–14.

Tigaret, X. C. M. *et al.* (2018). Channels to promote synaptic plasticity in the hippocampus, **38**(43), pp. 9252–9262.

Ting, J. T. *et al.* (2018). Preparation of acute brain slices using an optimized N-methyl-D-glucamine protective recovery method. *The Journal of Visualized Experiments*, **132**, pp. 1–13.

Tomita, S., Stein, V., *et al.* (2005). Bidirectional synaptic plasticity regulated by phosphorylation of stargazin-like TARPs. *Neuron*, **45**(2), pp. 269–277.

Tomita, S., Adesnik, H., *et al.* (2005). Stargazin modulates AMPA receptor gating and trafficking by distinct domains. *Nature*, **435**(7045), pp. 1052–1058.

Torborg, C. L. *et al.* (2010). Control of CA3 output by feedforward inhibition despite developmental changes in the excitation-inhibition balance. *The Journal of Neuroscience*, **30**(46), pp. 15628–15637.

Toth, K. *et al.* (2000). Differential mechanisms of transmission at three types of mossy fiber synapse. *The Journal of Neuroscience*, **20**(22), pp. 8279–8289.

Traub, R. D., Miles, R. and Wong, R. K. (1989). Model of the origin of rhythmic population oscillations in the hippocampal slice. *Science*, **243**(4896), pp. 1319–1325.

Traynelis, S. F. *et al.* (2010). Glutamate receptor ion channels: Structure, regulation, and function. *Pharmacological Reviews*, **62**(3), pp. 405–496.

Treves, A. and Rolls, E. T. (1992). Computational constraints suggest the need for two distinct input systems to the hippocampal CA3 network. *Hippocampus*, **2**(2), pp. 189–199.

Treves, A. and Rolls, E. T. (1994). Computational analysis of the role of the hippocampus in memory. *Hippocampus*, **4**(3), pp. 374–391.

Tripathy, S. J. *et al.* (2015). Brain-wide analysis of electrophysiological diversity yields novel categorization of mammalian neuron types. *The Journal of Neurophysiology*, **113**(10), pp. 3474–3489.

Tsai, H.-C. *et al.* (2009). Phasic firing in dopaminergic neurons is sufficient for

behavioral conditioning. *Science*, **324**(5930), pp. 1080–1084.

Tsodyks, M. V and Markram, H. (1997). The neural code between neocortical pyramidal neurons depends on neurotransmitter release probability. *Proceedings of The National Academy of Sciences of The United States of America*, **94**(2), pp. 719–723.

Tsumoto, T. (1993). Long-term depression in cerebral cortex: A possible substrate of 'forgetting' that should not be forgotten. *Neuroscience Research*, **16**(4), pp. 263–270.

Tully, K. *et al.* (2007). Norepinephrine enables the induction of associative long-term potentiation at thalamo-amygdala synapses. *Proceedings of The National Academy of Sciences of The United States of America*, **104**(35), pp. 14146–14150.

Tully, K. and Bolshakov, V. Y. (2010). Emotional enhancement of memory: How norepinephrine enables synaptic plasticity. *Molecular Brain*, **3**(15), pp. 1–9.

Tulving, E. (1972). *Episodic and semantic memory*. In: Tulving, E and Donaldson, W (eds.). *Organization of Memory*. Oxford: Academic Press, pp. 423–423.

Turecek, J. and Regehr, W. G. (2018). Synaptotagmin 7 mediates both facilitation and asynchronous release at granule cell synapses. *The Journal of Neuroscience*, **38**(13), pp. 3240–3251.

Turner, R. W. *et al.* (2016). Assessing the role of IKCa channels in generating the sAHP of CA1 hippocampal pyramidal cells. *Channels*, **10**(4), pp. 313–319.

Uematsu, A., Tan, B. Z. and Johansen, J. P. (2015). Projection specificity in heterogeneous locus coeruleus cell populations: Implications for learning and memory. *Learning and Memory*, **22**(9), pp. 444–451.

Ul Haq, R. *et al.* (2012). Adrenergic modulation of sharp wave-ripple activity in rat hippocampal slices. *Hippocampus*, **22**(3), pp. 516–533.

Umbriaco, D. *et al.* (1995). Relational features of acetylcholine, noradrenaline, serotonin and GABA axon terminals in the stratum radiatum of adult rat hippocampus (CA1). *Hippocampus*, **5**(6), pp. 605–620.

Usher, M. *et al.* (1999). The Role of Locus Coeruleus in the Regulation of Cognitive Performance. *Science*, **283**(January), pp. 549–555.

Valentinol, R. J. and Foote, L. (1987). Corticotropin-releasing hormone increases tonic but not sensory-evoked activity of noradrenergic locus coeruleus neurons in unanesthetized rats, **8**(3), pp. 1016–1025.

Vanderwolf, C. H. (1969). Hippocampal electrical activity and the voluntary movement in the rat. *Electroencephalography and Clinical Neurophysiology*, **26**(4), pp. 407–418.

Vankov, A., Herve-Minvielle, A. and Sara, S. J. (1995). Response to novelty and its rapid habituation in locus coeruleus neurons of the freely exploring rat. *The European Journal of Neuroscience*, **7**(6), pp. 1180–1187.

Varga, V. *et al.* (2008). The presence of pacemaker HCN channels identifies theta rhythmic GABAergic neurons in the medial septum. *The Journal of Physiology*, **586**(16), pp. 3893–3915.

van de Ven, G. M. *et al.* (2016). Hippocampal offline reactivation consolidates recently formed cell assembly patterns during sharp wave-ripples. *Neuron*, **92**(5), pp. 968–974.

Vertes, R. P. (2005). Hippocampal theta rhythm: a tag for short-term memory. *Hippocampus*, **15**(7), pp. 923–935.

Vico Varela, E., Etter, G. and Williams, S. (2019). Excitatory-inhibitory imbalance in Alzheimer's disease and therapeutic significance. *Neurobiology Of Disease*, **127**, pp. 605–615.

Villalobos, C. (2004). SKCa channels mediate the medium but not the slow calcium-activated afterhyperpolarization in cortical neurons. *The Journal of Neuroscience*, **24**(14), pp. 3537–3542.

Voss, J. L. and Paller, K. A. (2008). Brain substrates of implicit and explicit memory: The importance of concurrently acquired neural signals of both memory types. *Neuropsychologia*, **46**(13), pp. 3021–3029.

Vyleta, Nicholas P., Borges-Merjane, C. and Jonas, P. (2016). Plasticity-dependent, full detonation at hippocampal mossy fiber–CA3 pyramidal neuron synapses. *eLife*, **5**, pp. 1–12.

Wagatsuma, A. *et al.* (2018). Locus coeruleus input to hippocampal CA3 drives single-trial learning of a novel context. *Proceedings of The National Academy of Sciences of The United States of America*, **115**(2), pp. 310–316.

Wainer, B. H. *et al.* (1985). Cholinergic and non-cholinergic septohippocampal pathways. *Neuroscience Letters*, **54**(1), pp. 45–52.

Walling, S. G. *et al.* (2012). Selective wheat germ agglutinin (WGA) uptake in the hippocampus from the locus coeruleus of dopamine-β-hydroxylase-WGA transgenic mice. *Frontiers In Behavioral Neuroscience*, **6**(23), pp. 1–8.

Walling, S. G. and Harley, C. W. (2004). Locus ceruleus activation initiates delayed synaptic potentiation of perforant path input to the dentate gyrus in awake rats: A novel β-adrenergic- and protein synthesis-dependent mammalian plasticity mechanism. *The Journal of Neuroscience*, **24**(3), pp. 598–604.

Waterhouse, B. D. *et al.* (1988). New evidence for a gating action of norepinephrine in central neuronal circuits of mammalian brain, **21**(3), pp. 425–432.

Waterhouse, B. D., Moises, H. C. and Woodward, D. J. (1998). Phasic activation of the locus coeruleus enhances responses of primary sensory cortical neurons to peripheral receptive field stimulation. *Brain Research*, **790**(1-2), pp. 33–44.

Waterhouse, B. D. and Navarra, R. L. (2019). The locus coeruleus-norepinephrine system and sensory signal processing: A historical review and current perspectives. *Brain Research*, **1709**, pp. 1–15.

Weisskopf, M. G. *et al.* (1994). Mediation of hippocampal mossy fiber long-term potentiation by cyclic AMP. *Science*, **265**(5180), pp. 1878–1882.

Wickman, K. *et al.* (2000). Brain localization and behavioral impact of the G-protein-gated K^+ channel subunit GIRK4. *The Journal of Neuroscience*, **20**(15), pp. 5608–5615.

Wieland, K. *et al.* (1996). Involvement of Asn-293 in stereospecific agonist recognition and in activation of the β2-adrenergic receptor. *Proceedings of The National Academy of Sciences of The United States of America*, **93**(17), pp. 9276–9281.

Wierenga, C. J. and Wadman, W. J. (2003). Excitatory inputs to CA1 interneurons show selective synaptic dynamics. *The Journal of Neurophysiology*, **90**(2), pp. 811–821.

Willadt, S., Nenniger, M. and Vogt, K. E. (2013). Hippocampal feedforward inhibition focuses excitatory synaptic signals into distinct dendritic compartments. *PloS ONE*, **8**(11), pp. 1–10.

Wills, T. J. *et al.* (2005). Attractor dynamics in the hippocampal representation of the local environment. *Science*, **308**(5723), pp. 873–876.

Wilson, M. A. and McNaughton, B. L. (1993). Dynamics of the hippocampal ensemble code for space. *Science*, **261**(5124), pp. 1055–1058.

Wilson, M. A. and McNaughton, B. L. (1994). Reactivation of hippocampal ensemble memories during sleep. *Science*, **265**(5172), pp. 676–679.

Wilson, R. I. and Nicoll, R. A. (2001). Endogenous cannabinoids mediate retrograde signalling at hippocampal synapses. *Nature*, **410**(6828), pp. 588–592.

Winson, J. (1978). Loss of hippocampal theta rhythm results in spatial memory deficit in the rat. *Science*, **201**(4351), pp. 160–163.

Wise, R. A. and Rompre, P. P. (1989). Brain dopamine and reward. *Annual Review of Psychology*, **40**, pp. 191–225.

Witten, I. B. *et al.* (2011). Recombinase-driver rat lines: Tools, techniques, and

optogenetic application to dopamine-mediated reinforcement. *Neuron*, **72**(5), pp. 721–733.

Wittenberg, G. M. and Wang, S. S. H. (2006). Malleability of spike-timing-dependent plasticity at the CA3-CA1 synapse. *The Journal of Neuroscience*, **26**(24), pp. 6610–6617.

Witter, M. P. *et al.* (1989). Functional organization of the extrinsic and intrinsic circuitry of the parahippocampal region. *Progress In Neurobiology*, **33**(3), pp. 161–253.

Woodward, D. *et al.* (1979). Modulatory actions of norepinephrine in the central nervous system. *Federation Proceedings*, **38**(7), pp. 2109–2116.

Ylinen, A. *et al.* (1995). Sharp wave-associated high-frequency oscillation (200 Hz) in the intact hippocampus: network and intracellular mechanisms. *The Journal of Neuroscience*, **15**(1 Pt 1), pp. 30–46.

Young, B. J., Fox, G. D. and Eichenbaum, H. (1994). Correlates of hippocampal complex-spike cell activity in rats performing a nonspatial radial maze task. *The Journal of Neuroscience*, **14**(11), pp. 6553–6563.

Zalutsky, R. A. and Nicoll, R. A. (1990). Comparison of two forms of long-term potentiation in single hippocampal neurons. *Science*, **248**(4963), pp. 1619–1624.

Zhang, J. C., Lau, P. M. and Bi, G. Q. (2009). Gain in sensitivity and loss in temporal contrast of STDP by dopaminergic modulation at hippocampal synapses. *Proceedings of The National Academy of Sciences of The United States of America*, **106**(31), pp. 13028–13033.

Zhang, Y. and Oertner, T. G. (2007). Optical induction of synaptic plasticity using a light-sensitive channel. Nature Methods, **4**(2), pp. 139–141.

Zhou, Q., Homma, K. J. and Poo, M.-M. (2004). Shrinkage of dendritic spines associated with long-term depression of hippocampal synapses. *Neuron*, **44**(5), pp. 749–757.

Zitnik, G. A. (2016). Control of arousal through neuropeptide afferents of the locus coeruleus. *Brain Research*, **1641**(Pt B), pp. 338–350.

Zucker, R. S. (1972). Crayfish escape behavior and central synapses. II. Physiological mechanisms underlying behavioral habituation. *The Journal of Neurophysiology*, **35**(5), pp. 621–637.

Zucker, R. S. and Regehr, W. G. (2002). Short-term synaptic plasticity. *Annual Review of Physiology*, **64**, pp. 355–405.